

The Potential of Anaerobic Digestion combined with Dissolved Air Flotation (AD-DAF) for Wastewater Treatment

Piaggio, A.L.

DOI

[10.4233/uuid:1bd92bed-2d18-45fa-8b1c-cc40f6d7f4ae](https://doi.org/10.4233/uuid:1bd92bed-2d18-45fa-8b1c-cc40f6d7f4ae)

Publication date

2023

Document Version

Final published version

Citation (APA)

Piaggio, A. L. (2023). *The Potential of Anaerobic Digestion combined with Dissolved Air Flotation (AD-DAF) for Wastewater Treatment*. [Dissertation (TU Delft), Delft University of Technology].
<https://doi.org/10.4233/uuid:1bd92bed-2d18-45fa-8b1c-cc40f6d7f4ae>

Important note

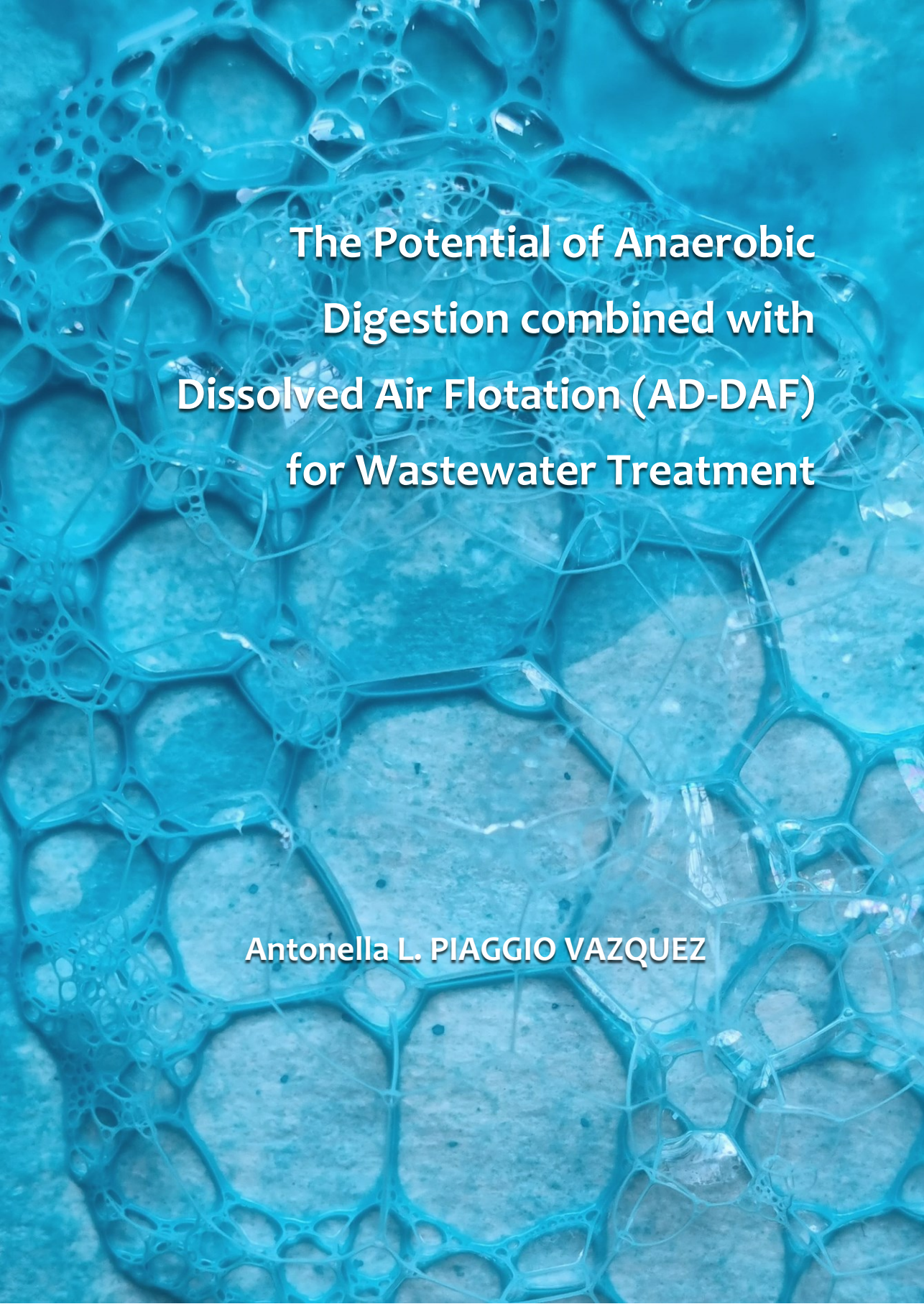
To cite this publication, please use the final published version (if applicable).
Please check the document version above.

Copyright

Other than for strictly personal use, it is not permitted to download, forward or distribute the text or part of it, without the consent of the author(s) and/or copyright holder(s), unless the work is under an open content license such as Creative Commons.

Takedown policy

Please contact us and provide details if you believe this document breaches copyrights.
We will remove access to the work immediately and investigate your claim.

The background of the entire page is a microscopic image of plant cells, showing a complex network of cell walls and large, irregularly shaped cells. A semi-transparent blue overlay is applied to the image, creating a monochromatic effect. The text is centered and overlaid on this background.

**The Potential of Anaerobic
Digestion combined with
Dissolved Air Flotation (AD-DAF)
for Wastewater Treatment**

Antonella L. PIAGGIO VAZQUEZ

The Potential of Anaerobic Digestion combined with Dissolved Air Flotation (AD-DAF) for Wastewater Treatment

Dissertation

for the purpose of obtaining the degree of doctor

at Delft University of Technology

by the authority of the Rector Magnificus, prof.dr.ir. T.H.J.J. van der Hagen,

Chair of the Board for Doctorates

to be defended publicly on

Tuesday 24 October at 12:30 o'clock

by

Antonella L. PIAGGIO VAZQUEZ

Master in Environmental Science, UNESCO-IHE, Netherlands

born in Montevideo, Uruguay

This dissertation has been approved by the promotors.

Composition of the doctoral committee:

Rector Magnificus	chairperson
Prof.dr.ir. M.K. de Kreuk	Technische Universiteit Delft, <i>promotor</i>
Dr.ir. R.E.F Lindeboom	Technische Universiteit Delft, <i>copromotor</i>

Independent members:

Prof.dr.ir. D. van Halem	Technische Universiteit Delft
Prof.dr.ir. I. Smets	Katholieke Universiteit Leuven, Belgium
Prof.dr. A. Malik	Indian Institute of Technology Delhi, India
Dr.ir. N. C. Boelee	Nijhuis Saur Industries, The Netherlands
Dr.ir. C. Hooijmans	IHE Institute for Water Education, The Netherlands
Prof.dr.ir. H. Schmitt	Technische Universiteit Delft (<i>reserve member</i>)

The research presented in this thesis was performed at the Sanitary Engineering Section, Department of Water Management, Faculty of Civil Engineering, Delft University of Technology, The Netherlands. The research was part of the LOTUS^{HR} project and was financially funded by the NWO, grant number 15424-2.

Front and back illustrations: bubbles created using watercolours, soap, and water, by A. L. Piaggio

Printed by Proefschrift-aio.nl

Keywords: anaerobic digestion (AD); dissolved air flotation (DAF); anaerobic membrane bioreactor (AnMBR); micro-aeration (MA); antibiotics

Copyright © 2023 by A. L. Piaggio

ISBN 978-94-6366-751-7

An electronic version of this dissertation is available at <http://repository.tudelft.nl/>.

To my dad, Juan E. Piaggio, who
always encouraged and guided
my academic journey

Contents

	Summary	viii
	Samenvatting	x
	Resumen	xiv
	Nomenclature	xvi
Chapter 1	Introduction	1
Chapter 2	Modelling of Dissolved Air Flotation (DAF). Application of an experimental filtration model for suspended solids removal prediction	23
Chapter 3	High suspended solids removal of Indian drain water with a down-scaled Dissolved Air Flotation (DAF) for water recovery	49
Chapter 4	Effects of low oxygen dosages on an anaerobic membrane bioreactor, simulating the oxygen supply in an anaerobic digester-dissolved air flotation (AD-DAF) system	77
Chapter 5	The fate of sulfamethoxazole and trimethoprim in a micro-aerated anaerobic membrane bioreactor (MA-AnMBR) and the occurrence of antibiotic resistance in the permeate	103
Chapter 6	Outlook	129
	Annexes	143
	Acknowledgements, About the author, List of Publications	183
	Bibliography	191

Summary

In the context of a worldwide scenario characterized by a progressively expanding human population, the combining effects of climate change, escalating water stress, and the degradation of freshwater resources, water reclamation has emerged as a viable solution to alleviate the critical issue of water scarcity. Several streams around the world are subjected to a wide range of pollutants concentration and water-born pathogens, like antibiotic-resistant bacteria (ARB), due to human activity. The latter can be considered as a global emerging threat, due to its potential to deteriorate the human health system. The juxtaposition of an increase in water demand, fluctuation of water availability, increased pollutant concentrations, and complexity of antibiotics removal, exacerbate water scarcity around the world. Thus, adequate treatment of these polluted streams is needed to overcome water scarcity.

While anaerobic membrane bioreactors (AnMBR) systems are a promising anaerobic digestion (AD) technology to treat municipal and concentrated wastewater, the application of membranes to separate solids from the bioreactor broth also has considerable constraints. An alternative physical separation method could be used to overcome the AnMBR limitations. Replacing the membrane unit of an AnMBR with a dissolved air flotation (DAF) system, and returning the flotation layer to the anaerobic reactor, may ensure high total suspended solids (TSS) retention while overcoming the membrane limitations. However, the oxygen-saturated flotation layer and the overall introduction of oxygen into the reactor through the DAF may negatively impact the anaerobic conversion process. This dissertation investigates the potential to use an AD coupled with a DAF system (AD-DAF) as a pre-treatment technology, specifically for the treatment of drain- and wastewater that mimics the ever-changing conditions of the Barapullah drain in New Delhi. Since testing an AD-DAF system on a laboratory-scale is not practically feasible, due to the constraints in downscaling a DAF unit, the implications of coupling these two technologies were assessed in two different systems: a column bench-scale DAF unit, and a lab-scale micro-aerated anaerobic membrane bioreactor (MA-AnMBR).

To begin with, a data-driven experimental DAF model was developed to predict TSS removal. Input values for the experimental model were particle and bubble characteristics. The experimental model outcomes were verified in a bench-scale column DAF and two full-scale DAF systems. Results showed a predicted TSS removal aligned with the measured one of Delft canal water, anaerobic sludge, and DAF₂ influents, $68 \pm 1\%$ vs. $66-96\%$, $77 \pm 3\%$ vs. $68-92\%$, and $98 \pm 1\%$ vs. $96 \pm 1\%$, respectively.

Afterwards, the bench-scale DAF was used to investigate the removal of suspended solids under four different influent conditions and seven DAF independent control variables (influent TSS, pH, temperature, DAF particles residence time, white water pressure, coagulants and flocculants concentration and mixing time). The influents simulated the Barapullah drain conditions under 1) dry and 2) monsoon times, and 3) close or 4) far from the pollution source. The results obtained indicated that TSS removal efficiency on the bench-scale DAF unit could mimic a full-scale system and that a DAF can remove over 90% of TSS for the four different tested influents. On the other hand, the effect of the performance variables altered depending on the influent type, with pressure showing a positive influence on the separation efficiency.

Secondly, to assess the effect of coupling the DAF system with AD, a lab-scale AnMBR system was subjected to an oxygen load similar to the one used on a DAF unit. The effects of the oxygen load were compared to a fully anaerobic system, and the MA-AnMBR performance was assessed, for removal of organic matter, biogas production, nutrient concentration, operation and maintenance, and removal of two antibiotics sulfamethoxazole, SMX, and trimethoprim, TMP). Results showed a slight significant increase in COD removal, from 98.2 to 98.5%, and an increase of 35% in the ammonium concentration in the MA-AnMBR permeate, which indicated improved hydrolysis. Furthermore, biogas production decreased by 27%, but methane concentration on both MA-AnMBR and AnMBR was high (85%).

Micro-aeration of the AnMBR had no negative effect in the removal of the tested antibiotics, which have a preferred anaerobic degradation pathway. TMP was rapidly adsorbed onto the sludge biomass and then degraded due to the long solids' retention time (27 days). SMX adsorption was minimal, but the system hydraulic retention time of 2.6 days allowed its biodegradation. The addition of SMX and TMP led to an increase in the relative abundance of all studied anti-microbial resistant genes (ARGs) (*sul1*, *sul2*, and *dfrA1*) and one mobile genetic element (*int1*) in the MA-AnMBR sludge. Furthermore, the presence of antibiotic-resistant bacteria and antibiotic-resistance genes in the reactor permeate indicated that further treatment was needed.

The outcomes obtained in this dissertation showed that an AD-DAF system has the potential to effectively remove total suspended solids under different influent conditions, and that the added oxygen load could improve hydrolysis with minimal impacts on the anaerobic conversion processes.

Samenvatting

In de context van een wereldwijde trend gekenmerkt door een groeiende bevolking, klimaatverandering, toenemende waterstress en de degradatie en uitputting van zoetwaterbronnen, is het hergebruik van gezuiverd afvalwater een haalbare oplossing om het kritieke probleem van waterschaarste het hoofd te bieden. Oppervlakte wateren over de hele wereld worden blootgesteld aan een breed scala van verontreinigende stoffen en watergedragen ziekteverwekkers, zoals antibiotica resistente bacteriën (ARB), als gevolg van menselijke activiteit. Het laatstgenoemde kan worden beschouwd als een opkomende wereldwijde dreiging vanwege het potentieel om het moderne gezondheidssysteem te ondermijnen. De combinatie van een toenemende vraag naar schoon water, schommelingen in waterbron en verontreinigingsconcentraties, en de complexiteit van het verwijderen van antibiotica verergeren de waterschaarste over de hele wereld. Een adequate behandeling van belangrijke vervuilde stromen is daarom nodig om waterschaarste tegen te gaan.

Hoewel anaërobe membraanbioreactors (AnMBR) veelbelovende AD-technologieën zijn om stedelijk en geconcentreerd afvalwater te behandelen, brengt het gebruik van membranen om vaste stoffen van de bioreactorvloeistof te scheiden aanzienlijke beperkingen met zich mee. Een alternatieve fysieke scheidingstechniek zou kunnen worden gebruikt om de beperkingen van AnMBR te overwinnen. Het vervangen van de membraaneenheid van een AnMBR door een opgelost luchtflotatie (DAF) systeem en het terugvoeren van de flotatielaag naar de anaërobe reactor kan zorgen voor een hoge TSS-retentie en zonder de membraanbeperkingen. Echter, de zuurstofverzadigde flotatielaag en de algemene introductie van zuurstof in de reactor als gevolg van de DAF kunnen een negatieve invloed hebben op het anaërobe vergistingsprocessen. Dit proefschrift onderzoekt de potentie om een AD gekoppeld aan een DAF-systeem (AD-DAF) te gebruiken als voorbehandelingstechniek, specifiek voor de behandeling van afvoer en afvalwater dat de voordurend veranderende omstandigheden van de Barapullah Drain in New Delhi, India nabootst. Aangezien het testen van een AD-DAF-systeem op laboratoriumschaal praktisch niet haalbaar is vanwege de beperkingen bij het verkleinen van een DAF-eenheid, werden de implicaties van het koppelen van deze twee technologieën geëvalueerd in twee verschillende systemen: een DAF-eenheid op kolomschaal en een laboratoriumschaal microbeluchte anaërobe membraanbioreactor (MA-AnMBR).

Om te beginnen werd er een experimenteel DAF-model ontwikkeld om de verwijdering van totale zwevende stoffen (TSS) te voorspellen, gebaseerd op observaties en gegevens. De eigenschappen van deeltjes en bubbels waren de invoerwaarden van het model. De resultaten van het experimentele model werden geverifieerd in een kolomschaal DAF-eenheid en twee DAF-systemen op volledige schaal. De resultaten toonden aan dat de voorspelde verwijdering van TSS overeenkwam met de gemeten verwijdering van Delfts kanaalwater ($68 \pm 1\%$ vs. $66-96\%$), anaëroob slib ($77 \pm 3\%$ vs. $68-92\%$) en DAF₂-influent ($98 \pm 1\%$ vs. $96 \pm 1\%$), en.

Daarna werd de DAF-eenheid op kolomschaal gebruikt om de verwijdering van zwevende stoffen te onderzoeken onder vier verschillende influentkenmerken en zeven onafhankelijke regelvariabelen van de DAF (influent TSS, pH, temperatuur, verblijftijd van DAF-deeltjes, druk van het witwater, concentratie van coagulantia en flocculantia, en mengtijd). De influenten simuleerden de kenmerken van de Barapullah-drain tijdens 1) droge en 2) moessonperiodes, en 3) met de bron van vervuiling dichtbij of 4) verweg. De resultaten wezen erop dat de verwijderingsefficiëntie van TSS op de DAF-eenheid op kolomschaal een volledig schaalmodel kon nabootsen en dat een DAF meer dan 90% van TSS kon verwijderen voor de vier verschillende geteste influenten. Bovendien varieerde het effect van de prestatievariabelen afhankelijk van het type influent, waarbij druk een positieve invloed had op de scheidingsrendement.

Ten tweede werd, om het effect van de koppeling van het DAF-systeem met AD te beoordelen, een laboratoriumschaal AnMBR-systeem onderworpen aan een zuurstofbelasting die vergelijkbaar was met die van een DAF-eenheid. De effecten van de zuurstofbelasting werden vergeleken met een volledig anaëroob systeem op het gebied van verwijdering van organische stoffen, biogasproductie, voedingsstofconcentratie, bedrijfsvoering en onderhoud, en verwijdering van twee antibiotica (sulfamethoxazol (SMX) en trimethoprim (TMP)). De resultaten toonden een lichte maar significante toename van de COD-verwijdering, van $98,2\%$ naar $98,5\%$, en een toename van 35% in de ammoniumconcentratie in het permeaat van het MA-AnMBR, wat wijst op verbeterde hydrolyse. De biogasproductie nam echter af met 27% , maar de methaanconcentratie in zowel het MA-AnMBR als het AnMBR was hoog (85%).

Microbeluchting van het AnMBR had geen negatief effect op de verwijdering van de geteste antibiotica, die een voorkeurspad hebben voor anaëroobe afbraak. TMP werd snel geabsorbeerd op de slibamenstelling en vervolgens afgebroken als gevolg van de lange retentietijd van de vaste stoffen (27 dagen). De adsorptie van SMX was

minimaal, maar de hydraulische retentietijd van het systeem van 2,6 dagen maakte biodegradatie mogelijk. De toevoeging van SMX en TMP leidde tot een toename van de relatieve overvloed van alle onderzochte antibioticaresistentiegenen (*sul1*, *sul2* en *dfrA1*) en een mobiel genetisch element (*intl1*) in het slib van het MA-AnMBR. Bovendien wees de aanwezigheid van antibioticaresistente bacteriën en antibioticaresistentiegenen in het permeaat van de reactor erop dat verdere behandeling nodig was.

De resultaten die in dit proefschrift zijn verkregen, tonen aan dat een AD-DAF-systeem het potentieel heeft om totaal zwevende vaste stoffen effectief te verwijderen onder verschillende influentomstandigheden, en dat de toegevoegde zuurstofbelasting de hydrolyse kan verbeteren met minimale invloed op de anaërobe omzettingsprocessen.

Resumen

La reutilización de aguas residuales adecuadamente tratadas ha surgido como una solución viable para aliviar el grave problema de la escasez de agua, en el contexto de un escenario mundial caracterizado por una población en constante expansión, incremento de cambio climático, estrés hídrico y degradación de la calidad del agua. Debido a la actividad humana, varios cursos de agua alrededor del mundo están ampliamente contaminados y presentan grandes concentraciones de patógenos, como las bacterias de resistencia antibacteriana (ARB, por su sigla en inglés). Estas últimas pueden considerarse como una amenaza emergente a nivel mundial, debido a su potencial para deteriorar el sistema de salud. La yuxtaposición del incremento en la demanda de agua, fluctuación de los flujos y disponibilidad del recurso, junto con la complejidad de la remoción de antibióticos y contaminantes, agravan la disponibilidad de agua para consumo. Por lo tanto, para superar su escasez, es indispensable el tratamiento adecuado de los cursos de agua.

Si bien los sistemas de biorreactores de membrana anaerobia (AnMBR, por su sigla en inglés) son una tecnología prometedora para el tratamiento de aguas residuales, la aplicación de las membranas para separar los sólidos tiene considerables limitaciones. Reemplazar la membrana de un AnMBR con otro sistema de separación física, como un sistema de flotación por aire disuelto (DAF, por su sigla en inglés), y reincorporar el sobrenadante al reactor anaeróbico podría garantizar una alta retención de sólidos, adquiriendo una remoción de sólidos suspendidos (SS) similar a la de los AnMBR. Sin embargo, la incorporación del sobrenadante saturado de oxígeno e introducción de oxígeno en el reactor anaerobio podrían tener un impacto negativo en los procesos de conversión. En esta disertación, se investigó el potencial de un digester anaeróbico (AD) acoplado a un DAF (AD-DAF), para el pretratamiento de drenajes y aguas residuales que imitan las condiciones del arroyo Barapullah en Nueva Delhi, India. Debido a que no es prácticamente factible testear un sistema AD-DAF a escala de laboratorio, en esta disertación se evaluaron las implicaciones de acoplar estas tecnologías en dos sistemas diferentes a escala laboratorio: una DAF corrido de forma discontinua, y un AnMBR sujeto a micro-aereación (MA-AnMBR).

Inicialmente, se desarrolló un modelo experimental del sistema DAF basado en datos, para predecir la remoción de sólidos en suspensión (SS). El modelo utilizó como valores de entrada las características de las partículas y las burbujas, y los resultados se verificaron en un DAF a escala laboratorio y en dos sistemas escala real. Los resultados mostraron una predicción de la remoción de SS en concordancia con los

valores obtenidos para el agua del canal de Delft, lodo anaeróbico y efluentes del DAF2, $68 \pm 1\%$ vs. $66-96\%$, $77 \pm 3\%$ vs. $68-92\%$ y $98 \pm 1\%$ vs. $96 \pm 1\%$, respectivamente.

Posteriormente, se investigó la remoción de SS en el DAF a escala laboratorio, utilizando cuatro influentes diferentes y siete variables de control independientes (SS del influente, pH, temperatura, tiempo de residencia de partículas en el DAF, presión del agua, concentración de coagulantes y floculantes, y tiempo de mezcla). Los influentes simulaban las condiciones del arroyo Barapullah en 1) época de sequía y 2) monzón, y 3) cerca o 4) lejos de la fuente de contaminación. Los resultados indicaron que la eficiencia de remoción de SS del DAF a escala laboratorio era similar a lo obtenido en un sistema a escala real, y que un DAF puede remover más del 90% de SS. Las variables de control no tuvieron el mismo efecto en todos los influentes testeados, salvo la presión que mostró una influencia positiva en la remoción de SS.

En segundo lugar, un AnMBR a escala laboratorio fue sometido a una adición de oxígeno similar a la utilizada en una unidad DAF, generando un MA-AnMBR. Los efectos de la adición de oxígeno se compararon con un sistema completamente anaerobio, y se evaluó el rendimiento del MA-AnMBR respecto a la remoción de materia orgánica, producción de biogás, concentración de nutrientes, operación y mantenimiento, y remoción de dos antibióticos (sulfametoxazol (SMX) y trimetoprima (TMP)). Los resultados mostraron un ligero aumento significativo en la remoción de DQO, de 98.2% a 98.5% , y un aumento del 35% en la concentración de amonio en el permeado del MA-AnMBR, lo que indica una mejora en la hidrólisis. Además, la producción de biogás disminuyó en un 27% , aunque la concentración de metano tanto en MA-AnMBR como en AnMBR fue alta (85%).

La remoción de los antibióticos testeados, los cuales tienen una vía preferencial de degradación anaerobia, no fue afectada por la micro-aereación del AnMBR. TMP fue rápidamente adsorbido en la biomasa y luego degradado debido al largo tiempo de retención de sólidos (27 días). La adsorción de SMX fue mínima, pero el tiempo de retención hidráulica del sistema de 2.6 días permitió su biodegradación. La adición de SMX y TMP provocó un aumento en la abundancia relativa de todos los genes de resistencia antibacteriana (ARGs por su sigla en inglés) estudiados (*sul1*, *sul2* y *dfrA1*) y un elemento genético móvil (*int1*). Además, la presencia de ARB y ARGs en el permeado del reactor indicó la necesidad de un tratamiento terciario.

Los resultados obtenidos en esta investigación demostraron que un sistema AD-DAF tiene el potencial de eliminar eficazmente los SS bajo diferentes tipos de influente, y que la adición de oxígeno podría mejorar la hidrólisis.

Nomenclature

AD	Anaerobic digestion
AD-DAF	Anaerobic digester – DAF
AnMBR	Anaerobic membrane bioreactor
ARB	Antibiotic-resistant bacteria
ARG	Antibiotic-resistant gene
CFD	Computational fluid dynamics
COD	Chemical oxygen demand
CSTR	Continuous stirred tank reactor
DAF	Dissolved air flotation
DBT	Department of Biotechnology
DO	Dissolved Oxygen
GC	Gas chromatography
HGT	Horizontal gene transfer
HRT	Hydraulic retention time
IITD	Indian Institute of Technology - Delhi
K_{ow}	Octanol-water partition coefficient
LOTUS ^{HR}	Local Treatment of Urban Sewage for Healthy Reuse
MA-AnMBR	Micro-aerated anaerobic membrane bioreactor
MBR	Membrane bioreactor
MGE	Mobile genetic elements
MF	Microfiltration
NF	Nanofiltration
NWO	The Dutch Research Council
OLR	Organic loading rate

ORP	Oxidation-reduction potential
PBD	Plackett-Burman Design
PBR	Photo bioreactor
PIV	Particle image velocimetry
PSD	Particle size distribution
qPCR	Quantitative polymerase chain reaction
RO	Reverse osmosis
SMA	Specific methanogenic activity
SMX	Sulfamethoxazole
SOD	Superoxide dismutase activity
SRT	Solids retention time
TERI	Energy and Resources Institute
TMP	Trimethoprim
TS	Total solids
TSS	Total suspended solids
UF	Ultrafiltration
UV	Ultraviolet
VFA	Volatile fatty acids
VS	Volatile solids
VSS	Volatile suspended solids
WWTP	Wastewater treatment plant



Bubbles created with watercolour, soap, and water.

1

Introduction

1.1 | WATER SCARCITY AND TREATMENT FOR REUSE

The availability of clean water and sanitation is one of the UN's seventeen sustainable development goals (SDGs) to “achieve a better and more sustainable future for all” (UN, 2018). This SDG shows the importance and relevance of water quantity and quality to humanity. Nevertheless, almost 40% of the global population endures water scarcity for one month per year, and 20% lives in countries with high or extremely high water vulnerability. Furthermore, water demand has been steadily increasing by at least 1% per year worldwide due to changes in consumption patterns, socioeconomic development, and population growth. Water consumption is expected to rise above one-quarter of the current consumption level by 2050 (WWAP, 2019). While agriculture is globally the largest consumer of water, with over 70% of the total consumption, the largest increase in water consumption is expected to originate from urban areas (FAO, 2020; Novoa et al., 2023).

Aside from the issues related to quantitative water scarcity, the deterioration of water quality only hampers, even more, the availability of adequate freshwater. Factors like salinity, nutrients, pathogens and other pollutants concentrations are key to the sustainable management of water resources (van Vliet et al., 2017). Freshwater pollution is largely caused by human activities, with anthropogenic water discharges such as industrial and domestic sewage, as well as agricultural run-off, being significant sources of pollution in both surface and groundwater systems (Calapez et al., 2019). Thus, adequate effluent treatment is crucial to alleviate water scarcity.

The total World population reaches around eight billion people, and the average human wastewater production is 130 L per day. Around 50% of the produced wastewater is discharged directly into the environment without treatment (Jones et al., 2021). Wastewater treatment can be categorised into physical, chemical and biological unit processes (Metcalf et al., 2013). Effective wastewater treatment generally consists of the following five steps: 1. preliminary treatment, mainly physical; 2. primary treatment, which can be chemical, physical or biological; 3. secondary treatment, generally biological and/or chemical; 4. tertiary treatment, mainly chemical and/or physical; and finally, 5. sludge treatment, which is usually a combination of physical, chemical and biological (Crini & Lichtfouse, 2019). The first two steps are commonly known as pre-treatment.

The most commonly used physical units for the pre-treatment of wastewater are screening, sedimentation, and flotation (Metcalf et al., 2014). Among these, dissolved air flotation (DAF) units have a small footprint and are characterised by a high

1
removal of suspended solids under a wide variety of hydraulic retention times (HRT) and organic loading rates (OLRs) (Kiuru, 1990). The ability to deal with a diversity of flows and solids makes DAF systems suitable for treating particularly challenging streams, especially those with high variation in their flows and biochemical composition. Compared to conventional settlers, DAF units need smaller surface areas for achieving similar solids removal efficiencies (between 60 to 99 %). This is a consequence of the short hydraulic retention time and high hydraulic loading rate needed to run a DAF system (Edzwald, 1995; Shammam et al., 2010).

The efficiency and reliability of biological wastewater treatment as part of the preliminary treatment have been well-established (Grady Jr et al., 2011; van den Berg, 2022). Biological wastewater treatment can be aerobic, anaerobic, or a combination of both. Anaerobic digestion (AD) is a widely used process due to its low sludge production when compared to aerobic treatment (up to one-tenth), the nutrient-rich effluent, and the production of energy as biogas (van Lier et al., 2008a). Amongst the AD systems, the anaerobic membrane bioreactor (AnMBR) is a promising technology to treat municipal wastewater from a resource-oriented perspective (van Lier, 2008). AnMBR units were first developed in the late 1980s for industrial wastewater treatment and are now considered one of the emerging anaerobic technologies that generate high-quality effluents of interest for subsequent reuse (Li, 1985).

Treated wastewater reuse has risen as a possibility to alleviate water scarcity caused by water stress (Saidan et al., 2020). Nevertheless, to reclaim treated wastewater, wastewater treatment plants (WWTPs) should be able to provide high-quality effluent. New and upgraded WWTPs should consider not only removing macro-contaminants, such as organic oxygen demand, suspended solids and nutrients but also pathogens and micropollutants (Roccaro & Verlicchi, 2018). A sharp increase in antibiotics consumption, due to their importance in human and veterinary medicine led to their abundance in wastewater. As much as 90% of these consumed antibiotics are excreted without any change (Balakrishna et al., 2017). Most conventional WWTPs are not designed for the removal of antibiotics (Gros et al., 2010; Radjenovic et al., 2007).

Minimal pharmaceutical removal can be observed in the physicochemical primary treatment of wastewater (Oulton et al., 2010). However, membrane bioreactors (MBR) are an effective technology in treating pharmaceutical wastewater containing various antibiotics and other micropollutants (Oberoi et al., 2019). The system solids retention time (SRT) and membrane pore size are the main operational parameters defining antibiotics removal on MBR units (Ji et al., 2020). Antibiotics might be

removed or transformed by two main different processes, biotic (biodegradation) or non-biotic (sorption, ion exchange, complex formation with metal ions, and polar hydrophilic interactions) (Díaz-Cruz et al., 2003; Michael et al., 2013). While some antibiotics' removal pathway is mainly due to adsorption, others are biodegraded (under aerobic or anaerobic conditions). Thus, the removal of all antibiotics from (waste)water is challenging.

The persistence of antibiotics in WWTPs and waterbodies can lead microbial communities to acquire antibiotic resistance. WWTPs are considered the major point of antibiotic resistance release into the environment (Czekalski et al., 2012; Kümmerer, 2009). The non-resistant bacteria can gain the resistance mechanisms from the antibiotic resistance bacteria (ARB) via an exchange of mobile genetic elements (MGE) like plasmids, integrons, and transposons, that contain antibiotic resistance genes (ARGs) (Blair et al., 2015). The O'Neil report, commissioned by the United Kingdom government, predicts that by 2050, antibiotic resistance infections will lead to 10 million annual deaths, with associated costs above 100 trillion USD (O'Neill, 2014). Furthermore, the World Health Organization established that the multi-resistance gained by bacteria is alarming and threatens global public health (Organization, 2015).

1.1.1 | India's Situation

Out of the four billion people that live under water scarcity, one fourth live in India, and 180 million Indians live under severe water scarcity (Mekonnen & Hoekstra, 2016). Annual per capita fresh-water availability is expected to decrease by 30% when compared to values of 2010, due to the increasing population and country development (Kaur et al., 2012). In 2017, the total renewable water resources per capita in India was at least five times lower than the global average, 1,000 versus 5,700 m³.person⁻¹.year⁻¹, respectively (Singh & Kumar, 2021).

India's population growth rate is around 1.0%, while New Delhi reaches values above 2.9% (India Census 2021). New Delhi has consistently been labelled as one of the most polluted and densely populated cities in the world (Balha et al., 2020; Mazhar et al., 2021). Rapid urbanization is hard to couple with infrastructure progress, especially related to the wastewater network system and treatment. A high percentage of sewage coming from India's capital is directly discharged into the river. Around 60% of New Delhi's untreated sewage, more than 2,500 MLD, is discharged into the Yamuna River, the second largest tributary to the Ganges River (Jassal et al., 2023; Lamba et al., 2020). Furthermore, the Yamuna is considered the most contaminated

1 river in the world (Patel et al., 2020). During monsoon time (around 90 days per year), New Delhi's total precipitation is around 1400 mm while the rest of the year totals only 180 mm (Sontakke et al., 2008). Like in several places around the world, the drains around Delhi are not only used for the discharge of rainwater but also wastewater, and municipal solid waste. The peak of water during monsoon times helps remove the accumulated piles of trash on the drains tributaries to the Yamuna, but increases the pollution downstream. These fluctuating flows and pollutant concentrations are challenging to manage in wastewater treatment plants fed with drain water, and contribute to the pollution of water resources.

Finally, India is one of the top five pharmaceutical manufacturers around the globe, with more than 2,300 MT of antibiotics produced per year and a turnover revenue above 40 billion euros (KPMG, 2006). It is expected that by 2050, around two million deaths in India will occur due to antimicrobial resistance (Dixit et al., 2019). The Isakavagu-Nakkavagu stream in Hyderabad, India, has been reported to have one of the highest antibiotic concentrations in Asia (Fick et al., 2009). The juxtaposition of water scarcity, increase in water demand, fluctuation of water flows and pollutants concentration, and complexity of antibiotics removal, exacerbate India's clean water availability.

1.2 | LOTUS^{HR}

The LOTUS^{HR} project, Local Treatment of Urban Sewage for Healthy Reuse, was launched at the beginning of 2017 and aims to further assess the situation of one of the tributary drains to the Yamuna River at New Delhi, the Barapullah drain. The collaboration between India and the Netherlands was set to investigate the possibility of constructing a resource-oriented wastewater treatment in order to treat the sewage from communities before entering the Barapullah drain, to keep the drain clean for rainwater transport. Treated effluent should be fit for reuse while energy and nutrients are recovered from wastewater. Additionally, the planned wastewater treatment plant should be able to deal with high and low-strength wastewater (corresponding to the dry and rainy seasons), high amounts of particulate matter, and (possibly) some toxic compounds coming from industry and hospital effluents.

The research baseline was set on the assessment of laboratory-scale technologies tested both in India and the Netherlands, that later could be established as pilot-scale technologies at the confluence between Barapullah drain and Yamuna River. Thus, LOTUS^{HR} is divided into three main research lines, each one related to one of the

treatment steps of the drain water. The first research line is about reducing the health risks of water reuse and compromising a microbial and chemical risk assessment of the treated wastewater. The second line corresponds to the sewage preliminary treatment and energy recovery, with (an)aerobic digestion. Finally, the third research line corresponds to the post-treatment and nutrient recovery via urban vital filters or micro-algae technology. The LOTUS^{HR} programme overview can be seen in **Figure 1-1**.

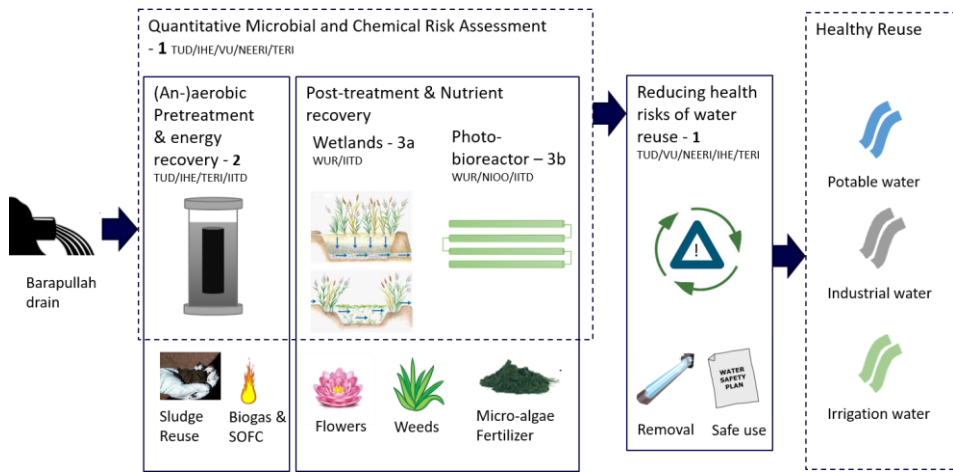


Figure 1-1. LOTUS^{HR} program overview. Source: T. Fernandez. Lotus^{HR} project proposal.

The research described in this document is framed as part of the second investigation line related to the preliminary treatment of high and low-strength wastewaters. As mentioned before, the preliminary treatment of wastewater is mainly done through physical separation or biological degradation. Thus, the next two sections describe the principles of Dissolved Air Flotation as a physical separation technology used for preliminary treatment, and the use of anaerobic digestion and anaerobic membrane bioreactors for biological wastewater treatment.

1.3 | DISSOLVED AIR FLOTATION

Dissolved air flotation (DAF) units are amongst the most commonly used physical units for the pre-treatment of wastewater (Metcalf et al., 2014). The first DAF systems were used in the 1920s and aimed at recovering ores and valuable materials from water suspensions for exploitation in industries (Kiuri, 2001). DAF units have been widely used since the beginning of the 1960s for clarification of drinking water (Edzwald & Haarhoff, 2011).

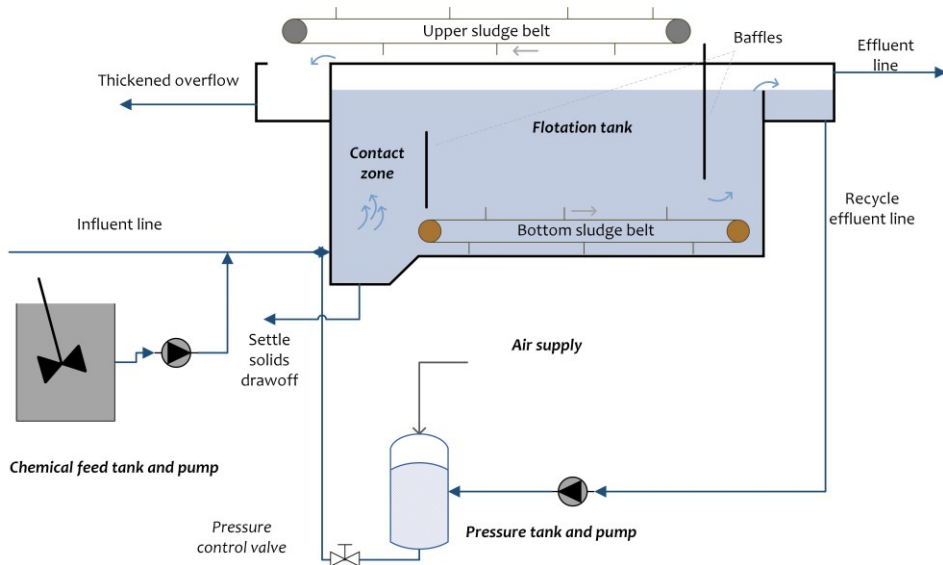


Figure 1-2. Schematic of dissolved air flotation systems with a pressurized recycle flow. Adapted from Metcalf et al. (2014).

A DAF system consists of five main components, which are the air supply, pressure tank and pump, chemical and mix tanks, the contact zone, and the flotation tank, as shown in **Figure 1-2**. DAF units have similar total suspended solids (TSS) removal efficiencies to settler tanks, but they do it in a shorter retention time and higher hydraulic loading rate. TSS removal efficiency is between 60 to 99 %, while retention time can be from 3 to 60 minutes and, hydraulic loading rate between 2.5 to 12.5 $\text{m}^3 \cdot \text{m}^{-2} \cdot \text{h}^{-1}$ (Edzwald, 1995; Kiuru, 1990; Shammass et al., 2010). **Table 1-1** shows typical DAF unit design parameters. The ability to deal with such a diversity of flows and solids makes DAF systems suitable for treating particularly challenging influents (Edzwald & Haarhoff, 2011).

Table 1-1. Typical DAF systems design parameters.

Parameters	Units	Ranges	Reference
Hydraulic Retention Time (HRT)	s	180 - 3600	Wang et al. (2005)
		1200 - 3600	Shammas et al. (2010)
Solids Organic Loading rate (SOLR)	gTSS·m ⁻² ·h ⁻¹	5,000 - 25,000	Metcalf et al. (2014)
Air to solids ratio (A/S)	gAir·gTSS ⁻¹ ·d ⁻¹	0.002 - 0.05	Wang et al. (2005)
Recycle flow	%	5 - 50	Wang et al. (2005)
		6 - 12	Edzwald (2010)
Pressure	10 ⁵ Pa	2 - 6	Wang et al. (2005)
		4 - 6	Edzwald (2010)
Coagulant concentration	g·L ⁻¹	0.5 - 2.0	Haydar and Aziz (2009)
Coagulation time	s	600 - 1800	Wang et al. (2005)

DAF removal efficiency of suspended solids is directly linked with the forming of bubble-particle aggregates (Wang et al., 2005). Flotation and sedimentation of the bubble-particle aggregates depend on the agglomerate density, bubble, and particle characteristics. Bubbles formed in DAF units generally have diameters between 10 to 150 μm and rise as rigid spheres following Stokes law under laminar flow conditions (De Rijk & den Blanken, 1994; Edzwald, 1995). If particles and the agglomerates are considered spheres, then Navier-Stokes can be used to calculate the rising or settling velocity v_r (Benjamin & Lawler, 2013; Jenicek et al., 2010), as shown in the equations below.

$$v_r = \frac{(\rho_w - \rho_{pb})gd_{pb}^2}{18\mu} \quad (1-1)$$

Equation 1-1 shows the rising (or settling) agglomerate velocity represented by Navier-Stokes as v_r , where g is the gravitational constant (9.8 m·s⁻²) and, ρ_w and μ are water density (kg·m⁻³) and viscosity (kg·m⁻¹·s⁻¹) respectively.

$$d_{pb} = \left(\frac{6V_{pb}}{\pi} \right)^{\frac{1}{3}} \quad (1-2)$$

$$\rho_{pb} = \frac{(n\rho_p V_p + \rho_b V_b)}{V_{pb}} \quad (1-3)$$

$$V_{pb} = \frac{\pi(n \times d_p^3 + d_b^3)}{6} \quad (1-4)$$

Where V_{pb} corresponds to the agglomerate volume (m^3), n is the number of particles attached to the bubble, d_p and d_b are the particle and bubble diameters respectively (m). d_{pb} is the agglomerate diameters (m), ρ_p and ρ_b are the particle and bubble densities ($kg \cdot m^{-3}$), and V_p and V_b are the particles and bubble volumes as solid spheres (m^3).

Bubble formation and concentration depend on the pressure set for DAF pressurized water. When air pressure is increased above atmospheric conditions in the saturation vessel, a higher concentration of dissolved air is present in the liquid. Gas concentration in the liquid phase follows Henry's law, depending on the set pressure, temperature and Henry's constant (van 't Hoff, 1884), as shown in equations 1.5 and 1.6.

$$H(T) = H^\theta e^{\left(\frac{-\Delta_{sol}H}{R} \left(\frac{1}{T} - \frac{1}{T^\theta} \right) \right)} \quad (1-5)$$

$$H(T) = \frac{c_a}{p} \quad (1-6)$$

where $H(T)$ corresponds to Henry's constant at temperature T , T^θ refers to the temperature of 298.15 K, T is the temperature in Kelvin, $\Delta_{sol}H$ corresponds to the dissolution enthalpy, R is the gas constant, c_a is the dissolved gas concentration, and p the partial pressure of the gas.

Considering that air contains mainly nitrogen and oxygen, 79 and 21 % respectively, and Henry's constant for these gases, $6.4 \times 10^{-6} \text{ mol} \cdot m^{-3} \cdot Pa^{-1}$ and $1.2 \times 10^{-5} \text{ mol} \cdot m^{-3} \cdot Pa^{-1}$, respectively (Sander, 2015), **Table 1-2** shows the dissolved gas concentrations at different temperatures and pressures, when air is pressurized. Once the pressurized liquid is released under atmospheric conditions, microbubbles are formed in the

liquid, giving it the impression of becoming white. Thus, the name of the pressurized water in the DAF system is also known as white water. The released bubbles are generally below 200 μm and are at least five times smaller than when fine bubble diffusers are used (De Rijk & den Blanken, 1994; Edzwald, 1995).

Table 1-2. Nitrogen and oxygen concentrations in water were calculated based on an air composition of 21% oxygen and 79%, and Henry's constants (Sander, 2015). Values are expressed in $\text{mg}\cdot\text{L}^{-1}$, under different pressures and temperatures. Nitrogen concentrations are seen in bold.

Temperature °C	Pressure (Pa)			
	1×10^5	4×10^5	5×10^5	6×10^5
35	11.9 / 6.8	47.6 / 27.4	59.5 / 34.2	71.4 / 41.1
29	13.2 / 7.5	52.7 / 30.2	65.9 / 37.7	79.1 / 45.3
25	14.2 / 8.1	56.6 / 32.3	70.8 / 40.3	84.9 / 48.4
20	15.5 / 8.8	62.1 / 35.1	77.6 / 43.9	93.1 / 52.7
15	17.1 / 9.6	68.2 / 38.4	85.3 / 48.0	102.3 / 57.6
10	18.8 / 10.5	75.3 / 42.1	94.1 / 52.6	112.9 / 63.2

There are two possible models to describe particle and bubble attachment, the flocculation and the filtration models (Benjamin & Lawler, 2013). Both models assume that particles are only able to attach to bubbles (not to each other) but differ in the particle-over-bubble diameter ratio. The flocculation model was developed by Tambo, Fukushi and Matsui (Fukushi et al., 1995, 1998; Matsui et al., 1998; Tambo & Fukushi, 1986). They assumed that the collision between bubbles and particles is only due to the turbulent fluid and that the particle-bubble agglomerate corresponds to a large particle attached to several smaller bubbles.

On the other hand, the filtration model developed by Edzwald and several co-workers (Edzwald, 1995; Fuller et al., 2010; Malley & Edzwald, 1991) assumes that one large bubble is attached to several smaller particles. This model is also known as the single spherical collector, where particle-bubble collisions can occur due to Brownian diffusion (η_{BD}), particle and bubble interception (η_I), and sedimentation of particles (η_S). Collision due to inertia (η_{IN}) can be neglected when compared to the other collision factors for bubbles and flocs diameters below 100 μm (Edzwald & Haarhoff,

2011). Small particles, below $10\ \mu\text{m}$, are mainly governed by Brownian diffusion (random movement), as shown in **Figure 1-3**.

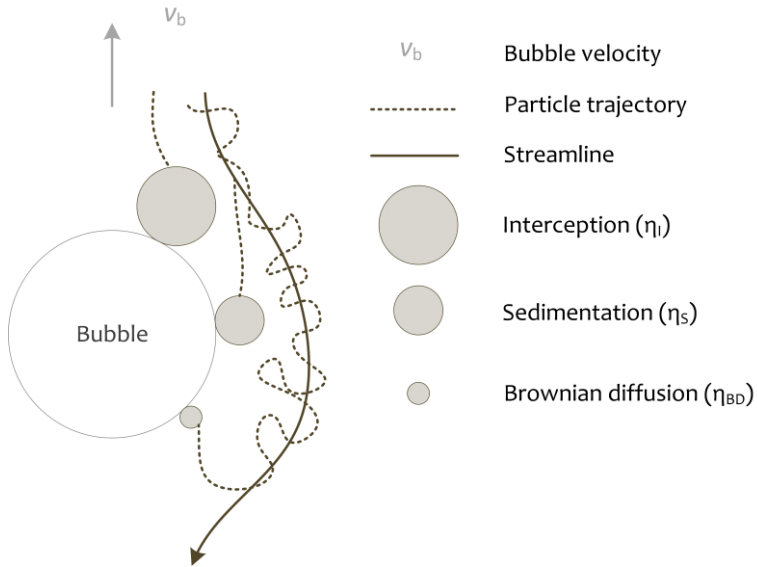


Figure 1-3. Single collector collision scheme, between a bubble and a particle. Adapted from Edzwald (2010).

Currently, DAF systems have been particularly useful in the pre-treatment of anaerobic digestion to remove suspended solids, with TSS removal efficiencies that vary between 75 to 98% (Cagnetta et al., 2019; Harris et al., 2017; Manjunath et al., 2000; McCabe et al., 2014; Penetra et al., 2003). Few articles have demonstrated the successful implementation of DAF units in wastewater reuse schemes. The reuse of fruit and vegetable processing wastewater and poultry slaughterhouse wastewater was achieved using a DAF system followed by Ultra Violet (UV) disinfection (De Nardi et al., 2011; Mundi & Zytner, 2015). Although the literature shows DAF systems have the potential to enable water reuse, particularly in combination with anaerobic digestion, the most typical applications still only consider DAF for conventional solid-liquid separation.

1.4 | ANAEROBIC DIGESTION

Anaerobic Digestion (AD) is a widely used process for wastewater pre-treatment. The first uses of anaerobic digestion date back to the 10th century B.C., where Assyrians used biogas produced under anaerobic degradation of faecal matter for heating bath water (Lusk, 1998). Since the 1970s, anaerobic treatment and specifically up-flow

anaerobic sludge blanket and anaerobic membrane bioreactors (AnMBR) are strongly established for wastewater treatment, due to several advantages in comparison with aerobic treatment. The most important advantages are the reduction of up to 90% of sludge production, a decrease of the needed footprint, a reduction of overall energy consumption, the production of energy as biogas, the possibility of dealing with high organic loading rates, the low usage of chemicals, and the nutrient-rich effluent for irrigation reuse (van Lier et al., 2008b). Anaerobic microorganisms and specifically methanogens grow relatively slowly in comparison with aerobic ones, making biomass retention key to providing enough solids retention time (SRT) for the methanogens (Liao et al., 2006).

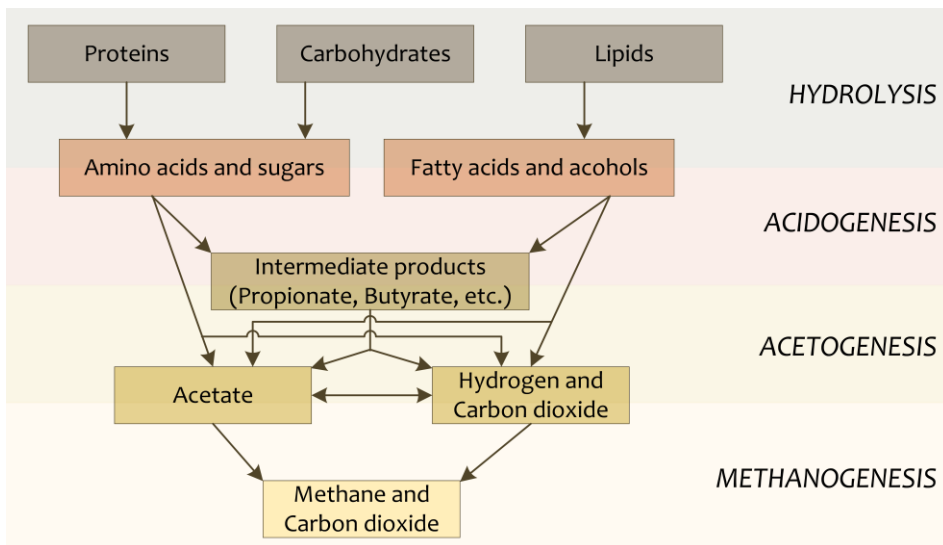


Figure 1-4. Anaerobic digestion scheme phases. Adapted from van Lier et al. (2008a)

AD has four main phases as shown in **Figure 1-4**; hydrolysis, acidogenesis, acetogenesis, and methanogenesis. Typically, either hydrolysis or methanogenesis determines the overall conversion rates (van Lier et al., 2008b). During hydrolysis, enzymes solubilise undissolved matter (lipids, proteins, and carbohydrates) into dissolved and less complex ones, which can then pass through the cell membranes. This process is the slowest and can be the bottleneck of anaerobic digestion, especially when treating wastewater with a high particulate matter content (Visvanathan & Abeynayaka, 2012). In the last step of AD, methanogenic archaea convert the compounds from acetogenesis (mainly acetate), into methane, carbon

1
dioxide and new cell material. Both steps (hydrolysis and methanogenesis) are affected by wastewater characteristics, like toxicity, nutrient content, and nature of the organics, among others, and reactor operation conditions such as pH, temperature, and organic loading rate.

The presence of complex organic matter in wastewater, hinders the hydrolysis phase of AD, leading to lower biogas yields, larger needed surface area and longer retention times (Nguyen et al., 2021). Thus, several researchers are focusing on the improvement of hydrolysis. In waste-activated sludge (WAS), numerous pre-treatment methods have been tested to improve sludge degradation under AD. Thermal, microwave, chemical and biological are amongst the most common WAS pre-treatments for hydrolysis improvement (Gonzalez et al., 2018).

Methanogens are known for being strict anaerobes (van Lier, 2008). However, various authors suggest that micro-aeration in anaerobic digesters can be advantageous for specific (bio)chemical conversion processes while having negligible impacts on the methanogenic biomass (Botheju & Bakke, 2011; Giroto et al., 2018; Sasidhar et al., 2022). The injection of small amounts of air in the AD sludge promotes the hydrolytic activity of both facultative and anaerobic bacteria, accelerating the hydrolysis of complex organic matter (Lim & Wang, 2013). Furthermore, aeration of the headspace of an AD reactor has proven to reduce concentrations of hydrogen sulphide in the biogas, improving the overall biogas quality (Kraakman et al., 2023).

1.4.1 | Anaerobic Membrane Bioreactors

AnMBR units were first developed in the late 1980s for industrial wastewater treatment (Li, 1985). From the AD technologies, AnMBR is a promising system to treat municipal wastewater from a resource-oriented perspective, leaving a solids-free effluent and removal of COD of above 90% (Robles et al., 2020). The membrane unit allows the decoupling of the hydraulic retention time (HRT) and solids retention time (SRT), promoting the growth of slow-growing micro-organisms and increasing degradation (Liao et al., 2006).

The principle of an AnMBR is a mixed anaerobic bioreactor connected to a physical membrane separation unit that is permselective, allowing some constituents to pass through the membrane material (Judd et al., 2008). There are four key membrane separation processes: micro-filtration (MF), ultra-filtration (UF), nano-filtration (NF) and reverse-osmosis (RO), determined by the average membrane pore size. Most commonly used AnMBR systems have an average pore size between 0.01 and 0.1 μm

and therefore, are in the UF and MF range (Lin et al., 2013). Macronutrients like ammonium and orthophosphate are not removed under UF anaerobic digestion. Domestic wastewater streams contain many different bacteria, viruses, protozoa, and helminth pathogens. Due to their sizes, not all the above-mentioned pathogens can be removed with UF membranes, as shown in **Figure 1-5**. Nevertheless, most of the UF effluent, known as permeate, is potentially suitable for agricultural uses (Ellouze et al., 2009).

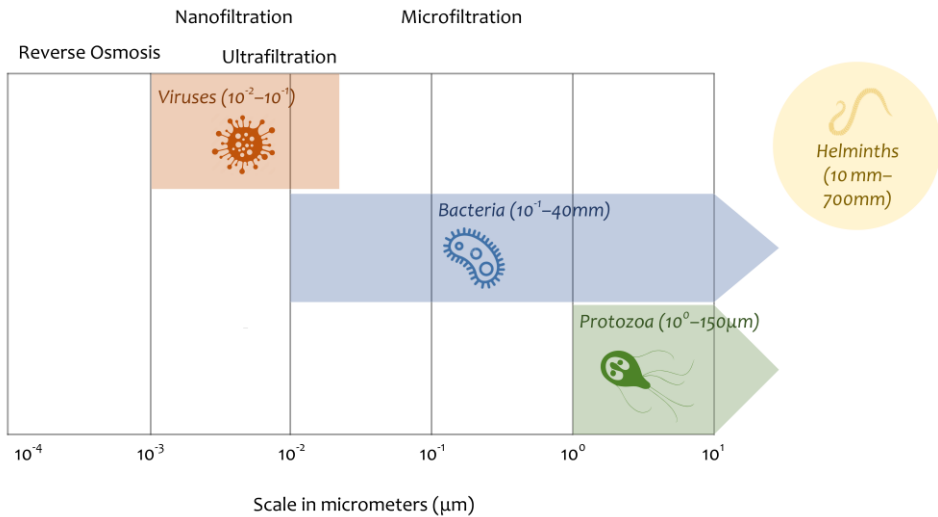


Figure 1-5. Membrane separation overview and water-borne pathogens. Based on Bridle (2020) and Judd et al. (2008)

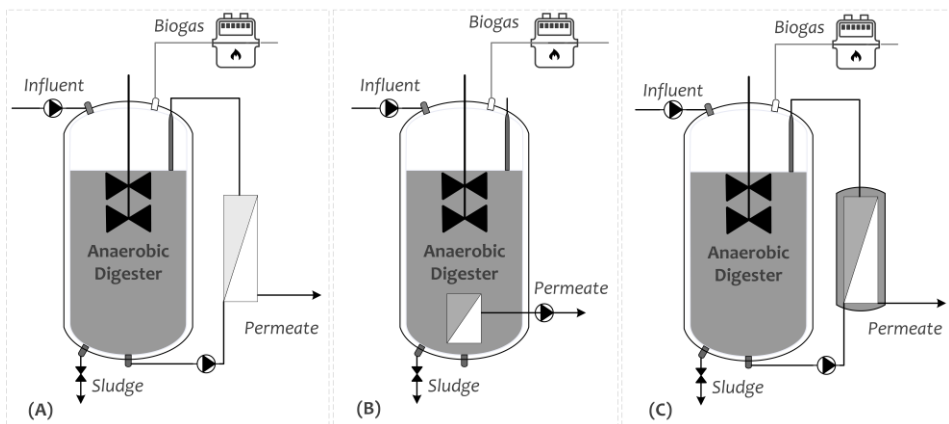


Figure 1-6. AnMBR process configuration when coupled with a CSTR tank. (A) External cross-flow. (B) Internal submerged. (C) External submerged.

The filtration unit of an AnMBR can have three different configurations, external cross-flow, internal submerged, and external submerged (Liao et al., 2006). Continuously stirred tank reactors (CSTR) are the most common combination with the membrane unit (Smith et al., 2012), as shown in **Figure 1-6**. Aside from the influent characteristics, the main AnMBR operational parameters affecting its performance are temperature, HRT, SRT and OLR (Stuckey, 2012). **Table 1-3** shows the most common operational parameters and their operational ranges for municipal wastewater treatment.

Table 1-3. AnMBR design parameters and operational ranges for municipal wastewater.

Operational parameter	Units	Ranges	Reference
Hydraulic Retention Time (HRT)	h	8 - 24	Stuckey (2012)
Solids retention time (SRT)	d	20 - 140	Ozgun, Dereli, et al. (2013)
		25 - 335	Stuckey (2012)
Temperature	°C	30 - 40*	Ozgun, Dereli, et al. (2013),
			Stuckey (2012)
Organic loading rate (OLR)	kgCOD·m ⁻³ ·d ⁻¹	0.3 - 12.5	Kanafin et al. (2021)
		1 - 15	Stuckey (2012)

*Temperature range for mesophilic conditions

1.5 | ANAEROBIC DIGESTION COMBINED WITH DISSOLVED AIR FLOTATION: AD-DAF SYSTEM

While AnMBR systems are a promising AD technology to treat municipal and concentrated wastewater, the application of membranes to separate solids from the bioreactor broth also has considerable constraints. These constraints are linked to membrane fouling, permeate flux limitations, and high operation and maintenance costs (Ozgun, Dereli, et al., 2013). Moreover, fluctuations in the influent OLR and hydraulic flow may negatively impact the sludge filterability and the membrane filtration capacity, decreasing the permeate flux (Dereli et al., 2012). Thus, an alternative physical separation method could be used to overcome the AnMBR limitations.

Replacing the membrane unit of an AnMBR with a DAF system, creating an AD-DAF system, and returning the flotation layer to the anaerobic reactor, may ensure high TSS retention while overcoming several main AnMBR limitations. However, the oxygen-saturated flotation layer and the overall introduction of oxygen into the reactor due to the DAF may negatively impact the anaerobic conversion process. Thus, further research needs to be carried out to assess the possibility of replacing the membrane of an AnMBR system with a DAF unit, creating an AD-DAF system. A scheme of the AD-DAF technology is shown in **Figure 1-7**.

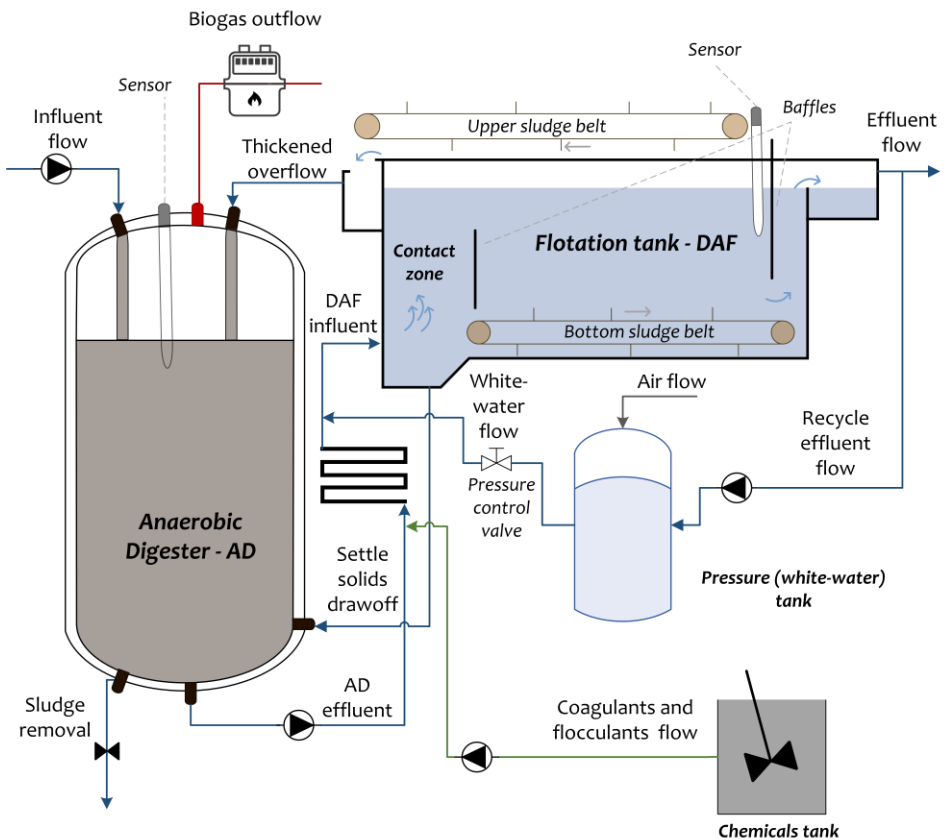


Figure 1-7. AD-DAF system scheme.

Furthermore, whilst recent research investigated the effect of aeration in AD, there is little understanding of how exactly aeration affects AD when simulating the coupling of an AD-DAF system. Moreover, to consider the large-scale applications of an AD-DAF system implemented for the treatment and reuse of storm-, drain- and wastewater, like what is conceived in the LOTUS^{HR} project at the Barapullah drain, it

is key to assess the removal of organic matter, suspended solids, nutrients, and micro-pollutants like antibiotics.

When a new wastewater treatment system is introduced, like the AD-DAF, the process is often firstly tested on laboratory-scale, and then further scaled up to pilot and full-scale (De Kreuk, 2006). The most common use of laboratory-scale DAF units is to empirically assess flow conditions, bubble formation, and bubble size, either by computational fluid dynamics (CFD) or other modelling tools (De Rijk & den Blanken, 1994; Han & Dockko, 1998; Han et al., 2002; Mudde & Simonin, 1999; Samstag et al., 2016; Yang et al., 2021). However, the systematic assessment of DAF process control variables on particle removal on a laboratory-scale is still missing. This difficulty arises due to the inherent challenge of accurately replicating the physical and hydraulic phenomena of full-scale applications on a down-scaled DAF system. This is primarily attributed to the inability to downscale microbubbles, which are a critical component of the process.

To mimic the rising bubble conditions on a laboratory-scale, avoiding the reactor wall causing changes in the hydrodynamic behaviour of the reactor medium, as described by Edzwald (1995), a DAF system should have at least 0.20 m in diameter and a height of 1.00 m, with the bubble injection in the centre. When using a cylinder shape, the dimensions above mentioned represent a total volume of 31.4 L. Furthermore, considering the average DAF HRT (**Table 1-1**), influent flows to the laboratory-scale DAF should be between 750 to 2,200 L·d⁻¹, and are therefore not suited for continuous operation with real or synthetic drainage and wastewater in a laboratory setting (Edzwald & Haarhoff, 2011). Thus, it is considered not practical to assess a continuous AD-DAF system on a laboratory-scale.

1.6 | DISSERTATION OBJECTIVES AND OUTLINE

This dissertation investigates the potential to use an AD coupled with a DAF system (AD-DAF) as a pre-treatment technology, specifically for the treatment of drain- and wastewater that mimics the ever-changing conditions of the Barapullah drain in New Delhi. While testing an AD-DAF system on a laboratory-scale is not possible, the implications of coupling these two technologies can be assessed in a laboratory but having two different systems. Thus, the investigation here presented comprehends two main objectives. Firstly, to assess the removal of suspended solids using a laboratory-scale DAF system, under different influent conditions that mimic the fluctuations of the Barapullah drain. Secondly, to evaluate the performance of an aerated AnMBR simulating the oxygen supply in an anaerobic digester-dissolved air

flotation system, bearing in mind the reuse possibilities of the treated effluent. The above-mentioned objectives derived into the research project structure shown in **Figure 1-8** and detailed below.

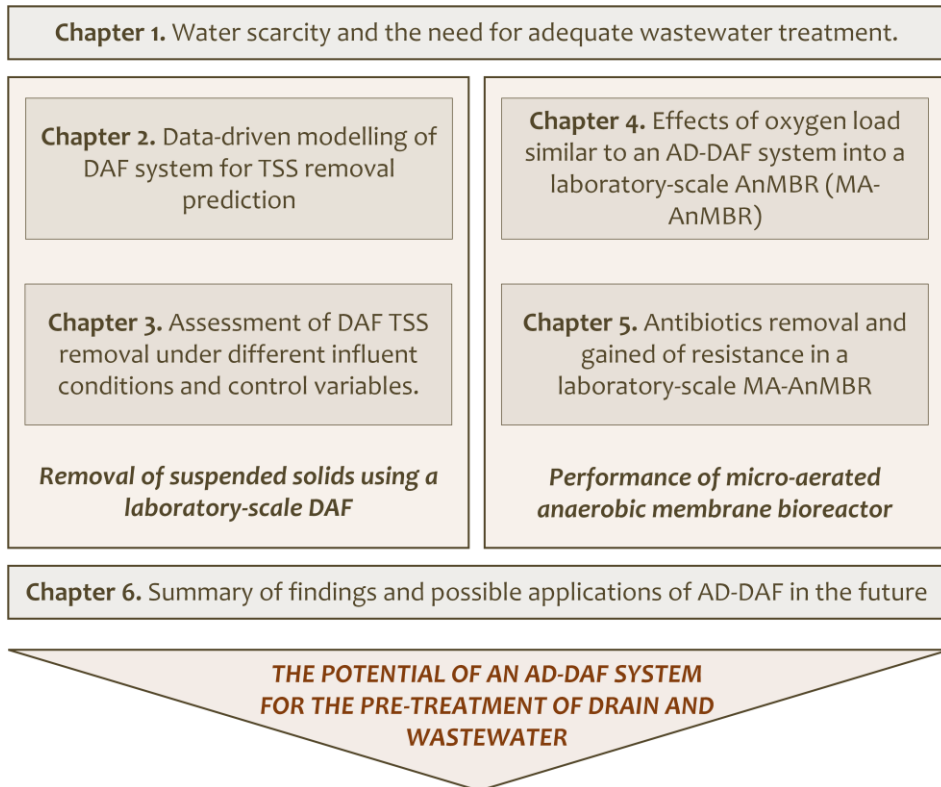


Figure 1-8. Scheme of dissertation outline and research project structure.

To begin with, based on the Filtration model developed by Edzwald (1995), a data-driven DAF model is developed in **Chapter 2**. This model is based on influent particle characteristics and bubble sizes. For the latter, bubble sizes are derived from their respective velocities, using particle image velocimetry (PIV) software for MATLAB, and a cell phone camera to record the videos. For the assessment of particle characteristics, particle sizes are analysed based on microscope images and the use of ImageJ-FIGI free software, which enables to create a particle size distribution profile. Finally, the model is tested in two full-scale DAF and a laboratory-scale unit.

Chapter 3 presents a laboratory-scale column DAF system designed and used to investigate the removal of suspended solids under four different influent conditions and seven DAF independent control variables (influent TSS, pH, temperature, DAF

1 particles residence time, white water pressure, coagulants and flocculants concentration and mixing time). The influents simulated the Barapullah drain conditions under 1) dry and 2) monsoon times, and 3) close or 4) far from the pollution source¹. The effect and statistical relevance of the different performance variables on the measured separation efficiencies were measured using a total of 60 batch DAF experimental runs.

After assessing the feasibility of using a DAF system to remove the suspended solids from drain- and wastewater, the effects of the AD-DAF system are investigated on a laboratory-scale, in **Chapter 4**. The tested system is an AnMBR treating synthetic concentrated domestic wastewater, subjected to an oxygen load similar to the one used on a DAF unit which aimed to replace the membrane filtration unit, making the system a micro-aerated AnMBR (MA-AnMBR). The effects of oxygen are compared to a fully anaerobic system, and the MA-AnMBR performance is assessed, for removal of organic matter, biogas production, nutrient concentration, and operation and maintenance. Furthermore, this chapter describes the effect of different oxygen loads in the influent degradation and sludge activity on batch tests. Finally, the enzymatic activity of superoxide dismutase (SOD) of the biomass, and microbial community shifts are monitored during the anaerobic and micro-aeration periods.

Chapter 5 builds upon knowledge gained in the previous chapter and investigates the performance of the Ma-AnMBR when two antibiotics are added to the system feed, sulfamethoxazole (SMX) and trimethoprim (TMP). The effect, removal, and gain of microbial resistance due to the addition of $150 \mu\text{g}\cdot\text{L}^{-1}$ of these two antibiotics are examined in detail. Both antibiotics have different preferable removal pathways (adsorption or biodegradation) and are mainly removed under anaerobic conditions. Thus, the consequences of the added aeration to the MA-AnMBR are also studied based on the antibiotic's removal. The ability of the system to remove antibiotic-resistant bacteria (ARB) and antibiotic-resistant genes (ARG) linked to SMX and TMP is assessed bearing in mind the reuse possibilities of the treated wastewater.

¹ At household level (close to the pollution source), or at the Barapullah' s mouth (28.58397, 77.27824).

Finally, **Chapter 6** gives a summary of the main findings of this investigation and discusses and evaluates them thoroughly. This chapter also highlights the possible applications of an AD-DAF technology, based on the results obtained on laboratory-scale, and gives recommendations for future research and applications linked to the development of this technology.



Concentrated suspended solids layer on the lab-scale DAF.

2

Modelling of Dissolved Air Flotation (DAF). Application of an experimental filtration model for suspended solids removal prediction

This chapter is an adapted version of Piaggio, A. L., Smith, G. de Kreuk, M. K., & Lindeboom, R. E. F. (*Under Review*). Modelling of Dissolved Air Flotation (DAF). Application of an experimental filtration model for suspended solids removal prediction. *Submitted to Separation and Purification Technology*.

ABSTRACT

Particle-bubble collisions in dissolved air flotation (DAF) systems play a crucial role in the removal of total suspended solids (TSS). The filtration model incorporates factors such as particle diameters, charge and density, bubble diameters, and collision factors. The challenge lies in accounting for the wide range of particle and bubble sizes and obtaining complex model inputs. To address this, an experimental model, for TSS removal in DAF units, based on the filtration model was established using low-cost laboratory measurements, including particle size distribution and density. Additionally, microbubble diameter profiles were derived from bubble velocities using particle image velocimetry software (PIV). Six independent variables, encompassing influent particle characteristics (such as particle size distribution and density) and DAF running characteristics (temperature, contact zone detention time, inflow and recycle flows), were employed in the experimental model. The model's accuracy was evaluated using a laboratory-scale DAF system with two different influents: Delft canal water and anaerobic sludge. The predicted TSS removal from the experimental model aligned well with the laboratory-scale DAF results, yielding removal efficiencies of $68 \pm 1\%$ and $77 \pm 3\%$ for Delft canal water and anaerobic sludge, respectively. Furthermore, when the experimental model was applied to two full-scale DAF systems, it successfully identified an underperforming system (DAF2) with a TSS removal efficiency of 91%, contrasting the theoretical filtration model-predicted efficiency of 98%. This study highlights the utility of combining bubble size distribution measured by PIVlab and particle size distribution obtained using FIJI-ImageJ as an economical and efficient approach to acquiring the necessary inputs for predicting TSS removal in DAF systems.

2.1 | INTRODUCTION

Dissolved air flotation (DAF) units have been widely used since the beginning of the 1960s for separating liquid and particle matter by flotation. The first DAF systems were used in the 1920s and aimed at recovering ores and valuable materials from water suspensions for exploitation in industries (Kiuri, 2001). Before the 1970s the Scandinavian countries were using DAF units for drinking water treatment, while some African countries were testing them for wastewater reclamation by algae removal on maturation ponds (Haarhoff, 2008). DAF units are capable to get similar solids removal efficiencies as in settler tanks, but they do it in a shorter retention time and higher hydraulic loading rate. Suspended solids removal efficiency is between 60 to 99 %, while retention time can be from 3 to 60 minutes and, hydraulic loading rate between 2.5 to 12.5 m³·m⁻²·h⁻¹ (Edzwald, 1995; Kiuru, 1990; Shamma et al., 2010). Furthermore, the influent suspended solids rate might vary from 5.0 to 25.0 kg·m⁻²·h⁻¹ (Benjamin & Lawler, 2013). The ability to deal with such a diversity of flows and solids content makes DAF systems suitable for treating particularly challenging streams, especially those with high variation in their flows and characteristics (Edzwald & Haarhoff, 2011).

DAF removal efficiency of suspended solids is directly linked with the forming of bubble-particle aggregates (Wang et al., 2005). Flotation and sedimentation of the bubble-particle aggregates depend on the agglomerate density, bubble, and particle characteristics. When the agglomerate density is lower than the water one, it will raise to the surface, but if it is higher it will settle (Benjamin & Lawler, 2013). Most bubbles formed in DAF have diameters below 100 μm and rise as rigid spheres following Stokes law under laminar flow conditions (Edzwald, 1995). If particles and the agglomerates are considered spheres, then Navier-Stokes can be used to calculate the rising or settling velocity v_r (Benjamin & Lawler, 2013; Jenicek et al., 2010), when one or more particles collide with one bubble, as shown in the equations below.

$$V_{pb} = \frac{\pi(n \times d_p^3 + d_b^3)}{6} \quad (2-1)$$

where V_{pb} corresponds to the agglomerate volume (m³), n is the number of particles attached to the bubble, d_p and d_b are the particle and bubble diameters respectively (m).

$$d_{pb} = \left(\frac{6V_{pb}}{\pi} \right)^{\frac{1}{3}} \quad (2-2)$$

$$\rho_{pb} = \frac{(n\rho_p V_p + \rho_b V_b)}{V_{pb}} \quad (2-3)$$

where d_{pb} is the agglomerate diameters (m), ρ_p and ρ_b are the particle and bubble densities ($\text{kg}\cdot\text{m}^{-3}$), and V_p and V_b are the particles and bubble volumes as solid spheres (m^3).

$$v_r = \frac{(\rho_w - \rho_{pb})gd_{pb}^2}{18\mu} \quad (2-4)$$

equation 2-4 shows the rising (or settling) agglomerate velocity represented by Navier-Stokes as v_r , where g is the gravitational constant ($9.8 \text{ m}\cdot\text{s}^{-2}$) and, ρ_w and μ are water density ($\text{kg}\cdot\text{m}^{-3}$) and viscosity ($\text{kg}\cdot\text{m}^{-1}\cdot\text{s}^{-1}$), respectively.

Table 2-1. Henry's law constants for water as a solvent for relevant gases. Adapted from Sander (2015)

	Henry's constant ($\text{mol}\cdot\text{m}^{-3}\cdot\text{Pa}^{-1}$)	$\Delta_{\text{sol}}H/R$ (K)
Nitrogen	6.40E-06	1600
Oxygen	1.20E-05	1500
Carbon Dioxide	3.30E-04	2400
Methane	1.40E-05	1600

Aside from density, the formation of the particle-bubble agglomerate also depends on the air bubbles' characteristics, like concentration and size. Bubble formation and concentration depend on the pressure set for DAF pressurized water. When air pressure is increased above atmospheric conditions in the saturation vessel, a higher concentration of dissolved air, mainly composed of nitrogen and oxygen is present in the liquid. Gas concentration in the liquid phase follows Henry's law, depending on the set pressure, temperature and Henry's constant (van 't Hoff, 1884) (equations 2-5 and 2-6). **Table 2-1** shows Henry's constant for relevant gases.

$$H(T) = H^\theta e^{\left(\frac{-\Delta_{sol}H}{R}\left(\frac{1}{T} - \frac{1}{T^\theta}\right)\right)} \quad (2-5)$$

$$H(T) = \frac{c_a}{p} \quad (2-6)$$

where $H(T)$ corresponds to Henry's constant at temperature T , T^θ refers to the temperature of 298.15K, T is the temperature in Kelvin, $\Delta_{sol}H$ corresponds to the dissolution enthalpy, R is the gas constant, c_a is the dissolved gas concentration, and p the partial pressure of the gas.

Once the air-pressurized liquid is released under atmospheric conditions, microbubbles are formed. These vary in diameter from 10 to 150 μm and are at least five times smaller than when fine bubble diffusers are used (De Rijk & den Blanken, 1994; Edzwald, 1995). The total amount of bubbles formed once the pressurized water is released under atmospheric conditions, also known as white water, depends on the bubble diameter. When air is used as a pressurizing gas, average microbubble diameters decrease with an increase in pressure, from 70 to 30 μm at 2 and 5×10^5 Pa respectively (Han et al., 2002). Nevertheless, when water is pressurized using CO_2 , average microbubble diameters increase when pressure rises, from 100 to 200 μm at 2 and 3×10^5 Pa respectively (Kwak & Kim, 2013). For a given dissolved gas concentration, the total amount of released microbubbles will increase if the bubble diameter decrease (De Rijk & den Blanken, 1994). A high quantity of microbubbles (at least 10^6 per mL) ensures sufficient surface area available to collide with particles (Rodrigues & Rubio, 2007).

Besides bubble characteristics, other factors also have an important effect on DAF performance. Particles' nature and size, solids loading rate, air-to-solids ratio (A/S), hydraulic retention time, and use of polymers and coagulants are among the most important factors to be considered (Wang et al., 2005). According to Van Nieuwenhuijzen (2002), most wastewater-suspended solids have a negatively charged surface. Similarly, air bubbles have a negative zeta potential and surface charge under a wide pH variation (M. Han & S. Dockko, 1998). Coagulants are used to neutralize particle surface charge, enhancing the collision between particles and bubbles. After adequate coagulation is achieved, flocculants are added to the agglomerates to neutralise particles and bubbles, creating bigger agglomerates. Thus, coagulation and flocculation are key to promoting particle-bubble collision agglomeration, and therefore, particle removal by flotation (Bratby, 1980).

The highest suspended solids removal efficiency in a DAF system can be expected when particles and bubbles are similar in diameter size, and both have a surface zeta

potential near zero (Han et al., 2001). Furthermore, the DAF unit should provide enough contact time to promote particle-bubble collision and agglomerate flotation. Therefore, the hydraulic retention time (HRT) and solids organic loading rate (SOLR) are fundamental to enhancing suspended solids removal. A summary of DAF units' design parameters is shown in **Table 2-2**.

Table 2-2. Typical DAF unit design parameters.

Parameters	Units	Ranges	Reference
Hydraulic Retention Time (HRT)	s	180 – 3600	Wang et al. (2005)
		1200 – 3600	Shammas et al. (2010)
Solids Organic Loading rate (SOLR)	gTSS·m ⁻² ·h ⁻¹	5,000 25,000	– Metcalf et al. (2014)
Air to solids ratio (A/S)	gAir·gTSS ⁻¹ ·d ⁻¹	0.002 - 0.05	Wang et al. (2005)
Recycle flow	%	5 – 50	Wang et al. (2005)
		6 – 12	Edzwald (2010)
Pressure	10 ⁵ Pa	2 – 6	Wang et al. (2005)
		4 – 6	Edzwald (2010)
Coagulant concentration	mg·L ⁻¹	500 – 2000	Haydar and Aziz (2009)
Coagulation time	s	600 – 1800	Wang et al. (2005)

The majority of laboratory-scale DAF units can be considered bench-scale, and involve jar tests (Edzwald & Haarhoff, 2011). Whilst jar tests are optimal for the assessment of adequate coagulation and flocculation concentrations depending on the treated wastewater, they cannot replicate the bubble-particle collision. Thus, pilot-scale DAF units are recommended for further testing. Reported DAF units need large influent flows (between 5 to 100 m³·h⁻¹), making it impossible to perform laboratory experiments with real wastewater (Edzwald & Haarhoff, 2011). Some authors have used laboratory-scale DAF units to empirically assess flow conditions, bubble formation, and bubble size (De Rijk & den Blanken, 1994; Han & Dockko, 1998; Han et al., 2002; Mudde & Simonin, 1999; Samstag et al., 2016).

Most recent literature on DAF is linked to the utilization of computational fluid dynamics (CFD) that is based on the Navier-Stokes equations, in order to enhance understanding of the separation and contact zones (Yang et al., 2021). The utilization of a mathematical model like CFD is key to understand the flux behaviour inside DAF units, but the multiphase assessment between liquid, particles and bubbles remains challenging (Wang et al., 2018). Verma and Padding (2020) developed a computational fluid dynamic – continuum particle model focused on gas-solids fluidized beds, comparable to what fundamentally occurs in DAF systems. While this model has a lower computational time when compared to other used models, it can still be considered complex, and it might introduce errors especially when assessing the collision between bubbles and particles around the system walls. Recent studies on DAF have also focused on the use of particle image velocimetry (PIV) as a tool to map the liquid velocity profile (Fanaie et al., 2019) and bubbles velocity profiles (Fanaie & Khiadani, 2020). The application of PIV has been mostly performed using high-speed cameras, to study bubbles and particle dynamics (Lindeboom et al., 2011). However, PIV has not been used to assess the bubbles diameter profile, and the possible interactions between liquid, bubbles, and particles.

Particle-bubble collision in the DAF contact zone has been modelled by Tambo and Fukushi (1986), Edzwald (1995), and Han (2002). The equations are based on particle diameters, charge and density, and bubble diameters. The complexity of applying these models lies in the fact that both particles and bubbles are present in a wide variety of sizes (Rodrigues & Rubio, 2007). To the authors' knowledge, no scientific studies have been conducted on an experimental version of the above-mentioned model, where low-cost laboratory measurements, such as particle size distribution and density, can be applied to achieve an initial approximation of suspended solids removal using a DAF unit. Furthermore, the authors' have not found further investigation on the coupling of these bubble-particle collision models with laboratory-scale DAF units. This coupling might lead to a better understanding and assessment of the removal potential of DAF systems for different influents.

2.2 | MATERIALS & METHODS

2.2.1 | Particle-bubble experimental collision model.

The filtration model developed by Edzwald and co-workers (Edzwald, 1995) was applied to calculate the expected suspended solids removal efficiency in the contact zone, using average bubble sizes and particle size distribution. This model, also known as the white-water bubble blanket model, considers the single-factor collision

approach, where one bubble collides with a particle or floc. It can be used when particle diameters are smaller than the average microbubble diameter (Edzwald, 2010). Average bubble sizes for pressures between 3 to 5 × 10⁵ Pa are expected to be below 65 μm (Han et al., 2002). While wastewater-suspended particles might vary in size, above 60% of the total amount of particles in wastewater are below 100 μm and therefore, more prone to float than to settle (Van Nieuwenhuijzen, 2002).

The single-factor collector efficiency equations are derived from Brownian diffusion and particle transport mechanisms. When microbubbles have diameters below 120 μm, they follow Stokes flow conditions (laminar flow). The model starts with the second-order rate kinetics to describe the rate at which particles change due to their impact with bubbles. From there, Equations (2-7) to (2-10) describe the total collision efficiency (η_T) and its components contributing to efficiency: Brownian diffusion (η_{BD}), interception (η_I), settling (η_S) and Equation (2-11) shows the total removal efficiency (E_{CZ}) from the DAF contact zone. Collision due to inertia (η_{IN}) can be neglected when compared to the other collision factors when bubbles and flocs diameters are below 100 μm (Edzwald & Haarhoff, 2011). Furthermore, the model assumes that both particles and bubbles can be considered spheres.

$$\eta_T = \eta_{BD} + \eta_I + \eta_S \quad (2-7)$$

$$\eta_{BD} = 6.18 \left[\frac{k_b T}{g(\rho_w - \rho_b)} \right]^{2/3} \left[\frac{1}{d_p} \right]^{2/3} \left[\frac{1}{d_b} \right]^2 \quad (2-8)$$

$$\eta_I = \left(\frac{d_p}{d_b} + 1 \right)^2 - \frac{3}{2} \left(\frac{d_p}{d_b} + 1 \right) + \frac{1}{2} \left(\frac{d_p}{d_b} + 1 \right) \quad (2-9)$$

$$\eta_S = \left[\frac{(\rho_p - \rho_w)}{(\rho_w - \rho_b)} \right] \left[\frac{d_p}{d_b} \right]^2 \quad (2-10)$$

where k_b is Boltzmann's constant ($1.4 \times 10^{-23} \text{J}\cdot\text{K}^{-1}$), T is the absolute temperature in kelvin, g is the gravitational constant ($9.8 \text{ m}\cdot\text{s}^{-2}$), ρ_p , ρ_b , and ρ_w are the particle-floc, air bubble and water density ($\text{kg}\cdot\text{m}^{-3}$) respectively, d_p and d_b are the particle and bubble diameter (m).

$$E_{CZ} = \left[1 - \exp \left(- \frac{3/2(\alpha_{pb}\eta_T v_b \Phi_b t_{CZ})}{d_b} \right) \right] \quad (2-11)$$

where α_{bp} is the collision efficiency factor for bubbles and particles, v_b is the air bubble velocity ($\text{m}\cdot\text{s}^{-1}$), Φ_b is the volume fraction of air in water, and t_{cz} is the DAF contact zone detention time (s).

Collision efficiency factors for bubbles and particles α_{bp} , vary between zero to one, were taken from Han (Han, 2002; Han et al., 2001) and were based on bubble average size and assumed particle zeta potential close to zero (due to the addition of coagulants and flocculants). The methods used to calculate average bubble size and particle size distribution are explained below (Bubble size and, Particle size). Furthermore, values of bubble velocity (v_b) were calculated based on the Navier-Stokes equation for rigid spheres (Constantin & Foias, 2020). The volume fraction of air in water (Φ_b) depends on the dissolved air concentration and therefore, on the applied pressure and temperature conditions, and the recycle flow (Equation (2-12)). A working pressure of 5×10^5 Pa was selected for the experimental model. Gas density and concentration were calculated based on the input temperature, Henry's constants for nitrogen and oxygen dissolution, air composition of 21% oxygen and 79% nitrogen, and assuming a 90% efficiency of air dissolution (Wang et al., 2005).

$$\Phi_b = \left(\Phi_{bQr} \frac{Q_r}{Q_r + Q_{in}} \right) \quad (2-12)$$

Where Φ_b is the volume fraction of air in water ($L_{\text{air}} \cdot L_{\text{water}}^{-1}$), Φ_{bQr} is the volume fraction of air in water in the recycle flow ($L_{\text{air}} \cdot L_{\text{water}}^{-1}$), calculated based on Henry's constant and applied pressure, and Q_r and Q_{in} are the recycle and influent flows, respectively.

For particles smaller than the average bubble size, the particle-bubble collision was measured discretized per intervals of particle diameters of $10 \mu\text{m}$, assuming a homogenous particle density, and then multiplied by particle frequency following the measured particle size distribution (PSD). The total collision efficiency per interval η_{π_i} , where i represents the particle interval, was calculated based on equation (2-7), and the total suspended particle removal was the sum of each interval removal. To obtain the removal of particles with diameters equal to or bigger than the average bubble size diameter, the frequency of these particles (when compared to the total amount of particles) was multiplied by either the lowest possible removal efficiency, 50%, or the highest expected removal efficiency, 90% (Fukushi et al., 1998). Thus, the model applied in this research predicts a removal range. A representation of the experimental model can be found in **Annex A-1**. The final inputs to run the model, as independent (measured) and dependent parameters, are enumerated in **Table 2-3**. For the experiments conducted in the laboratory-scale column DAF system, the

selected DAF characteristics were a running temperature of 303 K (30 °C), contact zone detention time of 1200 s, an inflow flow of $0.017 \pm 0.001 \text{ m}^3 \cdot \text{h}^{-1}$, and a recycle ratio of 1. These independent variables were selected based on the influent conditions to tests, and typical ranges of DAF parameters.

Table 2-3. Particle-bubble collision experimental model inputs and units.

		Inputs	Units
Independent variables	Particle characteristics	Particle size frequency in intervals of 10 μm^*	%
		Particle density	$\text{g} \cdot \text{cm}^3$
	DAF characteristics	Running temperature	K
		Contact zone detention time (τ_{cz})	s
		Inflow flow (Q_{in})	$\text{m}^3 \cdot \text{h}^{-1}$
	Recycle ratio (R)**	%	
Dependent variables	Particle-bubble interaction	Collision efficiency factor (α_{bp})	-
	Bubble characteristics	Average bubble diameter	μm

*As a percentage of the total amount of particles

** The recycle ratio (R) is equivalent to the white-water flow, and calculated as a percentage of the Q_{in}

The particle characteristics independent parameters used for the experimental model were selected based on the need to perform low-cost and simple laboratory measurements. Particle size distribution can be directly measured using laser diffraction analysis, like Microtrac Bluewave (Malvern Instruments Ltd., UK), or assessed directly with a digital microscope and FIJI-ImageJ software, as described below (**section 2.2.5**). This latter requires frugal instruments easily available in a laboratory.

Two dependent parameters were chosen for the model, the collision efficiency factor, and the average bubble diameter. While the latter is calculated based on PIV analysis of bubble velocities (described in **section 2.2.3**), values of bubble diameters are not directly measured but derived from the velocities and Navier-Stokes equation. Similarly, the collision efficiency factor is dependent on the average bubble size and the assumption of adequate coagulation and flocculation.

2.2.2 | Laboratory-scale DAF set-up

A laboratory-scaled column DAF reactor was designed to measure bubble sizes and particle removal, as shown in **Figure 2-1**. The column was made of polymethyl methacrylate because of its optical characteristics. The DAF column dimensions were 0.20 m in diameter with a height of 1.00 m and the width was chosen to avoid the reactor wall causing changes in the hydrodynamic behaviour of the reactor medium, as described by Edzwald (1995). Sample and injection points were located every 0.15 m (the first at 0.20 m from the column bottom). Tap water was stored in a stainless steel 10 L Thielman vessel, where the pressure was controlled and maintained by a pressure gauge (Festo pressure gauge, LR/LRS midi) at the desired value of 5.0×10^5 Pa. A pressurized water flow, also known as white water flow, was released at atmospheric conditions into the system from the lowest injection point using a polyurethane tubing of 4 mm internal diameter (PUN-6x1-SI, FESTO, Esslingen, Germany). The white-water flow rate was controlled through a one-way needle valve (Festo 193969, Esslingen, Germany). The laboratory-scale DAF column was located at TU Delft Water-lab (Delft, Netherlands).

The unit was equipped with an influent pump (Watson Marlow 520) set to provide an equal influent flow compared to the pressure-driven white-water flow. Both white-water flow and influent flow were introduced into the DAF column at the same location. The injection point into the column was placed vertically as shown in **Figure 2-1**, and positioned centrally to promote an upstream flow and enhance particle removal. Clean effluent was removed from the sample point located diametrically opposite to the injection one, in the lowest section of the column. Additionally, the concentrate flow was removed from a height of 0.65 m above the column bottom at the fourth collection point, from both sides of the column.

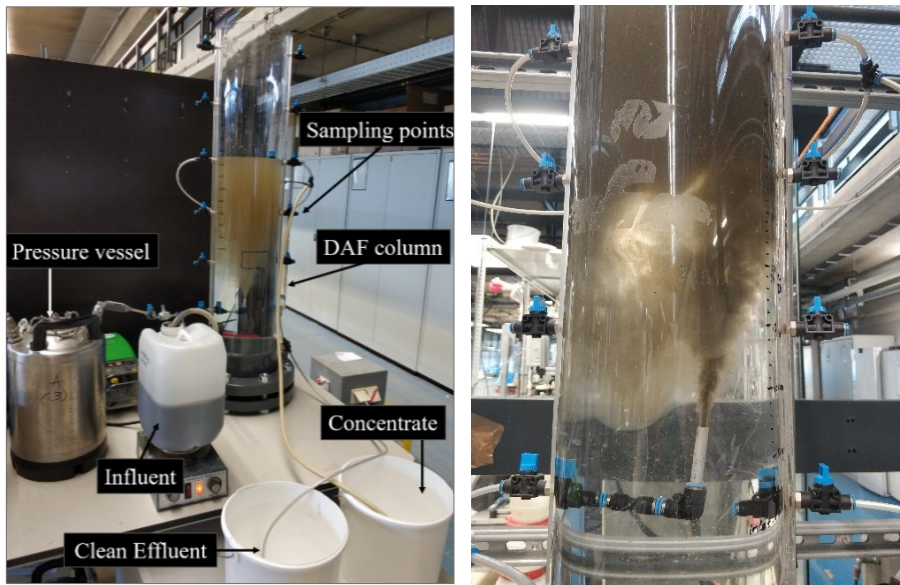


Figure 2-1. Images of the laboratory-scale column DAF system located in the Water Lab facilities (TU-Delft, The Netherlands). On the left, is the laboratory-scale DAF column system. On the right, the influent input point to the column DAF. The input influent is a combination of the tested selected influents and the pressurized water (white water).

Before the start of each trial, both for bubble size measurement and suspended particle removal assessment, the DAF column was filled with 20 L of tap water, corresponding to a height of 0.65 m. The pressure vessel was filled with tap water and pressurized to 5.0×10^5 Pa. Influent and white-water flows were set to be equal and entered the down-scaled DAF column together. No additional nozzles were provided, and white-water flow was controlled via a one-way flow needle valve (GR-QS 6 FESTO, New York, United States).

2.2.3 | Bubble size measurement using particle image velocimetry (PIV)

Bubble size measurement experiments were conducted in the laboratory-scale column DAF above mentioned. The experiments were conveyed using tap water, and a pressure of 5.0×10^5 Pa. LED lights were mounted at the top and back of the DAF column in a square formation. Then the DAF column with the LED lights was covered with a black bag to create opaque surroundings and enhance image quality (Thielicke & Stamhuis, 2014). A slit was created in the black bag at the front side of the DAF, big enough to locate a cellphone camera without enabling light infiltration from outside.

Unlike in previous work, no high-speed camera, but a cellphone camera (MI6, Xiaomi, Beijing, China) was used to record the bubble rise slow-motion videos. The camera was 12 megapixels, had a $1,334 \times 750$ -pixel resolution (high resolution – 4K), and was able to tape at slow motion taking 30 frames per second.

For the bubbles experimental trials, the influent (containing tap water) flow pump and white-water flow were opened at the same time, for a total duration of 145 s. After this period, both inlets to the laboratory-scale DAF column were stopped. Videos were recorded from the moment the influent and white water were on, and for a further 30 s after they were off, representing a total video time of 185 s. Afterwards, the videos were cut into 10 seconds sub-videos (equivalent to 300 frames). Two sub-videos per run, corresponding to times between 135 to 145 and 165 to 175 seconds were analyzed to assess bubble velocities. These videos were called “Tap water 2” (135-145 s), and “Tap water 3” (165-175 s). The selection of the first video frame was done bearing in mind that both inflows (influent and white-water) were on during the record, and bubbles movement was affected by water movement. For the second video frame, bubble movement was not affected by inlet flows.

Particle image velocimetry (PIV) was applied to analyse the recorded videos and compute the bubble velocities. Particularly, the PIVlab MATLAB package was used to process the videos (Thielicke & Stamhuis, 2014). The software can convert a string of consecutive images into velocity profiles by applying particle image velocimetry. Thus, in PIV, a velocity map is obtained based on a sequence of images, by determining the shift of particles from consecutive frames, at a defined time interval (Haidari & van der Meer, 2017). Vertical and horizontal velocity components every 0.5 mm were obtained in a grid of around $30 \text{ mm} \times 10 \text{ mm}$, giving a total of around 1200 velocity points in each grid. Calibration of the velocity vectors was performed based on the time elapsed between two consecutive video frames (30 fps), and a ruler was installed inside the DAF column system. The horizontal and vertical velocity outputs were then used to calculate the bubble diameters correlated to the obtained velocities using the Navier-Stokes (Equation 2-4). Finally, average bubble sizes per grid (of two consecutive frames) were determined based on the total bubble sizes calculated per each velocity point.

2.2.4 | Particle removal in the laboratory-scale DAF

Two different influents were assessed for suspended solids removal in the laboratory-scale column DAF. Firstly, drain water from a canal located in the vicinity of TU-Delft (Van der Burghweg, Delft, The Netherlands) was gathered using buckets.

This water was chosen due to its solid's characteristics since it is expected that canal water has a high content of small and inorganic solids. Delft canal water pH, total and suspended solids concentrations (TS and TSS) were 7.8 ± 0.1 , $840 \pm 48 \text{ mgTS}\cdot\text{L}^{-1}$, and $32 \pm 7 \text{ mgTSS}\cdot\text{L}^{-1}$. The second tested influent was anaerobically digested sludge from a domestic Wastewater Treatment Plant (WWTP), located at Den Hoorn, Netherlands (RWZI–Harnaspolder, Netherlands). To avoid clogging the laboratory-scale DAF, the sludge was sieved with a 0,71 mm filter. After sieving, the sludge pH was 6.9 ± 0.1 , TS concentration was $37.3 \pm 0.1 \text{ gTS}\cdot\text{L}^{-1}$, and TSS concentration was $36.8 \pm 1.5 \text{ gTSS}\cdot\text{L}^{-1}$. The anaerobic sludge was diluted with Delft canal water until a TSS concentration of $0.5 \text{ gTSS}\cdot\text{L}^{-1}$.

Laboratory-scale column DAF runs.

Suspended solids removal in the laboratory-scale DAF column was tested for Delft canal water and the anaerobically digested sludge. The total running time of each experiment was around 20 minutes (1200 s). Influent and white-water flows were fed into the system for the first 810 s. For the first 300 s, no valve was opened, and the DAF column height increased up to a total volume of 25 L. Then the effluent valve was opened (at 300 s) and kept open for another 300 s. The concentrate extraction points, located in the upper part of the lab column (**Figure 2-1**), were opened at 900 s, and the concentrate flow was discharged by gravity until the water height in the laboratory-scale column reached 0.65 m (extraction point). This process took on average 1200 s. A schematic of the laboratory-scale DAF runs can be seen in **Figure 2-2**.

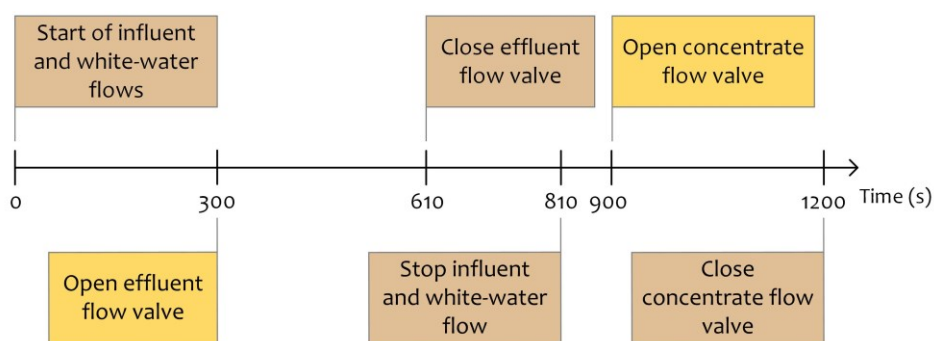


Figure 2-2. Laboratory-scale DAF column experimental times.

2.2.5 | Particle size

Particle characteristics and morphology was assessed using a digital microscope and FIJI-ImageJ processing software (Schindelin et al., 2012). At least nine high-definition

images were taken from the tested influent, with a digital microscope (VHX-5000 Series, KEYENCE, Osaka, Japan). The images were then stacked together to have a more representative sample condition and transformed into binary (black and white). Once the images were stacked, FIJI-ImageJ software was used to analyse the particles' morphological data. For each measured particle, FIJI-ImageJ software was set to give the measurements of particle area, perimeter, and circularity, using a known distance in the stacked pictures ($0.854 \text{ pixel} \cdot \mu\text{m}^{-1}$). Particle circularity can be between zero to one, being one a perfect circle and zero the most elongated shape, and is defined based on particle perimeter and area by FIJI-ImageJ (Ferreira & Rasband, 2012). Particle diameters were then calculated assuming all particles as spheres (similarly to the hypothesis taken for the experimental particle-bubble collision model), based on the values of particle area given by FIJI-ImageJ. Particle frequency every $10 \mu\text{m}$ was calculated by dividing the number of observed particles in a diameter range, by the total number of counted particles in the stacked image.

2.2.6 | Analytical methods

Total solids (TS) and total suspended solids (TSS) were measured following the Standard Method (American Public Health Association, 2013) and performed in triplicates. Measurements of pH at TU-Delft Lab facilities were conducted using and WTW multi720 pH meter, respectively. Finally, particle density was measured via a 100 mL pycnometer (Blaubrand, Wertheim, Germany), following the methods described by Blake and Hartge (1986).

2.3 | RESULTS AND DISCUSSION

2.3.1 | Microbubble sizes

The horizontal and vertical velocity vector components for each frame were extracted from PIVlab, and absolute average bubble horizontal and vertical velocities were calculated for the videos *Tap water 2* and *Tap water 3*. For *Tap water 2*, the average absolute bubble vertical velocity was $9.0 \times 10^{-3} \pm 1.3 \times 10^{-2} \text{ m} \cdot \text{s}^{-1}$, while for *Tap water 3* this value was $2.7 \times 10^{-3} \pm 1.2 \times 10^{-3} \text{ m} \cdot \text{s}^{-1}$. Similarly, average absolute bubble horizontal velocities were $6.5 \times 10^{-3} \pm 1.1 \times 10^{-2} \text{ m} \cdot \text{s}^{-1}$ and $5.3 \times 10^{-4} \pm 4.4 \times 10^{-2} \text{ m} \cdot \text{s}^{-1}$ for *Tap water 2* and *Tap water 3*, respectively. A higher absolute horizontal velocity and standard deviations were obtained for the *Tap water 2* video. This was also observed when absolute average velocities were calculated per frame and not only for the whole recording.

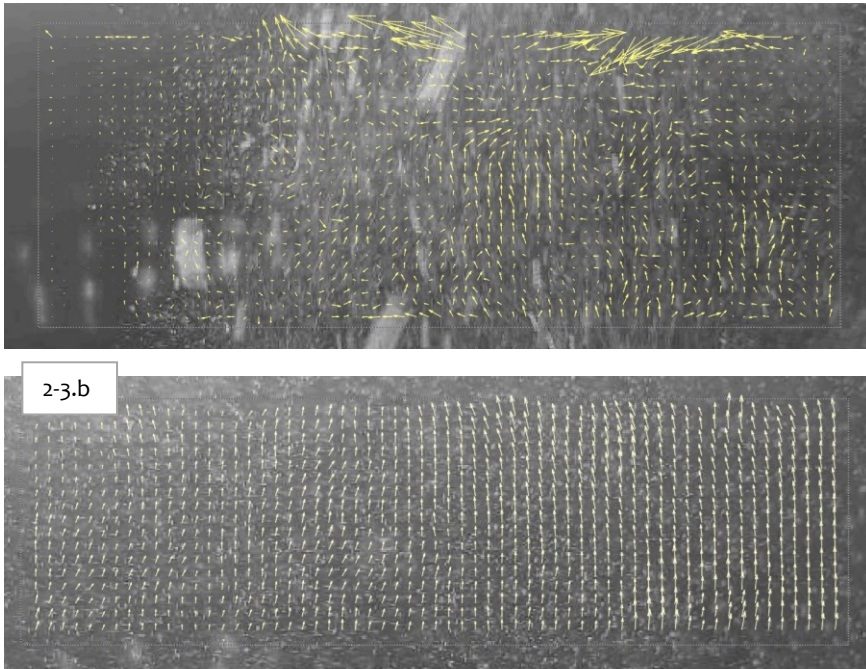


Figure 2-3. Velocity vectors from PIVlab. Fig 2-3.a corresponds to the velocity vector extracted from Tap water 2 at 140 s. Fig. 2-3.b shows the same conditions taken from Tap water 3 at 170 s. Both images are representative of what is observed in each tap water recording.

The difference between the bubble velocities of Tap water 2 and Tap water 3 can be due to the mixing conditions brought by the influent flow, which was running while recording the video Tap water 2 and closed for Tap water 3. Thus, in the latter, air bubbles flow was not disturbed by the water flow. Furthermore, bubbles observed during the recording of Tap water 2 were of a larger scale than the ones in the video Tap water 3. Baeyens et al. (1995) found that water depressurization can produce bubbles of around 1 mm in diameter which can disturb the laminar flow and floc formation and therefore, should be removed in the contact zone. The difference between the velocity vectors at 140 and 170 seconds (from Tap water 2 and Tap water 3 respectively) is shown in **Figure 2-3**. The first one has higher bubble flow disturbance leading to a vast variation in velocities direction, while at 170 seconds, bubbles velocity vectors are mostly vertically aligned.

Based on vertical velocities vectors, bubble sizes were calculated. Each video contained 150 frames of velocity information, and each frame was analyzed in a grid containing around 1200 velocity points. Bubble diameters per mesh point were

calculated based on velocity data and the Navier-Stokes Equation 2-4. The hypothesis to be able to apply Navier-Stokes are that the bubbles should be considered spherical spheres, with smooth surface, and flowing in a laminar flow. This latter means that the Reynolds number should be below 2000 (Ahmed & Giddens, 1983). Thus, after applying the Navier-Stokes equation to calculate the bubble diameters, the values of Reynolds numbers linked to each velocity and bubble diameter were calculated and assessed, following the equation below.

$$R_e = \frac{\rho_L \times v \times d_b}{\mu} \quad (2-13)$$

where ρ_L is water density, v and d_b are the absolute vertical velocity and diameter of the bubble, and μ is the water dynamic viscosity (all values were considered at 15 °C).

The application of Navier-Stokes for bubble diameter and Reynolds number, lead to the identification of a maximum bubble diameter of 1.4 mm in the recorded video *Tap water 2*, and a maximum Reynolds number of 1182. While this number is below the maximum Reynolds number for laminar flow (2000), Navier-Stokes' assumption of the movement of bubbles as solids spheres is valid for Reynolds numbers in the order of 1. Therefore, the video *Tap water 3* will be used for the assessment of bubble diameters, while the video *Tap water 2* will not be considered for this.

The average velocity per frame for the *Tap water 3* video (from 165 to 175 seconds) followed a linear decreased over time (R^2 of 0.92), as expected by Newton's law of motion (Newton, 1687) (**Annex A-2**). Concomitantly to the decrease in bubble velocity, a decrease in the standard deviation of these velocities was also observed. Based on the vertical velocity values, average bubble diameters were calculated (**Figure 2-4**). Average bubble sizes linearly decrease over time (R^2 of 0.92) from 83 to 69 μm . The obtained bubble velocity and diameter profiles are aligned with what is expected from the theory. When the pressurized influent was released into the laboratory-scale DAF column, a cluster of bubbles with varied sizes were formed. The larger the bubble diameter the higher the vertical velocity. Therefore, during the video *Tap water 3*, it is expected that larger bubbles with higher associated velocities will be observed at the beginning of the recording, in comparison to the end of the video. Furthermore, the smaller bubbles are expected to take longer periods inside the column in comparison to bigger ones and therefore, lower bubble diameters should be expected at the end of the recording in comparison to the beginning of it.

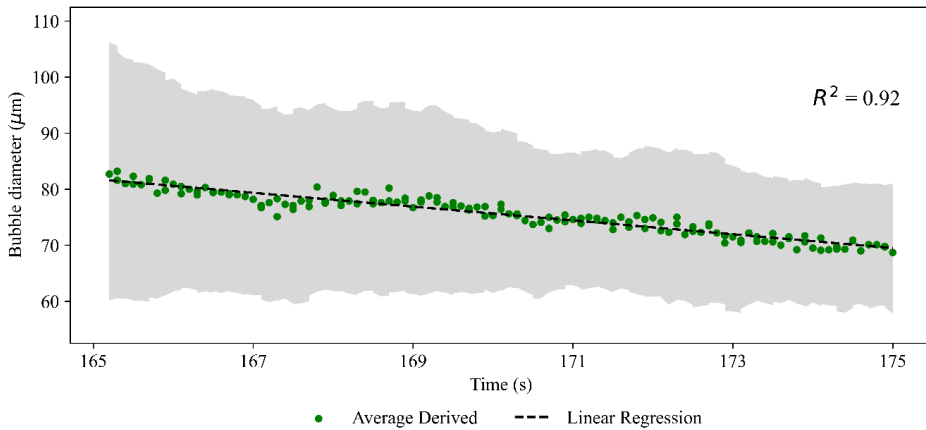


Figure 2-4. Average bubble diameter and standard deviation (in grey shadows). The diameters were calculated using Navier-Stokes and the velocity magnitudes were obtained from PIVlab. The figure is based on the video *Tap water 3*, recorded between 165 and 175 seconds, where there was no inflow into the laboratory-scale DAF column.

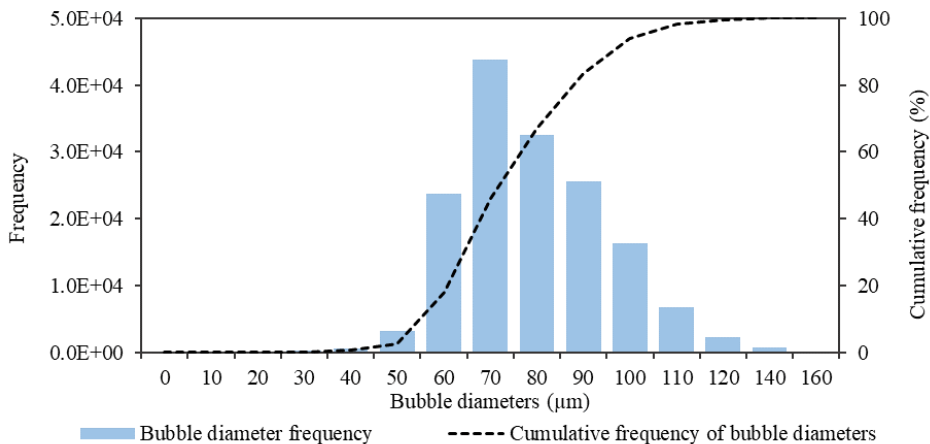


Figure 2-5. Bubble size distribution based on diameters, for the recorded video entitled *Tap water 3*.

From the whole *Tap water 3* recording, bubble sizes followed a normal distribution (**Figure 2-5**), where the average diameter was $74 \pm 15 \mu\text{m}$, and minimum and maximum values corresponded to $2 \mu\text{m}$ and $196 \mu\text{m}$. The 95% confidence interval showed that most bubbles have a size between 50 and 110 μm . These values are in the same range as what is stated by the literature, with sizes between 20 to 150 μm

(De Rijk & den Blanken, 1994; Han et al., 2002). Moreover, the bubble size distribution followed a similar trend to the one estimated by Vlyssides et al. (2004) and measured by Rodrigues and Rubio (2003). The distribution was positively skewed, where higher velocities far from the peak are more frequent than lower ones.

While the bubble size profile obtained using PIV resembles the results found in previous models, the average bubble diameter of $74\ \mu\text{m}$ at $5 \times 10^5\ \text{Pa}$ is bigger than the expected diameter, around 30 to $40\ \mu\text{m}$ (De Rijk & den Blanken, 1994; Rodrigues & Rubio, 2003). Several factors might affect bubble diameters. Firstly, the narrowing opening of a valve or nozzle, causing bubble formation due to cavitation, could cause bubble coalescence and therefore, bigger bubble diameters (De Rijk & den Blanken, 1994). Secondly, the recorded video was located right after the injection point of the white-water into the laboratory-scale DAF column. At further distances from the bubble generation (in the release valve from the pressurized vessel), bubble size and shape might vary and not behave like rigid spheres, but have an ellipsoidal shape (Brignell, 1974; Maldonado et al., 2013), which could cause deviations in bubble diameter determination. Finally, during image analysis, overlapping of bubbles can be observed, and bigger bubbles can be present. As a result, the velocity profile obtained using PIV will derive in larger bubble diameters (Rodrigues & Rubio, 2003). Even though this is a constraint of using PIV, bubble interactions inside a DAF system will naturally occur and the coalescence of several bubbles will form bigger ones. When using the average bubble diameter on the experimental model, suspended solid removal could be overestimated, smaller bubbles are beneficial for suspended solids removal since they provide higher surface areas available for collision (Edzwald, 2010).

2.3.2 | Experimental model results and verification with values from the laboratory-scale DAF

Average values of bubble diameter from *Tap water 3* ($74\ \mu\text{m}$) were used in combination with the particle's characteristics needed to run the experimental suspended solids removal model, PSD, and particle density. PSD results for both Delft canal water and Harnaschpolder anaerobic digested sludge are shown in **Figure 2-6**. More than half of the particles of Delft canal water had a diameter size below $10\ \mu\text{m}$, while this value was 35% for the Harnaschpolder anaerobic sludge. Furthermore, 5% of the anaerobic sludge particles had a size above $120\ \mu\text{m}$, while the maximum particle size for Delft canal water was $80\ \mu\text{m}$. **Annex A-3** includes particle images of both influents used for PSD calculations. Finally, the measured average particle

density was $1.08 \pm 0.02 \text{ g}\cdot\text{cm}^{-3}$ for Delft canal water and $1.04 \pm 0.03 \text{ g}\cdot\text{cm}^{-3}$ for the anaerobic sludge.

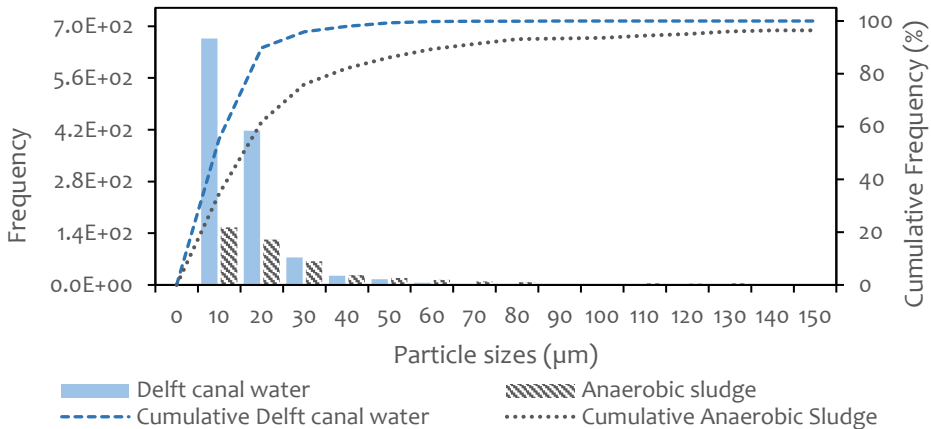


Figure 2-6. Particle size distribution (PSD) for Delft canal water and Harnaschpolder anaerobic digested sludge. The values were obtained using microscope images and the FIJI-ImageJ software to analyse particle shapes and their corresponding diameter. The calculations of PSD were conducted based on the total amount of measured particles. The microscope images used to gather particle shape and size can be found in Annex A-3.

Results of the filtration models applied to both influents showed that the suspended solids removal for Delft canal water should be $68 \pm 1\%$, while this value for Harnaschpolder anaerobic sludge was $78 \pm 3\%$. For both influents, the most important collision factor between bubbles and particles was interception (η_i). This coefficient was one or two orders of magnitude above the Brownian diffusion (η_{BM}) and settling (η_s) coefficients. Edzwald (1995) found that while Brownian diffusion governed the collision possibility with bubbles for particles below $1 \mu\text{m}$, interception governed particles above this size. In the experimental model, particles with sizes below $10 \mu\text{m}$ were the hardest to remove. These particles had the lowest chance of collision with bubbles, due to their small surface area available and interception coefficient, with 52 and 43% chance of collision for the anaerobic sludge and the Delft canal water, respectively.

To improve the suspended solids removal, it is key to have good coagulation and flocculation. Adequate coagulation will neutralize the particles' zeta potential, and improve the overall chances of particle-bubble collision (Han et al., 2001).

Furthermore, flocculation after coagulation will promote the formation of bigger agglomerates and therefore, increase the sizes of the suspended solid (Vandamme et al., 2015).

The laboratory-scale column DAF was used to evaluate the removal efficiency of suspended solids and compare the results to the predictive model. For the Delft canal water, with a TSS concentration of around $30 \text{ mgTSS}\cdot\text{L}^{-1}$, the removal varied between 66 to 96%, while for the anaerobic sludge with a concentration of $500 \text{ mgTSS}\cdot\text{L}^{-1}$, the removal was between 68 to 92%, when five experimental runs were conducted per influent type. The experimental model predicted removals of $68 \pm 1\%$ and $77 \pm 3\%$ for Delft canal water and the anaerobic sludge, respectively. These predicted values are aligned with the removals obtained in the laboratory-scale column. Furthermore, if the influents are subjected to good coagulation and flocculation, and the frequency of particles below $10 \mu\text{m}$ halved, the experimental model predicts an increase of suspended solids removal to 84 and 88% for the Delft canal water and anaerobic sludge, respectively.

While the experimental model gave a similar range of suspended solids removal to the one assessed in the laboratory-scale DAF column, the model has limitations. Firstly, the experimental model was run using only the average bubble diameter and not the full bubble size distribution shown in **Figure 2-5**. Depending on the bubble size distribution in the DAF unit, the experimental model can over or underestimate the suspended solids removal. A change in the average bubble size from 74 to $50 \mu\text{m}$ increases the predicted TSS removal efficiencies of Delft canal water and anaerobic sludge by 5%, to 76 and 82%. Contrary, an increase in average bubble size to $90 \mu\text{m}$ had a negative effect of reducing the predicted TSS removal by 3% to the Delft canal water and anaerobic sludge, respectively. Thus, the effect of average bubble size in the predicted removal efficiencies varies depending on the influent particle characteristics and might lead to significant changes. The sensitivity and uncertainty linked to this dependent model variable should be further assessed to better describe the interactions between particles and bubbles.

Secondly, values of the collision efficiency factor (α_{bp}) were taken from Han (Han et al., 2001). Trajectory analysis is used to calculate the α_{bp} factor, which depends on particle size and density, zeta potential, bubble wall effect, and fluid turbulence (T. Y. Liu & M. Schwarz, 2009). Generally, the rate of particle-bubble attachment has been analysed based on three main factors, which are the probability of actual collision, the probability of attachment occurring once the collision happened, and the collision frequency based on linear interception (Nguyen & Schultze, 2004). For particles

2

above 30 μm , the bubble surface effect on the particle drag force might decrease the collision efficiency and therefore, should be considered (T. Liu & M. Schwarz, 2009). The collision efficiency factor effect is mostly predominant in the removal of small particles. In the experimental model, an α_{bp} decrease of 20% shows a reduction of 4 and 2% in TSS removal of Delft canal water and anaerobic sludge. If α_{bp} further decreases to 60% of its original value, then the TSS removal prediction in Delft canal water plunges by 8%. Thus, the sensitivity of the collision efficiency factor in the experimental model should be further assessed to enhance model prediction.

The model considers that the influent particles and agglomerates have a zeta potential close to zero (adequate coagulation and flocculation), but zeta potential was not measured during the experiments carried out in the laboratory-scale DAF. Regular techniques of measuring adequate coagulation and flocculation involve jar tests for different polymer concentrations (Edzwald & Haarhoff, 2011). The method to measure PSD developed in this study could be useful as a complementary assessment of adequate coagulation and flocculation. Typical equipment employed to measure PSD, when particle sizes are smaller than a millimetre, uses light scatter techniques (Li et al., 2019). The use of this technique requires setting a liquid flow (water) with the particles to analyse, passing through a laser beam. Solids aggregates can be weak and get destroyed in the process (Bieganowski et al., 2018). Thus, the alternative method using microscope images and FIJI-ImageJ software can be considered to efficiently measure the particle aggregates.

Finally, the model considers that all particles have a homogenous density and surface. Drain- and wastewater particles are heterogenous, they can be inert or organic, and be categorised as settleable or not. Around 30% of the total suspended solids in domestic wastewater can be considered inert (Henze et al., 2008). From the tested influents, Delft canal water was expected to have a higher inorganic (inert) matter content than the anaerobically digested sludge. This can be observed based on the average particle density of both influents, 1.08 and 1.04 $\text{g}\cdot\text{cm}^{-3}$ for Delft canal water anaerobic sludge respectively, where organic matter is expected to have a lower density than inorganic matter. Nevertheless, both influents have a combination of organic and inorganic particles. Thus, considering that all particles from the influent have the same particle density might lead to wrong predictions of particle removal.

2.3.3 | Experimental prediction model and verification in full-scale DAF performance

Two full-scale DAF systems were used to compare the results of the experimental model and the suspended solids removal in the laboratory-scale DAF. The DAF systems were used as part of an industrial wastewater treatment plant. The treatment consisted of a DAF unit (DAF1) used for pre-treatment, followed by a biological nitrogen and phosphorus removal unit, with aerobic and anaerobic times. Finally a second DAF system (DAF2) was used as a polishing step after the biological unit. The DAF systems were in the Netherlands and supplied by Nijhuis Saur Industries. Samples of influents (after coagulation and flocculation), and effluents from the DAF systems we collected to process the average particle density and particle size distribution. DAF units' influent characteristics and suspended solids removal are shown in **Table 2-4**. The PSD of each influent can be seen in **Annex A-4**. Both units had influent flows around $10 \text{ m}^3 \cdot \text{h}^{-1}$, a recycle flow (R) ratio of 1, and were run under a white-water pressure of $5 \times 10^5 \text{ Pa}$.

Table 2-4. Full-scale DAF systems influent characteristics and suspended solids removal efficiencies. DAF1 was located at the beginning of the wastewater treatment train, while DAF2 was located after the biological removal of nitrogen and phosphorus.

	Particle density	Influent pH	Influent TSS	Influent VSS	Influent temperature	TSS removal	Predicted TSS removal
	$\text{g} \cdot \text{cm}^{-3}$	-	$\text{g} \cdot \text{L}^{-1}$	$\text{g} \cdot \text{L}^{-1}$	K	%	%
DAF1	1.06 ± 0.014	3.5	1.86 ± 0.06	1.86 ± 0.06	313	91 ± 2	98 ± 1
DAF2	1.07 ± 0.002	7.5	10.71 ± 0.32	10.71 ± 0.32	293	98 ± 1	96 ± 1

Results from the application of the experimental model with an average bubble size of $74 \mu\text{m}$ showed that both DAF units could reach a high suspended solids removal efficiency of $98 \pm 1\%$ and $96 \pm 1\%$ for DAF1 and DAF2, respectively. While this was the case in practice for DAF2 that reached 98% removal, the DAF1 unit was running under a lower removal efficiency than the predicted one, namely 91%. The suspended removal efficiencies obtained in the tested full-scale DAF systems are similar to what several researchers observed. Ansari et al. (2018) found a TSS removal of 98.5% when a full-scale DAF system was used as a pre-treatment of wastepaper-recycling

wastewater. Furthermore, Rattanapan et al. (2011) observed a suspended solids removal efficiency of almost 100% when using a DAF unit with acidification and coagulation to treat biodiesel wastewater. Finally, Koivunen and Heinonen-Tanski (2008) achieved a 95% reduction of suspended solids when a pilot-scale DAF was used to treat primary effluent of municipal wastewater.

When taking the full-scale DAF samples for testing, the DAF1 was not working under optimal conditions. Influent pH after coagulation and flocculation was too low (around 3.5), and prone to affect the further treatment steps. This was reflected in the results of the experimental model, where under optimal coagulation and flocculation, the DAF1 unit is expected to achieve a suspended solids removal of around 98%. Chemical pre-treatment, to neutralize particle charge and form bigger agglomerates, is essential for DAF efficiencies (Al-Shamrani et al., 2002; Leppinen, 2000). When inorganic coagulants and flocculants are used, like aluminium or iron salts, low pH promotes coagulation by accelerating the hydrolysis of coagulants to Al^{+3} and Fe^{+3} (Zouboulis et al., 2008). Zhao et al. (2021) concluded that to obtain adequate coagulation of oily wastewater the pH should be kept below 7. Furthermore, anionic polymer flocculants are highly affected by small changes in pH, and pH values below 4.5 are not recommendable (Zhao et al., 2021). Thus, the difference between the expected removal of the DAF1 and the actual obtained TSS removal could be because the influent pH was too low.

Moreover, the influent of the DAF1 presented a temperature of (40 °C) and therefore, a lower amount of bubbles can be expected to be released under these conditions in comparison to normal conditions (van 't Hoff, 1884). Air dissolution in water at a pressure of 5×10^5 Pa decreases around 30% when temperatures increase from 20 to 40 °C. Thus, fewer bubbles can be expected to form under higher temperatures, reducing the chances of collision between bubbles and particles. Furthermore, the air and water density and the water viscosity are also affected by the increase in temperature. These affect the velocities of the microbubbles inside the DAF. For an average bubble size of 74 μm , the bubble velocity increases by 50% at a temperature increase from 20 to 40 °C; 0.30 and 0.45 $\text{cm}\cdot\text{s}^{-1}$, respectively. The rise in bubble velocities reduces the time the bubbles are inside the DAF system, reducing the chances of collision with particles.

Finally, the experimental model for DAF suspended solids removal proved to be aligned with the results obtained in the full-scale DAF systems and gave information regarding the level of optimization of the systems. While the DAF2 was working under optimal suspended solids removal conditions, the model results clearly

indicated that DAF₁ performance could be enhanced, resulting in the advice to improve the influent pH and temperature control.

2.4 | CONCLUSIONS

An experimental model for total suspended solids (TSS) removal on dissolved air flotation (DAF) units was developed using the single factor collision approach. A set of six independent variables were used for the experimental model. These variables, referred to influent particle characteristics: particle size distribution (PSD) and particle density, and DAF running characteristics: temperature, contact zone detention time, inflow and recycle flows. Two dependant variables, collision efficiency factor and average bubble diameter, were used as model inputs. The latter was derived from measurements of bubble velocities using particle image velocimetry. The model was verified using a laboratory-scale DAF system tested for two different influents (Delft canal water and anaerobic sludge), and on two full-scale DAF installations. The main conclusions of this chapter are as follows:

- The developed experimental model was able to predict the TSS removal efficiencies of a laboratory-scale column DAF system when two different influents were used. Results from the model showed a TSS removal of $68 \pm 1\%$, and $77 \pm 3\%$ for Delft canal water and the anaerobic sludge, respectively, while experimental removals were between 66 to 96% for Delft canal water and 68 to 92% for anaerobic sludge.
- When modelling two full-scale DAF units, results from the experimental model showed that one of the units was underperforming, with a measured TSS removal of 91% and an expected one of 98%. Thus, the model was able to identify potential improvements.
- The sizes of microbubbles produced when depressurizing water can be measured using easily available materials, like a cell phone camera, and PIV software. Furthermore, the derived bubble size distribution using the method described in this research proved to be aligned with theory.
- The average bubble diameter, influent particle size distribution and density, were key inputs for the experimental model. The measurement of these parameters was performed using easily available computational tools and simple experimental procedures. These methods could overcome the difficulties of performing laboratory or pilot-scale TSS removal tests for assessing the efficiency of DAF systems.



Column bench-scale DAF system located at TU-Delft

3

High suspended solids removal of Indian drain water with a down- scaled Dissolved Air Flotation (DAF) for water recovery

This chapter is an adapted version of Piaggio, A. L., Soares, L. A., Balakrishnan, M., Guleria, T., de Kreuk, M. K., & Lindeboom, R. E. (2022). High suspended solids removal of Indian drain water with a down-scaled Dissolved Air Flotation (DAF) for water recovery. Assessing water-type dependence on process control variables. *Environmental Challenges*, 8, 100567. DOI: 10.1016/j.envc.2022.100567

ABSTRACT

3

The Barapullah drain crosses New Delhi, India, and transports millions of cubic meters of stormwater, municipal sewage, and industrial sewage to the Yamuna River. Seasonal variations and ambiguous annual discharges cause 20-fold fluctuations in hydraulic flows, pollutants type and concentration. Given New Delhi's high population density, limited surface area, and water stress, addressing these challenges is crucial. This study focuses on a down-scaled column Dissolved Air Flotation (DAF) system designed to assess total suspended solids (TSS) removal efficiencies under different influent conditions. Three influents that resemble the Barapullah drain seasonal variations in composition, and a fourth that imitates the feed of DAF when located after an anaerobic bioreactor were tested. Sixty batch DAF experiments evaluated seven control variables: influent Total Suspended Solids (TSS), pH, temperature, DAF particles residence time, white water pressure, coagulants and flocculants concentration, and coagulation and flocculation time. Results showed that the down-scaled DAF could be steered from low to high removal efficiencies, comparable to full-scale systems. Maximum TSS removal varied between 92 to 96%. The impact of performance variables varied depending on the influent type, with pressure exhibiting a positive influence on separation efficiency. The system exhibited lower removal efficiency for particles with spherical shapes and diameters below 10 μm . The results indicate that a full-scale DAF system could effectively remove suspended solids from the Barapullah drain, offering a robust and space-efficient solution for water recovery in densely populated areas.

3.1 | INTRODUCTION

In recent years, New Delhi has consistently been labelled one of the most polluted and densely populated cities in the world (Balha et al., 2020; Mazhar et al., 2021). Annual per capita fresh-water availability is expected to decrease by 30% when compared to values of 2010, due to the increasing population and country development (Kaur et al., 2012). Sewage is discharged into clean water bodies contaminating them, which is exemplified by the water recovery challenges related to the Barapullah stormwater drain. This drain is currently heavily polluted with municipal sewage and industrial effluent year-round. At the Barapullah drain mouth, the Chemical Oxygen Demand (COD) and Total Suspended Solids (TSS) varied from 320 to 1500 mg·L⁻¹ and 30 to 510 mg·L⁻¹ respectively throughout the year 2019 (Indian Institute of Technology Delhi, 2019). Aside from temperature fluctuations, ranging from 11 to 35°C over the year, the Barapullah drain volumetric flow rates increase 20 times during the monsoon season in contrast to the dry season (Sontakke et al., 2008). These fluctuations in both influent quality and quantity, pose serious concerns for conventional and highly advanced wastewater treatment technologies. Giokas et al. (2002) concluded that the performance of the wastewater treatment plant of Ioannina (Greece) was affected by shifts in wastewater quality and quantity. Efficiency decreased during high wastewater flows or a rise in feed flow pollutants concentration. Furthermore, a lack of stability in a bioreactor operation when insufficient shower water was produced was observed in a system developed for water reuse for manned life support in Space (Lindeboom et al., 2020). A Dissolved Air Flotation (DAF) is proposed as pre-treatment for a multi-stage treatment train, focused on healthy reuse of the Barapullah water. A DAF unit has a small footprint, high separation efficiency, robustness under a wide range of hydraulic loading rate, possibility of removing particles from 10 to 2000 µm (Kiuru, 1990).

DAF units have been widely used since the beginning of the 1960s for separating particulate matter from the liquid by flotation (Kiuri, 2001). Currently, these systems have been particularly useful in the pre-treatment of anaerobic digestion, to remove suspended solids. Cagnetta et al. (2019) found the removal of up to 78% of TSS when a high-rate activated sludge process was followed by a DAF. Penetra et al. (2003) reported a TSS removal of 96.7% when a DAF was located after an expanded bed anaerobic reactor. Some studies reported an increased overall performance by placing a DAF before the anaerobic digestion of municipal slaughterhouse wastewater (Harris et al., 2017; Manjunath et al., 2000; McCabe et al., 2014). Few articles have demonstrated the successful implementation of DAF units in

wastewater reuse schemes. For example, DAF followed by Ultra Violet (UV) disinfection allowed the reuse of fruit and vegetable processing wastewater (Mundi & Zytner, 2015). One study even reported drinking water quality standards could be achieved when treating poultry slaughterhouse wastewater with a laboratory-scale Sequencing Batch Reactor (SBR), followed by a batch DAF (2.0 L cylinder and 10 cm diameter) and UV disinfection (De Nardi et al., 2011). Although the literature shows DAF systems have the potential to enable water reuse, particularly in combination with anaerobic digestion, the most typical applications still only consider DAF for conventional solid-liquid separation.

3 DAF performance has been measured by the efficiency at which particles and liquid are separated. Particle removal in a DAF depends on particle buoyancy and the possibility of forming bubble-particle aggregates (Wang et al., 2005). Therefore, liquid flow, hydraulic retention time, influent particle concentration, and bubble concentration and size are key control variables that can be used to increase particle separation. According to Van Nieuwenhuijzen (2002), sludge particles from domestic wastewater have a negatively charged surface. Similarly, air bubbles have a negative zeta potential and surface charge through a wide variation of pH (M. Han & S. Dockko, 1998). Coagulants are needed to neutralize particle surface charge and promote particle-bubble collision, while flocculants are needed to agglomerate neutralized particles. Depending on incoming water quality, particle removal can thus, be enhanced by adding coagulants and flocculants (Bratby, 1980). While extensive knowledge in full-scale DAF systems removal was gained during the 1990s, the development of mathematical models and computers algorithms, for solving the equations governing the flow and particle-liquid-bubble interactions, are key to developing more efficient DAF units (Bondelind et al., 2010).

Most recent literature on DAF is linked to the utilization of computation fluid dynamics (CFD) for further understanding the separation and contact zones (Yang et al., 2021). Lundh et al. (2001) used CFD and found that two flow structures are present in a DAF, a stratified flow, and a downwards-vertical transport. A 3D CFD model was developed to analyse the optimization of the DAF in the wastewater treatment plant of Kluizen, Belgium by Satpathy et al. (2020). While the results of this model showed alignment with what was found before in relation to the stratification of the water flow, it lacked to fully address particle-bubble agglomerates. Rodrigues and Béttega (2018) formulated a two-phase (bubble-liquid) 2D CFD model to assess the flow behaviour on a 1.50 m³ pilot-scale DAF treating 10 m³.h⁻¹ of influent. Results showed that the Eulerian approach and κ - ϵ turbulence model where an adequate

representation of the real flow behaviour inside the DAF. Lakghomi et al. (2015) developed an analytical and computational fluid dynamic model to assess the multiphase of particle-bubble-liquid. Their research was based on simulations for a fix bubble size. Nevertheless, both particles and bubbles vary in diameter, and therefore, findings are limited. Furthermore, a comparison to a full or down-scaled DAF unit is recommended to compare mathematical and real results. While mathematical models are being developed to understand fluxes inside DAF units, the multi-phase interactions between bubbles, liquid and particles remain complex and limited (Wang et al., 2018). An assessment of full and down-scaled DAF units, treating different influents and particles, should be fixed to complement and contrast the information gathered from mathematical models.

Some authors have used laboratory-scale DAF units to empirically assess flow conditions, bubble formation, and bubble size (De Rijk & den Blanken, 1994; Han & Dockko, 1998; Han et al., 2002; Mudde & Simonin, 1999; Samstag et al., 2016). However, to the author's knowledge, no scientific studies are available that systematically assess the influence of all process control variables mentioned above, on particle removal for different types of particles, representing different 'real' wastewater. Potentially, this is because, on a down-scaled DAF, it is difficult to simulate the exact physical/hydraulic phenomena remaining representative for full-scale applications, since microbubbles are impossible to down-scale. Reported DAF units need large influent flows (between 5 to 100 m³ per test) and are therefore not suited for experiments with real drainage and wastewater in a laboratory setting (Edzwald & Haarhoff, 2011).

The application of experimental design has been used to evaluate the effects of many different variables at the same time for a wide range of environmental technologies, such as gasifiers, and solar reactors, among others (Al-Muraisy et al., 2022; Feroso et al., 2010; Inayat et al., 2020; Raheem et al., 2015). The experimental design enables the gathering of maximum information from a dataset using a limited number of experiments (Fisher & Bennett, 1990). It does so by assuming that the influence of one variable stays the same despite the change in others. In addition, this tool provides information about variations generated by the system itself and also regarding uncertainties or errors present in experimental data (Mäkelä, 2017). The use of experimental design in down-scaled DAF systems is therefore proposed to predict particle removal efficiency for a set of control variables under different operational conditions. These conditions can resemble a wide variety of complex urban water reuse schemes, like the Barapullah drain wastewater.

This study analyses the performance of a down-scaled DAF, treating four different influents. Two influents imitate the varying conditions of the Barapullah drain, one influent is taken from the drain itself and tested in-situ, and the last influent is from a bioreactor that also mimics locating the DAF closer to a household (upstream and concentrated). A novelty of this study is the assessment of seven DAF control variables (**Annex B-1**) on suspended solids removal, using the Plackett-Burman design, which resulted in a total of 60 batch DAF experiments. Based on the results, it will be evaluated to what extent the different control variables are key to enhancing suspended solids removal for different characteristic wastewaters. Additionally, down-scaled DAF solids removal performance will be compared to full-scale system performance, and the outcomes will be extrapolated for the treatment of the raw Barapullah drain water and/or bioreactor effluent. This culminates in the assessment of the possibility of using a DAF as part of a treatment train for water recovery in high population density megacities, like New Delhi, where available surface area and fluctuating hydraulic loads are considered serious barriers to water recovery, as a scarce resource.

3.2 | MATERIALS & METHODS

3.2.1 | Experimental set-up

Two identical down-scaled column DAF reactors were designed and then operated at TU-Delft WaterLab (Delft, The Netherlands), and the LOTUS^{HR} test site at the Barapullah drain (New Delhi, India), shown in **Figure 3-1**. The systems materials and equipment are identical to what was described in **section 2.2.2**. Before the start of each trial, the DAF column was filled with 20 L of tap water, corresponding to a height of 0.65 m. The pressure vessel was filled with tap water and pressurized following the experimental run requirements. Influent and white-water flows were set to be equal (at $1.62 \text{ L}\cdot\text{h}^{-1}$) and entered the down-scaled DAF column together. No additional nozzles were provided for the laboratory set-up, and white-water flow was controlled via a one-way flow needle valve (GR-QS 6 FESTO, New York, United States).

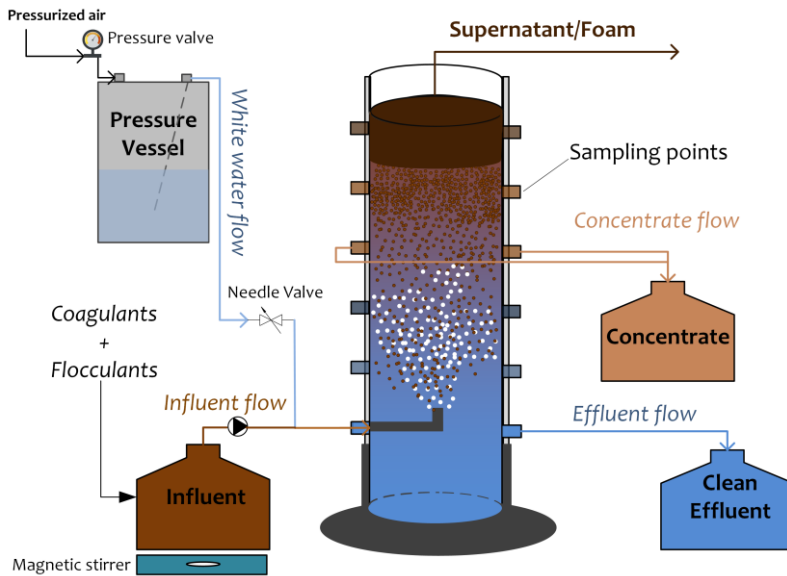


Figure 3-1. A schematic image of the down-scaled DAF system.

3.2.2 | Tested influents

Four different influents were selected based on possible DAF locations for wastewater treatment: as part of the primary treatment receiving raw drain water from the Barapullah drain or as the sludge and water separation mechanism after an anaerobic digester, which also mimics locating the DAF at household levels (closer to the pollution source).

The Barapullah drain water - BDW (New Delhi, India)

Water from the Barapullah drain was collected close to the drainage mouth with the Yamuna River by a pump and stored in 100 L containers at the LOTUS^{HR} site. Drain water characteristics were measured immediately after collection.

Delft canal water - DCW (Delft, The Netherlands)

Drain water from a canal located next to TU-Delft Water Laboratory (Van der Burghweg, Delft, The Netherlands) was gathered using buckets. Canal water was collected in May. This water was chosen to be representative of the Barapullah drain pollutants concentration throughout the monsoon season (June to September).

Anaerobic Digested Sludge - ADS (Harnaschpolder wastewater treatment plant, The Netherlands)

Anaerobic digested sludge was taken from a domestic wastewater treatment plant (RWZI–Harnaschpolder, Den Hoorn, The Netherlands). The digester treats both primary and secondary sludge and operates under 22 days of Solids Retention Time (SRT) at 35°C. ADS influent was chosen to mimic the feed conditions of a DAF system when located after a bioreactor, or at a household level (close to the pollution source). Due to the down-scaled DAF reactor requirements, the collected sludge was sieved with a 0.71 mm filter before use.

Mix of Anaerobic digested sludge and Delft canal water - MIX

Harnaschpolder anaerobic digested sludge and canal water were mixed at TU Delft Lab facilities. This mix influent was considered to mimic conditions of the Barapullah drain throughout the dry season. The sludge was sieved again with a 0.71 mm filter. The two components were mixed in a given ratio following the desired TSS content for each experiment.

3.2.3 | Influent preparation

Calcium hydroxide $\text{Ca}(\text{OH})_2$ was selected as coagulant and cellulose as flocculant due to their local commercial availability in India, and digestibility under anaerobic conditions. The same concentration of cellulose and $\text{Ca}(\text{OH})_2$ was incorporated (ratio 1:1), where a rapid mixing at 100 rpm for one minute followed by slow mixing at 40 rpm was performed. Furthermore, pH was corrected after the addition of the coagulant and flocculant. Two of the key independent control variables assessed were concentration of coagulants and flocculants, and coagulation time. Thus, these values vary between 5.0 and 500.0 $\text{mg}\cdot\text{L}^{-1}$ and, 10 to 30 minutes respectively. The exact values are explained below.

Canal water from Delft was heated up to a temperature of around 30°C using a water bath. Additionally, the pH of canal water and Harnaschpolder sludge was increased to 8.5 when needed to mimic the Barapullah drain conditions. This was done by adding sodium hydroxide (NaOH). Since the TSS concentration of influent was a variable to be tested, the Barapullah drain and canal water were either concentrated or diluted (with tap water) to reach TSS values between 30 to 510 $\text{mg}\cdot\text{L}^{-1}$, while sludge was diluted to have solids concentration between 500 and 5000 $\text{mg}\cdot\text{L}^{-1}$.

3.2.4 | Removal efficiencies calculation

To calculate the suspended solids removal for each experiment, an influent TSS dilution factor had to be determined. This dilution factor accounted for the 20 L of tap water inside the column, and the white water introduced into the system. The volume of white water incorporated per experiment was calculated based on the reactor mass balance, where the known inputs and outputs to the system were the volumes of influent, effluent, concentrate, and foam. The total volume of water inside the down-scaled DAF was kept at 20 L. Then, the diluted influent TSS concentration was calculated following the equation below (3-1). TSS removal efficiencies were determined considering the diluted influent and effluent TSS concentrations.

$$\text{Diluted inf. TSS} = (\text{Original inf. TSS} \times \text{Influent Volume}) / (\text{Influent volume} + \text{White water volume} + 20) \quad (3-1)$$

3.2.5 | Key performance control variables and Plackett-Burman Design

Seven key control variables were selected to assess down-scaled DAF suspended solids removal efficiency. These variables were TSS, temperature, pH, residence time, pressure, coagulant and flocculants concentration, and coagulation time, as already delineated in the introduction. All independent control variables were studied at two levels (1, -1) and one centre point (0), based on the Plackett-Burman Design (PBD) (Plackett & Burman, 1946). The levels and centre point corresponded to the maximum, minimum, and mean values of each set of variables. TSS, pH, and temperature are influent control variables, while pressure, residence time, and coagulant concentration are defined as DAF operational control variables. To define the former three influent variables, the Barapullah drain water conditions and variations during the year were considered. Maximum and minimum values of TSS and temperature for canal- and drain water influents were set to 30 and 500 mg·L⁻¹, and 29 and 35 °C respectively (Indian Institute of Technology Delhi, 2019). Suspended solids concentrations between 500 to 5000 mg·L⁻¹ were selected for the sludge and mix influents. Maximum, minimum, and central values of residence time, pressure, coagulants and flocculants concentration, and retention time are shown in **Table 3-1**.

Table 3-1. Plackett-Burman design (PBD) for screening of independent control variables.

Control Variables	Value	Units	Delft canal water -DCW	Barapullah drain water - BDW	Anaerobic digested sludge - ADS	Mix influent - MIX
Total Suspended Solids	30	mg·L ⁻¹	+	+		
	270	mg·L ⁻¹	+	+		
	510	mg·L ⁻¹	+	+		
	500	mg·L ⁻¹			+	+
	2750	mg·L ⁻¹			+	+
	5000	mg·L ⁻¹			+	+
Temperature	29	°C	+			
	32	°C	+			
	35	°C	+			
Residence time	780	s	+	+	+	+
	990	s	+	+	+	+
	1200	s	+	+	+	+
pH	6.7		+			
	7.2		+			
	7.6		+			
	7.0				+	
	7.8				+	
	8.5				+	
Pressure	3.0	10 ⁵ Pa	+	+	+	+
	4.0	10 ⁵ Pa	+	+	+	+
	5.0	10 ⁵ Pa	+	+	+	+

Table 3-1 (Continuation). Plackett-Burman design (PBD) for screening of independent control variables.

Control Variables	Value	Units	Delft canal water -DCW	Barapullah drain water - BDW	Anaerobic digested sludge - ADS	Mix influent - MIX
Coagulant and flocculants concentration	5.0	mg·L ⁻¹	+	+	+	+
	252.5	mg·L ⁻¹	+	+	+	+
	500.0	mg·L ⁻¹	+	+	+	+
Coagulation time	600	s	+	+	+	+
	1200	s	+	+	+	+
	1800	s	+	+	+	+

Plackett-Burman Design (PBD) was conducted by taking between five and seven control variables, depending on the experiment. Screening design was selected as the methodology to identify the effect of the chosen variables and the selection of the most important ones (statistical p-value below 10%). Furthermore, PBD was applied to formulate the experimental matrix, resulting in 12 different experiments and triplicates of the central point, summing up to 15 experiments per influent type (see **Annex B-2** with PBD matrix). The central point experiments were then used to calculate the standard deviation that later was applied in the analysis.

The analysis of the experimental data was performed using the Statistica 7.0 software and Protimiza software. The linear model to predict the main effects is described in the equation below (3-2).

$$x_i = a + \sum b_i * X_i \quad (3-2)$$

where x_i is the value of the independent variable in terms of TSS removal (%), a is the model intercept, X_i represents different levels of independent variables, and b_i is the coefficients as predicted by the equation.

3.2.6 | Analytical methods

Total and volatile solids were measured according to Standard Methods (American Public Health Association, 2013), and triplicate samples were taken and analysed. Temperature, pH, and dissolved oxygen (DO) measurements were conducted with a

multi720 pH meter (WTW, Weilheim, Germany). COD measurements were done using HACH test kits LCK 314, 514, and 014 (HACH, Tiel, The Netherlands). Particle density was measured following the methods described by Blake and Hartge (1986) using a 100 mL pycnometer (Blaubrand, Wertheim, Germany). Finally, particle zeta potential was measured based on the electrophoretic light scattering technique with a Zetasizer nano (Malvern Panalytical, Almelo, The Netherlands).

Particle characteristics and morphology was assessed using a digital microscope and FIJI-ImageJ, following the method described in **section 2.2.5**. For ADS, DCW, and MIX, high-definition images were taken with a digital microscope (VHX-5000 Series by KEYENCE). The Barapullah drain water images were captured with a digital microscope (NIKON ECLIPSE E600, illustrated 3.5b). These images were then processed using FIJI-ImageJ and morphological data, i.e., particle size and circularity were analysed in MS Excel. Circularity is defined based on particle perimeter and area by FIJI-ImageJ, following equation (3-3). A value of 1.0 indicates a perfect circle, while one closer to 0.0 shows an elongated shape. DCW had the lowest number of particles with a circularity above 0.7, 67% of the total amount of solids.

$$\text{circularity} = 4\pi \times (\text{area}/\text{perimeter}^2) \quad (3-3)$$

3.3 | RESULTS

3.3.1 | Influent characteristics

Table 3-2. Summary of tested influents characteristics. BDW stands for the Barapullah drain water, DCW for Delft canal water, and ADS for anaerobic digested sludge.

Parameter	Units	Influents		
		BDW	DCW	ADS
Temperature	°C	32.3 ± 1.8	9.4 ± 0.1	35.0 ± 1.0
pH	-	7.2 ± 0.2	7.8 ± 0.1	6.9 ± 0.1
Dissolved Oxygen	mg·L ⁻¹	0.5 ± 0.3	10.5 ± 0.2	0.09 ± 0.01
Chemical Oxygen Demand	mgCOD·L ⁻¹	328.4 ± 65.1	77.3 ± 7.5	39,500 ± 3,200
Total Solids	mgTS·L ⁻¹	782 ± 240	840 ± 48	37,300 ± 100
Total Suspended Solids	mgTSS·L ⁻¹	97 ± 64	32 ± 7	36,800 ± 1,500

The characteristics of the used influents DCW, BDW, and ADS are presented in **Table 3-2**. The BDW was collected during the dry season (June 2019). To mimic BDW during the dry season, DCW (of an average temperature of 9.4 ± 0.1 °C) mixed with ADS was used.

3.3.2 | Delft canal water (DCW)

Table 3-3. Summary of TSS removal efficiencies performed in the down-scaled column DAF units, with the following four diverse types of influents: Delft canal water (Delft, The Netherlands), the Barapullah drain water (New Delhi, India), anaerobic digested sludge (Harnaspolder, Den Hoorn, The Netherlands), and mix of anaerobic digested sludge and Delft canal water.

	Delft canal water (DCW)	The Barapullah drain water (BDW)	Anaerobic digested sludge (ADS)	Mixed water (MIX)
Maximum removal	96%	94%	92%	95%
Minimum removal	45%	69%	66%	29%
Standard deviation	4%	3%	4%	2%
Runs with removal efficiency below 80 %	9	3	4	6
Runs with removal efficiency above 90 %	1	3	2	4

Raw DCW with a minimum and maximum TSS of $30 \text{ mg}\cdot\text{L}^{-1}$ and $500 \text{ mg}\cdot\text{L}^{-1}$ respectively was treated by DAF according to the PBD. TSS removal efficiencies were between 45 and 96% (**Annex B-3**), with a standard deviation of 4% (obtained from the central point runs) and is summarized for all tested influents in **Table 3-3**. The highest suspended solids removal efficiency achieved was $96 \pm 4\%$ when the influent had a TSS concentration of $30 \text{ mg}\cdot\text{L}^{-1}$, temperature of 29 °C, residence time of 1200 s, pH of 7.6, pressure of 5.0×10^5 Pa, coagulant concentration of $5.0 \text{ mg}\cdot\text{L}^{-1}$ and coagulation time of 1800 s. Suspended solids removal efficiency below 80% were considered a low DAF efficiency, which was observed in nine out of fifteen runs in DCW.

Influent particle size and shape were assessed and compared to their respective effluents. DCW influent contained $67 \pm 8\%$ of particles with a diameter below 10 μm , which was the lowest fraction of small particles compared to the other influents. In contrast, a total of $97 \pm 1\%$ of effluent particles were observed to be below 10 μm , representing the highest percentage for all effluents.

Table 3-4. Heat map of ANOVA statistical results showing the effect of influent TSS concentration, temperature, down-scaled column DAF residence time, pH, pressure, coagulant and flocculants concentration, and, coagulation time, for TSS removal efficiencies from all types of influents. Acronym DCW corresponds to Delft canal water, BDW to the Barapullah drain water, ADS to anaerobic digested sludge, and MIX for the mixed influent of Delft canal water and anaerobic digested sludge. Red cells correspond with negative effects and green ones with a positive one. Additionally, in bold are those effects that corresponded to statistical p-values below 0.1.

Independent Variables	DCW	BDW	ADS	MIX	Effect
Total Suspended Solids concentration	12.16	-0.09	-4.03	15.30	High positive effect
Temperature	-0.50		-4.22		
Residence time	15.50	-0.01	4.06	5.80	Neutral effect
pH	2.16		-0.42		
Pressure	5.50	0.02	10.50	15.10	
Coagulant and flocculants concentration	1.16	0.04	1.33	14.80	
Coagulation time	22.16	-3.80	-0.05	7.70	High negative effect

Statistical analysis of the selected performance variables was conducted on each of the four different types of influents. A summary of the effect and p-value of each variable is shown in **Table 3-4**. Statistical significance was considered when p-values were below 10% (0.10). A negative effect means that an increase in the variable leads to a decrease in the total suspended solids removal. Furthermore, for a given influent, a high absolute effect of a variable entitles a more preponderant outcome. DCW had three control variables with a statistically important effect on TSS removal. These variables were TSS concentration, residence time, and coagulation time, with p-values of 0.03, 0.02, and 0.01 respectively. All control variables had a positive (dimensionless) effect, the highest being coagulation time.

3.3.3 | The Barapullah drain water (BDW)

TSS removal efficiencies were between 69 to 94 ± 3% for BDW (**Annex B-3**). Under the same conditions of DCW mentioned above, TSS removal of the BDW only reached 83 ± 3%. Different results were obtained under the same experimental conditions. While the central point parameters were the same for DCW and BDW, removal

efficiency for the latter was 1.7 times higher than the one obtained for DCW, $88 \pm 3\%$ and $51 \pm 4\%$ respectively. Furthermore, in six out of seven runs that had the same conditions for both influents, solids removal of BDW was between 1.2 to 1.9 times higher.

BDW influent had the highest fraction of particles smaller than $10 \mu\text{m}$ when compared to other influents, corresponding to $94 \pm 2\%$ of the total particles. Furthermore, the particle circularity of all influents was similar. Most particles have a circularity above 0.7 and can be considered spheres, $84 \pm 4\%$ on BDW, while the percentage of elongated particles with a circularity value below 0.3 was around 1% for this influent. Only one control variable had a significant effect on TSS removal from BDW. Influent total suspended solids had a negative effect (p-value of 0.06). While an increase in TSS resulted in a decrease in removal efficiency for this influent, the effect was contrary for DCW and the MIX influent.

3.3.4 | Anaerobic digested sludge (ADS)

Suspended solids removal efficiencies were between 66 to $92 \pm 4\%$ for ADS (**Annex B-3**). Nine out of the 15 experiments performed had a TSS removal between 80 and 90%. The maximum removal was obtained when TSS was $500 \text{ mg}\cdot\text{L}^{-1}$, residence time was 1200 s, pressure was $5.0 \times 10^5 \text{ Pa}$, coagulant concentration was $5.0 \text{ mg}\cdot\text{L}^{-1}$, coagulation time of 1800 s, temperature was at $35 \text{ }^\circ\text{C}$, and pH was set at 8.5.

ADS influent had the highest fraction of particles between 10 and $40 \mu\text{m}$ when compared to the other influents ($16 \pm 7\%$), and $6 \pm 2\%$ were larger than $40 \mu\text{m}$. The effluent had the lowest fraction of small particles (diameters below $10 \mu\text{m}$), and the highest fraction of large particles (diameters above $40 \mu\text{m}$), $77 \pm 6\%$ and $5 \pm 1\%$ respectively. All effluents had a high fraction of circular particles, showing values between 78 to 93% of the total number of particles. On the other hand, elongated particles with circularities below 0.3 represented less than 2% of the particle fraction in all effluents.

Pressure, residence time, and coagulants and flocculants concentration had a positive effect on ADS, but only the pressure was significant (p-value of 0.04). When pressure, residence time, or concentration of coagulants and flocculants were increased, higher suspended solids removal was observed from the down-scaled column DAF system. A temperature rise resulted in a negative effect on both the removal of suspended solids in ADS and DCW but was not significant (p-value > 0.1). Besides temperature, pH variations had no statistical effect on any of the tested influents, nor consistency in its positive or negative impact on the effect.

3.3.5 | Anaerobic digested sludge and Delft canal water mix (MIX)

This influent presented the largest number of experiments with high removal efficiencies above 90%, i.e., four out of 15, but the sufficient removal efficiencies (between 80 to 90%) were not extraordinary with 9 out of 15 runs. The TSS removal efficiency varied between 29 and $95 \pm 2\%$ for the mixed influent (**Annex B-3**). Under equal experimental conditions, TSS removal was 1.1 to 1.3 times higher for the MIX than ADS in four out of seven runs. The latter had a better removal only in one run ($87 \pm 4\%$ in comparison to $29 \pm 2\%$ of the MIX influent). The lowest removal efficiency of $29 \pm 2\%$ was obtained under an influent TSS of $500 \text{ mg}\cdot\text{L}^{-1}$, residence time of 1200 s, pressure of $3.0 \times 10^5 \text{ Pa}$, coagulant concentration of $5.0 \text{ mg}\cdot\text{L}^{-1}$, and 1800 s coagulation time.

All effluents but the MIX had a smaller frequency of particles above $40 \mu\text{m}$ when compared to particles in the corresponding influents. Frequencies of particle sizes for the four different influents and their respective DAF effluents can be seen in **Figure 3-2**. Even though elongated particles were predominant in all four influents and their respective effluents, the MIX effluent had the lowest proportion of particles with a circularity above 0.7 ($78 \pm 9\%$) and the highest one with circularity between 0.3 and 0.7 ($19 \pm 5\%$). **Figure 3-3** shows particle images of all influents and effluents, and particle circularity frequency can be found in **Annex B-4**.

For the MIX runs, three independent control variables positively affected the solids removal, i.e., influent total suspended solids (p-value of 0.06), pressure (p-value of 0.06), and coagulant and flocculants concentration (p-value of 0.07). The highest effect was found for TSS concentration (12.16), which means that small changes in influent TSS had the highest impact on suspended solids particle removal of the down-scaled DAF.

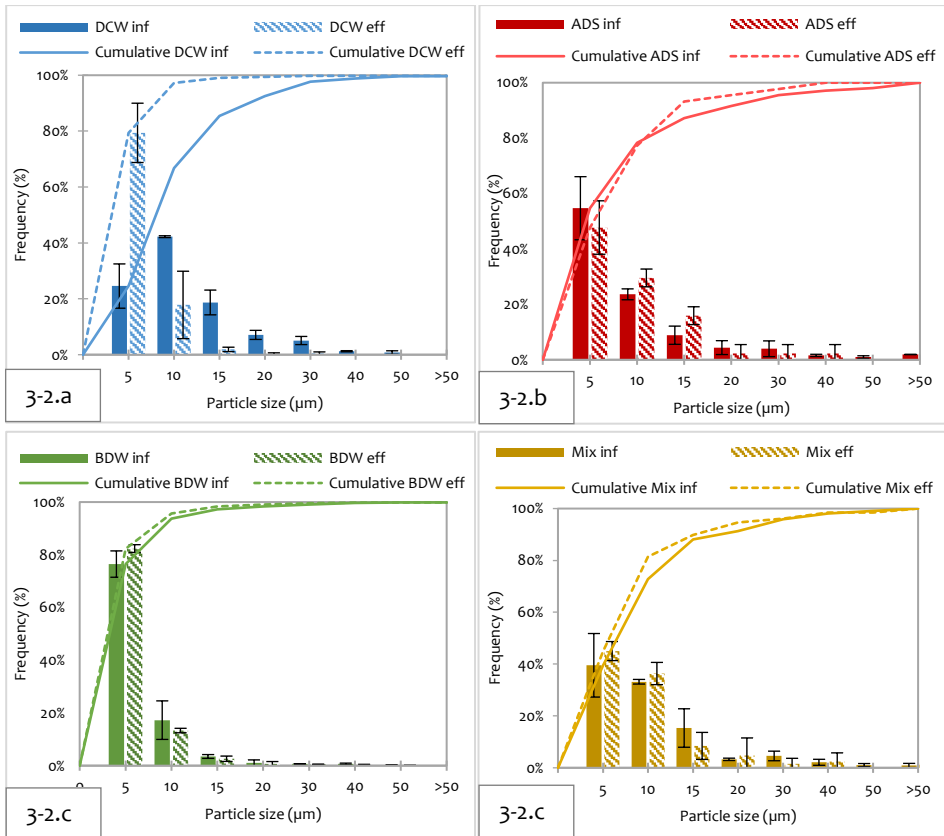


Figure 3-2. Particle size distribution and frequency for all influents (inf) and their respective effluents (eff) were performed at the central point condition of Plackett-Burman Design. Results are based on particle image analysis performed using FIJI-ImageJ. Figures 3-2.a and 3-2.c show the results for Delft canal water and the Barapullah drain, respectively. Both runs were conducted under the following conditions: $270 \text{ mg}\cdot\text{L}^{-1}$, residence time of 990 s, pressure of $4.0 \times 10^5 \text{ Pa}$, coagulant concentration of $252.5 \text{ mg}\cdot\text{L}^{-1}$, and coagulation time of 1200 s. Additionally, Delft canal water had a pH of 7.15 and a temperature of $32 \text{ }^\circ\text{C}$. Figures 3-2.c and 3-2.d show the results for anaerobic digested sludge and mix influent respectively. Both runs were conducted under the following conditions: $2750 \text{ mg}\cdot\text{L}^{-1}$, residence time of 990 s, pressure of $4.0 \times 10^5 \text{ Pa}$, coagulant concentration of $252.5 \text{ mg}\cdot\text{L}^{-1}$, coagulation time of 1200 s. Additionally, anaerobic digested sludge had a pH of 7.8 and a temperature of $30 \text{ }^\circ\text{C}$.

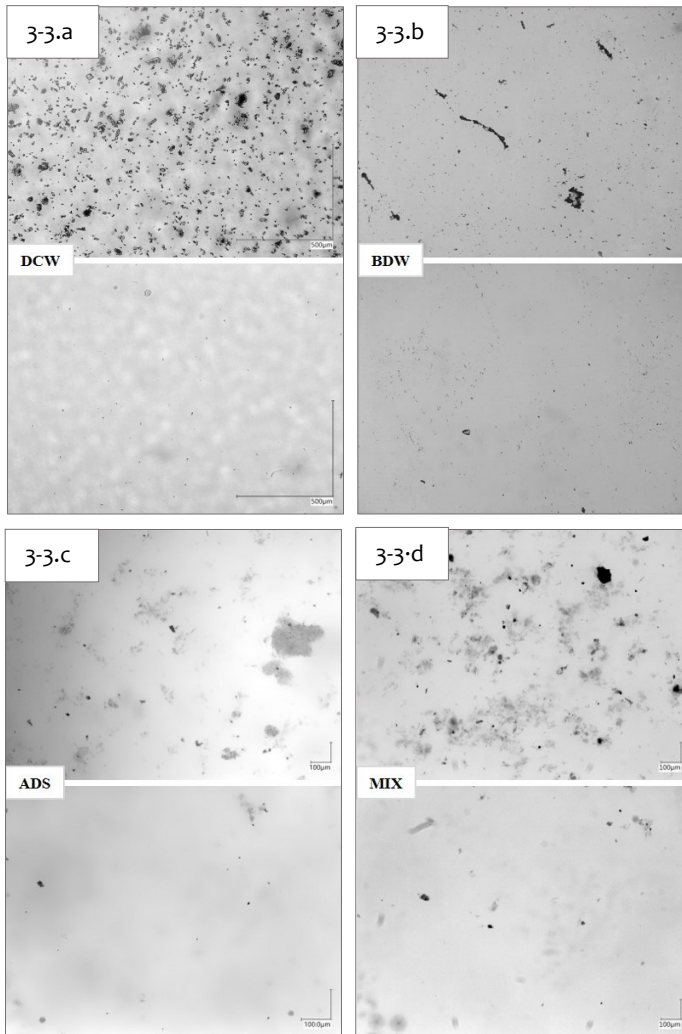


Figure 3-3. Particle images of the four different influents and their respective effluents. For each stream, the top panel is the influent to the DAF, and the bottom panel is the corresponding effluent. All pictures were taken for the runs of the central points (runs seven, eight, and nine), following the Plackett-Burman Design shown in Annex B-2. Figure 3-3.a shows the particles of the Delft canal water (DCW). Figure 3-3.b shows the particles of the Barapullah drain water (BDW), in New Delhi, India. Figure 3-3.c displays particles of the anaerobic digested sludge (ADS) taken from Harnaspolder (Den Hoorn, Delft). Finally, Figure 3-3.d shows the particles of the MIX influent, which entitles a combination of ADS and DCW. All these images were used to analyse particle size and circularity (among other characteristics) with the software FIJI-ImageJ.

3.4 | DISCUSSION

A total of 55 out of 60 experiments showed that removal efficiencies were in the ranges of 50 to 96%, while only 5 experiments had removal efficiencies below 50%. Moreover, 32 out of the 54 experiments had TSS removal efficiency above 80%, which was considered sufficient removal for DAF application. In the study conducted by Penetra and Reali (Penetra et al., 2003), a pilot-scale DAF treating $100 \text{ m}^3 \cdot \text{h}^{-1}$ of the effluent of an anaerobic expanded bed system fed with domestic wastewater, had a suspended solids removal efficiency between 49.4 and 96.4%. Similarly, Cagnetta et al. (2019) investigated the removal of organics and suspended solids on a pilot-scale DAF treating an effluent flow of $2 \text{ m}^3 \cdot \text{h}^{-1}$ from a high-rate activated sludge process of domestic wastewater. The DAF influent had a TSS concentration of $1.0 \text{ g} \cdot \text{L}^{-1}$ and total removal of 78%. Finally, TSS removal reached up to 98.5% on a full-scale DAF treating $188 \text{ m}^3 \cdot \text{h}^{-1}$ of wastepaper-recycling wastewater, with an influent TSS of around $7.0 \text{ g} \cdot \text{L}^{-1}$ (Ansari et al., 2018). Thus, the tested down-scaled column DAF system has a representative removal when compared to pilot and full-scale systems, enabling suspended solids removal studies under down-scaled systems. The results obtained in the down-scaled DAF presented in this work are, therefore, comparable to literature and conventional pilot and full-scale DAF systems. Furthermore, the down-scaled column can be used to predict DAF suitability and definition of the operational conditions. Finally, the down-scaled DAF is of particular use for mathematical models developed to understand the flows and particle removal from different types of wastewaters. This system could be used to contrast the suspended solids removal efficiency obtained from the models.

Aside from achieving a comparable suspended solids removal efficiency to full-scale systems conventionally used in water reuse applications, the down-scaled column DAF proved to be able to efficiently remove suspended solids when located either at the end of the Barapullah drain or after a biological digester (closer to the pollution source). Maximum solids removal for BDW and ADS were 94 and 92% respectively. The down-scaled DAF had a footprint below 0.3 m^2 and was able to handle almost 400 L of influent per day. According to the Central Pollution Control Board of India, daily per capita wastewater production reaches around 220 L in New Delhi, and around 100 L in class I cities (CPCB, 2009). Consequently, the designed column DAF could be used for treating the wastewater produced on a household level, where the surface area is scarce. The focus of the investigation was on DAF suspended solids removal, as a pre-treatment step. Post-treatment for the removal of dissolved organic matter and nutrients (phosphorus and nitrogen) is recommended for further

water utilization. Most biological systems for nutrient removal require the presence of organic matter. Conventionally a 100:5:1 COD:N:P ratio is recommended for aerobic systems (Metcalf et al., 2014). Thus, to enable post-treatment and nutrient recovery, the DAF unit should not remove all organic matter, but mostly the particulate one. Furthermore, systems like wetlands and algae photo-bioreactors (PBR) benefit from the absence of particulate matter (Chen et al., 2018; Langergraber et al., 2003). The potential of DAF as an alternative pre-treatment for water reuse could be useful for policymakers, water authorities, environmental planners, and technologists among others, to reduce the stress on land and drinking water availability, while reducing pollutants concentration in drain water streams.

3.4.1 | Delft canal water versus anaerobic digested sludge suspended solids removal.

DCW and ADS are compared due to their differences in particle characteristics and concentration. While ADS intends to emulate the feed of a DAF system when located after an anaerobic bioreactor, DCW mimics the rainy season conditions of the Barapullah drain. DCW has between 50 to 500 mg·L⁻¹ of suspended solids, whereas ADS TSS concentration tends to be 10 times higher. Moreover, around 75% of ADS solids are organics, while this was only 65% for DCW. Suspended solids characteristics, such as density, size, shape, and organic content have an impact on particle removal by flotation. Based on Navier-Stokes, lower particle densities correspond to lower settling velocities and therefore, higher rising velocities when bubbles collide with particles and form agglomerates (Constantin & Foias, 2020). DCW had an average particle density of $1.077 \pm 0.022 \text{ g}\cdot\text{cm}^{-3}$, while the ADS influent particle density was $1.044 \pm 0.030 \text{ g}\cdot\text{cm}^{-3}$. Benjamin and Lawler (2013) reported that activated sludge from municipal wastewater has a density between 1.01 and 1.10 g·cm⁻³, while Forster-Carneiro et al. (2010) have stated that anaerobic digested sludge from a municipal wastewater treatment plant had a density of 1.054 g·cm⁻³. Particles with lower densities had higher residence time in the column, enhancing the collision chances. Residence time had the highest positive impact on DCW among the other analysed parameters, as shown in **Table 3-4**. Thus, particle density has a high impact on their residence time inside the down-scaled DAF column and consequently on suspended solids removal efficiency. DCW had the highest particle density compared to all tested influents, which explains why this influent had nine out of 15 experimental runs with poor removal efficiency, considered below 80%.

Besides density, suspended solids are assessed based on particle size (diameter), shape, and organic content. Around $97 \pm 1\%$ of the suspended solids from DCW

effluent had diameters below 10 μm , whilst this frequency was $77 \pm 6\%$ for ADS. Both influents had a similar cumulative particle size frequency for particles above 10 μm , as shown in **Figure 3-2**. The best particle removal is achieved when particles and bubbles have similar sizes (Edzwald, 1995). Bubble sizes in DAF (at pressures between 2.0 to 5.0 $\times 10^5$ Pa) can vary from 10 to 140 μm having an average bubble size of around 60 μm (De Rijk & den Blanken, 1994; Edzwald, 1995; Han et al., 2002). Further studies can be done to assess the effect of bubble size distribution on particle removal, in the down-scaled DAF column, and correlate the changes in bubble size distribution with white water pressure.

Ellipsoidal particles cover a greater horizontal area than circular ones, enabling greater collision possibilities with bubbles (Gjaltema et al., 1997). Thus, higher removal by flotation is expected when particles resemble an ellipse in contrast to when they are circular. When compared to the other influents, DCW had the highest number of ellipsoidal particles with a circularity below 0.3 and the lowest number of round ones (**Annex B-4**). Furthermore, particles with the lowest circularities corresponded overall to the ones with higher Ferret's number and hence, greater shape irregularity. This enhances the chances that after bubbles collide with particles, they form a more stable agglomerate. Therefore, due to the irregularity and elongation of the particles, an increase in particle concentration can also lead to higher removal efficiencies in flotation, as seen in DCW and the MIX influent.

Coagulant and flocculants concentration and coagulation time had a positive effect on DCW. The coagulant used was calcium hydroxide (lime), an inorganic compound classified as a strong base with low solubility (Farhad & Mohammadi, 2005). Lime addition showed to be an effective coagulant due to the increase in particle zeta potential when added to several Calcium Silica Hydrates synthesized from silica, and dehydrated and decarbonated calcium hydroxide (Viallis-Terrisse et al., 2001). Both DCW and ADS had negative zeta potentials of -11.6 ± 1.1 and -18.2 ± 1.0 mV respectively. Similarly, air bubbles have a negative zeta potential between 0 to -58 mV when formed in diverse conditions and mediums (Elmahdy et al., 2008; Fan et al., 2004; Li & Somasundaran, 1991; McTaggart, 1922; Yang et al., 2001). According to Han et al. (2001), collision efficiency between particles and bubbles increases when particle zeta potential is close to zero. Coagulants, such as lime, are usually added to reduce particle surface charge to zero, promoting particle-particle or particle-bubble collisions. Since ADS had a higher concentration of particles than DCW, and higher absolute zeta potential, more coagulant is needed for ADS than for DCW to increase particle zeta potential. Thus, to achieve high TSS removal, an increase in coagulants

and flocculants concentration can be expected for the Barapullah drain water during the dry season, compared to the rainy season.

Flocculation is used after coagulation to promote the formation of larger flocs. In contrast to inorganic flocculants, organic ones do not harm the biomass (sludge) with metal salts (Vandamme et al., 2015), which is advantageous for biological post-treatment of the separated suspended (bio)solids. Cellulose-based flocculants are promising due to their biodegradability, abundance, and low cost. Furthermore, cellulose has a neutral charge and for this type of polymeric substance, bridging has been considered the main flocculation method (Kitchener, 1972). The time and concentration needed to promote particle bridging vary substantially based on particle characteristics. Coagulation and flocculation time had the highest (and statistically important) positive impact on DCW, while it had a mostly neutral effect on ADS (**Table 3-4**). The maximum coagulation and flocculation time in these experiments was 30 minutes, in comparison to the 60 to 120 minutes reported in other works (Agarwal et al., 2001; Mishra et al., 2002). Thus, coagulation and flocculation time might not have been enough to promote the formation of bigger flocs. The impact of $\text{Ca}(\text{OH})_2$ and cellulose on zeta potential and TSS removal of all influents at different concentrations and retention times should be assessed in further research.

3.4.2 | The Barapullah drain water versus mix influent suspended solids removal.

Nine out of the fifteen runs of BDW had a TSS removal between 80 to 90%, while for the MIX influent, this value was reduced to five (**Table 3-3**). The MIX influent was selected to represent the Barapullah drain over the dry season, where the concentration of pollutants and solids is high, while the BDW influent was tested during the monsoon season. Suspended solids content had an important impact on removal for three of the influents but not the same expected effect. For BDW, an increase in the solids content was linked with a decrease in the removal efficiency (negative effect). The opposite happened for the Mix influent, where characteristics of the ADS (charge, size, shape, and organic content) are expected to be dominant.

BDW was the influent with the highest fraction of particle diameters below 10 μm , $94 \pm 2\%$ versus $73 \pm 11\%$ on the Mix influent (**Figure 3-2**). This difference in particle size could explain the negative impact of influent TSS concentration on BDW removal efficiencies. From the effluent particle size distribution, the fraction with diameters below 10 μm is poorly removed in the down-scaled DAF set-up. While both influents

have similar particle shapes, the high fraction of small particles (below 10 μm) of BDW implies lower chances for collision between particles and bubbles. According to Edzwald (1995), particle collection efficiency depends on the transport of the particle to bubble surfaces and is governed by Brownian diffusion, interception, and sedimentation (when particles' and bubbles' diameters are less than 100 μm). Small particles are mainly governed by Brownian diffusion (random movement). Collision efficiency between different particle sizes and a bubble is shown in **Annex B-5**. To promote interception and flotation (or sedimentation) of particles, the interaction between particles and bubbles is key. Bigger particles of up to 100 μm have higher chances to collide with microbubbles (Edzwald, 1995). Thus, if an influent has a big share of small particles, an increase in the influent suspended solids can lead to a decrease in removal efficiency, due to the lack of available surface area needed to promote collision between particles and bubbles.

Flotation and sedimentation of particle-bubble agglomerates also depend on their density, since they determine the agglomerate density, and therefore, flotation velocity (Constantin & Foias, 2020). BDW had the lowest average particle density of $1.004 \pm 0.005 \text{ g}\cdot\text{cm}^{-3}$ when compared to the other influents. The MIX influent solids are expected to have a similar density to ADS ($1.044 \pm 0.030 \text{ g}\cdot\text{cm}^{-3}$). For the same particle size and shape (spheres), a solid with a density of $1.044 \text{ g}\cdot\text{cm}^{-3}$ settles down almost 10 times faster than a particle with a density of $1.004 \text{ g}\cdot\text{cm}^{-3}$ ($0.90 \text{ cm}\cdot\text{h}^{-1}$ versus $0.12 \text{ cm}\cdot\text{h}^{-1}$ respectively for 10 μm particles). Since the average diameters for bubbles and particles of all influents are around 60 and 10 μm respectively, the moment a particle collides with a bubble, the floating velocity is mostly governed by the bubble diameter. A higher particle density implies higher settling velocities, which can be linked with shorter times in the DAF column. Hence, fewer chances of collision with bubbles. Thus, a greater collision between bubbles and particles can be expected for the influent with the lowest particle density (BDW). This is aligned with what was observed for the BDW, where the number of experiments with TSS removal efficiencies above 80% (sufficient) was the highest.

An increase in bubble concentration enhances the chances of collision (Edzwald, 2010). White water pressure is directly linked with bubble concentration and size. According to Henry's law; air concentration in the liquid depends on set pressure, temperature, and Henry's constant (van 't Hoff, 1884). The amount of microbubbles formed upon pressure release to atmospheric conditions directly relates to the dissolved air concentration under pressurized conditions. For example, the dissolved air concentration increases 1.6 times when pressure changes from 3 to 5 $\times 10^5 \text{ Pa}$.

3

Next to more microbubbles formation at higher pressure, this phenomenon is enhanced due to a decrease in average bubble size at increased pressures up to 5.0×10^5 Pa (De Rijk & den Blanken, 1994; Han et al., 2002). De Rijk and den Blanken (1994) found that the average bubble diameter changed from 107 to 74 μm at 3.0 and 5.0×10^5 Pa respectively. The rising velocity of the bubbles will decrease with microbubble size, according to the Navier-Stokes equation (Constantin & Foias, 2020), which will enhance the residence time in the column and thus the chance for collision. Considering the dissolved air concentration at each pressure, white water flow, the bubble diameters, and the air density at 20°C , the number of bubbles generated at 3.0×10^5 Pa and 5.0×10^5 Pa in the experiment were 9.4×10^7 and 4.7×10^8 respectively. Thus, an increase in pressure has the following cumulative effects on air bubbles: an increase in quantity due to increased gas solubility, a decrease in size, and thus a decrease in rising velocity. All three aspects are conducive to particle and bubble collision. The stability of floc and bubble agglomerates, however, mostly depends on particle and bubble charge and therefore, appropriate coagulation and flocculation, as described in **section 3.4.1**.

The MIX influent has more than 99% of its particles coming from ADS, thus, coagulation and flocculation are expected to behave similarly to ADS. Organic content and particle zeta potential are key aspects to further assessing and understanding the effect of coagulants and flocculants concentration and time. However, these two characteristics were not possible to measure on BDW, due to the unavailability of technical equipment in-situ. BDW is expected to have a high concentration of inorganic solids (clay), and thus it is expected to have a negative zeta potential.

3.5 | CONCLUSIONS

A Dissolved Air Flotation (DAF) has been studied in a down-scaled column system as part of an open sewage treatment train to recover water, for the Barapullah drain in New Delhi (India). Four different types of influents were tested. Three influents resemble the Barapullah drain seasonal variations in composition, BDW, DCW, and MIX influent (combination of DCW and ADS). The fourth tested influent (ADS) mimics the feed of DAF when located after an anaerobic bioreactor or closer to the pollution source (household level). Design of experiments was used as a tool to assess the effect of a set of control variables on the down-scaled DAF suspended solids removal, namely suspended solids, temperature, pH, residence time, pressure, coagulants and

flocculants concentration, and coagulation time. Below are the conclusions from the study.

- Suspended solids removal obtained from the down-scaled DAF are comparable to full-scale systems. The use of design of experiments proved to enable the analysis of a set of seven DAF performance control variables (influent TSS concentration, pH, temperature, residence time, pressure, coagulant and flocculant concentration and, coagulation time), obtaining suspended solids removal that fluctuates from 29 to 96%. DAF high suspended solids removal is in accordance with requirements for a post-treatment focus on nutrient removal.
- The Barapullah drain suspended solids were efficiently removed by a DAF system. The maximum TSS removal efficiency obtained was $96 \pm 4\%$ for DCW. Similarly, the maximum BDW TSS removal was $94 \pm 3\%$, whilst for the MIX influent TSS removal reached $95 \pm 2\%$. Furthermore, DAF proved to be efficient in the removal of TSS when located after an anaerobic bioreactor (ADS influent) or next to the pollution source, with maximum removal of $92 \pm 4\%$.
- Particles with a diameter below $10 \mu\text{m}$ and more rounded shapes are less prone to be removed by DAF. Small particles' collision with air bubbles is governed by Brownian diffusion. They have fewer chances of collision with bubbles and less available surface area to attach to bubbles, even when their small size allows them to have longer residence time inside the down-scaled column. All tested influents had effluents with a high frequency of round particles and diameters below $10 \mu\text{m}$, above 78 and 77% respectively.
- The positive or negative effect of DAF control variables on suspended solids removal depends on the influent characteristics. An increase in pressure had a positive effect on all influents' TSS removal, and a significant impact on the most concentrated influents, ADS and MIX. Influent TSS concentration had a variable effect, due to the difference in density, size, shape, charge, and organic matter of particles, in the tested influents. Finally, the addition of $\text{Ca}(\text{OH})_2$ and cellulose as a coagulant and organic flocculant respectively had a positive impact on the TSS removal of all influents.
- The easy availability of materials to build the system, low cost of analytical methods, and usage of free software to measure particle size and shape,

made the down-scaled DAF system a promising tool to test full-scale DAF performance, for inflows as low as $15 \text{ L}\cdot\text{h}^{-1}$.

- The robustness and compactness of DAF installations, in combination with the high hydraulic loading rate and low TSS concentration in the effluent, make DAF systems useful for the pre-treatment of open-drain sewage. Due to the DAF's small surface area and high suspended solids removal, it could be located either downstream or closer to the pollution source. The knowledge of DAF usage as an alternative pre-treatment for water reuse could be beneficial for policymakers, water authorities, environmental planners, and technologists, among others, to reduce the stress on land and drinking water availability, while minimizing pollutants concentration in drain water streams.



Lab-scale micro-aerated anaerobic membrane bioreactor

4

Effects of low oxygen dosages on an anaerobic membrane bioreactor, simulating the oxygen supply in an anaerobic digester-dissolved air flotation (AD-DAF) system

This chapter is an adapted version of Piaggio, A. L., Sasidhar, K.B., Khande, P., Balakrishnan, M., van Lier, J. B., de Kreuk, M. K., & Lindeboom, R. E. F. (*Under Review*). Effects of low oxygen dosages on an anaerobic membrane bioreactor, simulating the oxygen supply in an anaerobic digester-dissolved air flotation (AD-DAF) system. *Submitted to Environmental Science and Technology*.

ABSTRACT

This study reports the effects of micro-aeration on a laboratory-scale AnMBR (MA-AnMBR) fed with synthetic concentrated domestic sewage. The imposed oxygen load mimics the oxygen load coming from a dissolved air flotation (DAF) unit, replacing the membrane filtration unit of an AnMBR, establishing an anaerobic digester - DAF (AD-DAF) system. Results showed a reduced COD concentration in the MA-AnMBR effluent in comparison to the AnMBR effluent, from 90 to 74 mgCOD·L⁻¹, and a concomitant 27% decrease in biogas production. The MA-AnMBR effluent ammonium (NH₄⁺) concentration increased by 35%, to 740 mgNH₄⁺·N·L⁻¹, indicating a rise in the hydrolytic capacity. Furthermore, the MA-AnMBR biomass seemingly adapted to an increased oxygen load, which corresponded to 1% of the influent COD load. Concomitantly, an increase in the superoxide dismutase activity (SOD) of the biomass was observed. Meanwhile, negligible changes were observed in the specific methanogenic activity (SMA) of the micro-aerated biomass that was subjected to an oxygen load equivalent to 3% of the influent COD load in batch tests. The obtained results showed that an AD-DAF system could be a promising technology for the treatment of concentrated domestic wastewater, improving sewage sludge hydrolysis and overall organic matter removal when compared to an AnMBR.

4.1 | INTRODUCTION

Anaerobic digestion (AD) is a widely used technology for wastewater treatment due to its low sludge production when compared to aerobic treatment (up to one-tenth), the nutrient-rich effluent, and the production of energy as biogas (van Lier et al., 2008a). Amongst the AD technologies, the anaerobic membrane bioreactor (AnMBR) is a promising alternative to treat municipal wastewater from a resource-oriented perspective (van Lier, 2008). AnMBR units were first developed in the late 1980s for industrial wastewater treatment and are now considered one of the emerging anaerobic technologies that generate high-quality effluents of interest for subsequent reuse (Li, 1985). The principle of an AnMBR is a mixed anaerobic bioreactor connected to a physical membrane separation unit retaining all suspended solids.

Various studies showed 80 to 99% COD removal from municipal wastewater using an anaerobically operated CSTR combined with either a side-stream or submerged membrane (Aslam et al., 2022; Ozgun, Dereli, et al., 2013). Furthermore, a pilot-scale submerged AnMBR treating sewage from the city of Valencia, Spain, produced an effluent with 25% higher ammonium and above 85% lower sulphate (SO₄) and COD concentrations than the influent, whilst the phosphate removal was negligible (Giménez et al., 2011). Even though a high SO₄ removal was achieved, it was converted into hydrogen sulphide, which is considered a contaminant gas that hampers biogas utilization (Abatzoglou & Boivin, 2009).

The use of AnMBR for sewage treatment can result in high COD removal and a solids-free effluent, but the technology has considerable constraints, which are linked to membrane fouling, flux limitations, increased process complexity, and higher costs related to capital investment and operation, compared to conventional anaerobic technologies (Ozgun, Dereli, et al., 2013; van Lier, 2008). In fact, all constraints are linked to the membrane filtration device, which is considered limiting for the treatment capacity.

The use of membranes to separate solids and liquids is one of the main hydraulic constraints of an AnMBR. Even though the footprint of membrane units is relatively small, large membrane area is required in municipal wastewater treatment (Ozgun, Dereli, et al., 2013). Moreover, fluctuations in influent organic loading rate (OLR) and hydraulic flow may negatively impact the sludge filterability and the membrane filtration capacity, decreasing the permeate flux (Dereli et al., 2012). Most solids' physical separation units in wastewater treatment plants are based on screening,

flocculation, filtration, adsorption, sedimentation, or flotation (Metcalf et al., 2014). Among these, dissolved air flotation (DAF) units have a small footprint and are characterised by a high removal of suspended solids under a wide variety of HRTs and OLRs (Kiuru, 1990). When located after a pilot-scale anaerobic digester treating domestic wastewater, DAF removal of suspended solids was reported to reach 96% (Cagnetta et al., 2019). Moreover, previous research showed that a laboratory-scale DAF could remove up to 95% of the influent total suspended solids (TSS) in the range of 0.03 - 5.0 g·L⁻¹, resembling the TSS content of municipal wastewater and the real wastewater from our project target area, Barapullah drain in New Delhi, India (Piaggio et al., 2022). Hence replacing the membrane unit of an AnMBR for a DAF, and returning the flotation layer to the anaerobic reactor, may ensure high TSS retention while overcoming the AnMBR limitations. However, the O₂-saturated flotation layer may negatively impact the anaerobic conversion process.

4 Although methanogens are strict anaerobes (van Lier et al., 2008a), research suggests that exposure of anaerobic biomass to limited amounts of oxygen may only have a negligible impact (Botheju & Bakke, 2011). Limited aeration in a thermophilic digestion system, treating municipal solid waste, showed minor differences in the microbial community when compared to a complete anaerobic system (Tang et al., 2004). Kato et al. (1993) suggested that the tolerance of methanogens to oxygen was mainly due to the activity of facultative bacteria located at the outside of granular consortia in an expanded granular sludge bed reactor. Brioukhanov et al. (2002) found high specific superoxide dismutase enzyme (SOD) activities in both methanogens and acetogens. SOD catalyses the disproportionation of the superoxide radical, preventing toxic conditions in cells due to oxygen reduction. The observed increased SOD activity suggests that methanogens may adapt to limited oxygen concentration.

Various authors suggest that micro-aeration in anaerobic digesters can be advantageous for specific (bio)chemical conversion processes (Botheju & Bakke, 2011; Giroto et al., 2018; Sasidhar et al., 2022). There is no alignment between researchers in what refers to micro-aeration. Nguyen and Khanal (2018) defined micro-aeration when the system ORP is between -200 to -300 mV, while Botheju and Bakke (2011) preferred the terminology of “*limited aeration*” to talk about a process where a certain amount of oxygen is introduced to a basically anaerobic biochemical process. Limited aeration (below 2% v/v) incorporated in the headspace or liquid phase of a pilot plant digester processing mixed sludge, showed 98% lower hydrogen sulphide concentrations in the biogas with a negligible impact on the methane yield

(Díaz et al., 2011). Using micro-aeration in a laboratory-scale reactor, inoculated with mesophilic anaerobic sludge, Lim and Wang (2013) found that the methane yield increased by more than 20% when fed with food-waste and concentrated black water. Furthermore, an intermittently micro-aerated laboratory-scale anaerobic digester CSTR, fed with lignocellulosic feedstock, showed a 50% reduction in volatile fatty acids (VFA) accumulation in comparison to the no micro-aeration conditions, under an organic loading rate (OLR) of 5 gVS·L⁻¹·d⁻¹ (Nguyen et al., 2019). On the other hand, Botheju et al. (2010) found a negative effect on the methane yield when an oxygen load equivalent to 10% of the influent COD was added to a laboratory-scale CSTR.

To the authors' knowledge, no research has been conducted on the replacement of the membrane unit in an AnMBR with a DAF unit, establishing an anaerobic digester - DAF (AD-DAF) system. Due to constraints related to DAF design loading rates and air bubble sizes in downscaled reactor systems (Raheem et al., 2015), it is not possible to test an AD-DAF system at laboratory-scale. Therefore, in our present study, typical DAF oxygen fluxes were calculated and experimentally simulated in a laboratory-scale intermittently micro-aerated AnMBR (MA-AnMBR), fed with synthetic concentrated domestic sewage. The objective of this study is to assess the performance of an MA-AnMBR, mimicking the impact of oxygen supply in an AD-DAF system. The research was focused on the changes in nutrient removal efficiency, especially nitrogen and phosphorus, the overall performance of the MA-AnMBR under various total O₂ fluxes (in the micro-aeration range), and the microbial community shifts in response to these.

4.2 | MATERIALS & METHODS

4.2.1 | Experimental set-up and tested influent

A laboratory-scale AnMBR was set-up to study the effects of micro-aeration in AD. Here, micro-aeration was defined as the aeration range at which no significant changes in the oxidation-reduction potential (ORP) were observed in the reactor (below 10%). The AnMBR consisted of an anaerobic CSTR connected to a side stream inside-out tubular ultrafiltration PVDF membrane, with a pore size of 30 nm (Helyx, Pentair, Minnesota, United States), an inner diameter of 5.2 mm and 640 mm length. The CSTR had a liquid volume of 6.5 L and 1.5 L of headspace. The AnMBR was equipped with feed, permeate extraction, aeration, and recirculation pumps (Watson Marlow 120U and 323U, Falmouth, United Kingdom). Reactor ORP, pH, and temperature were continuously measured with a Memosens CPS16D (Endress+Hauser, Reinach, Switzerland). The operational conditions of the AnMBR

are described in **Table 4-1**, and the reactor setup and scheme can be seen in **Figure 4-1**.

Table 4-1. AnMBR operational conditions.

	Unit	Value
Feed flow	L·d ⁻¹	2.5
Permeate flow	L·d ⁻¹	2.3
Reactor volume	L	6.5
Temperature	°C	37
Hydraulic retention time	d	2.6
Solids retention time	d	28
Organic loading rate	gCOD·L ⁻¹ ·d ⁻¹	1.9
Recirculation flow	L·d ⁻¹	1300
Cross flow velocity	m·s ⁻¹	0.6
Membrane flux	LMH	10.0

The synthetic influent composition was adapted from Ozgun et al. (Dereli et al., 2012) and adjusted to an average COD of $5.2 \pm 0.6 \text{ g}\cdot\text{L}^{-1}$, $60 \pm 9 \text{ mgPO}_4^{3-}\cdot\text{P}\cdot\text{L}^{-1}$ of phosphate, and $249 \pm 54 \text{ mgNH}_4^+\cdot\text{N}\cdot\text{L}^{-1}$ ammonium concentration. Feed composition is further detailed in **Annex C-1**. The AnMBR was inoculated with approximately 3.5 L of sludge from a pilot-scale blackwater anaerobic reactor located at NIOO-KNAW facilities (Wageningen, Netherlands). The sludge had a COD of $43.7 \pm 3.4 \text{ gCOD}\cdot\text{L}^{-1}$, total suspended solids (TSS) of $45.8 \pm 0.9 \text{ gTSS}\cdot\text{L}^{-1}$ and volatile suspended solids (VSS) of $36.0 \pm 1.2 \text{ gVSS}\cdot\text{L}^{-1}$ (Kuramae et al., 2020).

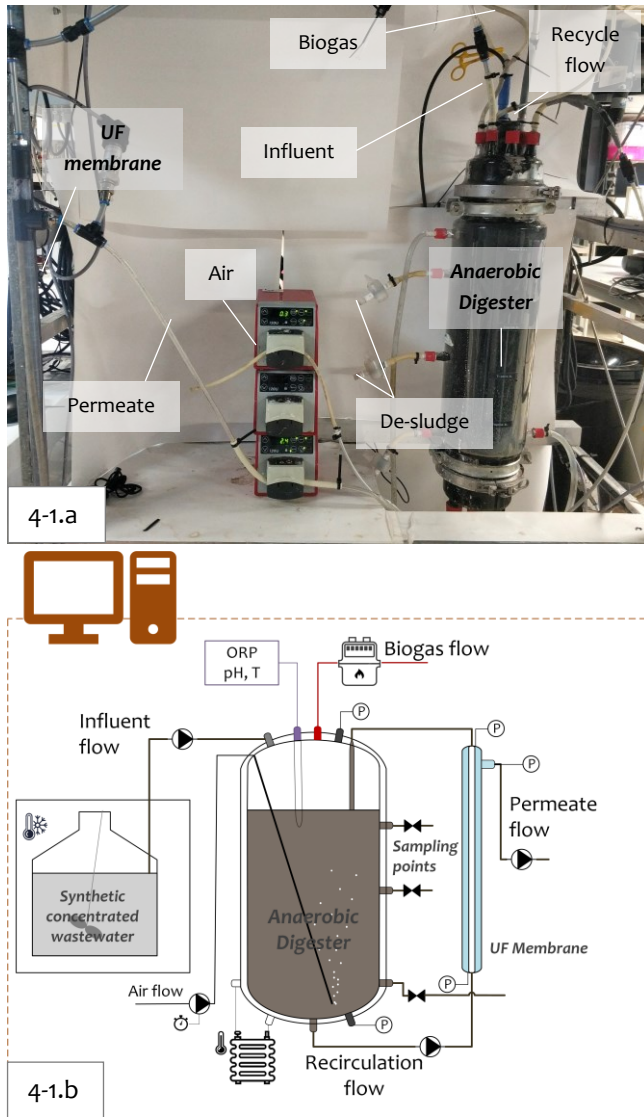


Figure 4-1. Anaerobic membrane bioreactor (AnMBR) and Micro-aerated AnMBR (MA-AnMBR) set up. Figure 4-1.a shows the laboratory-scale set up, while Figure 4-1.b shows the schematic representation of the laboratory-scale unit. The system is composed of a side stream inside-out tubular ultrafiltration membrane, with a pore size of 30 nm, and a CSTR (Anaerobic Digester) of 6.5 L liquid. The system was equipped with a probe to continuously measure ORP, pH and temperature, and a biogas meter (Ritter, Germany). The AnMBR and MA-AnMBR were operated under similar conditions, but the MA-AnMBR had an intermittent air flow. The aeration was introduced in the liquid phase of the anaerobic digester in three cycles of four hours, and it corresponded to an oxygen-over-influent COD load of 1.0%.

Reactor periods

In the first operational period, the AnMBR was operated under complete anaerobic conditions for 180 days (referred to as “AnMBR state”). Sludge extracted from this period was named S₀. In this research, micro-aeration is defined as the introduction of a certain amount of air into an anaerobic biochemical process, where ORP changes are below 10%. Micro-aeration of the AnMBR started afterwards and was performed in steps to acclimate the biomass to the aeration dose. Based on the AD-DAF system mass balance, the given final daily aeration was calculated to be 1.0% of oxygen in comparison to the total COD load, considering an air oxygen content of 21% at standard temperature and pressure conditions. Reactor aeration was directly performed in the liquid phase via intermittent cycles of four hours of aeration, followed by four consecutive hours of no aeration. Aeration intensity was gradually increased, where each aeration step lasted three HRTs. The airflow increases in each step corresponded to one-third of the final aeration: 0.3, 0.6, and 1.0% when compared to the influent COD. Sludge extracted from the reactor at each aeration step (airflows of 0.3, 0.6, and 1.0%) were named S₁, S₂, and S₃ respectively. Once the micro-aeration flux of 1% influent COD was reached, the MA-AnMBR was continuously operated under these conditions. The MA-AnMBR was considered to operate at stabilised performance after 100 days from the first aeration step. Thus, the period between the first added aeration and the stable conditions was called “Adaptation”, while the period under stable micro-aeration conditions was denominated “MA-AnMBR state”. This period lasted 300 days and the sludge extracted in this period was denominated S₄. A schematic representation of the reactor periods is shown in **Figure 4-2**.

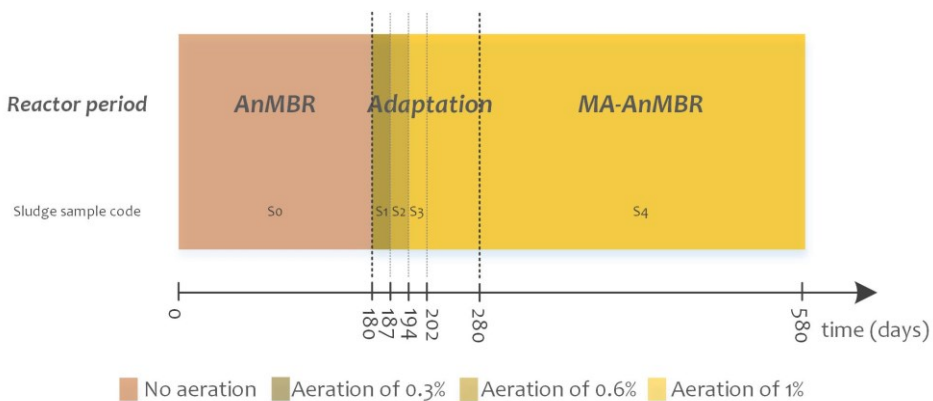


Figure 4-2. Schematic representation of reactor periods.

4.2.2 | Analytical methods

Total and volatile solids were measured according to standardised methods (American Public Health Association, 2013), and analysis was performed in triplicates. Sludge temperature, pH, and ORP were continuously measured with a Memosens CPS16D (Endress+Hausser, Reinach, Switzerland). COD measurements were done using HACH Lange test kits LCK 314, 514, and 014 (HACH, Tiel, The Netherlands). Total phosphorus (TP), orthophosphate (PO₄³⁻-P), total nitrogen (TN), ammonium-nitrogen (NH₄⁺-N), and nitrate-nitrogen (NO₃⁻-N) were measured with HACH Lange test kits (LCK 349, LCK238 LCK 303, and LCK 339). Samples were taken bi-weekly.

The composition of volatile fatty acids (VFA) in samples extracted from effluent and sludge was analysed using Agilent tech 7890A gas chromatography (GC) (Agilent, Santa Clara, CA, U.S.A.) with helium as a carrier gas. The gas flow rate was 2.45 mL.min⁻¹, the pressure was 0.76 bar, and detector and injector temperatures were 225 °C and 240 °C, respectively. The samples were collected in 2 mL Eppendorf every week and measured following the procedure described by García Rea et al. (2020).

For biogas analysis, weekly gas samples were collected using 1.5 mL gas-lock syringes after which they were immediately injected into a GC (Agilent, Santa Clara, CA, U.S.A.) with a thermal conductivity detector (TCD). To analyse the composition of the gas samples, two separate columns, HP-PLOT U and a Molesieve GC column (Agilent 19095P-MS6, Santa Clara, CA, U.S.A) of 60 m x 0.53 mm x 200 µm were used. Helium was used as a carrier gas at a flow rate of 10 mL.min⁻¹. The operational temperatures for the injector and detector were 40 °C and 200 °C, respectively (Ceron-Chafla et al., 2020).

Protein and carbohydrates degradation in serum bottles

Soluble and total protein concentrations in the reactor were measured via the modified Lowry method (Frølund et al., 1995), while soluble and total carbohydrate concentrations were measured using the anthrone-sulfuric acid method by Dubois et al. (1956), in serum bottles of 180 mL. A total of four aeration conditions were performed in triplicate, during an incubation period equivalent to the AnMBR solids retention time (SRT), i.e., 28 days. Tests were performed to mimic the micro-aeration conditions of the laboratory-scale MA-AnMBR, but also to compare the effect of different aeration in the degradation of proteins and carbohydrates. Thus, four aeration conditions, called Ovalbumin A0-A3, were tested. The supplied oxygen represented 0, 1, 2, and 5% of the substrate COD. As inoculum, 100mL of sludge from

the AnMBR period was used. The selected substrate was ovalbumin and micronutrients, mimicking the AnMBR synthetic influent concentrations. Ovalbumin was chosen as the main substrate due to its high ratio of added proteins to the influent. An inoculum over substrate ratio of 2 was considered, and the serum bottles were placed in a shaker at 110 rpm and 36 °C (Spanjers & Vanrolleghem, 2016). Aeration was incorporated in pulses during the first six experimental days, into the liquid phase. Produced biogas was removed twice per day during the first 10 days, and afterwards daily. Proteins and carbohydrates were measured at the beginning of the experiment and after 28 days of incubation. Finally, the measured concentrations of proteins and carbohydrates were converted to COD assuming the typical composition of protein ($C_{14}H_{12}O_7N_2$) and carbohydrate ($C_{10}H_{18}O_9$), following Sophonsiri and Morgenroth (Sophonsiri & Morgenroth, 2004).

Rheometry and particle size distribution (PSD) analysis

A rotational rheometer model MCR 302 (Anton Paar GmbH, Graz, Austria) was used to measure shear stress and shear rate. A smooth measuring cylinder model B-CC27 (0.026 m diameter) and a measuring cup model C-CC27 (0.030 m diameter) were used. A volume of 15 mL of sludge was used to perform the assay, which was done at 35 ± 0.2 °C. Since the sludge samples were stored in the fridge, a pre-shear stage was selected before starting the rheometric analysis. The methods followed were as described by Gonzalez et al. (2022).

PSD was assessed with a Microtrac Bluewave diffraction analyser (Malvern Instruments Ltd., UK), measuring particles between 0.01 to 2000 μm , via a light scattering technique. The results are shown as volume-based PSD and are indicative of the presence of large-size particles. When PSD is expressed in this way, small particles are neglected due to their insignificant volume when compared to larger particles. PSD was reported as percentiles D_{10} , D_{50} , and D_{90} , where D_{10} represents the particle diameter of which only 10% of the particles are smaller than the given diameter.

Specific methanogenic activity (SMA)

SMA tests were performed to analyse the effects of different aeration rates on the SMA of the AnMBR sludge, under the different operating periods: AnMBR state, adaptation, and MA-AnMBR state. The tests were carried out for five triplicate sludge samples extracted from the laboratory-scale reactor. The first tests were carried out with the inoculum of AnMBR (So). The second set of tests was performed using

adapted sludge as inoculum (S1-S3). Finally, the last inoculum used was MA-AnMBR (S4). All sludge samples were stored at 4 °C before the SMA test.

The tests were performed with an automated methane potential test system (AMPTS, Bioprocess Control, Sweden), at 37°C. Bottles of 250 mL with a liquid volume of 200 mL were used. Acetate, micro, and macronutrients were added as substrates in accordance with the method described by Spanjers and Vanrolleghem (2016), and different aerations were incorporated in pulses. The aeration pulse was injected at the beginning of the SMA test in the liquid phase, and the bottles were sealed for 20 minutes while being constantly mixed at 80 rpm. After this period, the connections between the bottles and the AMPTS were opened. Gas measurements were done after the first hour of operation. Three aerations were selected to test the SMA of the sludge and represented a ratio of oxygen over substrate COD of 3, 8 and 13%. These aerations were selected firstly to mimic the conditions of the laboratory-scale MA-AnMBR (3%), and to exceed those conditions and test the inhibition on methane production due to different oxygen contents. Since the tests were performed in serum bottles of 250 mL, the volume error of injecting aerations below 3% of the substrate COD was considered inappropriate and therefore, the minimum given aeration was set at 3%. All aeration conditions were compared to a positive control where no aeration was added. The calculated amount of injected air was based on oxygen content in the air of 21%, and an oxygen density of 1.43g·L⁻¹ at 20°C (room temperature).

Superoxide dismutase (SOD) activity analysis

SOD activity of AnMBR inoculum sludge from NIOO-KNAW and the MA-AnMBR sludge was measured using a colourimetric method by Invitrogen (EIASOD, Thermo Fisher Scientific, Waltham, MA, U.S.A). Sample preparation was performed in triplicates, with a dilution factor of 10 and following the kit guidelines. The samples were kept in a freezer at -20 °C until further analysis on the 96 well-plate. One SOD unit is defined as the amount of enzyme causing inhibition of 50% in the reduction of 1.5 mM Nitro blue tetrazolium, in the presence of riboflavin at 25°C and pH 7.8. SOD values were obtained in Units·mL⁻¹, but final SOD activity was expressed in SOD Units·mgProtein⁻¹ as per Kato et al. (1997).

4.2.3 | Chemical speciation

PhreeqC software was used to model the effect of micro-aeration on biogas composition and phosphorus speciation (Parkhurst & Appelo, 2013). PhreeqC enables the calculation of saturation indexes and distribution of aqueous species (among

others), based on detailed influent characteristics and composition. The developed code was applied to four different scenarios, corresponding to two scenarios of the AnMBR, and two of the MA-AnMBR states. The input data were derived from the synthetic influent characteristics and the laboratory-scale reactor characteristics (reactor and headspace volume of 6.5 and 2.0 L, respectively). The PhreeqC code is described in the supplementary material, **Annex C-2**. Ammonium concentration in the liquid phase was taken from the reactor analytical measurements, 583 mg·L⁻¹ and 740 mg·L⁻¹ for the AnMBR and the MA-AnMBR stable periods, respectively. Two initial biogas conditions were selected for each reactor period. Both conditions only include carbon dioxide and methane, in ratios of 50:50 and 20:80. The final analysed results were considered at pH values like the laboratory-scale experiments, i.e., 7.42 and 7.65 for the AnMBR state and MA-AnMBR state, respectively.

4.2.4 | Microbial community analysis

DNA extraction

Three triplicate sludge samples were taken to perform microbial population analysis, one from the AnMBR state (after 150 days of operation), and two from the MA-AnMBR state (after 370 and 580 days of operation). A homogenised sludge sample of 1.5 mL was transferred into an Eppendorf tube and centrifuged in a micro-centrifuge (Eppendorf, Hamburg, Germany), to extract DNA. Around 50 mg of sludge pellet were added to the extraction tubes from the soil FastDNA spin kit (MP Biomedicals, Irvine, CA, U.S.A). DNA extraction was performed following the protocol established by Albertsen et al. (2015). The concentration of the extracted DNA was measured using a Qubit dsDNA assay kit (Thermo Fisher, Waltham, MA, U.S.A). Finally, the DNA samples were frozen at -25 °C until they were sent for gene amplification.

16S rRNA Gene Amplicon Sequencing and Data Analysis

The 16S rRNA gene was selected for amplification and paired-end sequence, in an Illumina NovaSeq 6000 platform by Novogene (Beijing, China). The primer set chosen to amplify and sequence the hypervariable region V3-V4 was 341F [50'CCTAYGGGRBGCASCAG-3'] and 806R [5'-GGACTACNNGGTATCTAAT-3']. Subsequently, the Sequence Read Archive (SRA) of the National Centre for Biotechnology Information (NCBI) was used for reading the raw data. The gene sequence provided by Novogene was further processed and analysed following the procedure developed by Toja Ortega et al. (2021).

4.3 | RESULTS AND DISCUSSION

4.3.1 | Reactor performance

Variations in reactor pH, ORP, and maximum biogas production under the three studied periods (AnMBR, Adaptation, and MA-AnMBR states) are shown in **Table 4-2**.

Table 4-2. Summary of reactor performance during the different operational periods. Values correspond to averages and standard deviation of samples (in triplicates) taken bi-weekly during each period. AnMBR refers to the period in which the membrane bioreactor was operated under strictly anaerobic conditions (around 180 days). Adaptation refers to the period in which aeration was introduced to the reactor in steps (100 days). MA-AnMBR refers to the period that the system was operated under the full set-up aeration conditions, showing the stabilised performance (10 months). For particle size distribution, values of D_{90} , D_{50} , and D_{10} represent the particle diameters at which 90, 50, and 10% of the total number of particles are smaller than the given diameter, respectively. Values shown in bold correspond to those which had statistically significant changes between the different reactor periods.

	Unit	AnMBR	Adaptation	MA-AnMBR
Operation time	Days	180	100	300
Sludge pH	-	7.42 ± 0.02	7.52 ± 0.14	7.65 ± 0.13
Sludge Oxidation-Reduction Potential (ORP)	mV	-516 ± 44	-533 ± 16	-533 ± 42
Maximum biogas production	L·d ⁻¹	3.6	3.7	3.0
Average biogas production	L·d ⁻¹	2.5 ± 0.8	2.1 ± 0.8	1.8 ± 0.5
Chemical Oxygen Demand (COD) removal efficiency	%	98.2 ± 0.1	98.3 ± 0.1	98.5 ± 0.4
Ortho-phosphate removal	%	16.8 ± 5.4	24.3 ± 1.3	48.3 ± 18.8
Sulphate removal	%	88.4 ± 0.6	89.3 ± 0.3	89 ± 4.7
Ammonium concentration increase factor		2.3	2.6	3.0
Methane concentration in biogas	%	82 ± 2	84 ± 3	84 ± 6

Table 4-2 (Continuation). Summary of reactor performance during the different operational periods. Values correspond to averages and standard deviation of samples (in triplicates) taken bi-weekly during each period. AnMBR refers to the period in which the membrane bioreactor was operated under strictly anaerobic conditions (around 180 days). Adaptation refers to the period in which aeration was introduced to the reactor in steps (100 days). MA-AnMBR refers to the period that the system was operated under the full set-up aeration conditions, showing the stabilised performance (10 months). For particle size distribution, values of D_{90} , D_{50} , and D_{10} represent the particle diameters at which 90, 50, and 10% of the total number of particles are smaller than the given diameter, respectively. Values shown in bold correspond to those which had statistically significant changes between the different reactor periods.

	Unit	AnMBR	Adaptation	MA-AnMBR
Sludge Total solids	$\text{g}\cdot\text{L}^{-1}$	4.8 ± 1.0	5.9 ± 0.3	5.8 ± 0.9
Sludge Volatile solids	$\text{g}\cdot\text{L}^{-1}$	2.7 ± 0.6	3.6 ± 0.3	2.9 ± 0.6
Ash content	$\text{g}\cdot\text{L}^{-1}$	2.1 ± 1.2	2.3 ± 0.4	2.9 ± 1.1
Particle size distribution*				
D_{90}	μm	10.6 ± 0.7	13.0 ± 1.4	19.5 ± 0.6
D_{50}	μm	4.4 ± 0.3	5.2 ± 0.8	6.7 ± 0.2
D_{10}	μm	2.7 ± 0.2	3.2 ± 0.4	4.3 ± 0.1

* Values based on total particle numbers.

Single-factor ANOVA test showed no statistical difference between the ORP of all reactor periods. All three reactor periods showed values below -500 mV, and therefore, prevailing conditions could be considered fully anaerobic (Pepper & Gentry, 2015). These results align with the research conducted by Lim and Wang (2013), who observed negligible ORP variations when micro-aeration corresponding to 1.0% of the soluble influent COD load was added as a pre-treatment of anaerobic digestion. In our present research, anaerobic conditions were maintained during the adaptation period and the reactor ORP remained around -533 mV, showing that the oxygen introduced to the reactor was rapidly consumed and undetectable in the higher part of the liquid phase, where the ORP probe was located. However, the adaptation period was characterized by a slight increase in VFA concentrations during the first month of micro-aeration. Iso Caproic acid (I C6) and Caproic Acid (C6) increased to a maximum value of $50 \text{ mg}\cdot\text{L}^{-1}$ and decreased to undetectable values after this first adaptation. Under the MA-AnMBR state, VFA concentrations were negligible.

Whilst no statistical changes were observed in the reactor ORP, biogas quantity decreased during the MA-AnMBR period. Average biogas production decreased by 25%, from 2.5 L·d⁻¹ to 1.8 L·d⁻¹ in the AnMBR and MA-AnMBR periods, respectively. A high relative standard deviation of biogas production was observed during the operation of the reactor (30%). This was mainly due to tube obstructions (primarily on the feed line) and reactor headspace variations due to daily operation and maintenance. The difference in biogas production between the AnMBR and MA-AnMBR corresponded to a COD load of around 1300 mgCOD·d⁻¹, while theoretical calculations of aerobic degradation due to the supplied oxygen load corresponded to potential degradation of 112 mgCOD·d⁻¹. Thus, while aerobic degradation could have contributed to the observed decrease in biogas production (and methane content), the changes in biogas quantity cannot be attributed to aerobic degradation of the influent COD alone.

No statistical difference was observed in the biogas quality (p-value of 0.13), which showed high methane concentrations reaching 82 ± 2% to 84 ± 6% for the AnMBR and MA-AnMBR states, respectively. Similar observations were made by Ferrari et al. (2019) who found methane concentration in the biogas between 85-95%, while operating a laboratory-scale AnMBR treating concentrated synthetic municipal sewage in the temperature range 17-34 °C and HRT from 1 to 1.5 days. Methane concentrations reaching 70-80% are commonly found at full-scale anaerobic reactors treating dilute municipal sewage at relatively low HRTs, which can be attributed to the relatively high CO₂ solubility in the effluent (Chernicharo et al., 2015). The resulting CO₂ concentration in the biogas of these reactors is only 5-10%, while the remainder consists of atmospheric N₂ gas that was dissolved in the influent. The observed high methane concentrations in our present study and that of Ferrari et al. (2019) might be attributed to the presence of urea, which was used as the main nitrogen source in the synthetic influent. It should be noted that each mmol of urea is hydrolysed in two mmol of NH₄⁺, which increases the alkalinity and chemically binds two mmol CO₂ as bicarbonate to the liquid. In addition, also the proteins present in the influent will generate NH₄⁺, which binds CO₂.

The main protein sources of the influent were ovalbumin (200 mg·L⁻¹), milk powder (600 mg·L⁻¹) and yeast extract (510 mg·L⁻¹). The protein percentage of milk powder and yeast extract are around 25% w/w (Kamizake et al., 2003; Klotz et al., 2017). Food proteins contain 16% of nitrogen (by weight) (Moore et al., 2010), therefore, the NH₄⁺ generated by the influent proteins represents less than 15% of the total ammonium produced by urea, thus having a minor impact on the binding of CO₂. Research

showed that under a high acid neutralization capacity (ANC) to total inorganic produced carbon (TIC) ratio, a decrease in carbon dioxide content in the biogas can be expected (Lindeboom et al., 2012). The observed methane concentration in the biogas of the AnMBR and MA-AnMBR are therefore in line with the literature.

An increase in carbon dioxide in the biogas of less than 50 mL·d⁻¹ can be expected under aerobic respiration due to the added oxygen into the AnMBR (representing around 1% of the influent COD). To better understand the biogas composition, the AnMBR and MA-AnMBR conditions were modelled using the Ammonium database of the PhreeqC software. Results of the model showed concentrations of CH₄ and CO₂ of 87.8 and 6.7% respectively for the AnMBR, and 90.0 and 4.5% for the MA-AnMBR state. Relatively low discrepancies between the model outputs and observed biogas composition of 5.8 and 6% for the AnMBR and MA-AnMBR, respectively, were observed. Further discussions on the PhreeqC model results and biogas composition dependency on feed characteristics can be found in the supplementary material, **Annex C-4**.

Finally, a COD mass balance was calculated for the AnMBR and MA-AnMBR states. For the biogas COD, the maximum daily biogas production was considered instead of the average values, due to the high standard deviation (due to operational and maintenance issues). Influent, effluent, and sludge flows were considered as defined by the operation conditions specified in **Table 4-1**. Results showed an off-balance of 5% for the AnMBR and 9% for the MA-AnMBR when compared to the influent COD load. Biogas COD corresponded to 93 and 79% of the influent COD at the AnMBR and MA-AnMBR states respectively, while the effluent and sludge COD load did not vary significantly between the reactor states. The COD balance for each reactor period is presented in **Annex C-5**.

4.3.2 | Microbial conversions kinetics

Substrate degradation potential with micro-aeration

Following the observed changes in ammonium and phosphate concentration between the AnMBR and MA-AnMBR operational period, protein degradation was assessed. One of the main protein sources in the synthetic influent was ovalbumin; the degradation of which was tested under different aeration conditions in batch tests. Results showed that protein and carbohydrate concentrations in sludge decreased when aeration increased (**Figure 4-3**). When no aeration was applied (further referred to as Ovalbumin A₀), total proteins and carbohydrates

concentrations were 732 ± 10 and 400 ± 1 mgCOD·L⁻¹ respectively. Whilst degradation of total proteins and carbohydrates seemed to increase with aeration, the change was statistically insignificant (p-value above 0.05). Nevertheless, the difference was notable in the soluble fraction. Soluble protein concentration was 10.3 mgCOD·L⁻¹ when the supplied oxygen was 5% of the substrate COD load (further referred to as Ovalbumin A₃), and 14.3 mgCOD·L⁻¹ for Ovalbumin A₀, showing a significant 28% reduction (p-value < 0.001). Moreover, soluble carbohydrates concentration decreased from 18.2 to 17.0 mgCOD·L⁻¹ in A₀ and A₃ respectively, (p-value < 0.05). From these results, we concluded that the added aeration contributed to an increased degradation in soluble protein and carbohydrates.

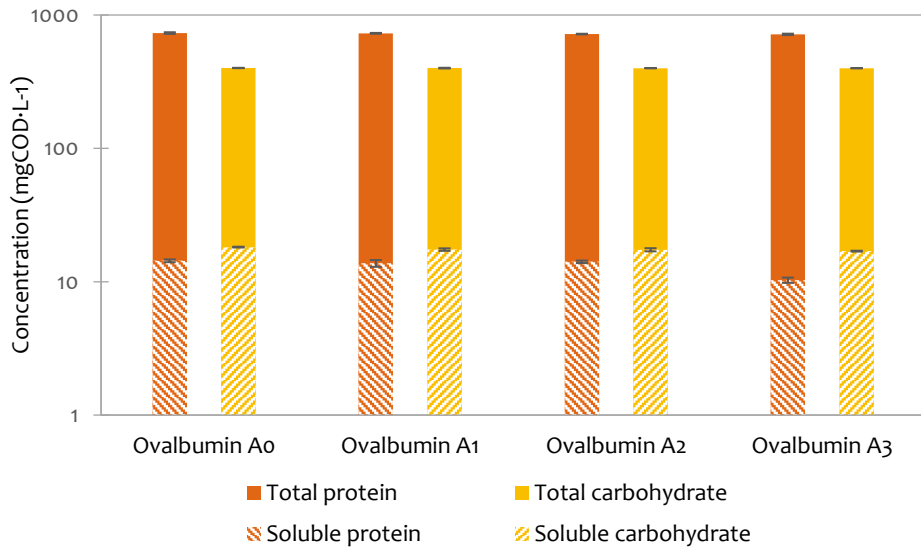


Figure 4-3. Concentrations of total and soluble proteins and carbohydrates. The substrate used for the batch experiments was ovalbumin, macronutrients, and micronutrients, in a similar composition as the one selected for the reactor feed. The inoculum used was AnMBR state sludge. The batch tests were conducted for 28 days, and aeration took place on the first 6 days. Values displayed are the mean over the triplicate samples followed by the standard deviation.

Sludge specific methanogenic activity under different aeration conditions.

The SMA of the MA-AnMBR sludge was measured under different aerations conditions, using biomass from the laboratory-scale reactor as inoculum that was harvested from the AnMBR stage (S₀), during adaptation (S₁-S₃) and after full adaptation to micro-aeration (S₄). The SMA results

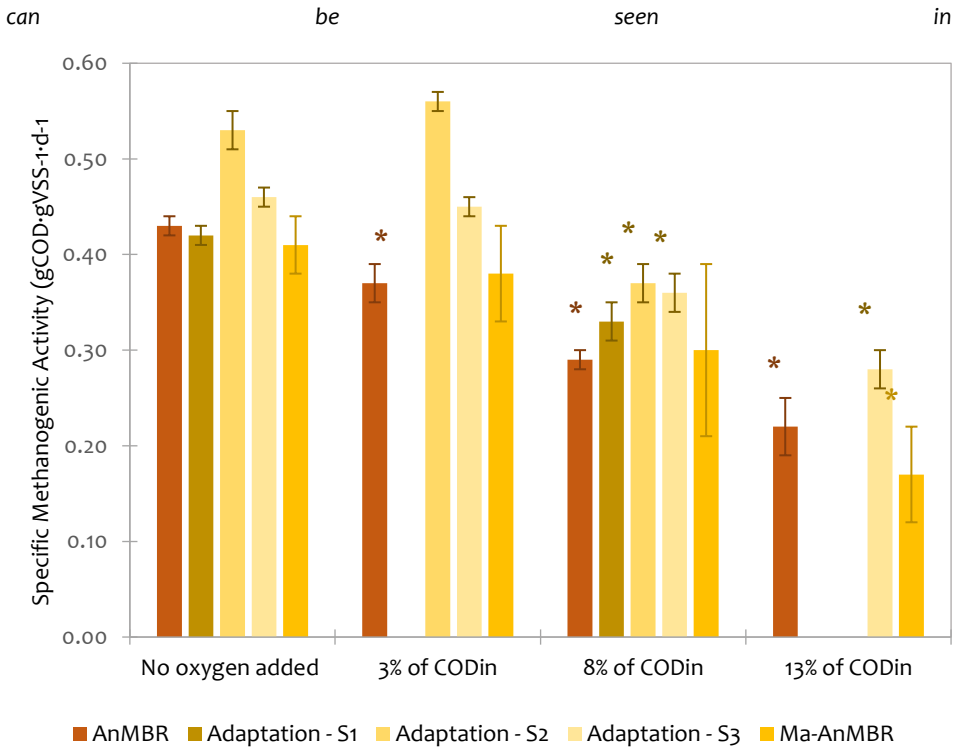


Figure 4-4. The aeration during the SMA test corresponded to ratios of oxygen over substrate COD loads of 3, 8 and 13%. For any given inoculum, an increase in aeration resulted in a decreased SMA.

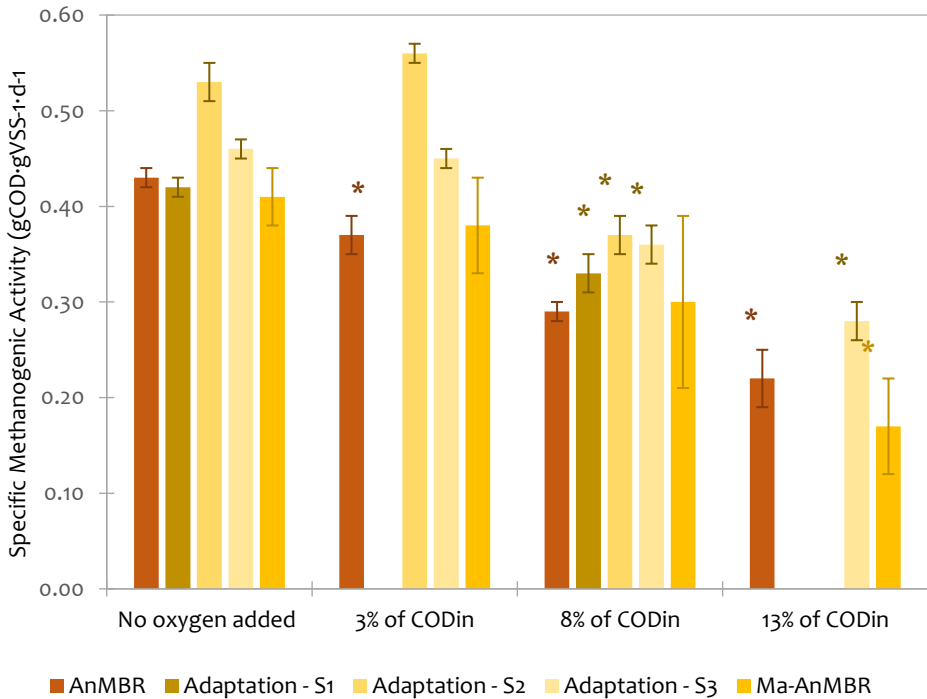


Figure 4-4. Specific Methanogenic Activity (SMA) in $\text{gCOD}\cdot\text{gVSS}^{-1}\cdot\text{d}^{-1}$ of sludge inoculums under different aerations. The oxygen supplied to each SMA bottle was calculated based on oxygen overload of substrate COD (COD_{in}) ratio, at 20°C , and considering an air composition of 21% Oxygen and 79% Nitrogen. Blank results under the different aerations indicate no measurements. Columns with an * show that the difference between the SMA of the sample was significant when compared to the no oxygen added conditions (p values <0.05).

Significant SMA decrease (with p -values below 0.01) of 14, 33, and 48% for the AnMBR state inoculum were observed with increasing aerations corresponding to 3, 8 and 13% of substrate COD load, respectively. The tests performed with inoculums from the Adaption period showed a statistically significant decrease in SMA for all three stages (S1, S2 and S3) of 20 and 35% when added oxygen corresponded to 8 and 13% of substrate COD, respectively (p -values below 0.01). No statistical variation was observed for the aeration corresponding to 3% of substrate COD (p -values above 0.4). SMA results showed a tendency of biomass adaptation to small amounts of added oxygen. A negligible impact on SMA was also observed for the MA-AnMBR state sludge for the lowest aeration (p -value of 0.6). Furthermore, this inoculum also had an insignificant reduction in SMA when the added oxygen was 8% of substrate COD. Nevertheless, the absence of significant differences could be linked to the high

standard deviations. Relative standard deviations above 20% were observed in all SMA tests conducted for the MA-AnMBR state inoculum subjected to an oxygen increase of 8% of substrate COD, which was performed five times and in triplicates. Finally, IC_{50} , an SMA decrease above 50% (p-value of 0.04), was observed for the MA-AnMBR state inoculum exposed to oxygen that corresponded to 13% of the substrate COD load. All p-values are given in the supplementary material, **Annex C-6**.

Even though SMA deterioration was observed for an added oxygen content of 8 and 13%, no variation in the lag-phases in the methane production of the different inoculums was observed. Furthermore, the negligible change in SMA of the MA-AnMBR sludge subjected to an oxygen-over-substrate COD load of 3%, suggested that the acetotrophic methanogenic biomass can tolerate small amounts of added oxygen, apparently creating resistance towards it.

4.3.3 | Nutrient removal in the MA-AnMBR vs AnMBR

Although the difference in total protein concentration between the MA-AnMBR and the AnMBR was statistically insignificant, the change in soluble proteins showed an increase in protein degradation when oxygen was added to the reactor (**Figure 4-3**). Soluble protein concentration in the micro-aerated sludge was 30-35% lower than the one in the AnMBR sludge. It is hypothesized that the 30% reduction in soluble protein concentration is directly linked to an increase in the hydrolytic capacity of the biomass, and the decrease in the effluent COD from 90.6 to 74.6 mgCOD·L⁻¹. This hypothesis was confirmed by the fact that the ammonium concentration during the MA-AnMBR period was 1.3 times higher than during the AnMBR period. Hydrolysis is commonly considered the rate-limiting step when treating wastewater with high concentrations of particulate matter (Visvanathan & Abeynayaka, 2012). Since hydrolysis occurs under a wide range of redox conditions, the observed increased protein hydrolysis, suggests that the addition of oxygen may enhance the hydrolysis rate and thus the overall digestion performance (Azman et al., 2015; Sun et al., 2013).

The N:P ratio in the effluent of the MA-AnMBR almost tripled when compared to the AnMBR, i.e., from 10 to 26. While the ammonium concentration increased from 547 to 740 mgNH₄⁺·N·L⁻¹, the phosphate concentration decreased from 55 to 28 mgPO₄³⁻·P·L⁻¹ under the AnMBR and MA-AnMBR periods, respectively. In comparison to AnMBR operation, phosphate removal almost tripled once the MA-AnMBR stable performance was attained, (p-value < 0.01). An increased buffer capacity and reactor pH were observed, which coincided with an increase in NH₄⁺ concentration. The pH

increase of 0.2, from 7.43 to 7.65, resulted in increased precipitation of inorganic matter.

The results of PhreeQC modelling showed that the reactor broth was supersaturated for amongst others hydroxyapatite, Ca₅(PO₄)₃OH, and vivianite, Fe₃(PO₄)₂·8H₂O, under both AnMBR and MA-AnMBR periods. Furthermore, both saturation indexes (SI) increased under the MA-AnMBR operational conditions compared to the AnMBR state. Hydroxyapatite SI increased by 12% to 6.4, while the vivianite SI doubled, from 0.2 to 0.4. Notably, vivianite precipitation can only be expected under strict anaerobic conditions, due to the required oxidation state of iron (Nriagu, 1972). Aside from vivianite and hydroxyapatite, aragonite, and calcite (carbonate minerals) saturation indexes increased from the AnMBR to the MA-AnMBR periods, from 0.4 and 0.5 to 0.5 and 0.7 respectively. This increase in carbonate minerals can be further linked to a decrease in the partial pressure of CO₂ in biogas. Since under all conditions, ORP levels showed values below -250 mV, it can be assumed that anaerobic conditions were maintained in the laboratory-scale reactor. Even though the vivianite SI is above zero and is therefore expected to precipitate, researchers found no measurable precipitation in similar water matrices when the SI is below four (Goedhart et al., 2022). Hydroxyapatite SI indicated precipitation of the mineral under both AnMBR and MA-AnMBR states. The precipitation of hydroxyapatite can be further linked to an increase in the concentration of calcium and phosphate in the sludge of the laboratory-scale reactor. When compared to the AnMBR, phosphate concentration in the MA-AnMBR effluent reduced to half, from 55.1 to 27.6 mgPO₄³⁻·P·L⁻¹.

4.3.4 | Effects of micro-aeration on physical sludge characteristics

Solids concentration, particle size, and viscosity varied for each of the reactor periods. While the sludge total solids concentration increased with micro-aeration, from 4.6 ± 0.3 to 5.8 ± 0.5 g·L⁻¹, no significant change was observed in the volatile solids. The ash content of the MA-AnMBR sludge was higher than the one of the AnMBR, i.e., 2.9 ± 1.1 and 2.1 ± 1.2 g·L⁻¹ respectively. Changes in TSS content are in line with the increased precipitation of phosphate compounds (like hydroxyapatite). The supplied oxygen would maximally result in an increase of 0.04 gVSS·L⁻¹ of aerobic biomass, assuming a yield of 0.5 gVSS·gCOD⁻¹ (Metcalf et al., 2014), which is considered negligible for the prevailing AnMBR and MA-AnMBR TSS concentrations, viz. 4.8 and 5.8 gTSS·L⁻¹ respectively.

Sludge viscosity and PSD varied while changing from AnMBR to MA-AnMBR periods. Based on the rheometer results, MA-AnMBR sludge viscosity decreased when

compared to the AnMBR. Under shear rates of 1.0 s^{-1} and 100.0 s^{-1} , MA-AnMBR showed shear stress values of 0.001 and 0.098 Pa, respectively, while for the AnMBR sludge, these values were 0.031 and 0.205. The shear stress against the shear rate for the different sludges is shown in **Annex C-7**. Furthermore, the PSD of the MA-AnMBR sludge showed a statistical increase in D_{10} , D_{50} and D_{90} compared to the AnMBR sludge (p-values below 0.05). The highest difference was observed for the D_{90} particles, where the average particle diameter from the MA-AnMBR sludge, i.e., 19.5 μm , was almost 90% larger than the ones from the AnMBR sludge, i.e., 10.6 μm (**Table 4-2**). A lower apparent viscosity can be potentially linked to better mixing and higher biogas production rates (Wei et al., 2019).

4.3.5 | Microbial community shifts

Microbial SOD activity of the MA-AnMBR sludge increased by a factor of 3 compared to that of the AnMBR inoculum sludge, i.e., 4.3 ± 0.4 and $1.4 \pm 0.1 \text{ U}\cdot\text{mgProtein}^{-1}$, respectively. An increase in SOD activity of the MA-AnMBR sample is linked to a higher amount of antioxidant enzymes that protect against oxidant stress situations (De Raeve et al., 1997). Enzymatic production requires an extensive energy investment in enzyme synthesis and excretion, consuming up to 5% of bacterial productivity (Christiansen & Nielsen, 2002; Frankena et al., 1988). Thus, an increase in the SOD activity can be linked to an additional need for organic matter from the microorganisms to produce the enzyme, resulting in a lower sludge yield.

The surge in SOD activity is associated with a higher tolerance to oxygen since it is likely related to the neutralization of superoxide anion-radicals and a localised decrease in redox potential (Fridovich, 1995). Because no changes in the reactor ORP were observed, a rise in the enzyme activity could be responsible for regulating the oxygen tolerance of the biomass at a localised level. Results of the SOD activity can also be linked to MA-AnMBR sludge SMA. The negligible decrease in SMA of the MA-AnMBR subjected to an oxygen load equivalent to 3% of the substrate COD load, indicated an increase in oxygen tolerance of the MA-AnMBR methanogenic biomass, and it could therefore be related to the rise in SOD activity. Even though SMA changes were negligible, biogas production in the laboratory-scale reactor decreased by 25% during the MA-AnMBR versus the AnMBR operation. This decrease potentially might be attributed to an increased anabolism to produce the SOD enzyme, as well as microbial community shifts, but further studies are necessary to verify this.

To obtain insight into the micro-organism's specific response to the induced oxygen stress DNA analysis was performed for the three samples, the AnMBR state (after 150

days of operation), and two from the MA-AnMBR state (after 370 and 580 days of operation). The two most relatively abundant taxa for the MA-AnMBR samples were bacteria family *Thermofonsia* or SBR103 and archaeal family *Methanosaetaceae*, while these taxa were the second and fifth most abundant in the AnMBR samples, respectively. Alpha and beta diversity analyses were conducted to identify further differences between the two reactor states. The diversity within samples (alpha diversity) showed that the phylogenetic distance between taxa in each sample was statistically different (p-value of 0.03), whilst the community evenness within samples was insignificant. Even though the diversity analysis showed a statistical difference between the AnMBR and MA-AnMBR sludge samples, it cannot be linked to differences in AD performance (Lin et al., 2023).

However, the sequencing of the 16rRNA might not be useful to define microorganisms that are responsible for specific processes (De Vrieze et al., 2018). For instance, whilst the *Methanosaetaceae* family relative abundance increased from 6.2 to 20.7% from the AnMBR to the MA-AnMBR samples (taken after 150 and 370 days respectively), no statistical difference was observed in this group due to the low relative abundance of *Methanosaetaceae* in the Archaea kingdom. While most hydrogenotrophic methanogens are members of the family of *Methanobacteriaceae* (Whitman et al., 2001), acetoclastic methanogens belong to the family of *Methanosaetaceae* (Ferry, 1992). No changes were observed between the sludge samples from the AnMBR and MA-AnMBR in the relative abundance of both families in the Archaea kingdom. *Methanobacteriaceae* represented around 3.5% of the Archaea while the acetoclastic methanogens were around 95.5%. Since hydrogenotrophic and acetoclastic archaea's relative abundance between the reactor periods did not vary, and SMA results showed no statistical changes in the MA-AnMBR sludge subjected to small aeration, changes in biogas production were not expected.

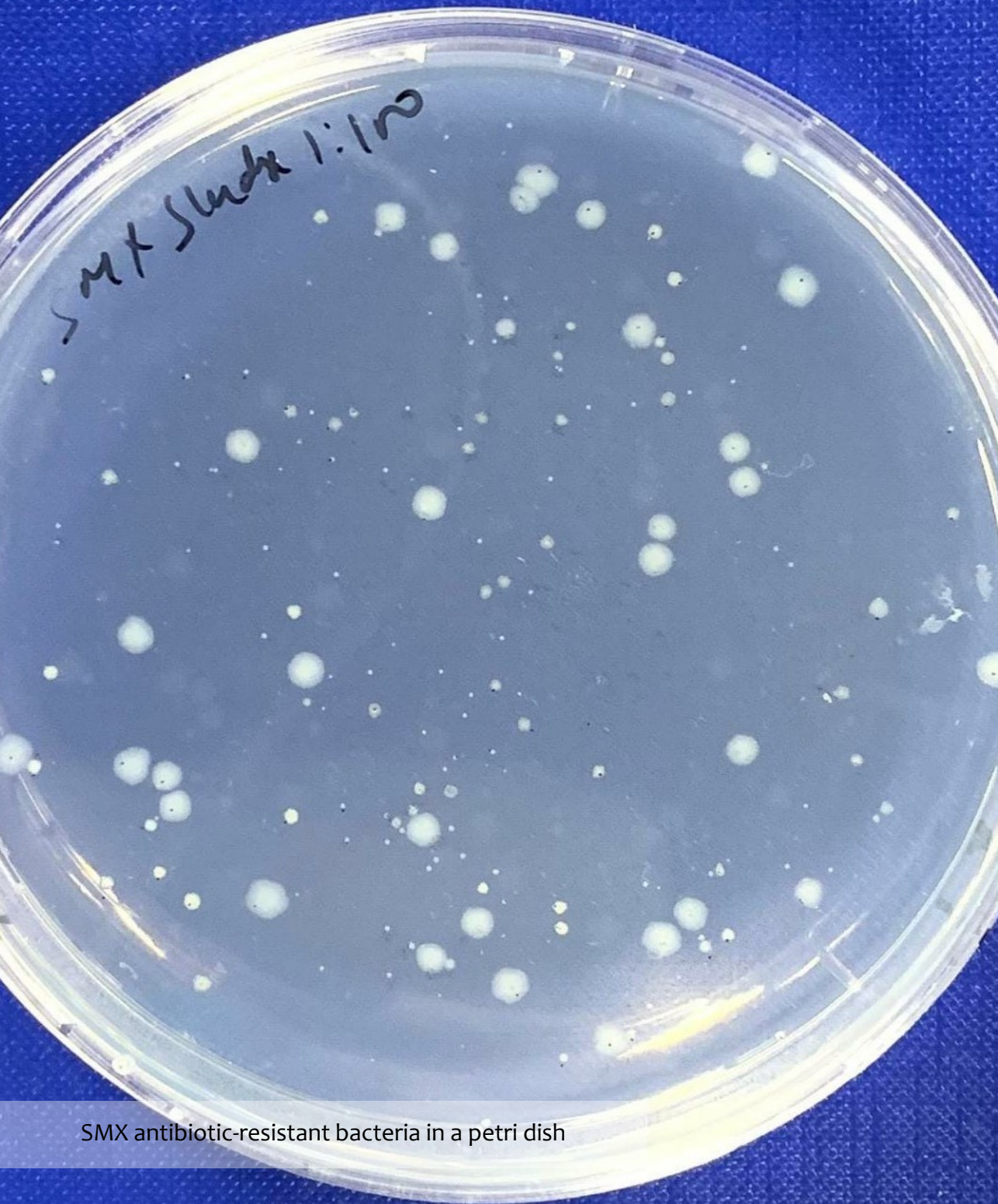
4.4 | CONCLUSIONS

A research was performed on the effects of micro-aeration on a laboratory scale anaerobic membrane bioreactor (MA-AnMBR), where the given oxygen load mimics the conditions of replacing the membrane system of an AnMBR for a dissolved air flotation (DAF) unit. The study focused on the overall performance during MA-AnMBR operation in comparison to strict anaerobic conditions (AnMBR period), as well as to changes in the permeate nutrient content and microbial community shifts. The main conclusions of the research are as follows:

- The addition of micro-aeration, representing an oxygen over influent chemical oxygen demand (COD) loading ratio of 1.0%, showed negligible effects on the operation of the MA-AnMBR, and performance remained stable. A statistically significant improvement of 0.2% increase in COD removal was observed shifting from AnMBR to the MA-AnMBR period. This was linked to a permeate COD decrease from 90.6 ± 4.4 during AnMBR to 74.6 ± 19.0 $\text{mgCOD}\cdot\text{L}^{-1}$ during MA-AnMBR operation. On the other hand, the produced biogas quantity decreased by 27%, which could not be solely attributed to aerobic conversions;
- The observed high biogas methane concentration of around 85% during AnMBR and MA-AnMBR operation, was due to the urea content of the synthetic concentrated domestic sewage. The hydrolysis of urea, where 1 mmol of urea produces 2 mmol of NH_4^+ , increased the alkalinity and chemically bound bicarbonate to the liquid;
- Ammonium concentration in the permeate increased from 547 to 740 $\text{mgNH}_4^+\text{-N}\cdot\text{L}^{-1}$, following AnMBR to MA-AnMBR respectively, suggesting a higher hydrolytic capacity of the latter. The increased ammonium concentration led to a higher buffer capacity, increased pH and a slight decrease in the biogas CO_2 concentration;
- When compared to the AnMBR, orthophosphate concentration in MA-AnMBR permeate was halved, from 55.1 to 27.6 $\text{mgPO}_4^{3-}\text{-P}\cdot\text{L}^{-1}$. The measured change in pH from 7.42 to 7.65 resulted in an increased hydroxyapatite precipitation in the MA-AnMBR period and a decrease in the permeate orthophosphate concentration.
- Ma-AnMBR sludge adapted to oxygen exposure, representing 1% of the influent COD load. Microbial adaptation was revealed by the increase in superoxide dismutase (SOD) enzyme activity, which tripled from AnMBR to MA-AnMBR operation (1.4 ± 0.1 and 4.3 ± 0.4 $\text{U}\cdot\text{mgProtein}^{-1}$

respectively). The rise in SOD activity indicates an increase in oxygen tolerance. Furthermore, the specific methanogenic activity (SMA) of the MA-AnMBR sludge was not affected despite an oxygen exposure of 3% of the substrate COD load.

All obtained results showed that the given oxygen loads to an AnMBR, mimicking the coupling of an anaerobic digester with a DAF (AD-DAF), had negligible effects on the performance of the anaerobic conversion process, indicating the feasibility of an AD-DAF system.



SMX antibiotic-resistant bacteria in a petri dish

5

The fate of sulfamethoxazole and trimethoprim in a micro-aerated anaerobic membrane bioreactor (MA-AnMBR) and the occurrence of antibiotic resistance in the permeate

This chapter is an adapted version of Piaggio, A. L., Mittapalli, S., Calderón-Franco D., Weissbrodt, D.G., van Lier, J. B., de Kreuk, M. K., & Lindeboom, R. E. (*Under Review*). The fate of sulfamethoxazole and trimethoprim in a micro-aerated anaerobic membrane bioreactor and the occurrence of antibiotic resistance in the permeate. *Submitted to Water Science and Technology*.

ABSTRACT

Interest in using treated wastewater drives efforts to eliminate antibiotics from wastewater to prevent the spreading of antibiotic resistance. Micro-aerated anaerobic membrane bioreactors (MA-AnMBR) promote treated wastewater use, while converting wastewater organic matter to biogas, on a small footprint. However, the fate of antibiotics, antibiotic-resistant bacteria (ARB), and their antibiotic-resistance genes (ARGs) are not known in these systems. We studied the effects, conversions, and resistance induction, following the addition of $150 \mu\text{g}\cdot\text{L}^{-1}$ of two antibiotics, sulfamethoxazole (SMX) and trimethoprim (TMP), in a laboratory-scale MA-AnMBR. TMP and SMX were removed at 97 and 86%, indicating that micro-aeration did not hamper the removal of the antibiotics. These antibiotics only affected the pH and biogas composition of the process, with a significant change in pH from 7.8 to 7.5, and a decrease in biogas CH_4 content from 84 to 78%. TMP was rapidly adsorbed onto the sludge and subsequently degraded during the long solids residence time of 27 days. SMX adsorption was minimal, but the applied hydraulic retention time of 2.6 days was sufficiently long to biodegrade SMX. The levels of three ARGs (*sul1* and *sul2* for SMX, *dfrA1*) and one mobile genetic element biomarker (*int1*) were analysed by qPCR, in combination with ARB tracked by plating. Additions of the antibiotics increased the relative abundances of all ARGs and *int1* in the MA-AnMBR sludge, with the *sul2* gene folding 15 times after 310 days of operation. The MA-AnMBR was able to reduce the concentration of ARB in the permeate by 3 log.

5.1 | INTRODUCTION

Water demand has been increasing worldwide due to changes in consumption patterns, socioeconomic development, and population growth. Water consumption is expected to rise above one-quarter of the current consumption level by 2050. About 40% of the global population endures water scarcity for one month per year, and 20% lives in countries with high water stress (WWAP, 2019). The use of treated wastewater has risen as a possibility to alleviate water scarcity caused by water stress (Saidan et al., 2020). Nevertheless, to reclaim treated water, wastewater treatment plants (WWTPs) should be able to provide high-quality effluents. New and upgraded WWTPs should consider not only removing macro-contaminants, such as organic matter, suspended solids, and nutrients but also pathogens and micropollutants (Roccaro & Verlicchi, 2018). Most conventional WWTPs are not designed for the removal of antibiotics (Gros et al., 2010; Radjenovic et al., 2007) and only minimal removal of pharmaceutical compounds can be observed in the primary treatment of wastewater (i.e., by coagulation, flocculation, and sedimentation) (Oulton et al., 2010). Currently, several high-income countries are adopting regulations for the treatment of micropollutants and the extension of WWTPs with physical-chemical processes for their removal (Falås et al., 2016). However, for other regions, there is a need for affordable and implementable treatment processes with less energy and resource footprints.

Antibiotics are important components of human and veterinary medicines. Their consumption is increasing daily, leading to their occurrence in residual waters, such as municipal wastewater and urban and rural run-off. As much as 90% of the consumed antibiotics are excreted without any change in composition or functionality (Balakrishna et al., 2017). Among the available antibiotics, sulfamethoxazole (SMX) and trimethoprim (TMP) are found in significantly high concentrations all over the world, as these are some of the most commonly used antibiotics in human and veterinary medications (van Boeckel et al., 2014). TMP and SMX are frequently administered together for urinary tract infections (Masters et al., 2003). Surface water concentrations of SMX and TMP reached values of $49.7 \mu\text{g}\cdot\text{L}^{-1}$ in Kenya, and $610 \mu\text{g}\cdot\text{L}^{-1}$ in Ecuador (de Ilurdoz et al., 2022). Sim et al. (2011) found high concentrations of SMX and TMP in WWTPs treating wastewater from the pharmaceutical industry, with maximum values reaching 309 and $162 \mu\text{g}\cdot\text{L}^{-1}$, respectively. India's production of antibiotics is amongst the five top countries worldwide. The Isakavagu-Nakkavagu surface water stream in India carries one of the highest antibiotic concentrations in Asia, with a TMP concentration of $4 \mu\text{g}\cdot\text{L}^{-1}$ (Fick

et al., 2009). In the water of the Barapullah largest urban drain in Delhi, the average concentration of TMP was $0.25 \mu\text{g}\cdot\text{L}^{-1}$ (Shukla & Ahammad, 2023).

Antibiotics can be removed or transformed by either biotic (biodegradation) or abiotic (sorption, ion exchange, complex formation with metal ions, and polar hydrophilic interactions) processes (Díaz-Cruz et al., 2003; Michael et al., 2013). On the majority of WWTPs, the sorption and biodegradation of antibiotics occur in parallel. Pharmaceuticals can be biodegraded under aerobic, anoxic or anaerobic conditions, or in combination of all conditions, depending on the antibiotic. The centrally positioned amide group in SMX prevents its degradation under aerobic conditions. However, under anaerobic conditions it can be degraded by reductive cleavage of the molecule due to the adjacently located strong electron-withdrawing sulfonyl group. In the case of TMP, the substituted pyrimidine group can be readily bio transformed under anaerobic conditions (Alvarino et al., 2018).

Furthermore, the sorption potential of antibiotics is highly dependent on their molecular charge, polarity, and hydrophobicity, among other characteristics. Hydrophobic antibiotics have a great affinity to solid particles and therefore, have higher chances of being sorbed to sludge particles and reside long in the process to get degraded. The sorption capacity of antibiotics can be described as low, medium, or high, depending on their octanol-water partition coefficient (K_{ow}). High sorption is linked to $\log K_{ow}$ values above 4, while low sorption can be considered for antibiotics with $\log K_{ow}$ values below 0.25 (Rogers, 1996). SMX and TMP properties are presented in **Table 5-1**.

The persistence of antibiotics in WWTPs and waterbodies can lead microbial communities to acquire antibiotic resistance. The O'Neil report (O'Neill, 2014), commissioned by the United Kingdom government, predicts that by 2050, antibiotic resistance infections will lead to 10 million annual deaths, with associated costs above 100 trillion USD. Furthermore, the World Health Organization established that the multi-resistance gained by bacteria is alarming and threatens global public health (Organization, 2015). Wastewater catchment areas and WWTPs are considered one of the major points of antibiotic resistance release into the environment (Czekalski et al., 2012; Kümmerer, 2009). Wastewater carries the complex cocktails of chemicals and biological contaminants released from anthropogenic activities. The high density of microbes in WWTPs has been frequently hypothesised to promote the transfer of antibiotic resistance via vertical and horizontal gene transfer in the presence of the antibiotics or other chemicals (Zarei-Baygi et al., 2019). The non-resistant bacteria can gain the resistance mechanisms from the antibiotic-resistant bacteria (ARB) via an

exchange of mobile genetic elements (MGEs) like plasmids, integrons, and transposons, that contains antibiotic resistance genes (ARGs) (Blair et al., 2015).

Table 5-1. Selected antibiotics and their characteristics. Adapted from NCBI (2005) and Alvarino et al. (2018). K_{OW} is the octanol-water partition coefficient and refers to the sorption capacity of antibiotics. The antibiotics removal pathways refer to the preferential ones, being either Aerobic or Anaerobic, and biodegraded or adsorbed.

Antibiotic	Molecular weight (g·mol ⁻¹)	Charge*	Preferential removal pathway		Log K_{OW}	Henry's constant (atm·m ³ ·mol ⁻¹)
SMX <chem>C10H11N3O3S</chem>	253.3	-	Anaerobic	Biodegraded	0.9	2.1×10^{-14}
TMP <chem>C14H18N4O3</chem>	290.3	+	Anaerobic	Adsorbed	1.3	6.4×10^{-13}

*Positive (+) or negative (-) charge is based on pH between 7 to 9

Previous research indicated that the high solids retention times (SRTs) of WWTPs can result in an increased abundance of ARGs in conventional and membrane-based activated sludge systems (Xiao et al., 2017; Zhang et al., 2018). However, low convergence in results across the regions has been obtained. The study of more than 60 installations in the Netherlands highlighted that WWTPs mostly abate ARGs of on average 1.8 log gene copies reduction from influent to effluent, i.e., more than 98% removal (Pallares-Vega et al., 2019). Lower removals of ARGs and ARB have been detected under rain events, highlighting the need to improve secondary clarifications under higher hydraulic loadings to remove microorganisms and their ARG pool (Pallares-Vega et al., 2021). Membrane systems can be one solution to enhance the solids-liquid separation.

Membrane bioreactors (MBRs) are potentially effective for treating pharmaceutical wastewater containing various antibiotics and other micropollutants (Oberoi et al., 2019). The long SRT and ultrafiltration (UF) membrane pore size are the main determining parameters for antibiotics removal in MBRs (Ji et al., 2020). Several authors found that the optimum SRT for enhanced antibiotics removal was around 30 days (Nguyen et al., 2017; Tadkaew et al., 2010; Xia et al., 2015). Due to its great affinity to solids, hydrophobic antibiotics can sorb to the sludge particles and then be subjected to biodegradation. The high SRT in MBRs promotes a diverse enzymatic

activity due to the manifestation of slowly growing bacteria, which in parallel may support the degradation of the antibiotics (Göbel et al., 2007; Le-Minh et al., 2010). Monsalvo et al. (2014) found that the removal of SMX and TMP in an AnMBR, fed with an influent containing $1.5 \mu\text{g}\cdot\text{L}^{-1}$ of each antibiotic and operated at 30 days SRT, was 95.2 and 40%, respectively. Furthermore, Wijekoon et al. (2015) observed a TMP removal of 98% in an AnMBR operated at an SRT of 180 days. Under aerobic conditions, SMX and TMP removal was around 80 and 90% in an MBR system with 70 days SRT (Göbel et al., 2007).

Whether antibiotics are degraded via aerobic, anoxic or anaerobic conversion pathways, determines the need to apply a specific treatment technique, or treatments that combine both redox conditions.

In **Chapter 4**, we researched the feasibility of a laboratory-scale MA-AnMBR, mimicking the oxygen dosage of a full-scale digester equipped with a dissolved air flotation DAF system for sludge retention instead of a membrane unit. Results showed improved hydrolysis and negligible effects of the oxygen dose on operation and maintenance of the system. However, thus far, the removal of antibiotics and specifically SMX and TMP in an MA-AnMBR, remains unclear. The application of micro-aeration in an AnMBR might negatively impact their removal efficiency and rate. Since TMP and SMX removal is a mixture of bio-sorption and bio-conversion, the complete solids retention and high SRT provided by the MA-AnMBR system may enhance the degradation of both antibiotics. Furthermore, little is known about the effect of a membrane system on the growth and on the separation of ARB, as well as on the spreading of ARGs, in conjunction with the presence and removal of antibiotics in the wastewater.

Therefore, this study focused on the fate of SMX and TMP, in a laboratory-scale MA-AnMBR and their effect on the presence of antibiotic resistance in the MA-AnMBR permeate. Antibiotics removal mechanisms (adsorption and/or degradation) and the effects of adding SMX and TMP to the MA-AnMBR feed on its operation and performance were assessed. Measurements of ARGs and ARB from the sludge and permeate of the MA-AnMBR were performed to further understand the complexities and risks linked to the presence of antibiotics in domestic wastewater, and to address the efficiency of MA-AnMBRs to possibly contribute in reducing the spreading of antibiotic resistance from urban water systems.

5.2 | MATERIALS & METHODS

5.2.1 | Experimental set-up

A laboratory-scale MA-AnMBR was set to study the fate of commonly used antibiotics. The used membrane system, operational conditions and tested influent were already described in **section 4.2.1**. Micro-aeration to the system was introduced in the reactors bulk liquid, in three sets of four hours of aeration and four hours of no aeration. The total daily air volume introduced to the system was around 120 mL, which corresponds to 25 mL O₂ (based on oxygen to air ratio of 0.21). The reactor scheme can be seen in **Figure 5-1**. The influent was synthetic concentrated wastewater, with an adapted recipe from Ozgun (Dereli et al., 2012). The synthetic feed had an average COD of $4.9 \pm 0.6 \text{ g}\cdot\text{L}^{-1}$, $66.4 \pm 3.4 \text{ mgPO}_4^{3-}\cdot\text{P}\cdot\text{L}^{-1}$, and $244 \pm 8 \text{ mgNH}_4^+\cdot\text{N}\cdot\text{L}^{-1}$. Feed composition and its recipe can be found in **Annex C-1**.

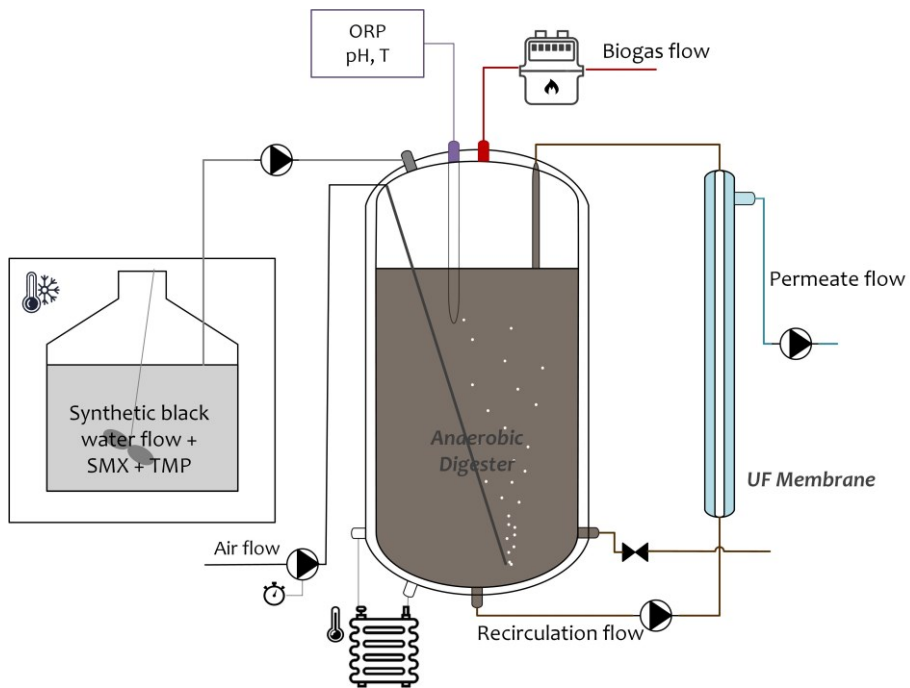


Figure 5-1. Micro-aerated AnMBR setup (MA-AnMBR). Adapted from Piaggio et al, 2023 (Submitted). The figure on the top shows the MA-AnMBR laboratory-scale setup. The figure on the bottom is a schematic representation of the laboratory-scale unit.

5.2.2 | Use of antibiotics SMX and TMP

Removal by adsorption and biodegradation of SMX and TMP was studied in both batch-scale systems and continuously operated MA-AnMBR system. From the literature, SMX and TMP concentrations in the influent of WWTPs vary from 10 to 500 $\mu\text{g}\cdot\text{L}^{-1}$. Considering that the synthetic influent of the MA-AnMBR is concentrated wastewater, 150 $\mu\text{g}\cdot\text{L}^{-1}$ of each antibiotic was added to the feed of the lab-scale MA-AnMBR. The addition of the antibiotics was done in steps and is described below. Moreover, SMX and TMP removal by adsorption was studied in batch tests (described in **section 5.2.5** hereafter) with concentrations between 10 and 150 $\mu\text{g}\cdot\text{L}^{-1}$.

5.2.3 | Reactor phases

A schematic view of the reactor phases is shown in **Figure 5-2**. The MA-AnMBR system was operated under stable conditions for 90 days before the addition of antibiotics was started. Hereafter, this phase is referred hereafter to as *P.I*.

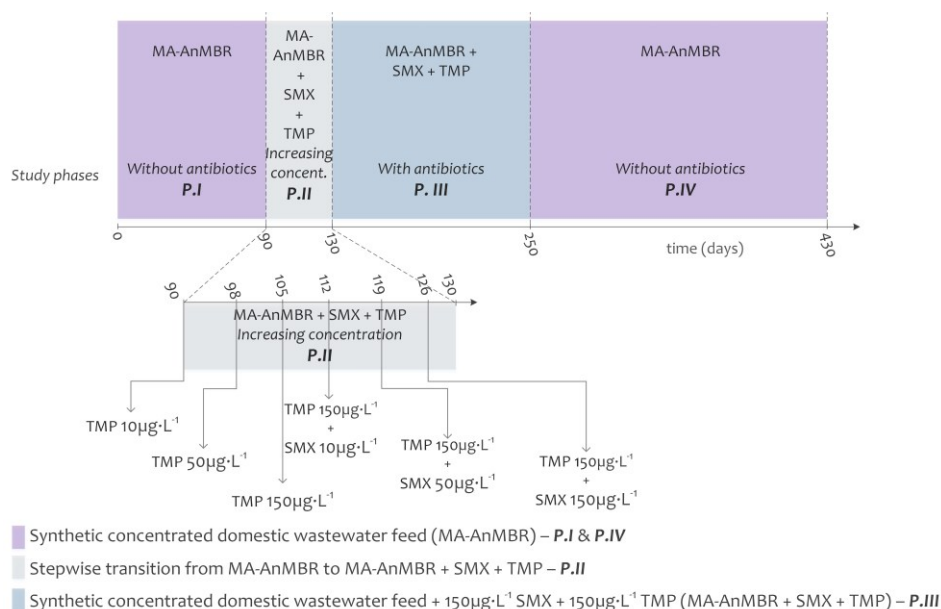


Figure 5-2. Schematic representation of the reactor phases.

The subsequent phase called *P.II* refers to the time frame in which the two antibiotics, TMP and SMX, were added step-wise to the reactor feed, as follows. Firstly, TMP was added to the feed in three steps of increasing concentrations: 10, 50, and 150 $\mu\text{g}\cdot\text{L}^{-1}$. The time lapse between each concentration shift corresponded to 3 hydraulic retention times (HRT), which was approximately one week. Thereafter, SMX addition

started and was done similarly to TMP in the same concentration steps and time. The whole *P.II* phase lasted 40 days.

Once both the SMX and TMP feed concentrations were $150 \mu\text{g}\cdot\text{L}^{-1}$, the reactor was continuously fed for a period of 120 days with the above-mentioned synthetic concentrated wastewater and $150 \mu\text{g}\cdot\text{L}^{-1}$ antibiotics. This phase is referred to as *P.III*.

Finally, the influent without antibiotics was fed again to the system from day 250 onwards and monitored for a further 180 days, reaching a total operational time of 430 days. This last monitoring phase was denominated *P.IV*.

5.2.4 | Analytical methods

COD measurements were done using HACH Lange test kits LCK 314, 514, and 014 (HACH, Tiel, The Netherlands). Nutrients, such as orthophosphate ($\text{PO}_4^{3-}\text{-P}$), total nitrogen (TN), ammonium-nitrogen ($\text{NH}_4^+\text{-N}$), and nitrate-nitrogen ($\text{NO}_3^-\text{-N}$) were measured with HACH Lange test kits (LCK238, LCK 303, and LCK 339). Total and volatile solids (in triplicates) were measured according to the APHA-Standard Methods (American Public Health Association, 2013). Sludge temperature, pH, and oxidation-reduction potential (ORP) were continuously measured with a Memosens CPS16D (Endress+Hauser, Reinach, Switzerland), installed in the reactor.

The composition of the volatile fatty acids (VFA) of the MA-AnMBR sludge were measured using an Agilent tech 7890A GC, with helium as a carrier gas. The gas flow rate was $2.45 \text{ mL}\cdot\text{min}^{-1}$ (at 0.76 bar), and detector and injector temperatures were 225°C and 240°C , respectively. The liquid samples were collected in 2 mL Eppendorf every week and measured following the procedure described by Garcia Rea et al (García Rea et al., 2020). Acetic, caproic (IC6), and propionic acids are measured in $\text{mg}\cdot\text{L}^{-1}$, and the final VFA concentration is expressed in $\text{mgCOD}\cdot\text{L}^{-1}$.

Biogas was analysed following the method described in **section 4.2.2**.

Antibiotics concentration measurement

Antibiotic concentrations in samples from batch experiments and the continuous-flow reactor were analysed using liquid chromatography-tandem triple quadrupole mass spectrometry (LC-MS). For feed and permeate samples, before analysis, a volume of 2 mL of sample was centrifuged in a micro-centrifuge (Eppendorf, Hamburg, Germany) at $10,000\times g$ for three minutes, and the supernatant was thereafter filtered through a $0.20 \mu\text{m}$ syringe filter (Chromafil® Xtra PES 20/25, Macherey-Nagel, Germany). Samples were stored at -20°C pending LC-MS analysis.

Antibiotic concentrations in the sludge from the continuous-flow reactor were measured using the methods described by Wijekoon et al. (2015). Homogenous sludge samples of 15 mL were centrifuged (Sorval ST 16R Centrifuge, Thermo Fisher Scientific, Waltham, MA, U.S.A) at $14,000 \times g$ for 15 minutes, and the supernatant was discarded. After freezing the remaining sludge samples at -80°C for at least one day, the samples were freeze-dried for 24 hours (BK-FD10, Biobase, Shandong, China). The dried sludge was then grounded to a fine powder using a hand mortar and pestle, and a mass of 0.4 g was transferred to a tube, where 4 mL of methanol (>99%) was added. The samples were mixed with a vortex and sonicated for 10 minutes with an amplitude set up of 20% and temperature less than 60°C (Branson 450 Digital Sonifier, Connecticut, U.S.A). Afterwards, the sample was centrifuged at $3,300 \times g$ for 15 min, and the supernatant was collected in a fresh 15 mL tube for further analysis. Finally, the solution was filtered through a $0.20 \mu\text{m}$ syringe filter (Chromafil® Xtra PES 20/25, Macherey-Nagel, Germany), and treated in a similar way to the permeate and liquid samples.

Chromatographic separation of the pharmaceuticals was performed by the ACQUITY UPLC® BEH C18 column ($2.1 \times 50 \text{ mm}$, $1.7 \mu\text{m}$, Waters, Ireland) with a gradient elution of ultrapure water. Acetonitrile was the mobile phase, and its flow rate was set to $0.35 \text{ ml}\cdot\text{min}^{-1}$ using an ACQUITY UPLC I-Class Plus pump (Waters, U.S.A). Ultrapure water and acetonitrile (LC-MS grade, Biosolve, France) were acidified with 0.1% formic acid (LC-MS grade, Biosolve, France). Detection of the pharmaceuticals by mass spectrometry (Xevo TQ-S micro, Waters, U.S.A) was conducted in the positive and negative electrospray ionization modes. The obtained data were analysed and compared to internal standards, based on the methods and information described by Zheng et al. (2022).

Heterotrophic plate count

Microbiological screening and quantification were performed by spread plate method according to APHA-Standard Methods (American Public Health Association, 2013). The total heterotrophic bacteria count was assessed by plating 0.1 mL of sample (either from the permeate or sludge) on a non-selective tryptone soya agar and low-nutrient Reasoner's 2A (R2A) agar. ARB were measured by adding concentrations of $50.4 \text{ mg}\cdot\text{L}^{-1}$ of SMX, or $16 \text{ mg}\cdot\text{L}^{-1}$ of TMP to the plate media (R2A). The antibiotics concentrations added to the R2A media were chosen based on the minimum inhibitory concentrations given by the Clinical and Laboratory Standards Institute (CLSI, 2019) and studies performed by Zarei-Baygi et al. (2019); (Zarei-Baygi et al., 2020).

5.2.5 | Adsorption batch tests

Adsorption tests were performed in 250 mL glass bottles at 10°C for seven hours, to retard biodegradation. A volume of 100 mL of acclimated sludge from the first phase *P.I.*, collected daily and stored at 4°C, was used to perform all adsorption experiments. For SMX and TMP, three different antibiotic concentrations were tested: 10, 50, and 150 µg·L⁻¹. Each antibiotic concentration was added to the 250 mL glass bottles. All experiments were performed in triplicates, summing up to a total of 18 bottles and six different analysis conditions. Immediately after the addition of the antibiotics, the bottles were placed on the magnetic stirrer at 160 RPM (C-MAG HS7, IKA®, Staufen, Germany), for over six hours. Sludge samples were collected in Eppendorf tubes of 2 mL volume and performed every five minutes for a period of 45 minutes, then every 15 minutes for two hours, and finally, every half an hour for the next four hours. After collecting, the samples were immediately centrifuged in a micro-centrifuge (Eppendorf, Hamburg, Germany), the supernatant was filtered through a 0.20 µm syringe filter, and the samples were stored at -20°C until further analysis of the residual dissolved pharmaceuticals in the LC-MS.

5.2.6 | Genetic analysis of ARGs

DNA extraction

Triplicate sludge and permeate samples from the MA-AnMBR were taken in the four studied phases, to extract DNA. The method followed to extract DNA was identical to the one described in **section 4.3.4**.

Quantitative polymerase chain reaction (qPCR) analysis of selected ARGs

Three ARGs were selected for qPCR analysis on the DNA fractions extracted from the sludge and permeate of the continuous MA-AnMBR lab-scale system. The chosen ARGs targeted the sulphonamide resistance genes *sul1* and *sul2*, and dihydrofolate reductase gene *dfrA1*, to assess the potential resistance gained by the sludge by the addition of SMX and TMP, respectively. Aside from the ARGs, one mobile genetic element (MGE) biomarker was selected to investigate gene mobility, namely the class I integron-integrase gene *intI1* (Ma et al., 2017). The 16S rRNA gene was selected as a proxy to quantify total bacteria. Standards, primers, and mix solutions were based on the work performed by Calderón-Franco et al. (2021), and are given in **Annex D-1** of the supplementary material.

5.3 | RESULTS

5.3.1 | MA-AnMBR performance

Changes in the MA-AnMBR performance before and after adding the antibiotics are shown in **Table 5-2**. The COD removal was always above 97%, with permeate COD values that varied between 50 and 90 mg·L⁻¹. The statistical difference between the reactor parameters was assessed using ANOVA single-factor between the MA-AnMBR parameters before and during the antibiotic's addition phases (P.I and P.III).

The reactor pH, system average biogas production, and biogas methane concentration showed statistical differences between the values obtained at the studied phases. The sludge pH decreased from 7.8 to 7.5 after the addition of antibiotics. Furthermore, while biogas production remained unchanged, around 1.4 L·d⁻¹, the biogas methane content decreased, from 84 to 78 %. Whilst the CH₄ concentration decreased, the carbon dioxide biogas concentration doubled, from 7 to 16%. No significant differences in sludge concentration, either suspended or total, was observed. Similarly, the nutrient content in the reactor permeate (as NH₄⁺ and PO₄³⁻) remained unchanged after the addition of 150 µg·L⁻¹ of SMX and TMP.

Antibiotics SMX and TMP removal was assessed during phase *P.II*, where the antibiotics were introduced stepwise until a concentration of 150 µg·L⁻¹ each (during 40 days in total), and during phase *P.III*, for 120 days. During *P.II*, TMP concentration in the MA-AnMBR permeate remained below 10 µg·L⁻¹, and SMX values were below 20 µg·L⁻¹. Once stable conditions were achieved at *P.III*, the SMX and TMP removal of the MA-AnMBR was 86 ± 5% and 97 ± 1% respectively. Antibiotics concentrations adsorbed in the MA-AnMBR sludge were similar to the ones found in the permeate, 9 ± 4 µg·L⁻¹ and 14 ± 6 µg·L⁻¹ of TMP and SMX respectively.

Table 5-2. Summary of the MA-AnMBR performance during the operational phases P.I, and P.III. Values correspond to averages and standard deviations of samples (in triplicates), and those in bold show statistical important variations (p -value < 0.05).

	Unit	P.I	P.III	p-value
Chemical Oxygen Demand (COD) removal efficiency	%	99 ± 1	98 ± 1	0.3
Volatile Fatty Acid (VFA) accumulation	mgCOD·L⁻¹	6.6 ± 1.1	10.8 ± 3.4	< 0.05
Ortho-phosphate removal efficiency	%	59 ± 5	55 ± 7	0.4
Sulphate removal efficiency	%	> 84*	> 88*	0.8
Ammonium concentration in the permeate	mgNH ₄ ⁺ -N·L ⁻¹	3.3 ± 0.4	3.5 ± 0.1	0.1
Sludge Total Suspended Solids (TSS)	g·L ⁻¹	694 ± 44	677 ± 49	0.1
Sludge Volatile Suspended Solids (VSS)	g·L ⁻¹	3.3 ± 0.4	3.5 ± 0.1	0.7
Sludge Total Solids (TS)	g·L ⁻¹	7.7 ± 1.3	7.5 ± 0.1	0.8
Sludge Volatile Solids (VS)	g·L ⁻¹	3.7 ± 0.8	3.6 ± 0.2	0.9
Sludge pH	-	7.8±0.2	7.5 ± 0.1	< 0.05
Sludge Oxidation-Reduction Potential (ORP)	mV	-538±14	-532±12	0.2
Average biogas production	L·d ⁻¹	1.4 ± 0.3	2.1 ± 0.6	0.8
Methane concentration in biogas	%	84 ± 3	78 ± 6	0.05
Carbon dioxide concentration in biogas	%	7 ± 3	16 ± 2	< 0.05

*MA-AnMBR permeate had values of sulphate concentration below the detection limit. The removal was calculated based on the minimum detection value

5.3.2 | Antibiotics adsorption batch tests

Batch tests with MA-AnMBR sludge, taken from the reactor during *P.I.*, were conducted to assess TMP and SMX adsorptions at 10 °C, for concentrations of 10, 50, and 150 $\mu\text{g}\cdot\text{L}^{-1}$. For all studied concentrations, adsorbed TMP was around 82% after six hours, as shown in **Figure 5-3**. TMP had a high level of adsorption in the first five minutes of testing. TMP concentrations in the liquid after 5 minutes were below 30% of the initial concentrations applying 10 and 50 $\mu\text{g}\cdot\text{L}^{-1}$, and 50% for the initial concentration of 150 $\mu\text{g}\cdot\text{L}^{-1}$. A single-factor ANOVA statistical analysis was conducted to assess the adsorption differences between the different initial TMP concentrations (10, 50, and 150 $\mu\text{g}\cdot\text{L}^{-1}$). No statistical differences were found after 6 hours of testing (*p*-value of 0.2).

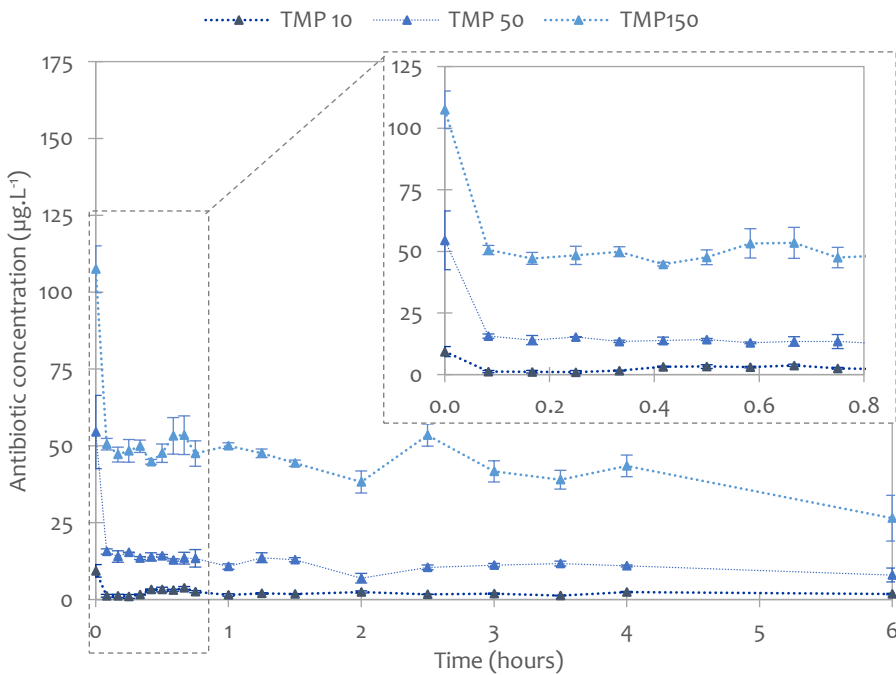


Figure 5-3. Adsorption batch tests of antibiotic TMP at 10°C, with MA-AnMBR sludge. The sludge's total solids concentration was 4.1 $\text{g}\cdot\text{L}^{-1}$.

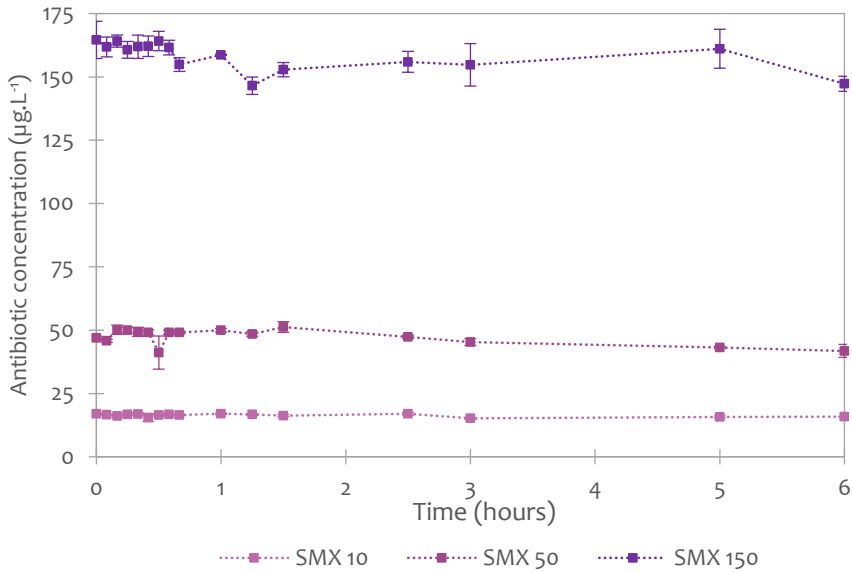


Figure 5-4. Adsorption batch tests of antibiotic SMX at 10°C, with MA-AnMBR sludge. The sludge's total solids concentration was 3.9 g·L⁻¹.

Adsorption of SMX onto the MA-AnMBR sludge was minimal, with values of 11% after six hours of testing (**Figure 5-4**). No statistical differences were found (p-value of 0.4) between the observed adsorption at the different SMX concentrations.

5.3.3 | Antibiotic-resistant bacteria

The levels of ARB in the MA-AnMBR bulk and permeate were measured by heterotrophic plate count in three out of the four study phases: *P.II*, *P.III*, and *P.IV*, while the total bacterial concentration was additionally measured during phase *P.I*. Results are shown in **Figure 5-5**. Total bacteria removal in the MA-AnMBR system was in the order of 3 log in all studied phases, 99.9% (difference between the bacteria count in the reactor bulk and the UF permeate). Removal of ARB varied and depended on the experimental phase. No resistant bacteria to SMX or TMP were found in the permeate after 21 days of TMP supply (day 111; influent TMP concentration was 150 µg·L⁻¹ and SMX was not yet added).

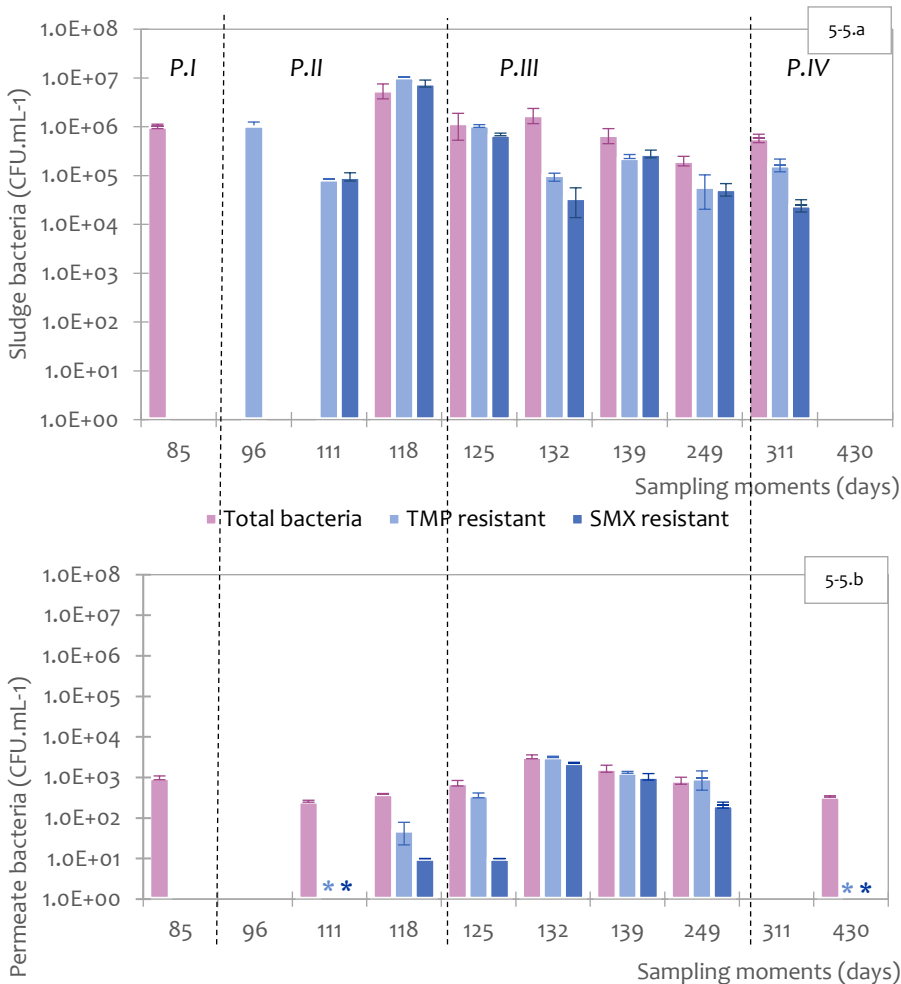


Figure 5-5. Antibiotic-resistant and total bacteria in the MA-AnMBR. Fig. 5-5.a shows the MA-AnMBR reactor bulk bacteria. Fig. 5-5.b shows the MA-AnMBR UF permeate bacteria. The reactor phases are visualized with dotted vertical lines. P. I to P.IV refer to the different reactor phases. More information can be found in **Figure 5-2**. Days with * refer to measured samples with values below the detection limit. Blank days indicate no measurements.

During P.IV, the MA-AnMBR influent was supplied again with a feed without antibiotics. No resistant bacteria to SMX nor TMP were detected anymore from the MA-AnMBR permeate. SMX-resistant bacteria followed a similar trend to TMP-resistant bacteria. SMX-resistant ones were removed by 5 log during P.II and by 2 log during P.III. Likewise, TMP-resistant bacteria were removed by 4 log during P.II and

by 2 log during P.III. Furthermore, during P.III, the concentration of total bacteria in the permeate was similar to the ARB ones.

5.3.4 | Antibiotic-resistant genes

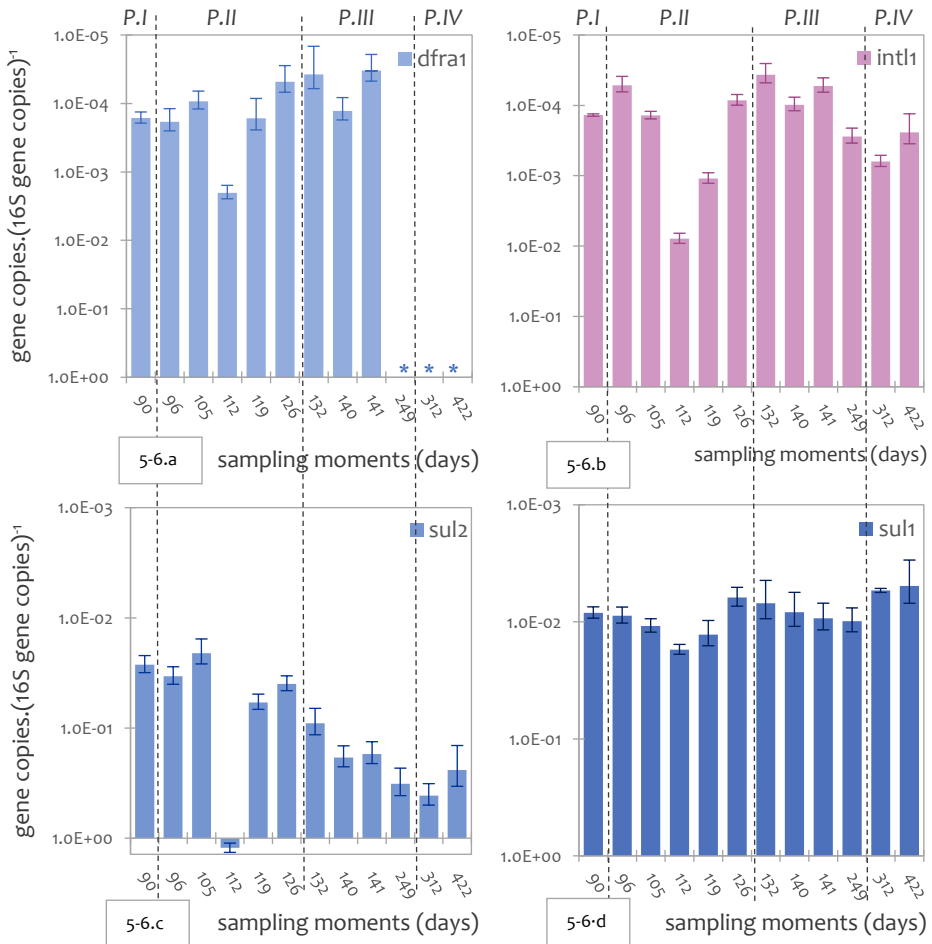


Figure 5-6. Antibiotic-resistant gene copies per 16S gene copies of the MA-AnMBR sludge. Fig. 5-6.a refers to *dfrA1* gene concentration. Fig. 5-6.b refers to *intI1* concentration. Fig. 5-6.c. refers to *sul2* concentration, and Fig. 5-6.d. refers *sul1* gene concentration. The reactor phases are visualized with dotted vertical lines P. I to P.IV refer to the different reactor phases. More information can be found in **Figure 5-2**. Values below the detection limit for *dfrA1* (5.2×10^3 *dfrA1* gene copies) are presented with *, and blank days indicate no measurements.

The ARGs *sul1*, *sul2* and *dfrA1*, and the MGE *intl1* were measured during the four reactor phases from the MA-AnMBR sludge. All genes were already found in the sludge sample that was taken before the addition of the antibiotics, on day 90 of operation. During *P.II*, all four genes showed an increase in their relative abundance (per 16S rRNA gene), as shown in **Figure 5-6**. A peak in all four gene relative abundances was observed on day 112, which corresponded to the start of the addition of $10 \mu\text{g}\cdot\text{L}^{-1}$ of SMX.

Relative abundances of the *sul2* gene were highest among the analyzed genes, with an average difference corresponding to two orders of magnitude. Aside from the peak on day 112, *sul2* increased during *P.II* and *P.III* to a value of 3.2×10^{-1} gene copies·(16S gene copies)⁻¹ at the end of *P.III* (day 249). During *P.IV*, the dosing of antibiotics in the influent was stopped, however, after 62 days in *P.IV* (day 312), *sul2* reached even 4.1×10^{-1} gene copies·(16S gene copies)⁻¹. This concentration decreased to only 2.4×10^{-1} gene copies·(16S gene copies)⁻¹ on the last day of reactor operation (day 422). A reduction in gene copies in phase *P.IV* was also observed for *dfrA1* and *sul1*, indicating a loss of antibiotic-resistance genes when antibiotic dosage to the MA-AnMBR was stopped. Concentrations of *sul1* during *P.IV* were even found to be below the values measured before the start of the antibiotic's addition: 5.0×10^{-3} and 8.4×10^{-3} gene copies·(16S gene copies)⁻¹ respectively. Finally, gene copies were below the detection limit of 5.2×10^{-3} for *dfrA1* at the end of *P.III* (day 249 days).

Gene copies from the UF permeate of the MA-AnMBR were measured during the first three reactor phases. UF permeate *dfrA1* gene copies were below the detection limit in all samples. For the rest of the studied genes, a difference of one to four orders of magnitude was found between the total abundance of gene copies (per mL of sample) in the bulk and the ones in the MA-AnMBR UF permeate, as shown for *sul1* in **Figure 5-7**. Apparently, the UF membrane of the MA-AnMBR retained the majority of the microorganisms that contained the studied genes, reducing 99.9% of the studied genes. Nevertheless, when considering the relative abundance of gene copies, the concentration of copies in the UF permeate and the reactor bulk tends to be in the same order of magnitude, as shown for the *sul1* gene in **Figure 5-7**. Permeate and sludge concentrations of gene *sul2* and MGE *intl-1* can be found in **Annex D-2**.

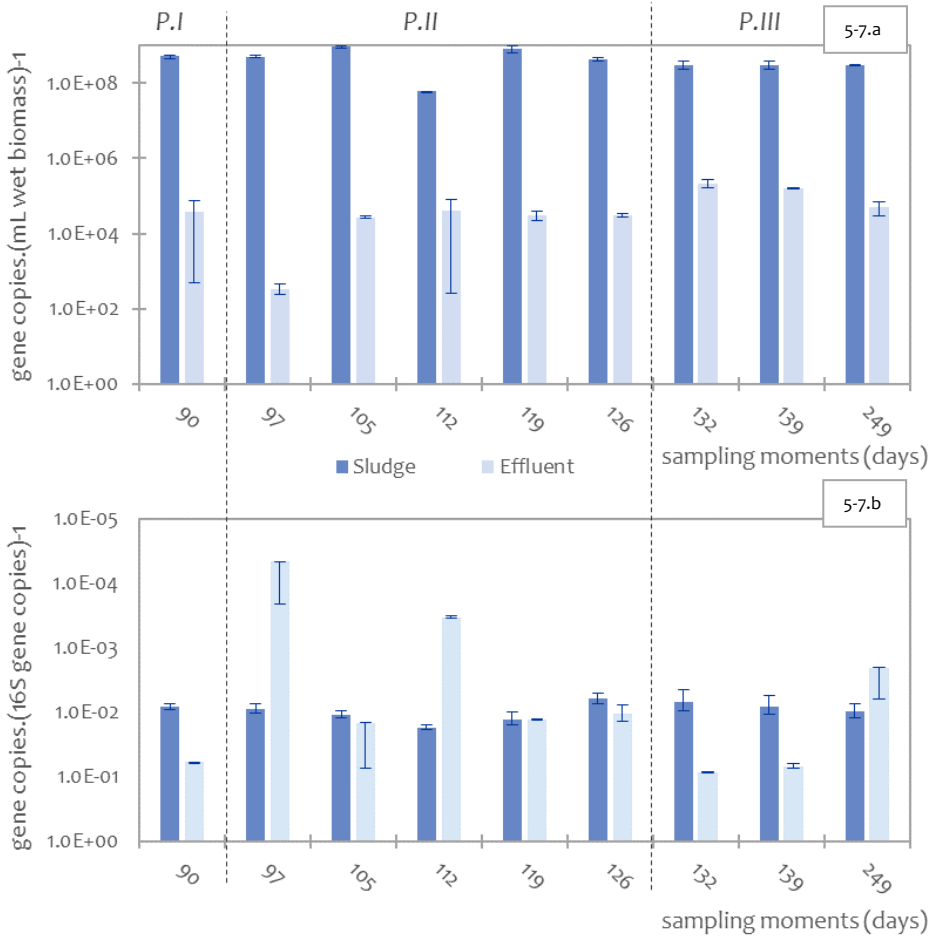


Figure 5-7. The concentration of gene *sul1* on the MA-AnMBR sludge and permeate. Fig. 5-7.a corresponds to the total gene copies per mL of wet biomass, while the values of Fig 5-7.b show *sul1* gene standardized per 16S gene copies. The reactor phases are visualized with dotted vertical lines P. I to P.IV refer to the different reactor phases. More information can be found in **Figure 5-2**.

5.4 | DISCUSSION

5.4.1 | Removal and consequences of TMP and SMX addition in the MA-AnMBR

Despite the addition of air in the MA-AnMBR, TMP removal was high, i.e., $97 \pm 1\%$. A similar TMP removal of around 94% was obtained in a lab-scale AnMBR treating

synthetic sewage (Xiao et al., 2017). Feng et al. (2017) have found that TMP removal during pig manure digestion under strict anaerobic conditions exceeded 99% after 10 days of digestion. In contrast, a TMP removal of only 26.4% has been measured from conventional activated sludge processes, that are mostly operated with aerobic conditions or in alternating redox conditions (Li & Zhang, 2010). Previously, the changes in AnMBR performance with and without micro-aeration had been assessed: it was concluded that the given micro-aeration (reaching an oxygen over influent COD load of 1.0%) had a negligible impact on the reactor performance (Piaggio et al, submitted). Thus, based on the efficiency measured in the MA-AnMBR, it can be inferred that the micro-aeration of the system has a negligible effect on TMP removal, and the MA-AnMBR is efficient in the removal of this antibiotic.

The log K_{ow} value of TMP and its positive charge at circumneutral pH results in quick adsorption onto the negatively charged biomass (Jia et al., 1996). Adsorption of TMP at 10 °C in batch tests showed a removal of TMP of around 75% after six hours of testing, as shown in **Figure 5-4**. In the continuous-flow MA-AnMBR, removal of TMP from the permeate reached 97%. From the results obtained in the adsorption tests, the sludge adsorption capacity for the highest TMP concentration tested ($107 \mu\text{g}\cdot\text{L}^{-1}$) was around $200 \mu\text{g}\cdot\text{gTSS}$. The MA-AnMBR has a TSS content of $6\text{g}\cdot\text{L}^{-1}$ and total volume of 6.5 L, resulting in a total biomass suspended biomass of 39 g. Considering the above-mentioned adsorption capacity, the MA-AnMBR is expected to be TMP saturated after 21 days of operation. Hereafter, if no biodegradation of TMP would have occurred, TMP would have accumulated, reaching increased concentrations. Since the overall removal of TMP in the MA-AnMBR is 97%, it can be concluded that TMP was indeed degraded in the MA-AnMBR. Antibiotic concentration in the MA-AnMBR sludge was measured during *P.II* and *P.III*. The residual TMP concentration increased from *P.II* to *P.III* until it reached a plateau, with a concentration of $9 \pm 4 \mu\text{g}\cdot\text{L}^{-1}$. Thus, TMP is quickly adsorbed onto the sludge and very likely subsequently digested. Apparently, the applied SRT of 27 days allowed enough time for the anaerobic degradation of TMP Alvarino et al. (2018); Feng et al. (2017).

The removal of SMX in the MA-AnMBR was $86 \pm 5\%$. This value was in the same range, between 70 to 90%, of reported SMX removal in fully anaerobic lab-scale AnMBR units treating domestic wastewater (Harb et al., 2021; Oberoi et al., 2022; Zarei-Baygi et al., 2020). SMX removal in an aerobic activated sludge process has been reported to be much lower than in the MA-AnMBR, i.e., 39.1% (Li & Zhang, 2010). ORP measurements showed that anaerobic conditions were kept in the MA-AnMBR even under micro-aeration, maintaining an ORP of -530 mV. Whilst a high removal of SMX was obtained

in the MA-AnMBR, batch adsorption tests at 10 °C showed SMX removal below 15% (**Figure 5-3**). The low adsorption of SMX onto the sludge is likely due to the negative charge of SMX at circumneutral pH, disfavoring its attraction to negatively charged biomass. The residual SMX concentration in the MA-AnMBR sludge was only $14 \pm 6 \mu\text{g}\cdot\text{L}^{-1}$ during *P.III*.

Most likely SMX was also degraded anaerobically in the MA-AnMBR, considering the measured removal efficiencies. With the measured low adsorption, the degradation rate of SMX is determined by the hydraulic loading rate, which resulted in an HRT of 2.6 days. The most important transformation reactions of the isoxazole ring of SMX and routes to co-metabolize SMX are hydroxylation, hydrogenation, acetylation, desulfurization and reductive cleavage, among others (Jia et al., 2017; Tang et al., 2022). Some of the degradation pathways of SMX, like hydroxylation and desulfurization as part of acetylation, take less than one day, ensuring SMX degradation when HRTs < 1 day are applied (Tang et al., 2022). According to Dermer and Fuchs (2012), dehydrogenases enzymes play a key role in the hydroxylation of SMX under anaerobic conditions, and hydroxylation can be considered one of the main SMX degradation pathways. Results indicate that antibiotics like TMP, which easily adsorb to the sludge, are efficiently degraded in anaerobic reactors that are characterized by a long SRT. However, antibiotics that remain solubilized, like SMX, require a minimum HRT for efficient conversion. Regarding SMX, an HRT of 2.6 days was already sufficient for a high removal efficiency. For practical purposes, further research on optimizing HRT values is recommended.

While biogas quality changes from *P.I* to *P.III* were statistically significant, no change in biogas quantity was observed. Cetecioglu et al. (2015) have shown that only concentrations above $45 \text{ mg}\cdot\text{L}^{-1}$ of SMX were lethal to the microbial community and hence, inhibit biogas production. Zarei-Baygi et al. (2020) have concluded that after the addition of $250 \mu\text{g}\cdot\text{L}^{-1}$ of SMX to a laboratory-scale AnMBR fed with synthetic wastewater, the abundance of methanogens remained the same, and the microbial community of biomass was stable throughout the study. Furthermore, Tang et al. (2022) concluded that addition of up to $2 \text{ mg}\cdot\text{L}^{-1}$ of SMX was beneficial for methane production in batch experiments, which was explained by the negative impact of SMX addition on acidogenic biomass, preventing the build-up of acid intermediates and low pH. As a consequence, the time required to reach the maximum methane production was distinctly shortened.

5.4.2 | TMP and SMX ARB and ARGs

The results of this long-term experiment indicated potential development of antibiotic resistance in the bacterial population when antibiotics are present in the wastewaters. In the MA-AnMBR permeate, no ARB bacteria were present in day 111 and 430. The latter sampling moment was performed when the MA-AnMBR was fed with synthetic feed without antibiotics, while the samples taken on day 111 corresponded to the moment that the MA-AnMBR was fed with the synthetic feed and $150 \mu\text{g}\cdot\text{L}^{-1}$ of TMP. ARB measurements performed after day 111 showed an increase in both TMP and SMX relative concentrations (to the total heterotrophic bacterial count), as shown in **Figure 5-5**. The highest concentration of TMP and SMX ARB in the UF permeate were obtained on *P.III*, having a relative abundance of 57 and 70% respectively. Furthermore, TMP ARB in the MA-AnMBR bulk increased from 4% of the total heterotrophic bacteria count at *P.II*, to 9% at *P.III* and finally 20% at *P.IV*. On the other hand, no significant difference was found in the relative abundance of the TMP and SMX ARB in the reactor bulk during the studied periods (p values of 0.3 and 0.8 respectively).

5 Both SMX and TMP-resistant bacteria were measured in the MA-AnMBR permeate during phases *P.I* to *P.III*, and SMX and TMP-resistant bacteria relative abundance significantly increased during *P.II*, while the antibiotics were being added in steps (p-value below 0.05). Moreover, no resistant bacteria were found 180 days after the antibiotic's dosage to the MA-AnMBR was stopped (day 430, *P.IV*). Whilst these results might indicate the loss of resistance once the antibiotics were removed from the feed solution, antibiotic-resistant genes for SMX were still found in abundance in the MA-AnMBR permeate in *P.IV*, on day 311, indicating the contrary. The antibiotic-resistant gene chosen for TMP, *dfrA1*, was below the detection limit in all phases of permeate samples. Thus, it is advised to assess the resistance towards this antibiotic in the MA-AnMBR on the ARB count, instead of the selected ARG.

The MA-AnMBR was equipped with a UF membrane with a nominal pore size of 30 nm, which was apparently too big for complete removal of total bacteria or ARB, under all the studied phases. Lousada-Ferreira et al. (2016) have found that particles 100 times bigger than the nominal pore size were found in several membranes' permeates, even when membrane integrity was not compromised. The authors concluded that the nominal membrane pore size given by the manufacturer is rather an indication of the average membrane pore size but might be very different from the maximum values. Most municipal wastewater bacteria sizes vary between 1 to 100 μm , for example, *E.coli* has an average size of 1-2 μm (Levine et al., 1985).

Therefore, it is possible that some bacteria will pass the UF membrane of the MA-AnMBR. Furthermore, the permeate of the laboratory-scale MA-AnMBR is rich in nutrients, such as nitrogen and phosphorus, and has an optimal temperature for bacterial re-growth. Nonetheless, the determined values around 10^3 CFU·mL⁻¹ for the laboratory-scale MA-AnMBR permeate, represented 3 log removal of total bacteria and ARB.

All measured ARGs and *intl1* concentrations in the MA-AnMBR sludge and UF permeate increased during phase *P.II*, but only *sul1* and *sul2* relative concentrations in the sludge kept increasing during phase *P.III*, as shown in **Figure 5-6**. These results are aligned with the results obtained by Guo et al. (2021), who found an increase in *intl1* mobile gene element, *sul1* and *sul2* due to an addition of oxygen equivalent to 1% of influent COD, in a sequencing batch reactor fed with blackwater. The increase in *sul1* and *sul2* genes due to the addition of SMX, has also been observed by Zarei-Baygi et al. (2019) and Blahna et al. (2006). Whilst SMX resistance genes increased during *P.II* and *P.III*, no statistical differences were found in the relative concentration of SMX-resistant bacteria and total bacteria between these phases (p-value of 0.4). Furthermore, the relative abundance of ARG in the permeate was similar to the one obtained in the sludge. Thus, while the UF membrane can retain 99.9% of the measured bacteria, the bacteria present in the permeate has a similar abundance of ARGs.

Pearson correlation tests were conducted between the measured levels of SMX-resistant bacteria and TMP-resistant bacteria, and the relative abundances of the different genes, for samples taken from the reactor bulk and the permeate of the MA-AnMBR. A strong linear correlation was assumed when the absolute value of the Pearson coefficient (ρ) was above 0.7. A strong linear positive correlation was observed between TMP- and SMX-resistant bacteria in the reactor bulk and UF permeate, with ρ values of 0.83 and 0.97 respectively (**Annex D-3**). Thus, SMX-resistant bacteria increased simultaneously with TMP-resistant bacteria, which might be attributed to the fact that both antibiotics were more or less simultaneously added to the MA-AnMBR, with only 20 days difference between the start of dosing TMP and SMX.

The gene *dfra1* was positively correlated to all studied genes in the sludge samples of the MA-AnMBR. When a concentration of $10 \mu\text{g}\cdot\text{L}^{-1}$ of SMX started to be added to the reactor on day 112, all studied genes reached their maximum concentration (**Figure 5-6**). Apparently, addition of SMX not only induced the concentration increase of *sul1* and *sul2*, i.e., the genes associated with this antibiotic, but also increased other ARGs.

The change in *dfrA1* gene concentration could be linked to both SMX and/or TMP addition, and therefore, TMP resistance is not only linked to changes in *dfrA1* concentration. Results showed that plate counts of resistant bacteria is a better estimation for measuring resistance towards TMP than the relative abundance of the *dfrA1* gene.

Finally, all measured relative abundances of the *sul1*, *sul2*, *dfrA1*, and *int1* genes decreased during phase P.IV, i.e., when the MA-AnMBR was fed without antibiotics. Biological digestion in the MA-AnMBR is favourable for the reduction of ARG levels in the sludge. Several authors have stated that biological treatment and membrane systems are efficient for the removal of ARGs, especially *sul1* and *sul2* (Munir et al., 2011; Zarei-Baygi et al., 2019; Zheng et al., 2019). Nevertheless, considering the relative abundance of genes (vs. 16S rRNA gene copy number), the UF membrane system of the MA-AnMBR did not retain all microorganisms, and the permeate still had ARGs. Thus, while the biological treatment achieved an increased removal of ARGs, it was not efficient in retaining all microorganisms, and the UF permeate showed a similar ARGs abundance to the one in the reactor bulk. Thus, for the complete removal of ARB and microorganisms containing the studied ARGs, a subsequent treatment step should be implemented.

5.5 | CONCLUSIONS

The fate of the SMX and TMP antibiotics was studied in a laboratory scale micro-aerated AnMBR fed with synthetic, concentrated domestic wastewater. The build-up of antibiotic resistance was assessed by measuring the concentrations of ARB, ARGs *sul1*, *sul2*, *dfrA1*, and MGE *int1* in the sludge and permeate. The effect of the additions of the antibiotics on the performance of the MA-AnMBR, their removal, and their relation to resistance induction were assessed for 430 days. The main conclusions of the research are the following:

- The addition of 150 $\mu\text{g}\cdot\text{L}^{-1}$ of SMX and TMP into the MA-AnMBR feed had negligible effects on the system performance. The sludge pH decreased from 7.8 to 7.5, which simultaneously entailed an increase of CO₂ concentration in the biogas (from 7 to 16%) and a decrease in the CH₄ partial pressure. These changes were statistically significant (p-value <0.05).
- A high removal of SMX and TMP was achieved in the laboratory-scale MA-AnMBR. SMX was poorly adsorbed into the sludge but rapidly degraded, reaching a total removal of 86%, measured in the MA-AnMBR permeate,

relative to the influent. In contrast, TMP was rapidly adsorbed onto the MA-AnMBR sludge while the long SRT of the system guaranteed its degradation, achieving a total TMP removal of 97%. Thus, micro-aeration of the membrane system had no negative effect on the removal of the antibiotics.

- ARB and ARGs were found in both the MA-AnMBR sludge and permeate. No significant difference was found in the relative abundance of the TMP and SMX ARB in the reactor bulk during the studied periods. While the system was able to reduce the ARB concentration by 3 log, the ARGs abundance (relative to the 16S-rRNA gene) was similar in the sludge and the ultrafiltration permeate. The addition of SMX and TMP led to an increase in the relative abundance of all ARGs and *int11* in the MA-AnMBR sludge.
- The relative abundance of the ARG *dfrA1* in the MA-AnMBR mixed liquor had a strong linear correlation with *sul1*, *sul2*, and the MGE *int11*. However, changes in relative abundance of the genes were not linked to ARB. Thus, the gain of resistance to TMP or SMX is better assessed by the heterotrophic plate count of ARB than by molecular detection of the genes.
- The relative abundance of the MGE *int11* in the sludge was positively and linearly correlated with all measured genes (p values above 0.82), reflecting the overall effect of antibiotics on the microbial gene pool.



Bubbles created with watercolour, soap, and water.

6

Outlook

6.1 | FOREWORD

Around 40% of the global population endures water scarcity for at least one month per year, an issue related to both water quantity and quality (UN, 2018). Human activity causes pollution of freshwater streams around the world. These streams are subjected to wastewaters with a wide range of pollutants, both in pollutant characteristics and concentration, as well as in fluctuating flows; these variabilities make it challenging to adequately treat the discharged wastewater. Nevertheless, adequately treating wastewater flow can ensure to keep fresh water streams healthy, and, in combination with aiming for water reuse, can alleviate the increasing water scarcity.

This dissertation studied the potential of anaerobic digestion combined with dissolved air flotation (AD-DAF) system when used as a pre-treatment technology, specifically for the treatment of drain- and wastewater. Synthetic water matrices were used, intended to mimic the ever-changing conditions of the Barapullah drain in New Delhi, the subject of study in the LOTUS-HR programme. The implications of coupling these two technologies were assessed on a laboratory-scale by having two separate systems: a column DAF unit, and a micro-aerated anaerobic membrane bioreactor (MA-AnMBR).

This chapter summarises the main conclusions drawn throughout the work presented in this dissertation. These conclusions are followed by practical implications of where AD-DAF technology could make a difference and an outlook on future research directions.

6.2 | SUMMARY OF CONCLUSIONS

Overall, based on the laboratory results, it can be concluded that an AD-DAF system has the potential to effectively remove total suspended solids under variable influent conditions. Furthermore, the oxygen load into the AD, coming from the DAF unit, might increase the anaerobic biomass hydrolytic capacity whilst reducing the system biogas production. The main conclusions of this dissertation are summarised as follows:

An experimental model, using low-cost laboratory measurements can be used to predict total suspended solids (TSS) removal of DAF systems. The experimental model described in **Chapter 2** used six independent variables: particle size distribution (PSD), particle density, influent temperature, DAF contact zone detention time, inflow and recycle flows; and two dependent ones: the collision

efficiency factor, and average bubble diameter. The influent PSD and density, and average bubble diameter, were key inputs for the experimental model. The measurement of these parameters was performed using easily available computational tools (PIVlab and FIJI-ImageJ software), a cell phone camera, and low-complexity experimental procedures. These methods could overcome the difficulties of performing pilot or full-scale TSS removal tests for assessing the efficiency of DAF systems. Furthermore, the verification of the experimental model results showed a predicted TSS removal aligned with the measured one of Delft canal water, anaerobic sludge, and DAF2 influents. The experimental model was able to identify that the full-scale DAF1 unit was underperforming, with a measured TSS removal of 91% and an expected one of 98%. Thus, the developed experimental model is able to predict TSS removal for variable influent characteristics.

Effective TSS removal can be achieved by a down-scaled DAF unit and used to predict the efficiency of the full-scale system. From the tested influents, three resemble the Barapullah drain seasonal variations in composition, and the fourth one mimicked the feed of a DAF when located after an anaerobic bioreactor or closer to the pollution source (household level), as described in **Chapter 3**. Maximum TSS removal varied between 92 and 96% for all studied influents. Seven performance variables were tested to assess their impact on TSS removal: influent TSS concentration, pH, temperature, residence time, pressure, coagulant and flocculant concentration, and coagulation time. The effect of the performance variables altered depending on the influent type, with pressure showing a positive influence on the separation efficiency for all tested influents. Moreover, the DAF unit showed lower removal efficiency for particles with spherical shapes and diameters below 10 μm . Finally, due to the DAF's compact design, small footprint and high TSS removal, it could be located either downstream at the drain or closer to the pollution source, highlighting its usage as a pre-treatment technology for water reuse.

The laboratory-scaled MA-AnMBR biomass studied in Chapter 4 seemingly adapted to the added oxygen dosage, which mimics the coupling of the AD to a DAF system (between 1 and 3% of the COD load), creating an AD-DAF system. Results showed a lower COD concentration in the MA-AnMBR effluent in comparison to the AnMBR effluent, from 90 to 74 $\text{mgCOD}\cdot\text{L}^{-1}$, and a concomitant 27% decrease in biogas production. Micro-aeration was defined as the aeration range at which no significant changes in the oxidation-reduction potential (ORP) were observed in the reactor (below 10%). A rise in hydrolysis of the MA-AnMBR biomass was achieved, based on an increase of 35% in the effluent ammonium (NH_4^+) concentration. Moreover, an

increase in the superoxide dismutase activity (SOD) of the biomass was observed. Meanwhile, negligible changes were observed in the specific methanogenic activity (SMA) of the micro-aerated biomass that was subjected to an oxygen load equivalent to 3% of the influent COD load in batch tests. These results showed that the given oxygen load did not affect the performance of the anaerobic conversion process, indicating the feasibility of an anaerobic digester–DAF (AD-DAF) system.

Antibiotics sulfamethoxazole (SMX) and trimethoprim (TMP) are highly removed from the MA-AnMBR effluent, but antibiotics-resistant bacteria (ARB) and antibiotics-resistant genes (ARGs) were found in abundance in the MA-AnMBR effluent. Chapter 5 evaluated the removal of $150 \mu\text{g}\cdot\text{L}^{-1}$ of SMX and TMP, in the laboratory-scale MA-AnMBR, reaching total removals of 86 and 97%, respectively. Since these removals are similar to the ones achieved under anaerobic conditions, it can be concluded that micro-aeration had no negative effect on the removal of the antibiotics. TMP was rapidly adsorbed onto the sludge biomass and then degraded due to the long solids' retention time (27 days). SMX adsorption was minimal, but the system hydraulic retention time of 2.6 days allowed its biodegradation. Moreover, the added antibiotics only affected the MA-AnMBR pH and biogas composition, with a significant change of pH from 7.8 to 7.5, and CH_4 biogas content from 84 to 78%. The assessment of the ARGs *sul1* and *sul2* for SMX, *dfrA1* for TMP, and one mobile genetic element, *int11*, showed that the addition of SMX and TMP led to an increase in the relative abundance of all ARGs and *int11* in the MA-AnMBR sludge. Finally, while the MA-AnMBR was able to reduce the ARB concentration by 3 log, relative ARG abundance (to the 16S-rRNA gene) was similar in the sludge and the effluent from the ultrafiltration membrane.

6.3 | AD-DAF SYSTEM AS A NEW TECHNOLOGY

The results presented in this dissertation aimed to assess the potential of an AD-DAF system used as a pre-treatment technology, specifically for the treatment of drain-and wastewater. The ability of DAF units to deal with a wide range of flows and suspended solids concentration allows this separation technology to efficiently work under different locations and conditions. Around the world, urban runoff and wastewater are vastly conveyed in combined sewer systems (CSS) (Quaranta et al., 2022). Due to climate change, a rise in the inter-annual variation of rainfall and intensification of extreme rain events can be expected (Singh et al., 2022; Tamm et al., 2023). When CSS are used, these extreme rainfalls drastically change the influent water quality and quantity to wastewater treatment plants (WWTPs). Conventional WWTPs do not deal well with these changes, and peak discharges of pollutants (like

ammonium) can be expected into the receiving water bodies due to increased loading from rainfall events (van Daal-Rombouts et al., 2017). Therefore, a technology like AD-DAF used for pre-treatment in WWTP could overcome the complexities of dealing with a wide range of flows and pollutant.

Furthermore, in the AD-DAF system, we will be able to decouple the hydraulic retention time and the solids retention time, reducing the system footprint and enhancing the anaerobic degradation of hardly biodegradable compounds. The DAF system will float and concentrate the influent solid fraction of organics, and the coupling with AD will promote the conversion to biogas. Cagnetta et al. (2019) studied the combination of a high-rate activated sludge system (HRAS) and a DAF unit, where the DAF was used to concentrate the sludge. A share of floated sludge from the DAF system was collected and returned to the HRAS (recycle ratio of around 0.025), while the rest was anaerobically digested. Almost 70% of the COD present in the latter was digested and transformed into biogas.

Moreover, the aeration given into the AD system due to the combination with DAF will potentially increase the biomass hydrolytic capacity, as shown in the laboratory-scale MA-AnMBR. This will enhance the removal and conversion of the organic biomass to biogas while leaving a nutrient-rich effluent. Finally, the laboratory-scale DAF system showed that it can achieve TSS removal efficiencies of around 95%. Thus, the AD-DAF system could potentially remove up to 95% of the particulate COD, convert most of the organic share into biogas, and its nutrient-rich effluent could be reclaimed for irrigation once the pathogens are adequately removed.

Although the AD-DAF system might be able to adequately remove particulate organic matter and further convert it into biogas, the high organic loading rate and low HRT (of around 30 to 60 minutes) present an important disadvantage for the removal of micropollutants such as antibiotics. Ejhed et al. (2018) concluded that the average removal efficiency of pharmaceuticals in WWTPs, had a linear correlation with HRT. Antibiotics that don't have a high octanol-water partition coefficient (K_{ow}), with Log K_{ow} values above four, have low sorption capacity and need higher HRTs to be degraded (Rogers, 1996). Therefore, whilst the long SRT of an AD-DAF system, of around 27 days, enables the sorption and subsequent anaerobic degradation of the antibiotics (Clara et al., 2005), the system HRT could be a critical parameter inhibiting the removal of pharmaceuticals with low sorption capacity. Post treatment for removal of these pharmaceuticals will be needed for safe water reuse.

6.3.1 | AD-DAF as part of LOTUS^{HR}

The LOTUS^{HR} project, a collaboration between India and the Netherlands, was set to investigate the possibility of constructing a resource-oriented wastewater treatment for drain water or domestic sewage before it enters the drain. The aim was to reuse treated effluent, in combination with energy and nutrients recovery from wastewater. The research baseline was set on the assessment of laboratory-scale technologies tested both in India and the Netherlands, that later could be established as pilot-scale technologies. The AD-DAF technology studied in this dissertation was part of the second research line of the project, as an (an)aerobic pre-treatment and energy recovery system.

Advantages of an AD-DAF system located at the Barapullah drain

The potential advantages of an AD-DAF unit as part of a centralised WWTP with combined sewer systems, were already mentioned in the above section, and the aforementioned advantages can be applied in the Indian context as well. The AD-DAF unit could be steered to treat different suspended solids concentrations and a wide range of flows, which typify the everchanging conditions of the Indian drains, where monsoon, dry weather, and illegal wastewater discharges play a key role in the dynamics of stormwater drains- and wastewater sewage.

Moreover, the AD-DAF technology could be used closer to the pollution sources, at household levels or as decentralized sanitation. The laboratory-scale DAF unit used for this research was able to reach a TSS removal of 90% when anaerobic digested sludge was used as an influent (with a TSS range between 500 to 5,000 mg·L⁻¹). According to the Central Pollution Control Board of India, New Delhi's daily per capita wastewater production is between 100 to 220 L (CPCB, 2009). The designed column laboratory-scale DAF was able to treat around 400 L·d⁻¹ of wastewater, with a surface area of 0.25 m². Considering an average HRT of 12 h for AnMBR systems treating domestic wastewater (Özgün, 2015), and an inflow of 400 L·d⁻¹, the surface area needed for the AD share of the unit is equivalent to 0.8 m². Thus, an AD-DAF system with a surface area of around 1 m² (volume of 1 m³) could be used for treating the wastewater produced on a household level, for a family of two to four people in India. Another advantage is that, when used close to the pollution source, the biogas produced could potentially be used for cooking or heating. Average COD concentration in sewage is around 0.5 g·L⁻¹ (Henze et al., 2008), corresponding to a load of 2.0 g·d⁻¹, and a biogas production of the AD-DAF system of around 550 L·d⁻¹ (assuming a 27% reduction in biogas due to aeration), of which 70% can be expected to be methane. This biogas volume could be used for one hour of cooking (Kurchania

et al., 2011) Furthermore, the pre-treatment of wastewater on a household level could reduce pollutants concentration in drain water streams, and uncontrolled biogas release from the drains caused by the suspended solids settling and degrading during transport.

AD-DAF in combination with secondary and/or tertiary treatment

To achieve water reclamation of the Barapullah drain, two post-treatments of the AD-DAF are proposed: algae photobioreactors (PBR) and constructed wetlands (CWs). The effluent of the AD-DAF will be rich in nutrient content while having minimal suspended solids. Fernandes et al. (2017) found that the optimal nitrogen to phosphorous (N:P) ratio in a PBR with *Chlorella sorokiniana* system may vary from 15 to 26. Furthermore, if phytoplankton species are used, higher N:P ratios should be considered (Klausmeier et al., 2004). Concerning CWs, N:P ratios can fluctuate from one to 100. Knight et al. (2020) investigated the performance of over 60 wetlands fed with municipal wastewater. When the influent N:P ratio was between 1 and 8, the authors observed that total phosphorus removal varied from 80 to 98 %, whilst nitrogen removal was between 40 to 94 %. Moreover, the effluent of AnMBR systems fed with domestic wastewater are reported to contain an N:P ratio from 10 to 15 (Berkessa et al., 2018; Giménez et al., 2011). A ratio below 10 is linked to N-limitation for biomass production and plant growth, while an N:P ratio above 20 indicates P-limitation (Güsewell, 2004).

The N:P ratio of the MA-AnMBR effluent studied in this dissertation, tripled when compared to the AnMBR effluent, i.e., from 10:1 to 29:1, at pH ranges from 7.4 to 7.8. The new N:P ratio corresponds to a P-limiting condition for biomass production and plant growth, compared to the N-limiting condition of the AnMBR effluent (Giménez et al., 2011). Under P-limiting conditions, microbial post-treatment with PBR or CWs will reach high levels of phosphorus removal (above 90%). Phosphorus is the most limiting nutrient for algae and bacteria growth in freshwater, and its concentration largely produces eutrophication and algae blooms (Smith et al., 2012).

Thus, if an AD-DAF system is located as a pre-treatment unit, and post-treatment of AD-DAF system effluent is done with either PBR or CWs, these treatment trains could potentially minimize the effects of nutrient discharge into water bodies. If the surface area is limiting, the combination of AD-DAF system and PBR could lead to optimal P removal and reuse, whilst AD-DAF combined with CWs could lead to maximum nitrogen and phosphorus reuse.

On the other hand, for safe re-use of the AD-DAF effluent for irrigation, this technology should be combined with a tertiary treatment aiming for pathogens and viruses' removal. Iron Electrocoagulation (Fe-EC) was investigated as part of the first research line of the LOTUS^{HR} project, seeking to reduce the risks associated with treated wastewater reuse. Other common steps developed for the disinfection of drinking water are UV radiation, chlorination and ozone, but these produced hazardous disinfection by-products (Pichel et al., 2019). According to Bicudo (2022), Fe-EC is a promising technology for municipal wastewater reclamation due to its ability to remove pathogens, certain organic micropollutants and recalcitrant organic compounds, among others.

Fe-EC is an electrochemical process, in which an electric current is used to release Fe²⁺ ions from an anode into the bulk liquid (Lakshmanan et al., 2009). At the cathode, microbubbles of hydrogen gas are released, which play a key role in the collision and flotation of the coagulated particles, forming flocs (Holt et al., 2002). The removal of the flocs by flotation or sedimentation is still one of the limiting steps of Fe-EC, with needs sedimentation times of at least four hours (Bicudo et al., 2022).

The above-mentioned limitation could be overcome if the Fe-EC unit is combined with pressurized water from the DAF unit of the AD-DAF system. Fe-EC hydrogen microbubbles are in the range of 20 to 50 µm, whilst DAF microbubbles are between 10 to 120 µm (De Rijk & den Blanken, 1994; Holt et al., 2005). The combination of these technologies could be beneficial for both. On one hand, the presence of small microbubbles formed due to electrocoagulation could improve the removal of small particles, as presented in **Chapter 2**. On the other hand, the abundance of microbubbles due to de-pressurization of the white-water stream in the DAF unit will enhance the floc flotation, reducing the time needed for the removal of the flocs in the Fe-EC. Although the synergy of these technologies might promote an increase in particle removal by flotation, further research should be done to better understand the effect of Fe-EC in combination with an AD-DAF system, especially on the usage of coagulants and flocculants, the impact on the sludge characteristics, and the influent of wastewater in an Fe-EC system.

6.4 | FUTURE RESEARCH

The research and results included in this dissertation were obtained exclusively from laboratory and bench-scale reactors, due to the practical limitations of downscaling DAF systems. This led to two main laboratory research lines, where a DAF and a micro-aerated AnMBR were studied in parallel. Whilst several conclusions drawn from both

systems can be extrapolated to the combined AD-DAF system, research on the potential and limitations of this new technology should be further assessed. To do so requires upscaling the process, meaning operating an AD-DAF system under pilot or full-scale, which is necessary towards a more in-depth understanding of the technology. Thus, the future research presented below is framed under the development and testing of the AD-DAF technology on pilot or full-scale.

DAF modelling and testing

Throughout **Chapter 2**, an experimental DAF model was designed based on the filtration model developed by Edzwald and co-workers. This model had six independent (measurable) variables, particle size distribution and density, DAF running time, contact zone detention time, influent and recycle flows, and two independent variables, the collision efficiency factor (α_{bp}) and the average bubble diameter. The above-mentioned dependent variables had an important impact on the overall particle removal.

The collision efficiency factor effect in DAF systems is the dominant variable in determining the removal of particles with a diameter below 20 μm . In this research, it was observed that a decrease in α_{bp} of 20%, reduced the maximum TSS removal of drain water from the Delft canal by around 8%. The study performed by Han et al. (2001) on α_{bp} was done on a laboratory-scale batch DAF system, made of a cylinder reactor of 60 mm diameter and an effective volume of 1.0 L. The dimensions of this laboratory-scale system are not enough to avoid the wall effect on the produced microbubbles (Edzwald, 1995). Therefore, further research should be performed on a laboratory-scale system with at least 20 cm diameter and 1 m height, to better understand the sensitivity of the collision efficiency. To perform the above, the bench-scale DAF system built for this research could be used, under a varied particle's zeta potential and bubble sizes.

Moreover, the experimental model developed in this research used the average bubble size under a certain pressure instead of the full bubble size distribution. A 50% reduction in the average bubble size had consequently a 5% increase in the TSS removal prediction of both anaerobic sludge and Delft canal water, while a 50% increase in the average bubble size reduced the TSS removal of both influents by around 3%. Therefore, using only one bubble size (the average), instead of the real bubble size distribution could lead to both, under and over-estimation of the suspended solids removal. A model that considers both, the particle size distribution

and the bubble size distribution on a DAF system should be developed to better assess the particle-bubble collision and TSS removal.

Sludge characteristics on the AD-DAF technology

Changes in the biomass characteristics of a micro-aerated AnMBR were assessed on **Chapter 4**. In this chapter, the micro-aeration load into the AnMBR simulated having an AD-DAF system. However, in the MA-AnMBR the oxygen was introduced during the day in three different cycles of four hours, whilst the DAF has an average retention time of one hour. Thus, the AD sludge will be subjected to higher oxygen stress periods and longer recovery (anaerobic) ones. This will most probably affect sludge characteristics and microbial community. Therefore, further research on the effect of oxygen on the sludge characteristics of an AD-DAF system should be performed.

To begin with, the MA-AnMBR was tested by incorporating air into the bulk liquid of the AnMBR with a peristaltic pump. This created large bubbles of air. However, in a DAF unit, mainly oxygen and nitrogen microbubbles are formed. When compared to larger bubbles, these microbubbles have a higher available surface area that promotes particle-bubble collision, and overall gas-liquid-solids interactions. In an AD-DAF system, the release of these microbubbles should promote the formation of aggregates (flocs) that will predominantly float. Furthermore, the thickened sludge from the DAF system will be recirculated to the AD unit, while particles that do not tend to float will be released with the DAF effluent. Thus the sludge floating ability will be enhanced and promoted. This could lead to a reduction of needed coagulants and flocculants, shifts in the sludge morphology, density, viscosity, and changes in the microbial community. To further assess the effect of micro bubbles on the AD-DAF system, a pilot- or full-scale should be built and run for at least 6 months. Measurements on sludge rheology, such as particle size distribution, density, and viscosity should be performed frequently.

Furthermore, the potential shifts of the microbial community would not only be affected by the flocculation of the sludge, but also by the higher “oxygen stress” periods that the anaerobic biomass will be subjected to. Organisms that are not able to survive a higher oxygen content will potentially perish. Under these conditions, the increase in SOD activity could play a significant role to promote sludge adaptation and increase biomass oxygen tolerance. The addition of oxygen could also lead to an increase in the sludge hydrolytic capacity, and concomitantly, an increase in ammonium concentration. Therefore, in a pilot- or full-scale AD-DAF system, DNA

samples should be extracted regularly. These samples should be used to assess microbial community shifts and analyse SOD concentration, in a pilot or full-scale AD-DAF system.

Finally, the release of dissolved methane and carbon dioxide in the AD-DAF system should be further researched. The de-pressurization of white water in the DAF system promotes the formation of micro-bubbles, which are key for the flotation of particles and agglomerates. The over-saturation of gas and micro-bubbles movements could potentially induce the release of dissolved CH₄ and CO₂ into the atmosphere if the DAF system is not covered. The anthropogenic emissions of CO₂ and CH₄ gas are one of the biggest contributors to greenhouse gases (GHGs) and therefore, one of the drivers of climate change (Montzka et al., 2011). Thus, ways to measure and minimize the release of these GHG emissions in the AD-DAF system should be investigated.

Micropollutants removal on an AD-DAF system

The removal of pathogens and antibiotics in the AD-DAF unit can be expected to be lower than in the MA-AnMBR, investigated in **Chapter 5**. In the MA-AnMBR, the ultrafiltration membrane is the primary mechanism for the removal (or retention in the sludge) of pathogens and antibiotics. The membrane system enables an almost complete decoupling of the HRT and SRT, promoting longer SRT. According to the literature, a long SRT allows the digestion and biodegradation of antibiotics, which increases their removal. The exact removal of pathogens and antibiotics in an AD-DAF system is still unknown and could be a critical parameter to assess the suitability of this system for treated storm and wastewater reuse and should therefore be explicitly investigated. The AD-DAF system effluent will have certain level of solids, as their DAF TSS removal is expected to be below 99%. Thus, calculations on the exact SRT of the AD-DAF system should be carried out, and pathogens and antibiotics removal should be linked to the total HRT and SRT of the system.

As mentioned before, in the AD-DAF system, the biomass will be subjected to higher “oxygen stress” periods, which could impact the removal of certain antibiotics. In this dissertation, two anaerobically biodegradable antibiotics were tested, sulfamethoxazole (SMX) and trimethoprim (TMP). Aside from the antibiotic's structure and system HRT and SRT, the redox potential conditions are crucial in the biodegradation pathway of micropollutants. Thus, the effect of different redox potentials on the removal of antibiotics and pathogens in the AD-DAF system should be further developed. Moreover, more commonly found antibiotics in domestic

wastewater streams should be assessed on the AD-DAF, to analyse the water reuse potential.

Design and operation of an AD-DAF system

Finally, applied research should be performed related to the design, operation, and maintenance of a pilot or full-scale AD-DAF system. To begin with, different design options for the AD-DAF system could provide a vast diversity of effluent qualities. Instead of one AD reactor, several smaller reactors could be installed in parallel. While this will increase the operation and maintenance of the overall system, it could potentially provide an extensive anaerobic time, and reduce the risks linked to the “oxygen stress” period when the biomass enters the DAF system.

Furthermore, the effect of white-water recirculation ratios on redox potential, microbial community, and optimal loading rates, among others, should be investigated. Whilst an increase in the white-water recirculation flow can spike the TSS removal, it could have negative effects on the volatilization of methane and carbon dioxide gases. Moreover, an increase in the white water flow will affect the oxygen load into the system and amount of microbubbles produced, which will affect the overall AD-DAF system performance. Therefore, the effect of changes in operational parameters on the performance of an AD-DAF system should be further developed.



Bubbles created with watercolour, soap, and water.

Annexes

A.

Additional details on Modelling of Dissolved Air Flotation

A.1. Representation of the flotation experimental model

The filtration Model was developed by Edzwald and coworkers, and it is a model for collision between particles and bubbles. It is based on the fact that bubbles diameters are on average bigger than particle diameters ($d_p/dbb < 1$).

Analysis is done for P=5 bar

Name of influent		DAF ₂									
α_{bp} is an empirical number calculated by Han et al, 2001 and 2002 Select temperature by the number above (1=10°C)											
		1	2	3	5	6	7	8	9		
		10	15	20	30	35	40	50	60		
Temperature		3.0	Select the temperature based on the values given in "mean values" sheet								
diameter of bubble bb (μm)		74									
Particle density (g/cm^3)		1.066									
Q inflow (m^3/h)		10.3									
Recycle ratio *		1									
* The recycle ratio is set based on the inflow. E.g. A recycle ratio of 1 corresponds to the same recycle flow as the inflow											
τ_{cz} (sec):		1200	Retention time of the contact zone								
k [$\text{m}^3 \cdot \text{kg}/(\text{s}^2 \cdot \text{K})$]:		1.38E-23									
Removal of particles smaller than the average bubble diameter											
diameter of particle i	diameter of bubble bb	v_{bb}	η_{BM}	η_{li}	η_s	η_{T1}	Fractions of particles removed	Frequency per particle diameter	Final removal		
(μm)	(μm)	(cm/s)					%	%	%		
10	74	0.3	1.4E-04	2.6E-02	1.2E-03	2.8E-02	95%	0.66	0.63		
20	74	0.3	8.5E-05	1.0E-01	5.0E-03	1.1E-01	100%	0.16	0.16		
30	74	0.3	6.5E-05	2.2E-01	1.1E-02	2.3E-01	100%	0.08	0.08		
40	74	0.3	5.4E-05	3.9E-01	2.0E-02	4.1E-01	100%	0.04	0.04		
50	74	0.3	4.6E-05	5.9E-01	3.1E-02	6.2E-01	100%	0.03	0.03		
60	74	0.3	4.1E-05	8.4E-01	4.5E-02	8.8E-01	100%	0.01	0.01		
0	74	0.3	0.0E+00	0.0E+00	0.0E+00	0.0E+00	0%	0.01	0.00		
0	74	0.3	0.0E+00	0.0E+00	0.0E+00	0.0E+00	0%	0.01	0.00		
Remaining particles bigger than average bubble size 3%											
Removal of particles bigger than the average bubble size											
Frequency of particles above average bubble diameter (%)						0.031042129					
The removal of these big particles can go from 50 to 95%, and this can give us the expected error. Based on the paper by Fukushi (Dissolved air flotation: Experiments and kinetics, 1998)											
Then, removal efficiency will be			95%	--	97%						
TOTAL REMOVAL(%)			96%	±	1%						

This considers a particle range in between the particles diameters. E.g: Particles removed for a particle diameter of 5 μm corresponds to particle frequency of diameters between 2,5 and 7,5, where 5 is the average number.

Filtration model developed by Edzwald and coworkers (1995).
<https://doi.org/10.2166/wst.1995.0512>

Brownian diffusion:
$$\eta_{BM} = 6.18 \left[\frac{k_b T}{g(\rho_w - \rho_b)} \right]^{2/3} \left[\frac{1}{d_p} \right]^{2/3} \left[\frac{1}{d_b} \right]^2$$

Interception:
$$\eta_I = \left(\frac{d_p}{d_b} + 1 \right)^2 - \frac{3}{2} \left(\frac{d_p}{d_b} + 1 \right) + \frac{1}{2} \left(\frac{d_p}{d_b} + 1 \right)^{-1}$$

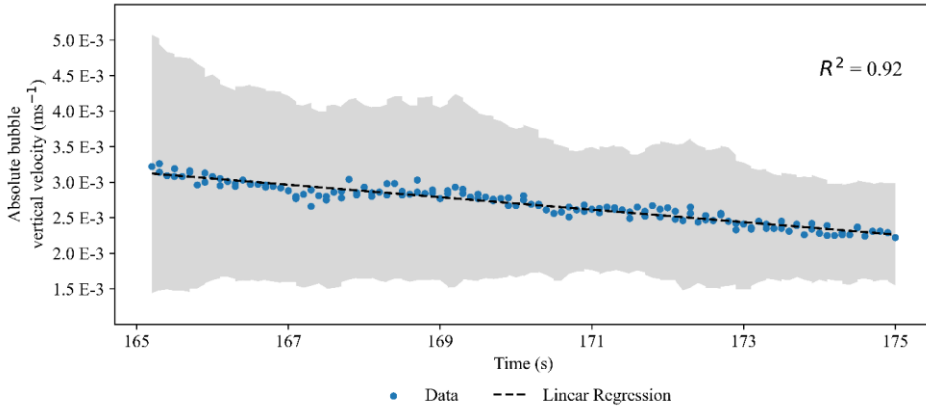
Differential settling of flocs:
$$\eta_S = \left[\frac{(\rho_p - \rho_w)}{(\rho_w - \rho_b)} \right] \left[\frac{d_p}{d_b} \right]^2$$

Total single collector efficiency:
$$\eta_T = \eta_{BM} + \eta_I + \eta_S$$

The total concentration of particles that remain unattached to a bubble can then be found by summing overall all the particle sizes

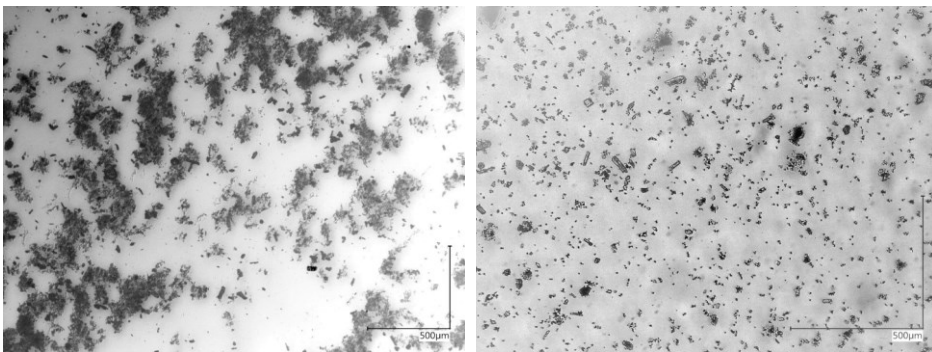
$$n_{T,out} = \sum_{\text{all } i} n_{i,in} \exp \left(- \frac{3 \alpha_{pbb} \eta_{T,i} \phi_{bb} v_{bb} \tau_{cz}}{d_{bb}} \right)$$

A.2. Average absolute bubble vertical velocity and standard deviation



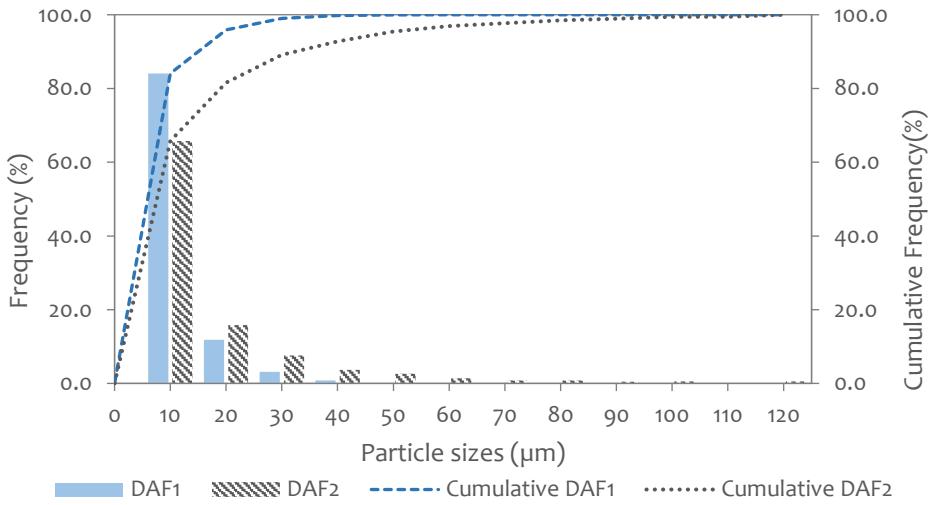
Average absolute bubble vertical velocity and standard deviation (in grey shadows). Average velocities were calculated via PIVlab, using a velocity grid containing around 1200 analysis points. The figure is based on the video Tap water 3, recorded between 165 and 175 seconds, where there was no inflow into the lab-scale DAF column.

A.3. Particle images of Delft canal water and Harnaschpolder anaerobic sludge microscope images.



On the left, is a digital microscope image of anaerobic sludge, and on the right, of Delft canal water.

A.4. Particle size distribution of the full-scale DAF systems



B.

Additional details on TSS removal on a down-scaled DAF

Annex B.1. Ranges of operating parameters that were used to define the lab-scale DAF experiments.

Parameter	Unit	Range	Reference
Influent TSS	mg·L ⁻¹	30 - 510*	Indian Institute of Technology Delhi (2019)
		6000 - 72000**	Speece (1988)
Temperature	°C	29 - 35	Indian Institute of Technology Delhi (2019)
Recycle flow	%	5 - 50	Wang et al. (2005)
		6 - 12	Edzwald (2010)
Pressure	10 ⁵ Pa	2 - 6	Wang et al. (2005)
		4 - 6	Edzwald (2010)
Coagulant concentration	mg·L ⁻¹	500 - 2000	Haydar and Aziz (2009)
Coagulation time	s	600 - 1800	Wang et al. (2005)
		180 - 3600	Wang et al. (2005)
Hydraulic Retention Time	s	1200 - 3600	Shammas et al. (2010)

*Represent values of suspended solids found in the Barapullah drain during one year of bi-weekly measurements.

**Following values of sludge from Anaerobic Digesters treating municipal wastewater.

Annex B.2. Plackett-Burman design for the effect of factors in drain waters and sludge for the experimental design. Plackett-Burman is a method for sensitivity analysis that considers several variables at the same time. The model scenarios are approximately twice as much as the tested variables and depend on the maximum, minimum, and average (central point) values of those variables. A value of 1 in the Plackett-Burman table, refers to the maximum value for the given variable. Similarly, a value of -1 represents the minimum value of the variable. Zero corresponds to the central point analysis.

Run	TSS mg.L ⁻¹	Temperature °C	Residence time s	pH	Pressure 10 ⁵ Pa	Coagulant and flocculants concentration mg.L ⁻¹	Coagulation time s
1	1	-1	1	-1	-1	-1	1
2	1	1	-1	1	-1	-1	-1
3	-1	1	1	-1	1	-1	-1
4	1	-1	1	1	-1	1	-1
5	1	1	-1	1	1	-1	1
6	1	1	1	-1	1	1	-1
7	-1	1	1	1	-1	1	1
8	-1	-1	1	1	1	-1	1
9	-1	-1	-1	1	1	1	-1
10	1	-1	-1	-1	1	1	1
11	-1	1	-1	-1	-1	1	1
12	-1	-1	-1	-1	-1	-1	-1
13	0	0	0	0	0	0	0
14	0	0	0	0	0	0	0
15	0	0	0	0	0	0	0

Annex B.3. Run performances for the different effluents and operational conditions.

Delft canal water (DCW) performed runs, with their selected parameters and removal efficiencies.

Run	Influent TSS mg·L ⁻¹	Coagulation time s	Residence time s	Coagulants and flocculants concentration mg·L ⁻¹	Pressure 10 ⁵ Pa	Temperature °C	pH	TSS removal efficiency %
1	30	600	780	500	5	29.0	7.6	47%
2	30	600	780	5	3	29.0	6.7	45%
3	30	1800	780	500	3	35.0	6.7	72%
4	30	600	1200	5	5	35.0	6.7	66%
5	30	1800	1200	500	3	35.0	7.6	81%
6	30	1800	1200	5	5	29.0	7.6	96%
7	270	1200	990	253	4	32.0	7.2	49%
8	270	1200	990	253	4	32.0	7.2	56%
9	270	1200	990	253	4	32.0	7.2	49%
10	510	600	780	5	3	35.0	7.6	60%
11	510	1800	780	5	5	35.0	7.6	85%
12	510	1800	780	500	5	29.0	6.7	88%
13	510	600	1200	500	3	29.0	7.6	81%
14	510	600	1200	500	5	35.0	6.7	78%
15	510	1800	1200	5	3	29.0	6.7	88%

Barapullah drain water (BDW) performed runs, with their selected parameters and removal efficiencies.

Run	Influent TSS concentration mg.L ⁻¹	Coagulation time s	Residence time s	Coagulant and flocculants concentration mg.L ⁻¹	Pressure 10 ⁵ Pa	TSS removal efficiency %
1	30	1800	1200	5	5	83%
2	30	600	1200	500	5	69%
3	30	1800	780	500	5	81%
4	30	1800	780	500	3	89%
5	30	600	1200	5	3	85%
6	30	600	780	5	3	70%
7	270	1200	990	253	4	92%
8	270	1200	990	253	4	85%
9	270	1200	990	253	4	87%
10	510	600	780	5	5	72%
11	510	600	1200	500	3	94%
12	510	600	780	500	5	83%
13	510	1800	1200	500	3	90%
14	510	1800	1200	5	5	83%
15	510	1800	780	5	3	88%

Anaerobic digested sludge (ADS) performed runs, with their selected parameters and removal efficiencies.

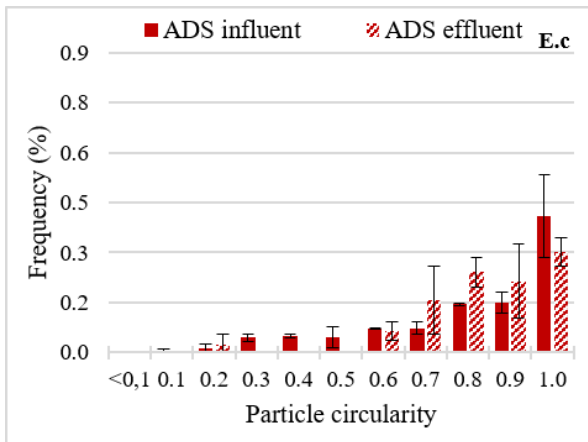
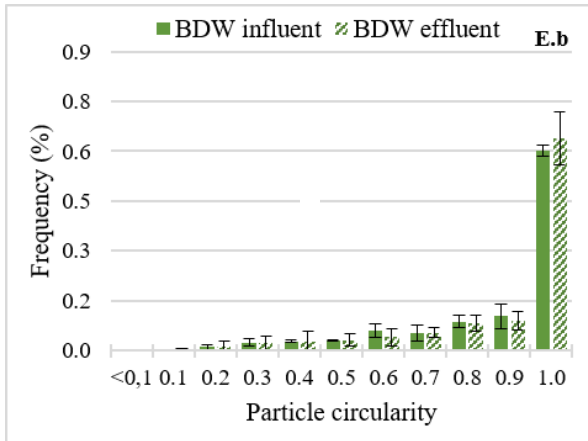
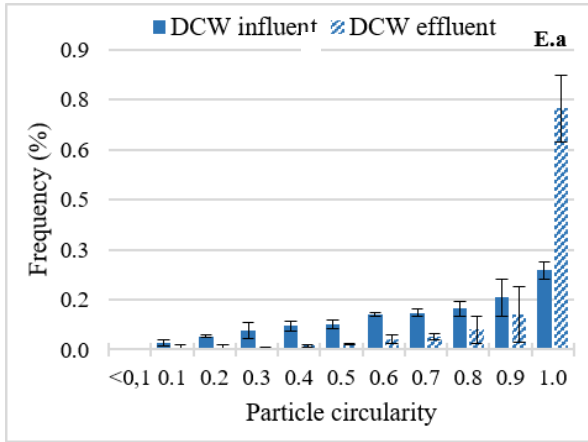
Run	Influent TSS mg.L ⁻¹	Coagulation time		Residence time s	Coagulants and flocclulants concentration		Pressure 10 ⁵ Pa	Temperature °C	pH	TSS removal efficiency %
		s	s		mg.L ⁻¹	mg.L ⁻¹				
1	500	600	600	780	5	5	3	25.0	7.0	87%
2	500	1800	1800	780	500	500	3	35.0	7.0	84%
3	500	600	600	780	500	500	5	25.0	8.5	88%
4	500	1800	1800	1200	500	500	3	35.0	8.5	66%
5	500	600	600	1200	5	5	5	35.0	7.0	68%
6	500	1800	1800	1200	5	5	5	25.0	8.5	92%
7	2750	1200	1200	990	253	253	4	30.0	7.8	79%
8	2750	1200	1200	990	253	253	4	30.0	7.8	87%
9	2750	1200	1200	990	253	253	4	30.0	7.8	84%
10	5000	600	600	780	5	5	3	35.0	8.5	72%
11	5000	1800	1800	780	5	5	5	35.0	8.5	88%
12	5000	1800	1800	780	500	500	5	25.0	7.0	90%
13	5000	1800	1800	1200	5	5	3	25.0	7.0	87%
14	5000	600	600	1200	500	500	3	25.0	8.5	87%
15	5000	600	600	1200	500	500	5	35.0	7.0	87%

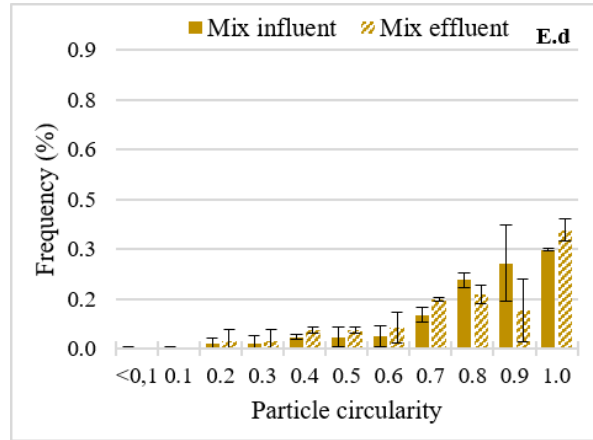
Mix influent performed runs, with their selected parameters and removal efficiencies.

Run	Influent TSS concentration	Coagulation time	Residence time	Coagulant and flocculants concentration	Pressure	TSS Removal Efficiency
	mg.L ⁻¹	s	s	mg.L ⁻¹	10 ⁵ Pa	%
1	500	600	780	5	3	29%
2	500	600	1200	5	3	59%
3	500	600	1200	500	5	78%
4	500	1800	780	500	3	86%
5	500	1800	780	500	5	80%
6	500	1800	1200	5	5	85%
7	2750	1200	990	253	4	89%
8	2750	1200	990	253	4	91%
9	2750	1200	990	253	4	93%
10	5000	600	780	5	5	86%
11	5000	600	780	500	5	93%
12	5000	600	1200	500	3	95%
13	5000	1800	780	5	3	72%
14	5000	1800	1200	5	5	87%
15	5000	1800	1200	500	3	77%

Annex B.4. Particle circularity frequency for all tested influents

B





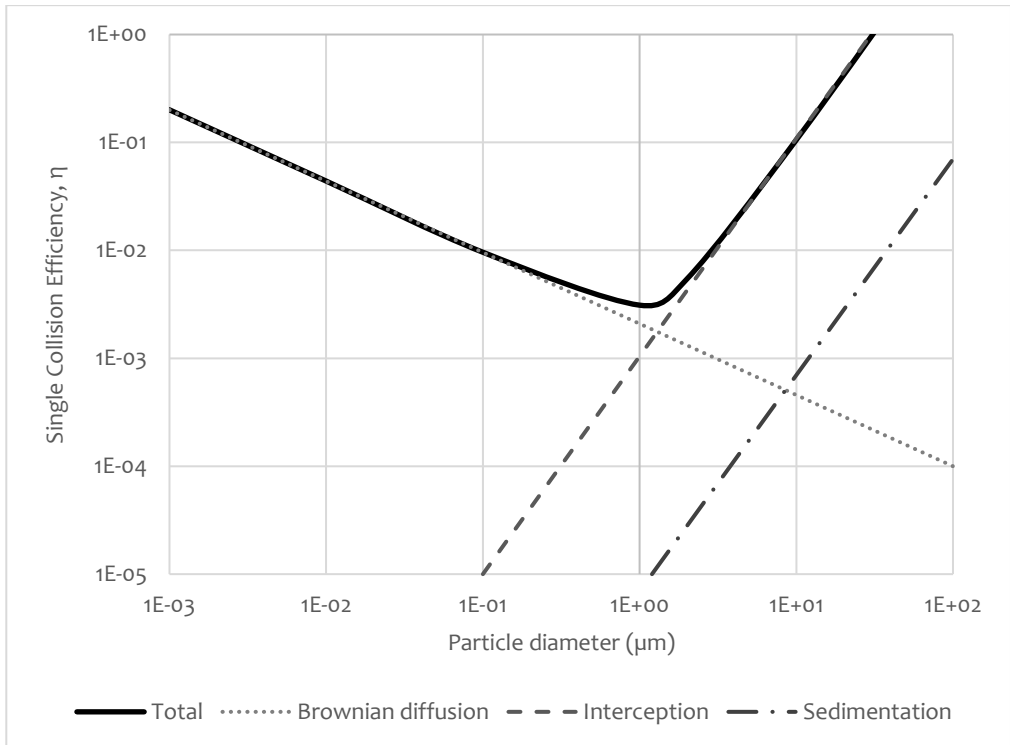
Particle circularity frequency for all influents and their respective effluents, performed under the central point parameters of the Design of Experiments. Results are based on particle image analysis performed using FIJI-ImageJ. The used acronyms correspond to Delft canal water(DCW), Barapullah drain water (BDW), and anaerobic digested sludge (ADS). and the mixed influent (MIX).

Summary of particle circularity frequency for all influents and their respective effluents, performed under the central point parameters of the Design of Experiments. Results are based on particle images. Particle circularity was divided into three categories: elongated particles with circularities below 0.3, round particles with circularity above 0.7, and particles with circularities between 0.3 and 0.7. Infl. refers to the influent, and Effl. to the effluent.

	DCW		BDW		ADS		MIX	
	Infl.	Effl.	Infl.	Effl.	Infl.	Effl.	Infl.	Effl.
Elongated Circ. <0.3	6 ± 1%	1 ± 1%	1 ± 1%	2 ± 2%	2 ± 2%	2 ± 3%	2 ± 2%	2 ± 3%
Circ. >0.3 and <0.7	31 ± 3%	7 ± 1%	14 ± 1%	12 ± 3%	21 ± 3%	6 ± 3%	12 ± 3%	19 ± 5%
Round Circ. >0.7	63 ± 6%	93 ± 7%	84 ± 4%	86 ± 3%	77 ± 3%	91 ± 10%	86 ± 10%	78 ± 9%

Annex B.5. Collision efficiency.

Single collector efficiency versus particle for particle density of $1.01\text{g}\cdot\text{cm}^{-3}$, bubble diameter of $40\ \mu\text{m}$, and temperature of 25°C . The total collection efficiency is the sum of the collection efficiencies of Brownian diffusion, interception, and sedimentation. Adapted from Edzwald (1995).



C.

Additional details on the Effects of low O₂ dosage on an AnMBR

Annex C.1. Micro-aerated AnMBR feed recipe and influent composition

Feed composition	Unit	Value	Micronutrients Solution	Unit	Value
Urea	g·L ⁻¹	1.0	FeCl ₃ ·6H ₂ O	mg·L ⁻¹	1000.0
Ammonium chloride	g·L ⁻¹	0.8	CoCl ₂ ·6H ₂ O	mg·L ⁻¹	1000.0
Sodium acetate trihydrate	g·L ⁻¹	2.6	MnCl ₂ ·4H ₂ O	mg·L ⁻¹	250.0
Ovalbumin	g·L ⁻¹	0.2	CuCl ₂ ·2H ₂ O	mg·L ⁻¹	15.0
Magnesium sulphate heptahydrate	g·L ⁻¹	0.1	ZnCl ₂	mg·L ⁻¹	25.0
Potassium phosphate monobasic	g·L ⁻¹	0.2	H ₃ BO ₃	mg·L ⁻¹	25.0
Calcium chloride dihydrate	g·L ⁻¹	0.1	(NH ₄) ₆ Mo ₇ O ₂₄ ·4H ₂ O	mg·L ⁻¹	45.0
Cellulose	g·L ⁻¹	1.5	Na ₂ SeO ₃ ·H ₂ O	mg·L ⁻¹	50.0
Milk powder	g·L ⁻¹	0.6	NiCl ₂ ·6H ₂ O	mg·L ⁻¹	25.0
Yeast extract	g·L ⁻¹	0.5	EDTA	mg·L ⁻¹	500.0
Sunflower oil	drops·L ⁻¹	2.0	HCl 36%	mg·L ⁻¹	0.5
Humic and Fulvic acid	drops·L ⁻¹	2.0	Resazurin sodium salt	mg·L ⁻¹	250.0
Micronutrients solution	g·L ⁻¹	10.6	Yeast extract	mg·L ⁻¹	1000.0

Micro-Aerated AnMBR feed composition

	Unit	Value
Chemical Oxygen Demand (COD)	mg·L ⁻¹	5200 ± 600
Ammonium (NH ₄ ⁺)	mgN·L ⁻¹	249 ± 54
Nitrate (NO ₃ ⁻)	mgN·L ⁻¹	1.3 ± 0.2
Phosphate (PO ₄ ³⁻)	mgP·L ⁻¹	60 ± 9
Sulphate (SO ₄ ²⁻)	mgS·L ⁻¹	235 ± 46
Total Suspended Solids (TSS)	mg·L ⁻¹	3073 ± 451
Volatile Suspended Solids (VSS)	mg·L ⁻¹	2938 ± 436

Annex C.2. PhreeqC model for the AnMBR and Ma-AnMBR phases**PhreeqC model for the Ma-AnMBR phase**

GAS_PHASE 1

Fixed_Pressure

-fixed_pressure # 0.33 L (default: 1.0 L)

-pressure 1.05

CO2(g) -0.282017616 # 50% (1.05bar)

H2S(g) -0.0 # not detectable in GC(1.05bar)

Amm(g) -0.00 # 0% (1.05bar)

CH4(g) -0.282017616 # 50% (1.05bar)

SOLUTION 1

pH 4.0

Temp 36.5

units mg/L

C(4) 2350

C(-4) 932

Ca 27.3

Co 0.0

S(-2) 13.01

Fe(+2) 0.86

Mn(+2) 0.73

Amm 583 # NH4+

Pb 0.001

Cu 0.06

Cr 0.0

Cd 0.0

Zn 0.12

Cl 587.35

Mg 9.87

Si 0.00

B 0.05

Ba 0.0

Al 0.01

Na 439.84

Ni 0.06

Sr 0.01

Ti 0.01

K 57.47

P 139.59 as PO4

N 714.71

SELECTED_OUTPUT

-file selectedoutput.sel

-temperature

INCREMENTAL_REACTIONS True # you can also choose False, if you do not want cumulative additions)

REACTION

NaOH 1.0; 1.0 moles in 1000 steps

USER_GRAPH 1

-headings head CO2 HCO3- CO3-2 CaHCO3+ CO2 (g)

-chart_title "pH effect carbon speciation"

-axis_titles "pH" "CO2 speciation (mol)" "Partial pressure (atm)"

-axis_scale x_axis 5 14 auto auto

-axis_scale y_axis 0.0 0.07 auto auto

-axis_scale sy_axis 0.00 0.7 auto auto

-initial_solutions true

-connect_simulations true

-plot_concentration_vs x

```
-start
10 graph_x -LA("H+")
20 graph_y MOL("CO2") MOL("HCO3-") MOL("CO3-2") MOL("CaHCO3+")
30 graph_sy PR_P("CO2(g)")

USER_GRAPH 2
-headings head H2S HS- S-2 Fe(HS)2 H2S(g)
-chart_title "pH effect sulphur speciation"
-axis_titles "pH" "S-speciation (mol)" "Partial Pressure (atm)"
-axis_scale x_axis      5 14 auto auto
-axis_scale y_axis      0 0.0016 auto auto
-axis_scale sy_axis     0 0.011 auto auto
-initial_solutions      true
-connect_simulations    true
-plot_concentration_vs  x
-start
10 graph_x -LA("H+")
20 graph_y MOL("H2S") MOL("HS-") MOL("S-2") MOL("Fe(HS)2")
30 graph_sy PR_P("H2S(g)")

USER_GRAPH 3
-headings head NH3(l) NH4+ NH3(g)
-chart_title "pH effect ammonia speciation "
-axis_titles "pH" "NH4-speciation (mol)" "Partial pressure
(atm)"
-axis_scale x_axis      4 14 auto auto
-axis_scale y_axis      0 0.05 auto auto
-axis_scale sy_axis     0 0.001 auto auto
-initial_solutions      true
-connect_simulations    true
-plot_concentration_vs  x
```


units mg/L

C(4) 2350

C(-4) 932

Ca 27.3

Co 0.0

S(-2) 13.01

Fe(+2) 0.86

Mn(+2) 0.73

Amm 714 # NH4+

Pb 0.001

Cu 0.06

Cr 0.0

Cd 0.0

Zn 0.12

Cl 587.35

Mg 9.87

Si 0.00

B 0.05

Ba 0.0

Al 0.01

Na 439.84

Ni 0.06

Sr 0.01

Ti 0.01

K 57.47

P 139.59 as PO4

N 714.71

SELECTED_OUTPUT

-file selectedoutput.sel

-temperature

```
INCREMENTAL_REACTIONS True # you can also choose False, if you
do not want cumulative additions)
```

```
REACTION
```

```
NaOH 1.0; 1.0 moles in 1000 steps
```

```
USER_GRAPH 1
```

```
-headings head CO2 HCO3- CO3-2 CaHCO3+ CO2(g)
-chart_title "pH effect carbon speciation"
-axis_titles "pH" "CO2 speciation (mol)" "Partial pressure
(atm) "
-axis_scale x_axis      5 14 auto auto
      -axis_scale y_axis      0.0 0.07 auto auto
-axis_scale sy_axis     0.00 0.7 auto auto
      -initial_solutions      true
      -connect_simulations    true
      -plot_concentration_vs  x
      -start
10 graph_x -LA("H+")
20 graph_y MOL("CO2") MOL("HCO3-") MOL("CO3-2") MOL("CaHCO3+")
30 graph_sy PR_P("CO2(g)")
```

```
USER_GRAPH 2
```

```
-headings head H2S HS- S-2 Fe(HS)2 H2S(g)
-chart_title "pH effect sulphur speciation"
-axis_titles "pH" "S-speciation (mol)" "Partial Pressure (atm) "
-axis_scale x_axis      5 14 auto auto
      -axis_scale y_axis      0 0.0016 auto auto
-axis_scale sy_axis     0 0.011 auto auto
      -initial_solutions      true
```



```
-connect_simulations    true
-plot_concentration_vs  x
-start
10 graph_x -LA("H+")
20 graph_y  MOL("H2S") MOL("HS-") MOL("S-2") MOL("Fe(HS)2")
30 graph_sy PR_P("H2S(g)")

USER_GRAPH 3
-headers head NH3(l) NH4+ NH3(g)
-chart_title "pH effect ammonia speciation "
-axis_titles "pH" "NH4-speciation (mol)" "Partial pressure
(atm)"
-axis_scale x_axis      4 14 auto auto
-axis_scale y_axis      0 0.05 auto auto
-axis_scale sy_axis     0 0.001 auto auto
-initial_solutions      true
-connect_simulations    true
-plot_concentration_vs  x
-start
10 graph_x -LA("H+")
20 graph_y  MOL("Amm") MOL("AmmH+")
30 graph_sy PR_P("Amm(g)")

USER_GRAPH 4
-headers head SI("Calcite") SI("Aragonite") SI("FeS(ppt)")
-chart_title ""
-axis_titles "pH" "Saturation index"
-axis_scale x_axis      3 14 auto auto
-axis_scale y_axis      -10 10 auto auto
-initial_solutions      true
-connect_simulations    true
```

```
-plot_concentration_vs x
-start
10 graph_x -LA("H+")
20 graph_y SI("Calcite") SI("Aragonite") SI("FeS(ppt)")

END
```

Annex C.3. Summary of effluent characteristics under the Anaerobic (AnMBR) and Micro-aerated (Ma-AnMBR) states.

	Unit	AnMBR		MA-AnMBR	
Chemical oxygen demand (COD) concentration	mgCOD·L ⁻¹	90.6	± 4.4	74.6	± 19.0
Ortho-phosphate concentration	mgPO ₄ -P·L ⁻¹	55.1	± 0.7	27.6	± 12.3
Sulphate concentration	mgSO ₄ -S·L ⁻¹	31.9	± 1.8	23.0	± 13.0
Ammonium concentration	mgNH ₄ -N·L ⁻¹	547	± 18	740	± 106

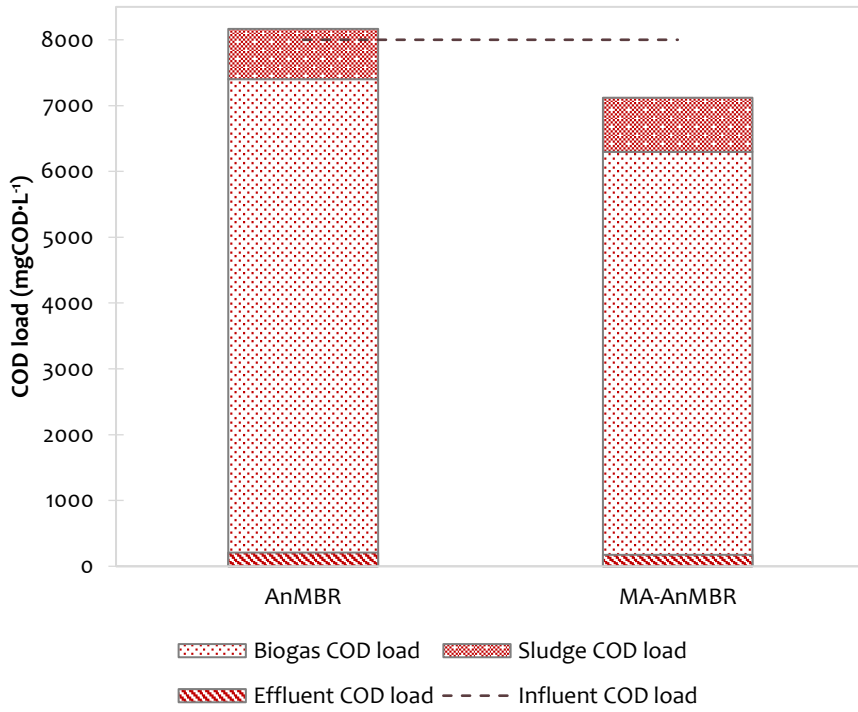
Annex C.4. AnMBR and MA-AnMBR biogas concentration

To further understand the reasons behind the high methane concentration in the biogas, the effect of pH in the dissolved concentrations of total inorganic carbon produced (TIC), HCO_3^- , CO_2 , and CO_3^{2-} , was assessed in the PhreeqC model. The total dissolved carbon concentration from these three species increased by around 3% in the MA-AnMBR compared to the AnMBR period. At a pH of 7.6, the MA-AnMBR had a dissolved carbon concentration of $0.42 \text{ g}\cdot\text{L}^{-1}$, while at a pH of 7.4, it was $0.41 \text{ g}\cdot\text{L}^{-1}$ for the AnMBR. The most significant change was observed for carbonic acid, where the model predicted an HCO_3^- concentration of $2.03 \text{ g}\cdot\text{L}^{-1}$ for the MA-AnMBR state and $1.92 \text{ g}\cdot\text{L}^{-1}$ for the AnMBR. Moreover, dissolved CO_2 concentration was also assessed at a neutral pH, and results showed that for both periods, the dissolved CO_2 concentration was $0.35 \text{ g}\cdot\text{L}^{-1}$. This value could also be linked to the predicted increase of CO_2 concentration in the biogas at pH 7, which was around 14 % for both reactor states.

Aside from an increase in the total inorganic carbon produced, the high acid neutralization capacity (ANC) of the AnMBR and MA-AnMBR could be linked to the urea concentration of the feed. A concentration of $1.0 \text{ g}\cdot\text{L}^{-1}$ of urea was added to the synthetic feed. Urea has a molar mass of $60 \text{ g}\cdot\text{mol}^{-1}$, and each mmol of urea is responsible for producing two meq of ammonia and one of carbon dioxide. At the lab-scale reactor pH, ammonia and carbon dioxide will be mainly in the form of NH_4^+ and HCO_3^- , obtaining a surplus of 17 meq of NH_4^+ cations. Most of the feed's COD content comes from sodium acetate and cellulose, added in concentrations of 2.6 and $1.5 \text{ g}\cdot\text{L}^{-1}$. The first one uses its own sodium as a buffer, and most of the sodium acetate is converted to methane and NaHCO_3 (Ferry, 1992). The produced CO_2 from cellulose will be chemically bound with the surplus of NH_4^+ cations coming from urea. This will decrease the CO_2 content in biogas, (increasing the partial content of CH_4), and improve the system buffer capacity, raising the ANC/TIC ratio. A rise in this ratio increases the HCO_3^- concentration in the liquid and decreases the biogas CO_2 concentration (Lindeboom et al., 2012). Therefore, the high methane concentration of the biogas for the AnMBR and MA-AnMBR could be attributed to the feed characteristics, high urea concentration, and CO_2 dissolution into the liquid.

Results of the PhreeqC model regarding methane and carbon dioxide biogas concentrations were further tested with the influent and reactor conditions given by Ozgun, Ersahin, et al. (2013), which uses urea as one of the main sources of ammonium. For the lab-scale reactor operated at a pH of 7, Ozgun, et al. obtained a CH_4 concentration of $61 \pm 5.7\%$, while the model predicted a methane concentration

of 61%. Moreover, for the same conditions, at a pH of 7.65, the results of the model showed an expected biogas methane concentration of 88%.

Annex C.5. COD balance for the AnMBR and Ma-AnMBR states.

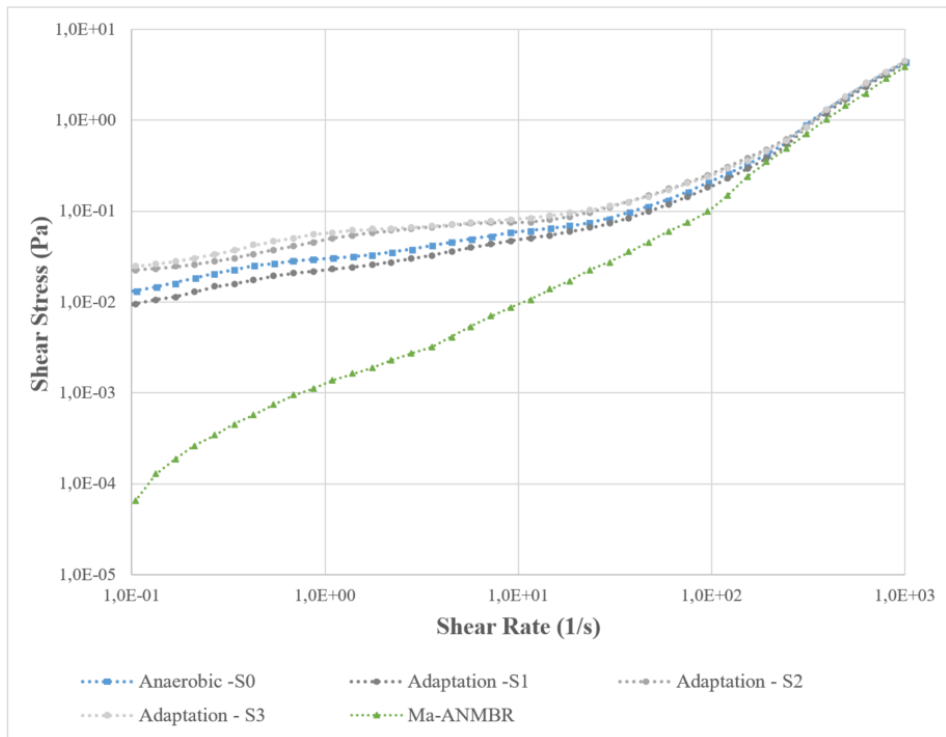
Annex C.6. P-values from the ANOVA single-factor tests performed for the specific methanogenic activity tests (SMA), when compared to the values of the control tests, with no extra aeration added.

Sludge S₀ corresponded to sludge from the Anaerobic Membrane Bioreactor (AnMBR) when operated under anaerobic conditions. Inoculums S₁ to S₃ corresponded to the first three weeks of adaptation to the addition of oxygen to the AnMBR. The last Sludge (S₄) corresponded to sludge from the fully adapted Micro-aerated AnMBR. The oxygen supplied to each SMA bottle was calculated as a percentage of the substrate COD load, at 20°C, considering an air composition of 21% Oxygen and 79% Nitrogen. In bold are the tests that showed no significant difference when compared to no aeration of the inoculum.

Inoculum		3 % of COD _{in}	8 % of COD _{in}	13 % of COD _{in}
S ₀	Anaerobic	0.011	0.000	0.001
S ₁		-	0.003	-
S ₂	Adaptation	0.613	0.000	-
S ₃		0.394	0.000	0.000
S ₄	MA-AnMBR	0.572	0.362	0.042

Annex C.7. Sludge viscosity curve of the Micro-Aerated AnMBR.

Sludge S₀ corresponded to sludge from the Anaerobic Membrane Bioreactor (AnMBR) when was operated under strict anaerobic conditions. Sludge S₁ to S₃ corresponded to the first three weeks of adaptation to the addition of oxygen to the AnMBR. The last sludge (S₄) corresponded to sludge from the fully adapted Micro-aerated AnMBR.



D.

Additional details on the Fate of SMX and TMP in an MA-AnMBR

Annex D.1. Mix solution and reaction conditions for qPCR.

All ARGs and *intl-1* qPCR reactions were conducted using a master mix per sample. The master mix consisted of a total volume of 20 μL , including IQTM SYBR green super mix BioRad 1x, of which 0.4 μL were of each forward and reverse primer (50 μM), 10 μL of SYBR green dye, 7.6 μL of qPCR grade water, and 2 μL of the DNA template. All the reactions were performed in technical triplicates, using a qTOWER3 Real-time PCR machine (Westburg, DE). The PCR cycles and amplification conditions depended on the selected gene.

Amplification conditions per selected ARGs, MGE and 16srRNA.

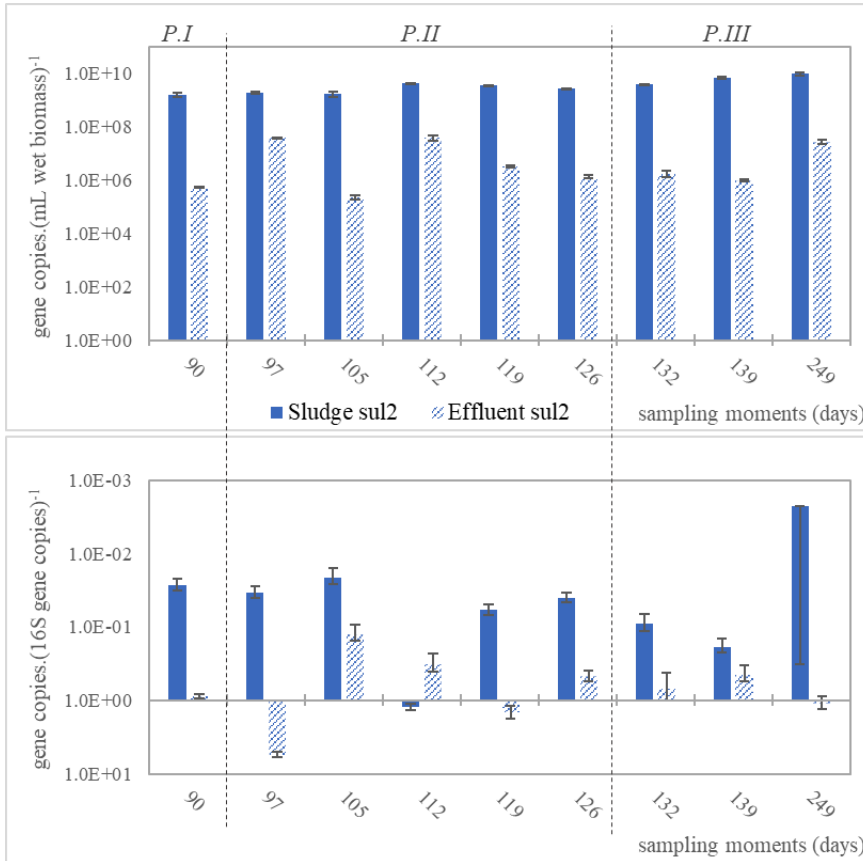
<i>Genes</i>	<i>Conditions</i>
<i>sul1</i>	5 minutes at 95 °C, 40 cycles of 15 seconds at 95 °C, annealing 30 seconds at 65 °C
<i>sul2</i>	5 minutes at 95 °C, 40 cycles of 15 seconds at 95 °C, annealing 30 seconds at 61 °C
<i>dfrA1</i>	5 minutes at 95 °C, 40 cycles of 10 seconds at 95 °C, annealing 30 seconds at 60 °C
<i>intl-1</i>	5 minutes at 95 °C, 40 cycles of 15 seconds at 95 °C, annealing 30 seconds at 60 °C
16s-rRNA	5 minutes at 95 °C, 40 cycles of 15 seconds at 95 °C, annealing 30 seconds at 60 °C

Forward and reverse primers of the selected ARGs, MGE and 16SrRNA.

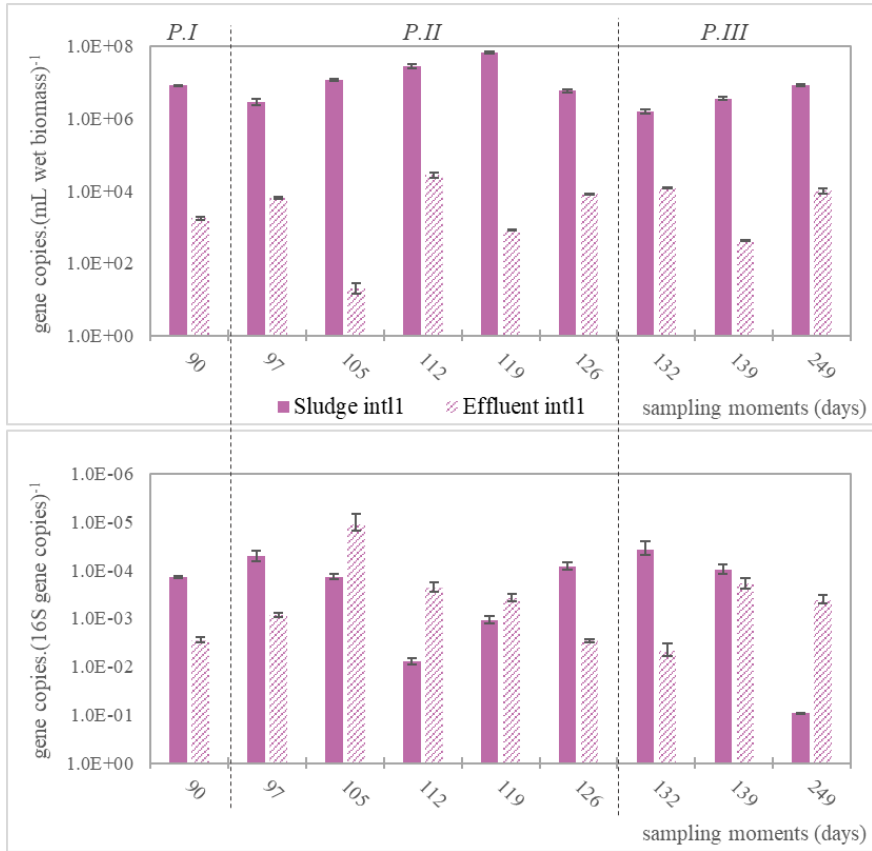
<i>Genes</i>	<i>Forward Primer 5'-3'</i>	<i>Reverse Primer 5'-3'</i>
<i>sul1</i>	CGCACCGGAAACATCGCTGCAC	TGAAGTTCCGCCGAAGGCTCG
<i>sul2</i>	TCCGGTGGAGGCCGGTATCTGG	CGGAATGCCATCTGCCTTGAG
<i>dfrA1</i>	TTCAGGTGGTGGGAGATATAC	TTAGAGGCGAAGTCTTGGGTAA
<i>intl-1</i>	GATCGGTGCGAATGCGTGT	GCCTTGATGTTACCCGAGAG
16s rRNA	ACTCCTACGGGAGGCAGCAG	ATTACCGCGGCTGCTGG

Standards were added to each PCR plate to generate the standard curve. At least 6 serial dilution points (in technical duplicate) were performed to create the standard curves. An average standard curve based on the curve generated in each run was created for every gene set. Finally, the gene concentration values were then calculated from the aforementioned curve. For *sul1*, *sul2*, *dfrA1* and *intl-1*, gene concentration values were standardized based on the 16srRNA gene concentration of each sample (sludge or permeate).

Annex D.2. Gene concentration in the MA-AnMBR



The concentration of gene *sul2* on the MA-AnMBR sludge and effluent. The figure on the top corresponds to the total gene copies per mL of wet biomass, while the values in the figure from the bottom are values of the *sul2* gene standardized per 16S gene copies. The graphs show the reactor periods in which the samples were taken P.I corresponds to the period before antibiotics were added to the MA-AnMBR feed; P.II entitles the period in which the antibiotics SMX and TMP were added in steps, in the concentration of 10, 50 and 150 $\mu\text{g}\cdot\text{L}^{-1}$. Each step lasted around 3 HRT (7.5 days). Finally, the P.III entitles 120 days in which SMX and TMP were present in the MA-AnMBR feed with a concentration equivalent to 150 $\mu\text{g}\cdot\text{L}^{-1}$ each.



The concentration of gene intl-1 on the MA-AnMBR sludge and effluent. The figure on the top corresponds to the total gene copies per mL of wet biomass, while the values in the figure from the bottom are values of the intl-1 gene standardized per 16S gene copies. The graphs show the reactor periods in which the samples were taken. P.I corresponds to the period before antibiotics were added to the MA-AnMBR feed; P.II entitles the period in which the antibiotics SMX and TMP were added in steps, in the concentration of 10, 50 and 150 $\mu\text{g}\cdot\text{L}^{-1}$. Each step lasted around 3 HRT (7.5 days). Finally, the P.III entitles 120 days in which SMX and TMP were present in the MA-AnMBR feed with a concentration equivalent to 150 $\mu\text{g}\cdot\text{L}^{-1}$ each.

Annex D.3. Pearson correlation

Pearson correlation tests were conducted between the measured SMX resistant-bacteria, TMP resistant-bacteria, and the different gene-relative concentrations, for samples taken from the sludge and the permeate of the MA-AnMBR. A strong correlation was assumed when the absolute value of the Pearson coefficient (ρ) was above 0.7.

The sludge SMX-resistant bacteria have no lineal correlation with any of the studied genes, but permeate values have a positive linear correlation with the *sul1* gene and *intI-1* MGE (with ρ values of 0.87 and 0.71 respectively). Results of the lack of correlation between SMX-resistant bacteria and genes *sul1* and *sul2* might indicate that the abundance of the selected resistant genes for SMX are not linked with the gain of resistance towards the antibiotics expressed in the genes. ARG *sul1*, *sul2*, *dfrA1*, and *intI-1* MGE were already present in the MA-AnMBR before the addition of SMX and TMP to the feed. The Ma-AnMBR was inoculated with real sludge from a pilot-scale blackwater anaerobic reactor located at NIOO-KNAW facilities (Wageningen, Netherlands) and therefore, some resistance towards the selected antibiotics could be expected. Thus, the MA-AnMBR could already have some ARGs, and the added concentrations of antibiotics might not be enough to assess the gain or loss in resistance.

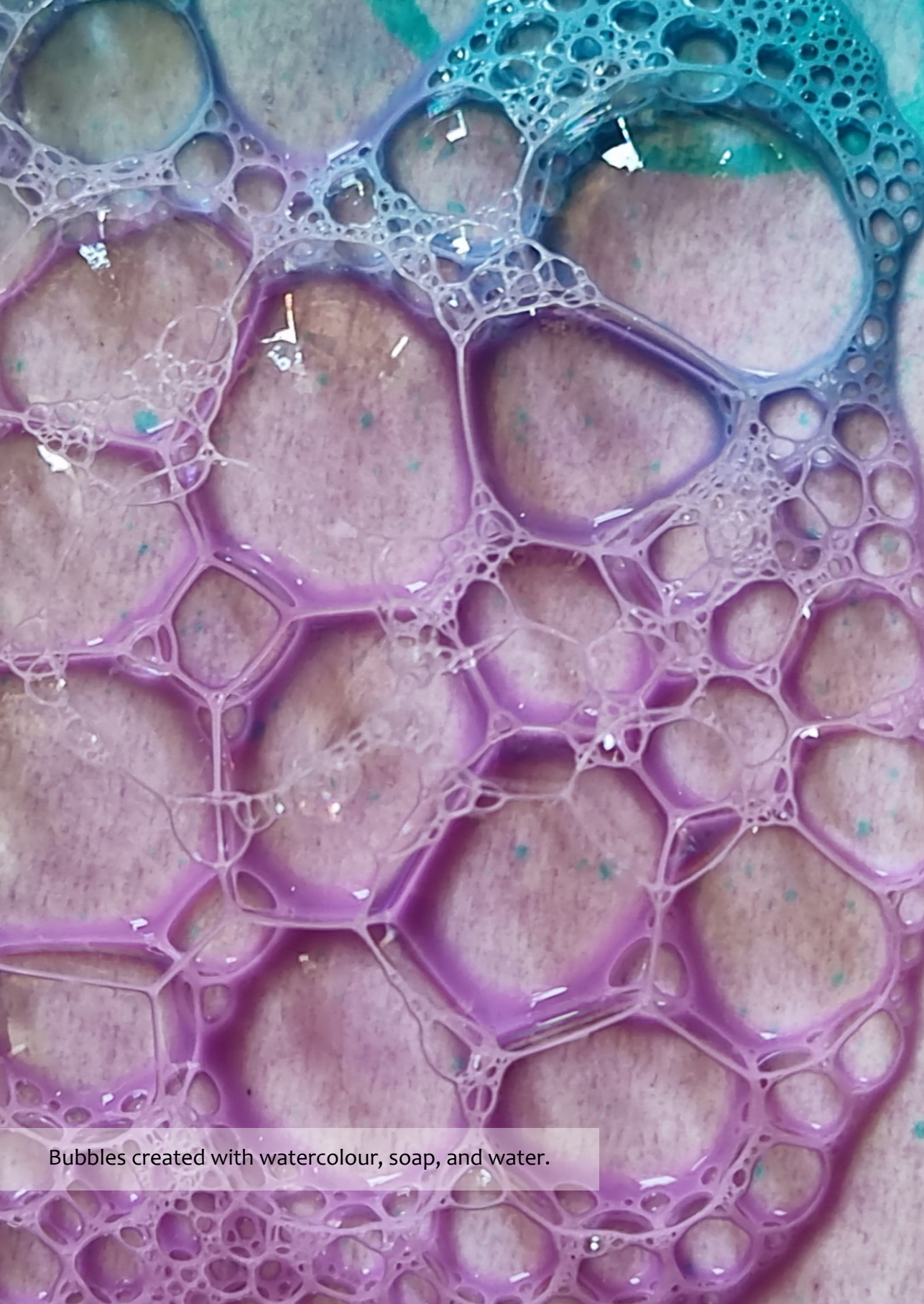
The table below shows the Pearson correlation coefficients for sludge samples taken between days 96 and 430 of the MA-AnMBR operation. The gene concentrations are considering their relative abundance (to 16S gene abundance), while the resistant bacteria to SMX or TMP correspond to the average plate count on each day. These days correspond to periods during the (stepwise) addition of antibiotics, P.II, after addition, where a concentration of $150 \mu\text{g}\cdot\text{L}^{-1}$ of SMX and TMP was added to the MA-AnMBR feed, P.III, and the period entitled P.IV, where SMX and TMP stopped being added to the feed. Strong correlations are shown in bold and with a green background and are defined for absolute values of Pearson coefficients above 0.7.

MA-AnMBR sludge	TMP resistant-bacteria	SMX resistant-bacteria	dfrA1 gene	sul1 gene	sul2 gene	intl-1 MGE
TMP resistant-bacteria	1.00					
SMX resistant-bacteria	0.83	1.00				
dfrA1 gene	-0.35	-0.23	1.00			
sul1 gene	0.00	0.36	0.86	1.00		
sul2 gene	-0.45	-0.30	0.99	0.66	1.00	
intl-1 MGE	-0.33	-0.04	0.99	0.82	0.94	1.00

The table below shows the Pearson correlation coefficients for UF permeate samples taken between days 86 and 250 of the MA-AnMBR operation. The gene concentrations are considering their relative abundance (over 16S gene abundance), while the resistant bacteria to SMX or TMP correspond to the average plate count on each day. A total of seven sample days were assessed for correlation, from periods P.I (before the addition of antibiotics), P.II (during the stepwise antibiotic addition) and P.III, when the concentration of $150 \mu\text{g}\cdot\text{L}^{-1}$ of SMX and TMP was added to the MA-AnMBR feed for around 180 days. Strong correlations are shown in bold and with a green background and are defined for absolute values of Pearson coefficients above 0.7.

MA-AnMBR permeate	TMP resistant-bacteria	SMX resistant-bacteria	sul1 gene	sul2 gene	intl-1 MGE
TMP resistant-bacteria	1.00				
SMX resistant-bacteria	0.97	1.00			
sul1 gene	0.94	0.87	1.00		
sul2 gene	-0.17	-0.11	-0.22	1.00	
intl-1 MGE	0.67	0.71	0.53	-0.27	1.00

Mobile genetic element *intl-1* had a positive linear correlation with all tested genes of the MA-AnMBR sludge. Due to their association with plasmids, the class 1 integron plays a key role in the transport of ARGs (Carattoli, 2003). The horizontal gene transfer (HGT) linked to *intl-1* concentrations might be responsible for a rise in the extracellular plasmid DNA, which hence intensified the harbouring of plasmid-based resistance within the microorganisms (Chaturvedi et al., 2021). The relative abundance of the *intl-1* gene in the permeate of the MA-AnMBR was similar to the one obtained in the sludge (**Annex D.2. Gene concentration in the MA-AnMBR**). A similar result, where the *intl-1* number of copies in raw and treated sewage had no significant difference was observed by Makowska et al. (2016). Furthermore, the *sul2* and *intl-1* are found to be co-located on conjugative plasmids generally. The gene cassettes with *sul2* and *intl-1* are found abundantly in wastewater, and the abundance of MGEs like *intl-1* is linked to the presence and distribution of ARG *sul2* (Zheng et al., 2018). This explains the strong correlation (ρ of 0.94) between *intl-1* and *sul2*. Moreover, the correlation results between *intl-1*, *dfrA1*, and *sul1* might indicate that the MGE *intl-1* could also be in cassettes with these genes.



Bubbles created with watercolour, soap, and water.

Acknowledgements

About the Author

List of Publications

Acknowledgements

Some people dream since they are little about having an academic career, doing research, and obtaining a PhD. This was not my case. But, along the way of studying and working, many people inspired, supported, and created opportunities for me to develop the researcher I have inside. This book represents the culmination of my PhD. It would not have been finished without the guidance and help of so many people, whom I would like to thank here.

Firstly, I would like to thank my supervisor, Ralph Lindeboom. From our first meeting back in 2017, you always encourage and supported my academic career. In our weekly meetings, we spent hours chatting and discussing my research and progress. I always left your office more uplifted than when I entered it, and with the feeling that I could accomplish what was ahead of me. Secondly, I would like to thank my promotor, Merle de Kreuk. You create a safe, supporting and encouraging environment around you, and your kindness inspires me to keep on learning. There was a moment in my PhD when I got completely lost and felt unsuitable for this job. Both Ralph and Merle allowed me to take time off, during which, I found back my strength and joy for learning. At the beginning of my PhD, I had an uncommonly large supervision team. Thank you Tineke Hooijmans and Hector Garcia, for being the bridge between my MSc. at IHE and my PhD at TU. Thank you Jules van Lier, for your sharp review of my research and papers, which made me a better researcher.

I am grateful for doing my PhD as part of the LOTUS^{HR} team. Thank you, Lucas, Bruno, Elackiya, Steef, Tania, Doris, Theo, Nora and Kasia. We spent endless hours in committee meetings in the Netherlands and India, but we also enjoyed dinners, bars, beers, chats, and trips. You were the perfect team to be part of and showed me what real collaboration looks like.

My work would have not been possible without the help of our section staff: Armand, Mohammed, Patricia, Jane, Jasper, Sabrina, Mariska, Riëlle and Tamara. Thank you for your guidance and for making our job easier. I spent my last two years at TU-Delft working as an Education support personnel, helping in the development of the new MSc. in Environmental Engineering. Thank you, Miriam, for giving me the space to develop my organizational skills as part of the Steppingstone module, and for your good energy and support. I also want to thank Kim and Doris, for the trust and hours spent thinking about B1. I learnt and I always felt welcomed by all the TU-Delft staff members that I got to work with, so thank you.

I was able to teach some during my time at TU-Delft, so thank you to all the students that were part of my journey. I can only hope that I was able to support and encourage your learning, as much as you encourage my growth as a teacher. I am especially thankful to the students that contributed in one way or another to this project: Tavishi, Sasidhar, Pravin, Shrilekha, Giorgio, Ben, Jelle, and Jing.

My PhD journey was full of bumpy roads and long hours spent at the office and lab, but I wouldn't have finished without the support of so many colleagues and friends. Thank you, Carina, Emiel, Sara, Lenno, Bin, Lihua, and Max. We started together and you all made me feel more at home. Thank you for organizing Sinterklaas, for the coffee breaks, lunches, and laughs. Thank you, Pamela, Javier (& Nicole), Magela and Victor, for welcoming me as part of the department and showing me the way. For the hours spent discussing science, how the lab worked, and sometimes how it didn't work. I cannot thank enough what I call "the new batch" of PhDs: Shreya, Simon M., Simon K., Roberto, Alex, Aashna, Joao, Sofia (& Ze), Iosif, Gladys, Roos, and many more. We spent hours in lunches next to the pond and on the 6th floor, chatting about some serious and non-serious topics. My PhD journey was interrupted by a global pandemic, but this didn't stop the PSOR group. Thank you Boran (& Luisa), Ties, Jerom, Robert, Jessica, Mike, Juancho, Bart, and Johanna for the beers, glühwein, Koningsdag parties, picnics, and beach moments.

I am beyond grateful to my Paranympths, Carina and Sofia. Carina, we started our PhDs the same day, and move from office to office always together. You are one of the greatest gifts this PhD brought to me. Your friendship kept me sane, and you were always a source of fun and awesome experiences. I can only dream about our next adventures, either at the beach, skiing, or surfing. Thank you Sofia, for your calmness and kindness. I love seeing how you take care of everyone around you, and how you make all of us at TU much more comfortable. I hope you have a great PhD journey, especially in the next years to come.

While my family was more than 11,000 km away, I had a group of friends in NL that were (and are) like my family. Thank you, Bruno, and Fio, for being my little piece of home in NL, for our pasta lunches on Sundays, and all your support. Thank you to all the Game Night group: Berend, Stefan, Claudia, Mona, Lauren, and Rafa. You were a source of joy, and I am beyond grateful for your friendship and support, especially during some dark moments.

Even when my PhD was in the Netherlands, back home I had a big group of supporters. Nato, Agus, Clari, Flo, Xime, Mati y Meche, I was always looking forward

to our “Chicas” meetings once I was back home. In our 20 years of friendship, we saw each other grow, and support each other in every step. Every time I went back home, I felt renewed and energized, and you were a big part of it!

Job, thanks for the laughs, dinners, walks, ice creams, research conversations and fun times we have shared. During my PhD journey, you supported, helped and believed in me, even when I didn’t believe in myself. You are one of the kindest people that I know, and that moves me to be a better person. Thank you for making me a better researcher. I hope we have more adventures and time to spend together in the future.

Finally, I want to thank my family: Papá, Vicky, Pol, Flopi, Fede, Pierre y Berto. These last six years were full of joy, growth, and some hard moments. Back in 2015, you encouraged me to come to the Netherlands to keep on studying, and you have never stopped supporting me. Your unconditional love has always been my energy source. With you, I learnt that physical and emotional distances are not the same, and that no matter what, we will be there for each other. Thanks for the laughs and smiles brought by my nieces and nephew, Lucas, Josefina, Pilar, and the next one to come. I cannot wait to see you grow and experience fun things together. My mom used to complain that at the end of every Sunday lunch or dinner, we always used to talk about disgusting things like poop (sorry, maybe it was my fault). I can only hope that one day, I would be able to share another dinner and hug her again.

About the Author



Antonella Lucia Piaggio Vazquez was born in Montevideo, Uruguay, on December 6th, 1986. She attended her elementary, primary and secondary education at Colegio Seminario in Montevideo. In 2005, she began with her bachelor's in civil engineering at the Universidad de la República (UdelaR). She developed an interest in water treatment and urban water management, doing an internship at the Industrial Effluents Department of Montevideo town hall, majoring in Hydraulics and Environment in 2012.

Next to her studies, Antonella worked for over 5 years in consultancy on urban water master planning and flood hazard risk maps. Parallely, she taught Math and Physics as a private tutor and at high-school level at Liceo Jubliar Juan Pablo II and coordinated the pastoral extracurricular activities at primary school level on the Colegio Seminario. In 2015, she received a full scholarship in UNESCO-IHE (Delft, Netherlands) to pursue an MSc. in Sanitary Engineering. Her thesis focused on assessing the feasibility of Reverse Osmosis Treatment of an Anaerobic Membrane Bioreactor permeate, and was done at Biothane (Veolia Water Technologies Center, Netherlands).

After graduating with her MSc. in 2017, Antonella started her PhD at the Delft University of Technology (TU-Delft), in the Water Management Department, under the supervision of Ralph Lindeboom and Merle de Kreuk. As part of the larger LOTUS^{HR} project, her PhD focused on wastewater pre-treatment, specifically on the potential of combining anaerobic digestion with dissolved air flotation as a suspended solids separation unit. Since 2022, she started as an Educational support personnel and helped in the development of the new MSc. in Environmental Engineering of TU-Delft.

List of Publications

Publications

Wasajja, H., Al-Muraisy, S. A., **Piaggio, A. L.**, Ceron-Chafla, P., Aravind, P. V., Spanjers, H., van Lier, J.B., Lindeboom, R. E. (2021). Improvement of Biogas Quality and Quantity for Small-Scale Biogas-Electricity Generation Application in off-Grid Settings: A Field-Based Study. *Energies*, 14(11), 3088. <https://doi.org/10.3390/en14113088>

Piaggio, A. L., Soares, L. A., Balakrishnan, M., Guleria, T., de Kreuk, M. K., & Lindeboom, R. E. (2022). High suspended solids removal of Indian drain water with a down-scaled Dissolved Air Flotation (DAF) for water recovery. Assessing water-type dependence on process control variables. *Environmental Challenges*, 8, 100567. <https://doi.org/10.1016/j.envc.2022.100567>

Piaggio, A. L., Sasidhar, K.B., Khande, P., Balakrishnan, M., van Lier, J. B., de Kreuk, M. K., & Lindeboom, R. E. F. (Under Review). Effects of low oxygen dosages on an anaerobic membrane bioreactor, simulating the oxygen supply in an anaerobic digester-dissolved air flotation (AD-DAF) system. *Submitted to Environmental Science and Technology*.

Piaggio, A. L., Mittapalli, S., Calderón-Franco D., Weissbrodt, D.G., van Lier, J. B., de Kreuk, M. K., & Lindeboom, R. E. (Under Review). The fate of sulfamethoxazole and trimethoprim in a micro-aerated anaerobic membrane bioreactor: implications for antibiotic resistance spreading. *Submitted to Water Science and Technology*.

Piaggio, A. L., Smith, G. de Kreuk, M. K., & Lindeboom, R. E. (Under Review). Modelling of Dissolved Air Flotation (DAF). Application of an experimental filtration model for suspended solids removal prediction. *Submitted to Separation and Purification Technology*.

Conference contributions

Piaggio A.L., Guleria Ta., Soares L., De Kreuk M.K. , Lindeboom R.E.F. (2020, June 3-4, Netherlands). Dissolved Air Flotation for particle removal in drain water treatment: a comparison between India and the Netherlands. *Environmental Technology for Impact*.

Piaggio A. L., Lindeboom R.E.F, Sasidhar K.B., de Kreuk M.K., van Lier J.B., Lindeboom R.E.F (2022, April 10-13, Poland). Specific Methanogenic Activity of AnMBR sludge subjected to limited aeration: an adaptation process. IWA Wastewater, Water and Resource Recovery Conference.

Piaggio A. L., Calderón-Franco D., Weissbrodt, D.G. (2022, April 4-6, Netherlands). Use of qPCR for antibiotics resistant genes, on a micro-aerated AnMBR. IWA Young Water Professionals Conference.

Piaggio A. L., Lindeboom R.E.F, Sasidhar K.B., Khande P., Mittapalli S., van Lier J.B., de Kreuk M.K. (2022, June 17-22, U.S.A.). Performance of a lab-scale Micro-aerated Anaerobic Membrane Bioreactor fed with synthetic concentrated black water. 17th IWA World Conference on Anaerobic Digestion.



Bubbles created with watercolour, soap, and water.

Bibliography

- Abatzoglou, N., & Boivin, S. (2009). A review of biogas purification processes. *Biofuels, Bioproducts and Biorefining*, 3(1), 42-71. <https://doi.org/10.1002/bbb.117>
- Agarwal, M., Srinivasan, R., & Mishra, A. (2001). Study on flocculation efficiency of okra gum in sewage waste water. *Macromolecular Materials and Engineering*, 286(9), 560-563. [https://doi.org/10.1002/1439-2054\(20010901\)286:9](https://doi.org/10.1002/1439-2054(20010901)286:9)
- Ahmed, S. A., & Giddens, D. P. (1983). Velocity measurements in steady flow through axisymmetric stenoses at moderate Reynolds numbers. *Journal of biomechanics*, 16(7), 505-516. [https://doi.org/10.1016/0021-9290\(83\)90065-9](https://doi.org/10.1016/0021-9290(83)90065-9)
- Al-Muraisy, S. A., Soares, L. A., Chuayboon, S., Ismail, S. B., Abanades, S., van Lier, J. B., & Lindeboom, R. E. (2022). Solar-driven steam gasification of oil palm empty fruit bunch to produce syngas: Parametric optimization via central composite design. *Fuel Processing Technology*, 227, 107118. <https://doi.org/10.1016/j.fuproc.2021.107118>
- Al-Shamrani, A., James, A., & Xiao, H. (2002). Destabilisation of oil–water emulsions and separation by dissolved air flotation. *Water Research*, 36(6), 1503-1512. [https://doi.org/10.1016/S0043-1354\(01\)00347-5](https://doi.org/10.1016/S0043-1354(01)00347-5)
- Albertsen, M., Karst, S. M., Ziegler, A. S., Kirkegaard, R. H., & Nielsen, P. H. (2015). Back to basics—the influence of DNA extraction and primer choice on phylogenetic analysis of activated sludge communities. *PloS one*, 10(7), e0132783. <https://doi.org/10.1371/journal.pone.0132783>
- Alvarino, T., Suarez, S., Lema, J., & Omil, F. (2018). Understanding the sorption and biotransformation of organic micropollutants in innovative biological wastewater treatment technologies. *Science of The Total Environment*, 615, 297-306. <https://doi.org/10.1016/j.scitotenv.2017.09.278>
- American Public Health Association. (2013). APHA. 2005. *Standard Methods for the Examination of Water and Wastewater*. 21st ed. American Public Health Association, Washington DC, 1220p.
- Ansari, S., Alavi, J., & Yaseen, Z. M. (2018). Performance of full-scale coagulation-flocculation/DAF as a pre-treatment technology for biodegradability enhancement of high strength wastepaper-recycling wastewater. *Environmental Science and Pollution Research*, 25(34), 33978-33991. <https://doi.org/10.1007/s11356-018-3340-0>
- Aslam, A., Khan, S. J., & Shahzad, H. M. A. (2022). Anaerobic membrane bioreactors (AnMBRs) for municipal wastewater treatment-potential benefits, constraints, and future perspectives: An updated review. *Science of The Total Environment*, 802, 149612. <https://doi.org/10.1016/j.scitotenv.2021.149612>
- Azman, S., Khadem, A. F., Van Lier, J. B., Zeeman, G., & Plugge, C. M. (2015). Presence and role of anaerobic hydrolytic microbes in conversion of lignocellulosic biomass for biogas production. *Critical Reviews in Environmental Science and Technology*, 45(23), 2523-2564. <https://doi.org/10.1080/10643389.2015.1053727>
- Baeyens, J., Mochtar, I., Liers, S., & De Wit, H. (1995). Plugflow dissolved air flotation. *Water environment research*, 67(7), 1027-1035. <https://doi.org/10.2175/106143095X133266>
- Balakrishna, K., Rath, A., Praveenkumarreddy, Y., Guruge, K. S., & Subedi, B. (2017). A review of the occurrence of pharmaceuticals and personal care products in Indian water bodies. *Ecotoxicology and environmental safety*, 137, 113-120. <https://doi.org/10.1016/j.ecoenv.2016.11.014>
- Balha, A., Vishwakarma, B. D., Pandey, S., & Singh, C. K. (2020). Predicting impact of urbanization on water resources in megacity Delhi. *Remote Sensing Applications: Society and Environment*, 20, 100361. <https://doi.org/10.1016/j.rsase.2020.100361>
- Benjamin, M. M., & Lawler, D. F. (2013). *Water quality engineering: Physical/chemical treatment processes*. John Wiley & Sons.

- Berkessa, Y. W., Yan, B., Li, T., Tan, M., She, Z., Jegatheesan, V., Jiang, H., & Zhang, Y. (2018). Novel anaerobic membrane bioreactor (AnMBR) design for wastewater treatment at long HRT and high solid concentration. *Bioresource technology*, 250, 281-289. <https://doi.org/10.1016/j.biortech.2017.11.025>
- Bicudo, B. (2022). *Municipal effluent disinfection by Iron Electrocoagulation* [Doctoral Dissertation, TU-Delft]. Delft.
- Bicudo, B., van der Werff, B.-J., Medema, G., & Van Halem, D. (2022). Disinfection during Iron Electrocoagulation: Differentiating between Inactivation and Floc Entrapment for *Escherichia coli* and Somatic Coliphage ϕ X174. *ACS ES&T Water*, 2(10), 1707-1714. <https://doi.org/10.1021/acsestwater.2c00230>
- Bieganowski, A., Zaleski, T., Kajdas, B., Sochan, A., Józefowska, A., Beczek, M., Lipiec, J., Turski, M., & Ryzak, M. (2018). An improved method for determination of aggregate stability using laser diffraction. *Land Degradation & Development*, 29(5), 1376-1384. <https://doi.org/10.1111/lfd.12369>
- Blahna, M. T., Zalewski, C. A., Reuer, J., Kahlmeter, G., Foxman, B., & Marrs, C. F. (2006). The role of horizontal gene transfer in the spread of trimethoprim-sulfamethoxazole resistance among uropathogenic *Escherichia coli* in Europe and Canada. *Journal of Antimicrobial Chemotherapy*, 57(4), 666-672. <https://doi.org/10.1093/jac/dkl020>
- Blair, J., Webber, M. A., Baylay, A. J., Ogbolu, D. O., & Piddock, L. J. (2015). Molecular mechanisms of antibiotic resistance. *Nature reviews microbiology*, 13(1), 42-51. <https://doi.org/10.1038/nrmicro3380>
- Blake, G., & Hartge, K. (1986). Particle density. *Methods of soil analysis: Part 1 physical and mineralogical methods*, 5, 377-382. <https://doi.org/10.2136/sssabookser5.1.2ed.c14>
- Bondelind, M., Sasic, S., Pettersson, T. J., Karapantsios, T. D., Kostoglou, M., & Bergdahl, L. (2010). Setting up a numerical model of a DAF tank: turbulence, geometry, and bubble size. *Journal of environmental engineering*, 136(12), 1424-1434. [https://doi.org/10.1061/\(ASCE\)EE.1943-7870.0000275](https://doi.org/10.1061/(ASCE)EE.1943-7870.0000275)
- Botheju, D., & Bakke, R. (2011). Oxygen effects in anaerobic digestion-a review. <http://dx.doi.org/10.2174/1876400201104010001>
- Botheju, D., Samarakoon, G., Chen, C., & Bakke, R. (2010). *An experimental study on the effects of oxygen in bio-gasification; Part 1* proceedings of the International Conference on Renewable Energies and Power Quality (ICRE PQ 10), Granada, Spain,
- Bratby, J. (1980). *Coagulation and flocculation* (first ed.).
- Bridle, H. (2020). *Waterborne pathogens: detection methods and applications*. Academic Press.
- Brignell, A. (1974). Mass transfer from a spherical cap bubble in laminar flow. *Chemical Engineering Science*, 29(1), 135-147. [https://doi.org/10.1016/0009-2509\(74\)85039-6](https://doi.org/10.1016/0009-2509(74)85039-6)
- Brioukhanov, A., Thauer, R., & Netrusov, A. (2002). Catalase and superoxide dismutase in the cells of strictly anaerobic microorganisms. *Microbiology*, 71(3), 281-285. <https://doi.org/10.1023/A:1015846409735>
- Cagnetta, C., Saerens, B., Meerburg, F. A., Decru, S. O., Broeders, E., Menkveld, W., Vandekerckhove, T. G., De Vrieze, J., Vlaeminck, S. E., & Verliefde, A. R. (2019). High-rate activated sludge systems combined with dissolved air flotation enable effective organics removal and recovery. *Bioresource technology*, 291, 121833. <https://doi.org/10.1016/j.biortech.2019.121833>
- Calapez, A. R., Elias, C. L., Almeida, S. F., Brito, A. G., & Feio, M. J. (2019). Sewage contamination under water scarcity effects on stream biota: biofilm, grazers, and their interaction. *Environmental Science and Pollution Research*, 26, 26636-26645. <https://doi.org/10.1007/s11356-019-05876-7>
- Calderón-Franco, D., van Loosdrecht, M. C., Abeel, T., & Weissbrodt, D. G. (2021). Free-floating extracellular DNA: Systematic profiling of mobile genetic elements and antibiotic resistance

- from wastewater. *Water Research*, 189, 116592. <https://doi.org/10.1016/j.watres.2020.116592>
- Carattoli, A. (2003). Plasmid-mediated antimicrobial resistance in *Salmonella enterica*. *Current issues in molecular biology*, 5(4), 113-122. <https://doi.org/10.21775/cimb.005.113>
- Ceron-Chafla, P., Kleerebezem, R., Rabaey, K., van Lier, J. B., & Lindeboom, R. E. (2020). Direct and indirect effects of increased CO₂ partial pressure on the bioenergetics of syntrophic propionate and butyrate conversion. *Environmental science & technology*, 54(19), 12583-12592. <https://doi.org/10.1021/acs.est.0c02022>
- Cetecioglu, Z., Ince, B., Gros, M., Rodriguez-Mozaz, S., Barceló, D., Ince, O., & Orhon, D. (2015). Biodegradation and reversible inhibitory impact of sulfamethoxazole on the utilization of volatile fatty acids during anaerobic treatment of pharmaceutical industry wastewater. *Science of The Total Environment*, 536, 667-674. <https://doi.org/10.1016/j.scitotenv.2015.07.139>
- Chaturvedi, P., Singh, A., Chowdhary, P., Pandey, A., & Gupta, P. (2021). Occurrence of emerging sulfonamide resistance (sul1 and sul2) associated with mobile integrons-integrase (int1 and int2) in riverine systems. *Science of The Total Environment*, 751, 142217. <https://doi.org/10.1016/j.scitotenv.2020.142217>
- Chen, X., Li, Z., He, N., Zheng, Y., Li, H., Wang, H., Wang, Y., Lu, Y., Li, Q., & Peng, Y. (2018). Nitrogen and phosphorus removal from anaerobically digested wastewater by microalgae cultured in a novel membrane photobioreactor. *Biotechnology for biofuels*, 11(1), 1-11. <https://doi.org/10.1186/s13068-018-1190-0>
- Chernicharo, C., Van Lier, J., Noyola, A., & Bressani Ribeiro, T. (2015). Anaerobic sewage treatment: state of the art, constraints and challenges. *Reviews in Environmental Science and Bio/Technology*, 14(4), 649-679. <https://doi.org/10.1007/s11157-015-9377-3>
- Christiansen, T., & Nielsen, J. (2002). Production of extracellular protease and glucose uptake in *Bacillus clausii* in steady-state and transient continuous cultures. *Journal of biotechnology*, 97(3), 265-273. [https://doi.org/10.1016/S0168-1656\(02\)00109-8](https://doi.org/10.1016/S0168-1656(02)00109-8)
- Clara, M., Kreuzinger, N., Strenn, B., Gans, O., & Kroiss, H. (2005). The solids retention time—a suitable design parameter to evaluate the capacity of wastewater treatment plants to remove micropollutants. *Water Research*, 39(1), 97-106. <https://doi.org/10.1016/j.watres.2004.08.036>
- CLSI. (2019). *Performance standards for antimicrobial susceptibility testing* (CLSI supplement M100, Issue.
- Constantin, P., & Foias, C. (2020). *Navier-stokes equations*. University of Chicago Press.
- CPCB. (2009). *Status of Water Supply, Wastewater Generation and Treatment in Class-I Cities and Class-II Towns of India*. Retrieved from www.cpcb.nic.in
- Crini, G., & Lichtfouse, E. (2019). Advantages and disadvantages of techniques used for wastewater treatment. *Environmental Chemistry Letters*, 17, 145-155. <https://doi.org/10.1007/s10311-018-0785-9>
- Czekalski, N., Berthold, T., Caucci, S., Egli, A., & Bürgmann, H. (2012). Increased levels of multiresistant bacteria and resistance genes after wastewater treatment and their dissemination into Lake Geneva, Switzerland. *Frontiers in microbiology*, 3, 106. <https://doi.org/10.3389/fmicb.2012.00106>
- de Ilurdoz, M. S., Sathwani, J. J., & Reboso, J. V. (2022). Antibiotic removal processes from water & wastewater for the protection of the aquatic environment—a review. *Journal of Water Process Engineering*, 45, 102474. <https://doi.org/10.1016/j.jwpe.2021.102474>
- De Kreuk, M. K. (2006). *Aerobic granular sludge: scaling up a new technology* [PhD Dissertation, TU Delft]. <http://resolver.tudelft.nl/uuid:a23ba934-3b4a-476e-a781-798723a74056>

- De Nardi, I., Del Nery, V., Amorim, A., Dos Santos, N., & Chimenes, F. (2011). Performances of SBR, chemical-DAF and UV disinfection for poultry slaughterhouse wastewater reclamation. *Desalination*, 269(1-3), 184-189. <https://doi.org/10.1016/j.desal.2010.10.060>
- De Raeve, H., Thunnissen, F., Kaneko, F., Guo, F., Lewis, M., Kavuru, M., Sedic, M., Thomassen, M., & Erzurum, S. (1997). Decreased Cu, Zn-SOD activity in asthmatic airway epithelium: correction by inhaled corticosteroid in vivo. *American Journal of Physiology-Lung Cellular and Molecular Physiology*, 272(1), L148-L154. <https://doi.org/10.1152/ajplung.1997.272.1.L148>
- De Rijk, S. E., & den Blanken, J. G. (1994). Bubble size in flotation thickening. *Water Research*, 28(2), 465-473. [https://doi.org/10.1016/0043-1354\(94\)90284-4](https://doi.org/10.1016/0043-1354(94)90284-4)
- De Vrieze, J., Pinto, A. J., Sloan, W. T., & Ijaz, U. Z. (2018). The active microbial community more accurately reflects the anaerobic digestion process: 16S rRNA (gene) sequencing as a predictive tool. *Microbiome*, 6(1), 1-13. <https://doi.org/10.1186/s40168-018-0449-9>
- Dereli, R. K., Ersahin, M. E., Ozturk, H., Ozturk, I., Jeison, D., van der Zee, F., & van Lier, J. B. (2012). Potentials of anaerobic membrane bioreactors to overcome treatment limitations induced by industrial wastewaters. *Bioresource technology*, 122, 160-170. <https://doi.org/10.1016/j.biortech.2012.05.139>
- Dermer, J., & Fuchs, G. (2012). Molybdoenzyme that catalyzes the anaerobic hydroxylation of a tertiary carbon atom in the side chain of cholesterol. *Journal of Biological Chemistry*, 287(44), 36905-36916. <https://doi.org/10.1074/jbc.M112.407304>
- Díaz-Cruz, M. S., de Alda, M. a. J. L., & Barcelo, D. (2003). Environmental behavior and analysis of veterinary and human drugs in soils, sediments and sludge. *TrAC Trends in Analytical Chemistry*, 22(6), 340-351. [https://doi.org/10.1016/S0165-9936\(03\)00603-4](https://doi.org/10.1016/S0165-9936(03)00603-4)
- Díaz, I., Pérez, S., Ferrero, E., & Fdz-Polanco, M. (2011). Effect of oxygen dosing point and mixing on the microaerobic removal of hydrogen sulphide in sludge digesters. *Bioresource technology*, 102(4), 3768-3775. <https://doi.org/10.1016/j.biortech.2010.12.016>
- Dixit, A., Kumar, N., Kumar, S., & Trigun, V. (2019). Antimicrobial resistance: progress in the decade since emergence of New Delhi metallo- β -lactamase in India. *Indian journal of community medicine: official publication of Indian Association of Preventive & Social Medicine*, 44(1), 4. https://doi.org/10.4103%2Fijcm.IJCM_217_18
- Dubois, M., Gilles, K. A., Hamilton, J. K., Rebers, P. t., & Smith, F. (1956). Colorimetric method for determination of sugars and related substances. *Analytical chemistry*, 28(3), 350-356. <https://doi.org/10.1021/ac60111a017>
- Edzwald. (2010). Dissolved air flotation and me. *Water Research*, 44(7), 2077-2106. <https://doi.org/10.1016/j.watres.2009.12.040>
- Edzwald, & Haarhoff. (2011). *Dissolved air flotation for water clarification* (first ed.). McGraw Hill Professional.
- Edzwald, J. (1995). Principles and applications of dissolved air flotation. *Water Science and Technology*, 31(3-4), 1-23. [https://doi.org/10.1016/0273-1223\(95\)00200-7](https://doi.org/10.1016/0273-1223(95)00200-7)
- Ejhed, H., Fång, J., Hansen, K., Graae, L., Rahmberg, M., Magnér, J., Dorgeloh, E., & Plaza, G. (2018). The effect of hydraulic retention time in onsite wastewater treatment and removal of pharmaceuticals, hormones and phenolic utility substances. *Science of The Total Environment*, 618, 250-261. <https://doi.org/10.1016/j.scitotenv.2017.11.011>
- Ellouze, M., Saddoud, A., Dhouib, A., & Sayadi, S. (2009). Assessment of the impact of excessive chemical additions to municipal wastewaters and comparison of three technologies in the removal performance of pathogens and toxicity. *Microbiological Research*, 164(2), 138-148. <https://doi.org/10.1016/j.micres.2006.11.007>
- Elmahdy, A., Mirnezami, M., & Finch, J. (2008). Zeta potential of air bubbles in presence of frothers. *International Journal of Mineral Processing*, 89(1-4), 40-43. <https://doi.org/10.1016/j.minpro.2008.09.003>

- Falås, P., Wick, A., Castronovo, S., Habermacher, J., Ternes, T. A., & Joss, A. (2016). Tracing the limits of organic micropollutant removal in biological wastewater treatment. *Water Research*, 95, 240-249. <https://doi.org/10.1016/j.watres.2016.03.009>
- Fan, X., Zhang, Z., Li, G., & Rowson, N. (2004). Attachment of solid particles to air bubbles in surfactant-free aqueous solutions. *Chemical Engineering Science*, 59(13), 2639-2645. <https://doi.org/10.1016/j.ces.2004.04.001>
- Fanaie, V. R., & Khiadani, M. (2020). Effect of salinity on air dissolution, size distribution of microbubbles, and hydrodynamics of a dissolved air flotation (DAF) system. *Colloids and Surfaces A: Physicochemical and Engineering Aspects*, 591, 124547. <https://doi.org/10.1016/j.colsurfa.2020.124547>
- Fanaie, V. R., Khiadani, M., & Ayres, T. (2019). Effects of internal geometry on hydrodynamics of dissolved air flotation (DAF) tank: an experimental study using particle image velocimetry (PIV). *Colloids and Surfaces A: Physicochemical and Engineering Aspects*, 575, 382-390. <https://doi.org/10.1016/j.colsurfa.2019.05.027>
- FAO. (2020). *The State of Food and Agriculture 2020. Overcoming water challenges in agriculture*. FAO.
- Farhad, A., & Mohammadi, Z. (2005). Calcium hydroxide: a review. *International dental journal*, 55(5), 293-301. <https://doi.org/10.1111/j.1875-595X.2005.tb00326.x>
- Feng, L., Casas, M. E., Ottosen, L. D. M., Møller, H. B., & Bester, K. (2017). Removal of antibiotics during the anaerobic digestion of pig manure. *Science of The Total Environment*, 603, 219-225. <https://doi.org/10.1016/j.scitotenv.2017.05.280>
- Fermoso, J., Gil, M. V., Arias, B., Plaza, M., Pevida, C., Pis, J., & Rubiera, F. (2010). Application of response surface methodology to assess the combined effect of operating variables on high-pressure coal gasification for H₂-rich gas production. *International Journal of Hydrogen Energy*, 35(3), 1191-1204. <https://doi.org/10.1016/j.ijhydene.2009.11.046>
- Fernandes, T. V., Suárez-Muñoz, M., Trebuch, L. M., Verbraak, P. J., & Van de Waal, D. B. (2017). Toward an ecologically optimized N: P recovery from wastewater by microalgae. *Frontiers in microbiology*, 8, 1742. <https://doi.org/10.3389/fmicb.2017.01742>
- Ferrari, F., Balcazar, J. L., Rodriguez-Roda, I., & Pijuan, M. (2019). Anaerobic membrane bioreactor for biogas production from concentrated sewage produced during sewer mining. *Science of The Total Environment*, 670, 993-1000. <https://doi.org/10.1016/j.scitotenv.2019.03.218>
- Ferreira, T., & Rasband, W. (2012). *ImageJ User Guide: IJ 1.46r*. National Institute of Health. Retrieved 17TH mARCH from <https://imagej.nih.gov/ij/docs/guide/>
- Ferry, J. G. (1992). Methane from acetate. *Journal of bacteriology*, 174(17), 5489-5495. <https://doi.org/10.1128/jb.174.17.5489-5495.1992>
- Fick, J., Söderström, H., Lindberg, R. H., Phan, C., Tysklind, M., & Larsson, D. J. (2009). Contamination of surface, ground, and drinking water from pharmaceutical production. *Environmental Toxicology and Chemistry*, 28(12), 2522-2527. <https://doi.org/10.1897/09-073.1>
- Fisher, R. A., & Bennett, J. H. (1990). *Statistical methods, experimental design, and scientific inference* (first ed.). Oxford University Press Inc.
- Forster-Carneiro, T., Riau, V., & Pérez, M. (2010). Mesophilic anaerobic digestion of sewage sludge to obtain class B biosolids: Microbiological methods development. *Biomass and Bioenergy*, 34(12), 1805-1812. <https://doi.org/10.1016/j.biombioe.2010.07.010>
- Frankena, J., Van Verseveld, H., & Stouthamer, A. (1988). Substrate and energy costs of the production of exocellular enzymes by *Bacillus licheniformis*. *Biotechnology and bioengineering*, 32(6), 803-812. <https://doi.org/10.1002/bit.260320612>
- Fridovich, I. (1995). Superoxide radical and superoxide dismutases. *Annual review of biochemistry*, 64(1), 97-112. <https://doi.org/10.1146/annurev.bi.64.070195.000525>

- Frølund, B., Griebe, T., & Nielsen, P. (1995). Enzymatic activity in the activated-sludge floc matrix. *Applied microbiology and biotechnology*, 43(4), 755-761. <https://doi.org/10.1007/BF00164784>
- Fukushi, K.-i., Matsui, Y., & Tambo, N. (1995). A kinetic study for dissolved air flotation system in water and wastewater treatment. *Water Sci. Technol.* (31), 10.
- Fukushi, K.-i., Matsui, Y., & Tambo, N. (1998). Dissolved air flotation: experiments and kinetic analysis. *Journal of Water Supply: Research and Technology—AQUA*, 47(2), 76-86. <https://doi.org/10.2166/aqua.1998.13>
- Fuller, M., Perreault, N., & Hawari, J. (2010). Microaerophilic degradation of hexahydro-1, 3, 5-trinitro-1, 3, 5-triazine (RDX) by three Rhodococcus strains. *Letters in applied microbiology*, 51(3), 313-318.
- García Rea, V. S., Muñoz Sierra, J. D., Fonseca Aponte, L. M., Cerqueda-García, D., Quchani, K. M., Spanjers, H., & Van Lier, J. B. (2020). Enhancing phenol conversion rates in saline anaerobic membrane bioreactor using acetate and butyrate as additional carbon and energy sources. *Frontiers in microbiology*, 11, 604173. <https://doi.org/10.3389/fmicb.2020.604173>
- Giménez, J., Robles, A., Carretero, L., Durán, F., Ruano, M., Gatti, M. N., Ribes, J., Ferrer, J., & Seco, A. (2011). Experimental study of the anaerobic urban wastewater treatment in a submerged hollow-fibre membrane bioreactor at pilot scale. *Bioresource technology*, 102(19), 8799-8806. <https://doi.org/10.1016/j.biortech.2011.07.014>
- Giokas, D., Vlessidis, A., Angelidis, M., Tsimarakis, G., & Karayannis, M. (2002). Systematic analysis of the operational response of activated sludge process to variable wastewater flows. A case study. *Clean Technologies and Environmental Policy*, 4(3), 183-190. <https://doi.org/10.1007/s10098-002-0145-z>
- Giroto, F., Peng, W., Rafieenia, R., & Cossu, R. (2018). Effect of aeration applied during different phases of anaerobic digestion. *Waste and Biomass Valorization*, 9(2), 161-174. <https://doi.org/10.1007/s12649-016-9785-9>
- Gjaltema, A., Vinke, J., Van Loosdrecht, M., & Heijnen, J. (1997). Abrasion of suspended biofilm pellets in airlift reactors: Importance of shape, structure, and particle concentrations. *Biotechnology and bioengineering*, 53(1), 88-99. [https://doi.org/10.1002/\(SICI\)1097-0290\(19970105\)53:1%3C88::AID-BIT12%3E3.0.CO;2-5](https://doi.org/10.1002/(SICI)1097-0290(19970105)53:1%3C88::AID-BIT12%3E3.0.CO;2-5)
- Göbel, A., McArdell, C. S., Joss, A., Siegrist, H., & Giger, W. (2007). Fate of sulfonamides, macrolides, and trimethoprim in different wastewater treatment technologies. *Science of The Total Environment*, 372(2-3), 361-371. <https://doi.org/10.1016/j.scitotenv.2006.07.039>
- Goedhart, R., Müller, S., van Loosdrecht, M. C., & van Halem, D. (2022). Vivianite precipitation for iron recovery from anaerobic groundwater. *Water Research*, 217, 118345. <https://doi.org/10.1016/j.watres.2022.118345>
- Gonzalez, A., Hendriks, A., Van Lier, J. B., & De Kreuk, M. (2018). Pre-treatments to enhance the biodegradability of waste activated sludge: Elucidating the rate limiting step. *Biotechnology Advances*, 36(5), 1434-1469. <https://doi.org/10.1016/j.biotechadv.2018.06.001>
- Gonzalez, A., van Lier, J. B., & de Kreuk, M. K. (2022). Effects of mild thermal pre-treatment combined with H₂O₂ addition on waste activated sludge digestibility. *Waste Management*, 141, 163-172. <https://doi.org/10.1016/j.wasman.2022.01.017>
- Grady Jr, C. L., Daigger, G. T., Love, N. G., & Filipe, C. D. (2011). *Biological wastewater treatment*. CRC press.
- Gros, M., Petrović, M., Ginebreda, A., & Barceló, D. (2010). Removal of pharmaceuticals during wastewater treatment and environmental risk assessment using hazard indexes. *Environment international*, 36(1), 15-26. <https://doi.org/10.1016/j.envint.2009.09.002>
- Guo, B., Yu, N., Weissbrodt, D. G., & Liu, Y. (2021). Effects of micro-aeration on microbial niches and antimicrobial resistances in blackwater anaerobic digesters. *Water Research*, 196, 117035. <https://doi.org/10.1016/j.watres.2021.117035>

- Güsewell, S. (2004). N: P ratios in terrestrial plants: variation and functional significance. *New phytologist*, 164(2), 243-266. <https://doi.org/10.1111/j.1469-8137.2004.01192.x>
- Haarhoff, J. (2008). Dissolved air flotation: progress and prospects for drinking water treatment. *Journal of Water Supply: Research and Technology—AQUA*, 57(8), 555-567. <https://doi.org/10.2166/aqua.2008.046b>
- Haidari, A., & van der Meer, W. (2017). *One Step Membrane Filtration: A fundamental study* [Doctoral Dissertation, Delft University of Technology]. Netherlands.
- Han. (2002). Modeling of DAF: the effect of particle and bubble characteristics. *Journal of Water Supply: Research and Technology—AQUA*, 51(1), 27-34. <https://doi.org/10.2166/aqua.2002.0003>
- Han, & Dockko. (1998). Zeta potential measurement of bubbles in DAF process and its effect on the removal efficiency. *KSCE Journal of Civil Engineering*, 2(4), 461-466. <https://doi.org/10.1007/BF02830128>
- Han, Park, Lee, & Shim. (2002). Effect of pressure on bubble size in dissolved air flotation. *Water Science and Technology: Water Supply*, 2(5-6), 41-46. <https://doi.org/10.2166/ws.2002.0148>
- Han, M., & Dockko, S. (1998). Zeta potential measurement of bubbles in DAF process and its effect on the removal efficiency. *KSCE Journal of Civil Engineering*, 2(4), 461-466. <https://doi.org/10.1007/BF02830128>
- Han, M., Kim, W., & Dockko, S. (2001). Collision efficiency factor of bubble and particle (abp) in DAF: theory and experimental verification. *Water Science and Technology*, 43(8), 139-144. <https://doi.org/10.2166/wst.2001.0484>
- Harb, M., Zarei-Baygi, A., Wang, P., Sawaya, C. B., McCurry, D. L., Stadler, L. B., & Smith, A. L. (2021). Antibiotic transformation in an anaerobic membrane bioreactor linked to membrane biofilm microbial activity. *Environmental Research*, 200, 111456. <https://doi.org/10.1016/j.envres.2021.111456>
- Harris, P. W., Schmidt, T., & McCabe, B. K. (2017). Evaluation of chemical, thermobaric and thermochemical pre-treatment on anaerobic digestion of high-fat cattle slaughterhouse waste. *Bioresource technology*, 244, 605-610. <https://doi.org/10.1016/j.biortech.2017.07.179>
- Haydar, S., & Aziz, J. A. (2009). Coagulation–flocculation studies of tannery wastewater using combination of alum with cationic and anionic polymers. *Journal of Hazardous Materials*, 168(2-3), 1035-1040. <https://doi.org/10.1016/j.jhazmat.2009.02.140>
- Henze, M., van Loosdrecht, M. C., Ekama, G. A., & Brdjanovic, D. (2008). *Biological wastewater treatment*. IWA publishing.
- Holt, P. K., Barton, G. W., & Mitchell, C. A. (2005). The future for electrocoagulation as a localised water treatment technology. *Chemosphere*, 59(3), 355-367. <https://doi.org/10.1016/j.chemosphere.2004.10.023>
- Holt, P. K., Barton, G. W., Wark, M., & Mitchell, C. A. (2002). A quantitative comparison between chemical dosing and electrocoagulation. *Colloids and Surfaces A: Physicochemical and Engineering Aspects*, 211(2-3), 233-248. [https://doi.org/10.1016/S0927-7757\(02\)00285-6](https://doi.org/10.1016/S0927-7757(02)00285-6)
- Inayat, A., Inayat, M., Shahbaz, M., Sulaiman, S. A., Raza, M., & Yusup, S. (2020). Parametric analysis and optimization for the catalytic air gasification of palm kernel shell using coal bottom ash as catalyst. *Renewable Energy*, 145, 671-681. <https://doi.org/10.1016/j.renene.2019.06.104>
- Indian Institute of Technology Delhi. (2019). *Unpublished work: Barapullah drain quality parameters*. IITD.
- Jassal, P. S., Kaur, D., Kaur, M., & Sharma, D. (2023). Level of antibiotic contamination in the major river systems: A review on South Asian countries perspective. *Journal of Applied Pharmaceutical Science*. 10.7324/JAPS.2023.56748

- Jenicsek, P., Koubova, J., Bindzar, J., & Zabranska, J. (2010). Advantages of anaerobic digestion of sludge in microaerobic conditions. *Water Science and Technology*, 62(2), 427-434. <https://doi.org/10.2166/wst.2010.305>
- Ji, J., Kakade, A., Yu, Z., Khan, A., Liu, P., & Li, X. (2020). Anaerobic membrane bioreactors for treatment of emerging contaminants: A review. *Journal of environmental management*, 270, 110913. <https://doi.org/10.1016/j.jenvman.2020.110913>
- Jia, X., Fang, H. H., & Furumai, H. (1996). Surface charge and extracellular polymer of sludge in the anaerobic degradation process. *Water Science and Technology*, 34(5-6), 309-316. [https://doi.org/10.1016/0273-1223\(96\)00660-9](https://doi.org/10.1016/0273-1223(96)00660-9)
- Jia, Y., Khanal, S. K., Zhang, H., Chen, G.-H., & Lu, H. (2017). Sulfamethoxazole degradation in anaerobic sulfate-reducing bacteria sludge system. *Water Research*, 119, 12-20. <https://doi.org/10.1016/j.watres.2017.04.040>
- Jones, E. R., Van Vliet, M. T., Qadir, M., & Bierkens, M. F. (2021). Country-level and gridded estimates of wastewater production, collection, treatment and reuse. *Earth System Science Data*, 13(2), 237-254. <https://doi.org/10.5194/essd-13-237-2021>
- Judd, S., Kim, B.-g., & Amy, G. (2008). Membrane Bio-reactors. In *Biological wastewater treatment* (Vol. 1). IWA publishing.
- Kamizake, N. K., Gonçalves, M. M., Zaia, C. T., & Zaia, D. A. (2003). Determination of total proteins in cow milk powder samples: a comparative study between the Kjeldahl method and spectrophotometric methods. *Journal of Food composition and analysis*, 16(4), 507-516. [https://doi.org/10.1016/S0889-1575\(03\)00004-8](https://doi.org/10.1016/S0889-1575(03)00004-8)
- Kanafin, Y. N., Kanafina, D., Malamis, S., Katsou, E., Inglezakis, V. J., Pouloupoulos, S. G., & Arkhangelsky, E. (2021). Anaerobic membrane bioreactors for municipal wastewater treatment: a literature review. *Membranes*, 11(12), 967. <https://doi.org/10.3390/membranes11120967>
- Kato, M., Field, J., & Lettinga, G. (1997). Anaerobe tolerance to oxygen and the potentials of anaerobic and aerobic cocultures for wastewater treatment. *Brazilian Journal of Chemical Engineering*, 14(4). <https://doi.org/10.1590/S0104-66321997000400015>
- Kato, M. T., Field, J. A., & Lettinga, G. (1993). High tolerance of methanogens in granular sludge to oxygen. *Biotechnology and bioengineering*, 42(11), 1360-1366. <https://doi.org/10.1002/bit.260421113>
- Kaur, R., Wani, S., Singh, A., & Lal, K. (2012). Wastewater production, treatment and use in India. *Safe Use of Wastewater in Agriculture*,
- Kitchener, J. (1972). Principles of action of polymeric flocculants. *British Polymer Journal*, 4(3), 217-229. <https://doi.org/10.1002/pi.4980040307>
- Kiuri, H. (2001). Development of dissolved air flotation technology from the first generation to the newest (third) one (DAF in turbulent flow conditions). *Water Science and Technology*, 43(8), 1-7. <https://doi.org/10.2166/wst.2001.0450>
- Kiuru, H. J. (1990). Unit operations for the removal of solids and their combinations in water treatment. In *Chemical water and wastewater Treatment* (pp. 169-186). Springer.
- Klausmeier, C. A., Litchman, E., & Levin, S. A. (2004). Phytoplankton growth and stoichiometry under multiple nutrient limitation. *Limnology and oceanography*, 49(4part2), 1463-1470. https://doi.org/10.4319/lo.2004.49.4_part_2.1463
- Klotz, S., Kuenz, A., & Prüße, U. (2017). Nutritional requirements and the impact of yeast extract on the d-lactic acid production by *Sporolactobacillus inulinus*. *Green Chemistry*, 19(19), 4633-4641. <https://doi.org/10.1039/C7GC01796K>
- Knight, R., Ruble, R., Kadlec, R., & Reed, S. (2020). Wetlands for wastewater treatment: performance database. In *Constructed wetlands for water quality improvement* (pp. 35-58). CRC Press.

- Koivunen, J., & Heinonen-Tanski, H. (2008). Dissolved air flotation (DAF) for primary and tertiary treatment of municipal wastewaters. *Environmental technology*, 29(1), 101-109. <https://doi.org/10.1080/09593330802009410>
- KPMG. (2006). *The Indian Pharmaceutical Industry: Collaboration for Growth* (Industrial Markets, Issue 110406).
- Kraakman, N. J. R., Diaz, I., Fdz-Polanco, M., & Muñoz, R. (2023). Large-scale micro-aerobic digestion studies at municipal water resource recovery facilities for process-integrated biogas desulfurization. *Journal of Water Process Engineering*, 53, 103643. <https://doi.org/10.1016/j.jwpe.2023.103643>
- Kümmerer, K. (2009). Antibiotics in the aquatic environment—a review—part II. *Chemosphere*, 75(4), 435-441. <https://doi.org/10.1016/j.chemosphere.2008.12.006>
- Kuramae, E. E., Dimitrov, M. R., da Silva, G. H., Lucheta, A. R., Mendes, L. W., Luz, R. L., Vet, L. E., & Fernandes, T. V. (2020). On-site blackwater treatment fosters microbial groups and functions to efficiently and robustly recover carbon and nutrients. *Microorganisms*, 9(1), 75. <https://doi.org/10.3390/microorganisms9010075>
- Kurchania, A., Panwar, N., & Pagar, S. D. (2011). Development of domestic biogas stove. *Biomass Conversion and Biorefinery*, 1, 99-103. <https://doi.org/10.1007/s13399-011-0011-5>
- Kwak, D.-H., & Kim, M.-S. (2013). Feasibility of carbon dioxide bubbles as a collector in flotation process for water treatment. *Journal of Water Supply: Research and Technology-AQUA*, 62(1), 52-65. <https://doi.org/10.2166/aqua.2013.156>
- Lakghomi, B., Lawryshyn, Y., & Hofmann, R. (2015). A model of particle removal in a dissolved air flotation tank: importance of stratified flow and bubble size. *Water Research*, 68, 262-272. <https://doi.org/10.1016/j.watres.2014.09.053>
- Lakshmanan, D., Clifford, D. A., & Samanta, G. (2009). Ferrous and ferric ion generation during iron electrocoagulation. *Environmental science & technology*, 43(10), 3853-3859. <https://doi.org/10.1021/es8036669>
- Lamba, M., Sreekrishnan, T., & Ahammad, S. Z. (2020). Sewage mediated transfer of antibiotic resistance to River Yamuna in Delhi, India. *Journal of Environmental Chemical Engineering*, 8(1), 102088. <https://doi.org/10.1016/j.jece.2017.12.041>
- Langergraber, G., Haberl, R., Laber, J., & Pressl, A. (2003). Evaluation of substrate clogging processes in vertical flow constructed wetlands. *Water Science and Technology*, 48(5), 25-34. <https://doi.org/10.2166/wst.2003.0272>
- Le-Minh, N., Khan, S., Drewes, J., & Stuetz, R. (2010). Fate of antibiotics during municipal water recycling treatment processes. *Water Research*, 44(15), 4295-4323. <https://doi.org/10.1016/j.watres.2010.06.020>
- Leppinen, D. (2000). A kinetic model of dissolved air flotation including the effects of interparticle forces. *Journal of Water Supply: Research and Technology—AQUA*, 49(5), 259-268. <https://doi.org/10.2166/aqua.2000.0022>
- Levine, A. D., Tchobanoglous, G., & Asano, T. (1985). Characterization of the size distribution of contaminants in wastewater: treatment and reuse implications. *Journal (Water Pollution Control Federation)*, 805-816. <https://www.jstor.org/stable/25042701>
- Li. (1985). Application of membrane anaerobic reactor system for the treatment of industrial wastewaters. Ind. Waste Conf. Purdue Univ.,
- Li, B., & Zhang, T. (2010). Biodegradation and adsorption of antibiotics in the activated sludge process. *Environmental science & technology*, 44(9), 3468-3473. <https://doi.org/10.1021/es903490h>
- Li, C., & Somasundaran, P. (1991). Reversal of bubble charge in multivalent inorganic salt solutions—effect of magnesium. *Journal of Colloid and Interface Science*, 146(1), 215-218. [https://doi.org/10.1016/0021-9797\(91\)90018-4](https://doi.org/10.1016/0021-9797(91)90018-4)

- Li, H., Li, J., Bodycomb, J., & Patience, G. S. (2019). Experimental methods in chemical engineering: particle size distribution by laser diffraction—PSD. *The Canadian Journal of Chemical Engineering*, 97(7), 1974-1981. <https://doi.org/10.1002/cjce.23480>
- Liao, B.-Q., Kraemer, J. T., & Bagley, D. M. (2006). Anaerobic membrane bioreactors: applications and research directions. *Critical Reviews in Environmental Science and Technology*, 36(6), 489-530. <https://doi.org/10.1080/10643380600678146>
- Lim, J. W., & Wang, J.-Y. (2013). Enhanced hydrolysis and methane yield by applying microaeration pretreatment to the anaerobic co-digestion of brown water and food waste. *Waste Management*, 33(4), 813-819. <https://doi.org/10.1016/j.wasman.2012.11.013>
- Lin, H., Peng, W., Zhang, M., Chen, J., Hong, H., & Zhang, Y. (2013). A review on anaerobic membrane bioreactors: applications, membrane fouling and future perspectives. *Desalination*, 314, 169-188. <https://doi.org/10.1016/j.desal.2013.01.019>
- Lin, Q., De Vrieze, J., Li, L., Fang, X., & Li, X. (2023). Interconnected versus unconnected microorganisms: Does it matter in anaerobic digestion functioning. *Journal of environmental management*, 331, 117307. <https://doi.org/10.1016/j.jenvman.2023.117307>
- Lindeboom, R., De Paepe, J., Vanoppen, M., Alonso-Fariñas, B., Coessens, W., Alloul, A., Christiaens, M., Dotremont, C., Beckers, H., & Lamaze, B. (2020). A five-stage treatment train for water recovery from urine and shower water for long-term human Space missions. *Desalination*, 495, 114634. <https://doi.org/10.1016/j.desal.2020.114634>
- Lindeboom, R., Smith, G., Jeison, D., Temmink, H., & van Lier, J. B. (2011). Application of high speed imaging as a novel tool to study particle dynamics in tubular membrane systems. *Journal of membrane science*, 368(1-2), 95-99. <https://doi.org/10.1016/j.memsci.2010.11.029>
- Lindeboom, R. E., Weijma, J., & van Lier, J. B. (2012). High-calorific biogas production by selective CO₂ retention at autogenerated biogas pressures up to 20 bar. *Environmental science & technology*, 46(3), 1895-1902. <https://doi.org/10.1021/es202633u>
- Liu, T., & Schwarz, M. (2009). CFD-based multiscale modelling of bubble-particle collision efficiency in a turbulent flotation cell. *Chemical Engineering Science*, 64(24), 5287-5301. <https://doi.org/10.1016/j.ces.2009.09.014>
- Liu, T. Y., & Schwarz, M. (2009). CFD-based modelling of bubble-particle collision efficiency with mobile bubble surface in a turbulent environment. *International Journal of Mineral Processing*, 90(1-4), 45-55. <https://doi.org/10.1016/j.minpro.2008.10.004>
- Lousada-Ferreira, M., Van Lier, J., & Van Der Graaf, J. (2016). Particle counting as surrogate measurement of membrane integrity loss and assessment tool for particle growth and regrowth in the permeate of membrane bioreactors. *Separation and Purification Technology*, 161, 16-24. <https://doi.org/10.1016/j.seppur.2016.01.033>
- Lundh, M., Jönsson, L., & Dahlquist, J. (2001). The flow structure in the separation zone of a DAF pilot plant and the relation with bubble concentration. *Water Science and Technology*, 43(8), 185-194. <https://doi.org/10.2166/wst.2001.0493>
- Lusk, P. (1998). *Methane recovery from animal manures the current opportunities casebook*.
- Ma, L., Li, A.-D., Yin, X.-L., & Zhang, T. (2017). The prevalence of integrons as the carrier of antibiotic resistance genes in natural and man-made environments. *Environmental science & technology*, 51(10), 5721-5728. <https://doi.org/10.1021/acs.est.6b05887>
- Mäkelä, M. (2017). Experimental design and response surface methodology in energy applications: A tutorial review. *Energy Conversion and Management*, 151, 630-640. <https://doi.org/10.1016/j.enconman.2017.09.021>
- Makowska, N., Koczura, R., & Mokracka, J. (2016). Class 1 integrase, sulfonamide and tetracycline resistance genes in wastewater treatment plant and surface water. *Chemosphere*, 144, 1665-1673. <https://doi.org/10.1016/j.envpol.2012.05.007>

- Maldonado, M., Quinn, J., Gomez, C., & Finch, J. (2013). An experimental study examining the relationship between bubble shape and rise velocity. *Chemical Engineering Science*, *98*, 7-11. <https://doi.org/10.1016/j.ces.2013.04.050>
- Malley, J., & Edzwald, J. (1991). Concepts for dissolved-air flotation treatment of drinking waters. *Aqua AQUAAA*, *40*(1).
- Manjunath, N., Mehrotra, I., & Mathur, R. (2000). Treatment of wastewater from slaughterhouse by DAF-UASB system. *Water Research*, *34*(6), 1930-1936. [https://doi.org/10.1016/S0043-1354\(99\)00337-1](https://doi.org/10.1016/S0043-1354(99)00337-1)
- Masters, P. A., O'Bryan, T. A., Zurlo, J., Miller, D. Q., & Joshi, N. (2003). Trimethoprim-sulfamethoxazole revisited. *Archives of internal medicine*, *163*(4), 402-410. <https://doi.org/10.1111/j.1365-2125.2010.03866.x>
- Matsui, Y., Fukushi, K., & Tambo, N. (1998). Modeling, simulation and operational parameters of dissolved air flotation. *Journal of Water Supply: Research and Technology—AQUA*, *47*(1), 9-20. <https://doi.org/10.2166/aqua.1998.0003>
- Mazhar, M. A., Ahmed, S., Husain, A., & Khan, N. A. (2021). Trends in Organic Contamination in River Yamuna: A Case Study of Delhi Stretch (2007-2016). <https://doi.org/10.1177/0975425321999081>
- McCabe, B. K., Hamawand, I., Harris, P., Baillie, C., & Yusuf, T. (2014). A case study for biogas generation from covered anaerobic ponds treating abattoir wastewater: Investigation of pond performance and potential biogas production. *Applied Energy*, *114*, 798-808. <https://doi.org/10.1016/j.apenergy.2013.10.020>
- McTaggart, H. A. (1922). XXXVIII. On the electrification at the boundary between a liquid and a gas. *The London, Edinburgh, and Dublin Philosophical Magazine and Journal of Science*, *44*(260), 386-395. <https://doi.org/10.1080/14786440808634012>
- Mekonnen, M. M., & Hoekstra, A. Y. (2016). Four billion people facing severe water scarcity. *Science Advances*, *2*(2), e1500323. <https://doi.org/10.1126/sciadv.1500323>
- Metcalf, Eddy, Abu-Orf, M., Bowden, G., Burton, F. L., Pfrang, W., Stensel, H. D., Tchobanoglous, G., Tsuchihashi, R., & AECOM. (2014). *Wastewater engineering: treatment and resource recovery*. McGraw Hill Education.
- Metcalf, Eddy, Tchobanoglous, G., Stensel, H. D., Tsuchihashi, R., Burton, F. L., Abu-Orf, M., Bowden, G., & Pfrang, W. (2013). *Wastewater Engineering: Treatment and Resource Recovery* (fifth ed.). McGraw-Hill Education. <https://books.google.com/cu/books?id=ZHbFsgEACAAJ>
- Michael, I., Rizzo, L., McArdell, C., Manaia, C., Merlin, C., Schwartz, T., Dagot, C., & Fatta-Kassinos, D. (2013). Urban wastewater treatment plants as hotspots for the release of antibiotics in the environment: a review. *Water Research*, *47*(3), 957-995. <https://doi.org/10.1016/j.watres.2012.11.027>
- Mishra, A., Agarwal, M., Bajpai, M., Rajani, S., & Mishra, R. (2002). Plantago psyllium mucilage for sewage and tannery effluent treatment. <https://www.sid.ir/en/journal/ViewPaper.aspx?id=33899>
- Monsalvo, V. M., McDonald, J. A., Khan, S. J., & Le-Clech, P. (2014). Removal of trace organics by anaerobic membrane bioreactors. *Water Research*, *49*, 103-112. <https://doi.org/10.1016/j.watres.2013.11.026>
- Montzka, S. A., Dlugokencky, E. J., & Butler, J. H. (2011). Non-CO₂ greenhouse gases and climate change. *Nature*, *476*(7358), 43-50. <https://doi.org/10.1038/nature10322>
- Moore, J. C., DeVries, J. W., Lipp, M., Griffiths, J. C., & Abernethy, D. R. (2010). Total protein methods and their potential utility to reduce the risk of food protein adulteration. *Comprehensive reviews in food science and food safety*, *9*(4), 330-357. <https://doi.org/10.1111/j.1541-4337.2010.00114.x>

- Mudde, R. F., & Simonin, O. (1999). Two-and three-dimensional simulations of a bubble plume using a two-fluid model. *Chemical Engineering Science*, 54(21), 5061-5069. [https://doi.org/10.1016/S0009-2509\(99\)00234-1](https://doi.org/10.1016/S0009-2509(99)00234-1)
- Mundi, G. S., & Zytner, R. G. (2015). Effective solid removal technologies for wash-water treatment to allow water reuse in the fresh-cut fruit and vegetable industry. *Journal of Agricultural Science and Technology A*, 5, 396-407. <https://doi.org/10.17265/2161-6256/2015.06.003>
- Munir, M., Wong, K., & Xagorarakis, I. (2011). Release of antibiotic resistant bacteria and genes in the effluent and biosolids of five wastewater utilities in Michigan. *Water Research*, 45(2), 681-693. <https://doi.org/10.1016/j.watres.2010.08.033>
- NCBI, N. C. f. B. I. (2005). *National Library of Medicine*. US Government. Retrieved 03/03 from <https://www.ncbi.nlm.nih.gov/>
- Newton, I. (1687). *The Principia: mathematical principles of natural philosophy* (1st ed. ed.). Dawson & Sons.
- Nguyen, A., Chaudhary, D. K., Dahal, R. H., Trinh, N. H., Kim, J., Chang, S. W., Hong, Y., La, D. D., Nguyen, X. C., & Ngo, H. H. (2021). Review on pretreatment techniques to improve anaerobic digestion of sewage sludge. *Fuel*, 285, 119105. <https://doi.org/10.1016/j.fuel.2020.119105>
- Nguyen, A., & Schultze, H. J. (2004). *Colloidal science of flotation* (Vol. 118). Marcel Dekker Inc. <https://doi.org/10.1201/9781482276411>
- Nguyen, D., & Khanal, S. K. (2018). A little breath of fresh air into an anaerobic system: How microaeration facilitates anaerobic digestion process. *Biotechnology advances*, 36(7), 1971-1983. <https://doi.org/10.1016/j.biotechadv.2018.08.007>
- Nguyen, D., Wu, Z., Shrestha, S., Lee, P.-H., Raskin, L., & Khanal, S. K. (2019). Intermittent microaeration: New strategy to control volatile fatty acid accumulation in high organic loading anaerobic digestion. *Water Research*, 166, 115080. <https://doi.org/10.1016/j.watres.2019.115080>
- Nguyen, T.-T., Bui, X.-T., Luu, V.-P., Nguyen, P.-D., Guo, W., & Ngo, H.-H. (2017). Removal of antibiotics in sponge membrane bioreactors treating hospital wastewater: Comparison between hollow fiber and flat sheet membrane systems. *Bioresour. Technol.*, 240, 42-49. <https://doi.org/10.1016/j.biortech.2017.02.118>
- Novoa, V., Rojas, O., Ahumada-Rudolph, R., Arumí, J. L., Munizaga, J., de la Barrera, F., Cabrera-Pardo, J. R., & Rojas, C. (2023). Water footprint and virtual water flows from the Global South: Foundations for sustainable agriculture in periods of drought. *Science of The Total Environment*, 161526. <https://doi.org/10.1016/j.scitotenv.2023.161526>
- Nriagu, J. O. (1972). Stability of vivianite and ion-pair formation in the system Fe³ (PO₄)₂-H₃PO₄-H₂O. *Geochimica et Cosmochimica Acta*, 36(4), 459-470. [https://doi.org/10.1016/0016-7037\(72\)90035-X](https://doi.org/10.1016/0016-7037(72)90035-X)
- O'Neill, J. (2014). *Antimicrobial Resistance: Tackling a Crisis for the Health and Wealth of Nations: December 2014*.
- Oberoi, A. S., Jia, Y., Zhang, H., Khanal, S. K., & Lu, H. (2019). Insights into the fate and removal of antibiotics in engineered biological treatment systems: a critical review. *Environmental science & technology*, 53(13), 7234-7264. <https://doi.org/10.1021/acs.est.9b01131>
- Oberoi, A. S., Surendra, K., Wu, D., Lu, H., Wong, J. W., & Khanal, S. K. (2022). Anaerobic membrane bioreactors for pharmaceutical-laden wastewater treatment: A critical review. *Bioresour. Technol.*, 127667. <https://doi.org/10.1016/j.biortech.2022.127667>
- Organization, W. H. (2015). *Global antimicrobial resistance surveillance system: manual for early implementation*. World Health Organization.
- Oulton, R. L., Kohn, T., & Cwiertny, D. M. (2010). Pharmaceuticals and personal care products in effluent matrices: a survey of transformation and removal during wastewater treatment and implications for wastewater management. *Journal of Environmental Monitoring*, 12(11), 1956-1978. <https://doi.org/10.1039/C0EM00068J>

- Özgül, H. (2015). *Anaerobic membrane bioreactors for cost-effective municipal water reuse* [Doctoral, TU-Delft]. Delft.
- Ozgun, H., Dereli, R. K., Ersahin, M. E., Kinaci, C., Spanjers, H., & van Lier, J. B. (2013). A review of anaerobic membrane bioreactors for municipal wastewater treatment: integration options, limitations and expectations. *Separation and Purification Technology*, *118*, 89-104. <https://doi.org/10.1016/j.seppur.2013.06.036>
- Ozgun, H., Ersahin, M. E., Tao, Y., Spanjers, H., & van Lier, J. B. (2013). Effect of upflow velocity on the effluent membrane fouling potential in membrane coupled upflow anaerobic sludge blanket reactors. *Bioresource technology*, *147*, 285-292. <https://doi.org/10.1016/j.biortech.2013.08.039>
- Pallares-Vega, R., Blaak, H., van der Plaats, R., de Roda Husman, A. M., Leal, L. H., van Loosdrecht, M. C., Weissbrodt, D. G., & Schmitt, H. (2019). Determinants of presence and removal of antibiotic resistance genes during WWTP treatment: A cross-sectional study. *Water Research*, *161*, 319-328. [10.1016/j.watres.2019.05.100](https://doi.org/10.1016/j.watres.2019.05.100)
- Pallares-Vega, R., Leal, L. H., Fletcher, B. N., Vias-Torres, E., van Loosdrecht, M. C., Weissbrodt, D. G., & Schmitt, H. (2021). Annual dynamics of antimicrobials and resistance determinants in flocculent and aerobic granular sludge treatment systems. *Water Research*, *190*, 116752. <https://doi.org/10.1016/j.watres.2020.116752>
- Parkhurst, D. L., & Appelo, C. (2013). *Description of input and examples for PHREEQC version 3—a computer program for speciation, batch-reaction, one-dimensional transport, and inverse geochemical calculations. In US geological survey techniques and methods (Version 3)* U.S. Geological Survey <https://pubs.usgs.gov/tm/06/a43/>
- Patel, P. P., Mondal, S., & Ghosh, K. G. (2020). Some respite for India's dirtiest river? Examining the Yamuna's water quality at Delhi during the COVID-19 lockdown period. *Science of The Total Environment*, *744*, 140851. <https://doi.org/10.1016/j.scitotenv.2020.140851>
- Penetra, R., Reali, M., & Campos, J. (2003). Influence of flocculation conditions in the performance of an experimental domestic sewage treatment plant consisting of an anaerobic expanded bed reactor followed by dissolved air flotation. *Water Science and Technology*, *48*(6), 285-293. <https://doi.org/10.2166/wst.2003.0414>
- Pepper, I. L., & Gentry, T. J. (2015). Earth environments. In *Environmental microbiology* (pp. 59-88). Elsevier. <https://doi.org/https://doi.org/10.1016/B978-0-12-394626-3.00004-1>
- Piaggio, A. L., Soares, L. A., Balakrishnan, M., Guleria, T., de Kreuk, M. K., & Lindeboom, R. E. (2022). High suspended solids removal of Indian drain water with a down-scaled Dissolved Air Flotation (DAF) for water recovery. Assessing water-type dependence on process control variables. *Environmental Challenges*, 100567. <https://doi.org/10.1016/j.envc.2022.100567>
- Pichel, N., Vivar, M., & Fuentes, M. (2019). The problem of drinking water access: A review of disinfection technologies with an emphasis on solar treatment methods. *Chemosphere*, *218*, 1014-1030. <https://doi.org/10.1016/j.chemosphere.2018.11.205>
- Plackett, R. L., & Burman, J. P. (1946). The design of optimum multifactorial experiments. *Biometrika*, *33*(4), 305-325. <https://doi.org/10.2307/2332195>
- Quaranta, E., Fuchs, S., Liefing, H. J., Schellart, A., & Pistocchi, A. (2022). A hydrological model to estimate pollution from combined sewer overflows at the regional scale: Application to Europe. *Journal of Hydrology: Regional Studies*, *41*, 101080. <https://doi.org/10.1016/j.ejrh.2022.101080>
- Radjenovic, J., Petrovic, M., & Barceló, D. (2007). Analysis of pharmaceuticals in wastewater and removal using a membrane bioreactor. *Analytical and bioanalytical chemistry*, *387*(4), 1365-1377. <https://doi.org/10.1007/s00216-006-0883-6>
- Raheem, A., WAKG, W. A., Yap, Y. T., Danquah, M. K., & Harun, R. (2015). Optimization of the microalgae *Chlorella vulgaris* for syngas production using central composite design. *Rsc Advances*, *5*(88), 71805-71815. <https://doi.org/10.1039/C5RA10503J>

- Rattanapan, C., Sawain, A., Suksaroj, T., & Suksaroj, C. (2011). Enhanced efficiency of dissolved air flotation for biodiesel wastewater treatment by acidification and coagulation processes. *Desalination*, 280(1-3), 370-377. <https://doi.org/10.1016/j.desal.2011.07.018>
- Robles, Á., Durán, F., Giménez, J. B., Jiménez, E., Ribes, J., Serralta, J., Seco, A., Ferrer, J., & Rogalla, F. (2020). Anaerobic membrane bioreactors (AnMBR) treating urban wastewater in mild climates. *Bioresource technology*, 314, 123763. <https://doi.org/10.1016/j.biortech.2020.123763>
- Roccaro, P., & Verlicchi, P. (2018). Wastewater and reuse. In (Vol. 2, pp. 61-63): Elsevier.
- Rodrigues, J., & Béttega, R. (2018). Evaluation of multiphase CFD models for Dissolved Air Flotation (DAF) process. *Colloids and Surfaces A: Physicochemical and Engineering Aspects*, 539, 116-123. <https://doi.org/10.1016/j.colsurfa.2017.12.015>
- Rodrigues, R., & Rubio, J. (2003). New basis for measuring the size distribution of bubbles. *Minerals engineering*, 16(8), 757-765. [https://doi.org/10.1016/S0892-6875\(03\)00181-X](https://doi.org/10.1016/S0892-6875(03)00181-X)
- Rodrigues, R. T., & Rubio, J. (2007). DAF–dissolved air flotation: Potential applications in the mining and mineral processing industry. *International Journal of Mineral Processing*, 82(1), 1-13. <https://doi.org/10.1016/j.minpro.2006.07.019>
- Rogers, H. R. (1996). Sources, behaviour and fate of organic contaminants during sewage treatment and in sewage sludges. *Science of The Total Environment*, 185(1-3), 3-26. [https://doi.org/10.1016/0048-9697\(96\)05039-5](https://doi.org/10.1016/0048-9697(96)05039-5)
- Saidan, M. N., Al-Addous, M., Al-Weshah, R. A., Obada, I., Alkasrawi, M., & Barbana, N. (2020). Wastewater reclamation in major Jordanian industries: a viable component of a circular economy. *Water*, 12(5), 1276. <https://doi.org/10.1016/j.coesh.2018.03.008>
- Samstag, R. W., Ducoste, J. J., Griborio, A., Nopens, I., Batstone, D., Wicks, J., Saunders, S., Wicklein, E., Kenny, G., & Laurent, J. (2016). CFD for wastewater treatment: an overview. *Water Science and Technology*, 74(3), 549-563. <https://doi.org/10.2166/wst.2016.249>
- Sander, R. (2015). Compilation of Henry's law constants (version 4.0) for water as solvent. *Atmospheric Chemistry & Physics*, 15(8).
- Sasidhar, K., Somasundaram, M., Ekambaram, P., Arumugam, S. K., Nataraj, G., & Murugan, M. A. (2022). A critical review on the effects of pneumatic mixing in anaerobic digestion process. *Journal of Cleaner Production*, 134513. <https://doi.org/10.1016/j.jclepro.2022.134513>
- Satpathy, K., Rehman, U., Cools, B., Verdickt, L., Peleman, G., & Nopens, I. (2020). CFD-based process optimization of a dissolved air flotation system for drinking water production. *Water Science and Technology*, 81(8), 1668-1681. <https://doi.org/10.2166/wst.2020.028>
- Schindelin, J., Arganda-Carreras, I., Frise, E., Kaynig, V., Longair, M., Pietzsch, T., Preibisch, S., Rueden, C., Saalfeld, S., & Schmid, B. (2012). Fiji: an open-source platform for biological-image analysis. *Nature methods*, 9(7), 676-682. <https://doi.org/10.1038/nmeth.2019>
- Shammas, N. K., Wang, L. K., & Hahn, H. H. (2010). Fundamentals of wastewater flotation. In *Flotation Technology* (Vol. 12, pp. 121-164). Humana Press. https://doi.org/https://doi.org/10.1007/978-1-60327-133-2_4
- Shukla, R., & Ahammad, S. Z. (2023). Performance assessment of a modified trickling filter and conventional activated sludge process along with tertiary treatment in removing emerging pollutants from urban sewage. *Science of The Total Environment*, 858, 159833. <https://doi.org/10.1016/j.scitotenv.2022.159833>
- Sim, W.-J., Lee, J.-W., Lee, E.-S., Shin, S.-K., Hwang, S.-R., & Oh, J.-E. (2011). Occurrence and distribution of pharmaceuticals in wastewater from households, livestock farms, hospitals and pharmaceutical manufactures. *Chemosphere*, 82(2), 179-186. <https://doi.org/10.1016/j.chemosphere.2010.10.026>
- Singh, R., Jaiswal, N., & Kishtawal, C. (2022). Rising surface pressure over Tibetan Plateau strengthens indian summer monsoon rainfall over northwestern India. *Scientific Reports*, 12(1), 8621. <https://doi.org/10.1038/s41598-022-12523-8>

- Singh, R., & Kumar, R. (2021). The suitability of water scarcity indicators to the Indian context. *Water Security*, 14, 100097. <https://doi.org/10.1016/j.wasec.2021.100097>
- Smith, A. L., Stadler, L. B., Love, N. G., Skerlos, S. J., & Raskin, L. (2012). Perspectives on anaerobic membrane bioreactor treatment of domestic wastewater: a critical review. *Bioresource technology*, 122, 149-159. <https://doi.org/10.1016/j.biortech.2012.04.055>
- Sontakke, N. A., Singh, N., & Singh, H. (2008). Instrumental period rainfall series of the Indian region (AD 1813—2005): revised reconstruction, update and analysis. *The Holocene*, 18(7), 1055-1066. <https://doi.org/10.1177/0959683608095576>
- Sophonsiri, C., & Morgenroth, E. (2004). Chemical composition associated with different particle size fractions in municipal, industrial, and agricultural wastewaters. *Chemosphere*, 55(5), 691-703. <https://doi.org/10.1016/j.chemosphere.2003.11.032>
- Spanjers, H., & Vanrolleghem, P. (2016). Respirometry. In *Experimental methods in wastewater treatment* (pp. 133-176). IWA publishing.
- Speece, R. (1988). A survey of municipal anaerobic sludge digesters and diagnostic activity assays. *Water Research*, 22(3), 365-372.
- Stuckey, D. C. (2012). Recent developments in anaerobic membrane reactors. *Bioresource technology*, 122, 137-148. <https://doi.org/10.1016/j.biortech.2012.05.138>
- Sun, L., Müller, B., & Schnürer, A. (2013). Biogas production from wheat straw: community structure of cellulose-degrading bacteria. *Energy, Sustainability and Society*, 3(1), 1-11. <https://doi.org/10.1186/2192-0567-3-15>
- Tadkaew, N., Sivakumar, M., Khan, S. J., McDonald, J. A., & Nghiem, L. D. (2010). Effect of mixed liquor pH on the removal of trace organic contaminants in a membrane bioreactor. *Bioresource technology*, 101(5), 1494-1500. <https://doi.org/10.1016/j.biortech.2009.09.082>
- Tambo, N., & Fukushi, K. (1986). *A kinetic study of dissolved air flotation* World Congress of Chemical Engineering, Tokyo.
- Tamm, O., Saaremäe, E., Rahkema, K., Jaagus, J., & Tamm, T. (2023). The intensification of short-duration rainfall extremes due to climate change—Need for a frequent update of intensity–duration–frequency curves. *Climate Services*, 30, 100349. <https://doi.org/10.1016/j.cliser.2023.100349>
- Tang, T., Liu, M., Chen, Y., Du, Y., Feng, J., & Feng, H. (2022). Influence of sulfamethoxazole on anaerobic digestion: Methanogenesis, degradation mechanism and toxicity evolution. *Journal of Hazardous Materials*, 431, 128540. <https://doi.org/10.1016/j.jhazmat.2022.128540>
- Tang, Y., Shigematsu, T., Morimura, S., & Kida, K. (2004). The effects of micro-aeration on the phylogenetic diversity of microorganisms in a thermophilic anaerobic municipal solid-waste digester. *Water Research*, 38(10), 2537-2550. <https://doi.org/10.1016/j.watres.2004.03.012>
- Thielicke, W., & Stamhuis, E. (2014). PIVlab—towards user-friendly, affordable and accurate digital particle image velocimetry in MATLAB. *Journal of Open Research Software*, 2(1). <http://dx.doi.org/10.5334/jors.bl>
- Toja Ortega, S., Pronk, M., & de Kreuk, M. K. (2021). Effect of an increased particulate cod load on the aerobic granular sludge process: A full scale study. *Processes*, 9(8), 1472. <https://doi.org/10.3390/pr9081472>
- UN. (2018). *Sustainable Development Goal 6: Synthesis Report 2018 on Water and Sanitation*. United Nations. <https://doi.org/10.18356/e8fc060b-en>
- van 't Hoff, J. H. (1884). *Etudes de dynamique chimique* (Vol. 1). Muller. <https://doi.org/10.1002/recl.18840031003>
- van Boeckel, T. P., Gandra, S., Ashok, A., Caudron, Q., Grenfell, B. T., Levin, S. A., & Laxminarayan, R. (2014). Global antibiotic consumption 2000 to 2010: an analysis of national pharmaceutical sales data. *The Lancet infectious diseases*, 14(8), 742-750. [https://doi.org/10.1016/S1473-3099\(14\)70780-7](https://doi.org/10.1016/S1473-3099(14)70780-7)

- van Daal-Rombouts, P., Benedetti, L., de Jonge, J., Weijers, S., & Langeveld, J. (2017). Performance evaluation of a smart buffer control at a wastewater treatment plant. *Water Research*, *125*, 180-190. <https://doi.org/10.1016/j.watres.2017.08.042>
- van den Berg, L. (2022). *Diffusion in Aerobic Granular Sludge* [doctoral thesis, TU-Delft]. Delft, Netherlands. <https://repository.tudelft.nl/islandora/object/uuid:2e5c2d37-20af-48f9-a926-593e8a7aa5a6?collection=research>
- van Lier, J. B. (2008). High-rate anaerobic wastewater treatment: diversifying from end-of-the-pipe treatment to resource-oriented conversion techniques. *Water Science and Technology*, *57*(8), 1137-1148. <https://doi.org/10.2166/wst.2008.040>
- van Lier, J. B., Mahmoud, N., & Zeeman, G. (2008a). Anaerobic wastewater treatment. In *biological wastewater treatment, principles, modelling and design* (pp. 415-456). IWA Publishing. https://doi.org/https://doi.org/10.2166/9781789060362_0701
- van Lier, J. B., Mahmoud, N., & Zeeman, G. (2008b). Anaerobic wastewater treatment. *biological wastewater treatment, principles, modelling and design*, 415-456.
- Van Nieuwenhuijzen, A. F. (2002). Scenario studies into advanced particle removal in the physical-chemical pre-treatment of wastewater. In: DUP Science.
- van Vliet, M. T., Flörke, M., & Wada, Y. (2017). Quality matters for water scarcity. *Nature Geoscience*, *10*(11), 800-802. <https://doi.org/10.1038/ngeo3047>
- Vandamme, D., Eyley, S., Van den Mooter, G., Muylaert, K., & Thielemans, W. (2015). Highly charged cellulose-based nanocrystals as flocculants for harvesting *Chlorella vulgaris*. *Bioresource technology*, *194*, 270-275. <https://doi.org/10.1016/j.biortech.2015.07.039>
- Verma, V., & Padding, J. T. (2020). A novel approach to MP-PIC: Continuum particle model for dense particle flows in fluidized beds. *Chemical Engineering Science: X*, *6*, 100053. <https://doi.org/10.1016/j.cesx.2019.100053>
- Viallis-Terrisse, H., Nonat, A., & Petit, J.-C. (2001). Zeta-potential study of calcium silicate hydrates interacting with alkaline cations. *Journal of Colloid and Interface Science*, *244*(1), 58-65. <https://doi.org/10.1006/jcis.2001.7897>
- Visvanathan, C., & Abeynayaka, A. (2012). Developments and future potentials of anaerobic membrane bioreactors (AnMBRs). *Membr. Water Treat*, *3*(1), 1-23. <https://doi.org/10.12989/mwt.2012.3.1.001>
- Vlyssides, A. G., Mai, S. T., & Barampouti, E. M. P. (2004). Bubble size distribution formed by depressurizing air-saturated water. *Industrial & Engineering Chemistry Research*, *43*(11), 2775-2780. <https://doi.org/10.1021/ie0307176>
- Wang, Fahey, & Wu. (2005). Dissolved air flotation. In *Physicochemical treatment processes* (Vol. 3, pp. 431-500). Humana Press. <https://doi.org/https://doi.org/10.1385/1-59259-820-x:431>
- Wang, G., Ge, L., Mitra, S., Evans, G. M., Joshi, J., & Chen, S. (2018). A review of CFD modelling studies on the flotation process. *Minerals engineering*, *127*, 153-177. <https://doi.org/10.1016/j.mineng.2018.08.019>
- Wei, P., Mudde, R. F., Uijttewaal, W., Spanjers, H., van Lier, J. B., & de Kreuk, M. (2019). Characterising the two-phase flow and mixing performance in a gas-mixed anaerobic digester: Importance for scaled-up applications. *Water Research*, *149*, 86-97. <https://doi.org/10.1016/j.watres.2018.11.049>
- Whitman, W., Boone, D., Koga, Y., & Keswani, J. (2001). Taxonomy of methanogenic Archaea. In *Bergey's Manual® of Systematic Bacteriology: Volume One The Archaea and the Deeply Branching and Phototrophic Bacteria* (pp. 211-213). Springer.
- Wijekoon, K. C., McDonald, J. A., Khan, S. J., Hai, F. I., Price, W. E., & Nghiem, L. D. (2015). Development of a predictive framework to assess the removal of trace organic chemicals by anaerobic membrane bioreactor. *Bioresource technology*, *189*, 391-398. <https://doi.org/10.1016/j.biortech.2015.04.034>

- WWAP. (2019). The United Nations World Water Development Report 2019: Leaving No One Behind. In: UNESCO Paris.
- Xia, Z., Xiao-Chun, W., Zhong-lin, C., Hao, X., & Qing-fang, Z. (2015). Microbial community structure and pharmaceuticals and personal care products removal in a membrane bioreactor seeded with aerobic granular sludge. *Applied microbiology and biotechnology*, 99(1), 425-433. <https://doi.org/10.1007/s00253-014-5984-0>
- Xiao, Y., Yaohari, H., De Araujo, C., Sze, C. C., & Stuckey, D. C. (2017). Removal of selected pharmaceuticals in an anaerobic membrane bioreactor (AnMBR) with/without powdered activated carbon (PAC). *Chemical Engineering Journal*, 321, 335-345. <https://doi.org/10.1016/j.cej.2017.03.118>
- Yang, del Pozo, D. F., Torfs, E., Rehman, U., Yu, D., & Nopens, I. (2021). Numerical simulation on the effects of bubble size and internal structure on flow behavior in a DAF tank: A comparative study of CFD and CFD-PBM approach. *Chemical Engineering Journal Advances*, 7, 100131. <https://doi.org/10.1016/j.cej.2021.100131>
- Yang, C., Dabros, T., Li, D., Czarnecki, J., & Masliyah, J. H. (2001). Measurement of the zeta potential of gas bubbles in aqueous solutions by microelectrophoresis method. *Journal of Colloid and Interface Science*, 243(1), 128-135. <https://doi.org/10.1006/jcis.2001.7842>
- Zarei-Baygi, A., Harb, M., Wang, P., Stadler, L. B., & Smith, A. L. (2019). Evaluating antibiotic resistance gene correlations with antibiotic exposure conditions in anaerobic membrane bioreactors. *Environmental science & technology*, 53(7), 3599-3609. <https://doi.org/10.1021/acs.est.9b00798>
- Zarei-Baygi, A., Harb, M., Wang, P., Stadler, L. B., & Smith, A. L. (2020). Microbial community and antibiotic resistance profiles of biomass and effluent are distinctly affected by antibiotic addition to an anaerobic membrane bioreactor. *Environmental Science: Water Research & Technology*, 6(3), 724-736. <https://doi.org/10.1039/c9ew00913b>
- Zhang, H., Jia, Y., Khanal, S. K., Lu, H., Fang, H., & Zhao, Q. (2018). Understanding the role of extracellular polymeric substances on ciprofloxacin adsorption in aerobic sludge, anaerobic sludge, and sulfate-reducing bacteria sludge systems. *Environmental science & technology*, 52(11), 6476-6486. <https://doi.org/10.1021/acs.est.8b00568>
- Zhao, C., Zhou, J., Yan, Y., Yang, L., Xing, G., Li, H., Wu, P., Wang, M., & Zheng, H. (2021). Application of coagulation/flocculation in oily wastewater treatment: A review. *Science of The Total Environment*, 765, 142795. <https://doi.org/10.1016/j.scitotenv.2020.142795>
- Zheng, J., Zhou, Z., Wei, Y., Chen, T., Feng, W., & Chen, H. (2018). High-throughput profiling of seasonal variations of antibiotic resistance gene transport in a peri-urban river. *Environment international*, 114, 87-94. <https://doi.org/10.1016/j.envint.2018.02.039>
- Zheng, W., Wen, X., Zhang, B., & Qiu, Y. (2019). Selective effect and elimination of antibiotics in membrane bioreactor of urban wastewater treatment plant. *Science of The Total Environment*, 646, 1293-1303. <https://doi.org/10.1016/j.scitotenv.2018.07.400>
- Zheng, X., Jiang, N., Zheng, H., Wu, Y., & Heijman, S. G. (2022). Predicting adsorption isotherms of organic micropollutants by high-silica zeolite mixtures. *Separation and Purification Technology*, 282, 120009. <https://doi.org/10.1016/j.seppur.2021.120009>
- Zouboulis, A., Moussas, P., & Vasilakou, F. (2008). Polyferric sulphate: Preparation, characterisation and application in coagulation experiments. *Journal of Hazardous Materials*, 155(3), 459-468. <https://doi.org/10.1016/j.jhazmat.2007.11.108>